COMPRESSIVE CERVICAL SPINE INJURY:
THE EFFECT OF INJURY MECHANISM ON STRUCTURAL INJURY PATTERN AND NEUROLOGIC INJURY POTENTIAL

Jarrod Wade Carter

A dissertation submitted in partial fulfillment of the requirements for the degree of

Doctor of Philosophy

University of Washington

2002

Program Authorized to Offer Degree: Department of Bioengineering

UMI Number: 3041013

ProQuest Information and Learning Company
300 North Zeeb Road
P.O. Box 1346
Ann Arbor, MI 48106-1346

In presenting this dissertation in partial fulfillment of the requirements for the Doctoral degree at the University of Washington, I agree that the Library shall make its copies freely available for inspection. I further agree that extensive copying of the dissertation is allowable only for scholarly purposes, consistent with "fair use" as prescribed in the U.S. Copyright Law. Requests for copying or reproduction of this dissertation may be referred to Bell and Howell Information and Learning, 300 North Zeeb Road, Ann Arbor, MI 48106-1346, to whom the author has granted "the right to reproduce and sell (a) copies of the manuscript in microform and/or (b) printed copies of the manuscript made from microform."

Signature: 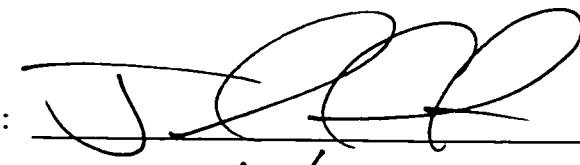

Date: 3/14/02

University of Washington
Graduate School

This is to certify that I have examined this copy of a doctoral dissertation by

Jarrod W Carter

and have found that it is complete and satisfactory in all respects,
and that any and all revisions required by the final
examining committee have been made.

Chair of Supervisory Committee:

Randal P. Ching

Reading Committee:

Randal P. Ching

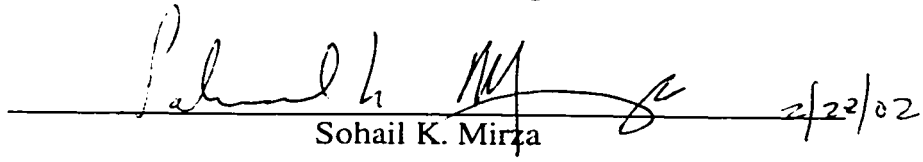

Sohail K. Mirza

Francis A. Spelman

Date: 2-28-02

University of Washington

ABSTRACT

COMPRESSIVE CERVICAL SPINE INJURY: THE EFFECT OF INJURY MECHANISM ON STRUCTURAL INJURY PATTERN AND NEUROLOGIC INJURY POTENTIAL

Jarrod Wade Carter

Chair of the Supervisory Committee:

Associate Professor Randal P. Ching
Department of Orthopaedics and Sports Medicine

Cervical spine trauma resulting in spinal cord injury is a particularly devastating musculoskeletal injury. Every year thousands of individuals are added to the ranks of those afflicted by it. And, the associated socioeconomic costs are extremely high. Researchers have put forth a considerable amount of effort to better understand, prevent, diagnose, and treat these injuries. However, some would argue that progress is hampered by difficulties and inconsistencies in communication among researchers. Specifically, there is no universally accepted method for classifying cervical spine injuries. Arguably the most commonly used classification is the "mechanistic classification," which describes injuries based on the mechanisms responsible for producing them. Although, the mechanistic classification is commonly used, its fundamental hypothesis that different injury mechanisms produce distinct injury patterns classifiable by mechanism alone remains untested. Furthermore, the relationship between injury mechanism and neurologic injury potential, which would make a valuable addition to the mechanistic classification, remains unexplored. Therefore, the objective of this research was to investigate the effect of compressive cervical spine injury mechanisms on structural

injury patterns and neurologic injury potential. The results demonstrate that different compressive injury mechanisms produced distinct injury patterns. And, that the injury patterns are accurately classifiable by the mechanism responsible for creating them. The results also suggest that neurologic injury potential is not significantly affected by injury mechanism in compressive cervical spine trauma. In addition, this study resulted in the development of a Quantitative Mechanistic Classification scheme. This classification scheme provides a way to classify an injury pattern by the mechanism that created it using the intact/injured status of a small subset of the structures comprising the cervical spine.

TABLE OF CONTENTS

1 LIST OF FIGURES

2 LIST OF TABLES

ACKNOWLEDGEMENTS

To start I would like to acknowledge my mother, Laurie L. Carter, for bringing reality into focus for me during the summer between my junior and senior years of high school. If she hadn't prodded me to live up to my potential I most likely wouldn't have made it this far. Furthermore, I would like to thank her for always having faith in me. Her faith has provided bottomless well of strength for me to draw on throughout my life.

I would like to acknowledge my grandparents, Robert and Sallie Keim. They have provided immeasurable amounts of love and support. I would especially like to acknowledge my grandfather for truly being a "grand" father. Of course he will deny that he had any great influence on my life, but if he hadn't been there as a role model for me growing up, who knows where I may have ended up.

I would like to acknowledge John L. Habberstad for filling the role of mentor early on in my educational career. Without John's encouragement I certainly would never have considered mechanical engineering or bioengineering for higher education. Moreover, without John's financial support during my undergraduate and graduate work I would have been hard pressed to make it.

I would like to acknowledge my advisor Randy Ching for his patience and encouragement, even when it looked like I might become a career student. So many times it was Randy reminding me to KISS (Keep It Simple Stupid) my project that prevented unnecessary diversions down useless rabbit trails. Also, I would like to thank Randy for being a good friend.

I would like to acknowledge the hard work of Grace Ku and Mike Eck. Without the efforts they put into helping me prepare the specimens for this study it may never have been finished. Additionally, in working with them I have come to consider them friends as well as colleagues.

I would like to acknowledge David Nuckley, who started out as a colleague and became my best friend. If only there were some way to convey with words how much his friendship and support have meant to me. There were so many instances when I just needed someone to hear me out, and David was there to lend an ear. Thanks Dave!

I would like to acknowledge the Centers for Disease Control for their support of the research presented in this dissertation.

And, last, but not least by any measure, I would like to acknowledge my wife Tama. She has a love for me that is too deep to fathom. She has given of herself to the utmost to support me through my graduate career. There were so many times when I considered abandoning my doctoral work and she was there to provide the encouragement I needed to keep going. My wife didn't perform any of the work involved in this dissertation and she didn't write a single word on any of these pages, but her unconditional love and support made it possible for me to do the work and write the words, which is, in my mind, just as significant.

DEDICATION

I would like to dedicate this dissertation to my wife Tama and the memory of my little brother John Wayne Carter.

3 ABBREVIATIONS

ANOVA – Analysis of variance

CI – Confidence interval

DA – Discriminant analysis

FSO – Full scale output

FSU – Functional spinal unit

LVDT – Linear variable differential transformer

MIV – Major injuring vector

MSD – Midsagittal diameter

SCOT – Spinal canal occlusion transducer

4 INTRODUCTION

Spinal trauma with concomitant cord injury is one of the most devastating musculoskeletal injuries an individual can sustain. The epidemiological literature indicates that the majority of spinal trauma, as well as the majority of spinal cord injuries, occur in the cervical spine.[11, 26, 75] It has been estimated that every year 10,000 new cases of cervical spine injury with quadriplegia occur, with the annual cost for treating all existing cases of quadriplegia approaching $10 billion (in 1982 dollars).[48, 52] These incidence and cost figures only increase if other degrees of neurologic deficit are considered. Unfortunately, these figures do not take into account loss of productivity, the potential costs of associated litigation, or, more importantly, the tremendous pain and suffering of those involved. Hence, cervical spine trauma, with concomitant cord injury, is a common occurrence, and is extremely costly, not only monetarily but also socially and psychologically.

Epidemiologists, clinicians, and biomechanicians have put forth a significant amount of effort to better understand, prevent, diagnose, and treat cervical spine trauma. However, progress is hampered by difficulties and inconsistencies in communication among and within these three disciplines.[52] Improved communication within and between these disciplines could lead to great strides in the effort to find better ways to diagnose, treat, manage, and prevent cervical spine trauma. To improve communication, though, each community should speak the same language.

A universally accepted cervical spine injury classification scheme could provide the common language and frame of reference needed to improve communication.[52, 92] A universal classification would provide unique descriptions of different injuries that could include information regarding the potential for neurologic damage. It could also provide a picture of the structures that may be damaged, an understanding of the loads involved in creating the injury, the amount and directionality of mechanical instability, and suggestions for the best possible treatment. In the end, a universal classification scheme

would provide a mechanism for seamless information exchange between epidemiologists, clinicians, and biomechanicians. This seamless exchange of information can only improve our understanding of cervical spine trauma, which would assuredly lead to improvements in treatment, management, and prevention strategies.

Numerous classification schemes have been developed based upon many different approaches, including: reviews of radiographs, case reports, retrospective patient reviews, cadaveric experimentation, and reconstruction of field injuries.[52] Unfortunately, no single classification has been accepted by both the injury prevention and clinical communities.

One method of classifying cervical spine injuries that has received much attention and is arguably the most widely used classification scheme is the mechanistic classification.[5, 52, 77, 90, 92, 93] The mechanistic classification attempts to relate the type of injury to the loading environment (mechanism) that produced the injury. This method of classification was originally established in 1972 by Roaf,[77] refined and popularized by White and Panjabi[89] and Allen et al.,[5] and has recently been reexamined by Myers and Winkelstein.[52]

A drawback to mechanistic classification is the unverified relationship between the loading mechanism and the resulting injury pattern. Thus far, the association between loading mechanism and injury pattern has been based primarily on the perceived loading mechanism that produced the observed injury pattern and, in some instances, on limited experimental data. To date no experimental studies exist which demonstrate that *different injury mechanisms produce different structural injury patterns*, nor does their exist a study which demonstrates that *injury patterns are classifiable based solely on injury mechanism.*

Likewise, there exists a dearth of knowledge with regard to the relationship between injury mechanism and neurologic injury potential. Since neural tissue injury cannot be

repaired with current technology, it is essential to understand what effect, if any, injury mechanism may have on the potential for spinal cord injury. A close review of the study of Allen et al.[5] indicates that there may be a relationship between injury mechanism and neurologic injury potential. They provided data regarding the frequency of neurologic injury associated with different injury mechanisms. Their data suggests that spinal cord injury frequency is related to the mechanism of cervical spine injury. Again, though, the mechanisms Allen et al.[5] used were perceived mechanisms. Nonetheless, it seems logical that the spinal cord injury may be related to the mechanism of cervical spine injury. At present, however, there are no available biomechanical studies that have investigated *the relationship between neurologic injury potential and injury mechanism.*

It is commonly accepted that the neurologic injury is a cascade of events driven by the initial mechanical deformation of the spinal cord during trauma.[62, 66, 87] It has also been shown that the amount of cord deformation and the velocity of deformation are related to the degree of neurologic deficit.[38] So, if deformation of the spinal canal is monitored dynamically during column trauma experiments then it would be possible to investigate the relationship between injury mechanism and the neurologic injury potential. At the Applied Biomechanics Laboratory a novel transducer has been developed to measure static and dynamic changes in the geometry of the spinal canal.[74] Using this transducer it is now possible to monitor canal geometry during column failure and examine how the external loading environment affects canal deformations and thus, the neurologic injury potential.

The ability to link all of the potential cervical spine injury mechanisms to specific injury patterns and neurologic injury potentials would be tremendously beneficial for both injury prevention and clinical outcomes. However, it would be impractical to investigate all of the different potential mechanisms of cervical spine injury in one study. Therefore, it was necessary to choose a subgroup of mechanisms to investigate. The epidemiological literature suggests that the most common cervical spine injuries are the

result of an axial-compressive load in the midsagittal plane resulting in flexion (forward) or extension (rearward) bending.[5, 96] Consequently, midsagittal plane compressive loading was the mechanism of injury chosen for investigation in this study.

> The objective of this research was to examine the effect of midsagittal plane compressive loading – compression, compression-flexion, and compression-extension – on structural injury patterns and neurologic injury potential in cervical spine trauma.

The following questions were addressed in this study:

1.) Do different injury mechanisms produce distinctly different structural injury patterns?

2.) Can structural injury patterns be accurately classified based on injury mechanism alone?

3.) Is the neurologic injury potential (magnitude of canal deformation) the same for different injury mechanisms?

4.) Are spinal canal deformations produced during injury observable post-injury, or are they transient in nature? In other words, can the actual neurologic injury potential present during injury be perceived post-injury?

5.) If canal deformations produced during injury are different from those observed post-injury is there a correlation between them? In other words, if the neurologic injury

potential present during injury is different from that perceived post-injury, is there a relationship between them?

5 BACKGROUND

The objective of this dissertation was to investigate the effect of loading mechanisms on structural injury patterns and neurologic injury potential, in cervical spine trauma. To understand the genesis of this objective will require some foundation. To start, the anatomy of the cervical spine will be discussed followed by coverage of motion and loading terminology. Then a review of the epidemiological literature will add to the foundation by providing an understanding of the incidence and most common loading mechanisms of cervical spine trauma, as well as the costs of cervical spine trauma, both monetary and non-monetary. The importance of cervical spine injury classifications as weapons in the effort to combat the scourge of cervical spine trauma will be elucidated. In particular the need for a universal classification to provide seamless communication between epidemiologists, clinicians, and biomechanicians will be discussed. From the available classifications the mechanistic classification will be highlighted for its potential to provide a universal classification. A close examination of the mechanistic classification will reveal that it relies on an untested, but logical, hypothesis that the *injury pattern is a function of, and accurately classified by, injury mechanism.* An examination of the literature concerning spinal cord injury mechanics will demonstrate that there is also a need to understand the relationship between injury mechanism and neurologic injury potential, which will complete the foundation.

5.1 Relevant Anatomy and Terminology

5.1.1 Anatomic Position, Anatomic Planes, and Anatomic Directions

Anatomic position is defined as an erect standing posture with the heels together, toes pointed slightly outward, arms at the sides, and palms facing forward (Figure 1). From the anatomic position three primary anatomic planes can be defined (Figure 1). The first is the transverse or horizontal plane that divides the body or a specific component of the anatomy into upper or lower parts in relation to the anatomic position. The second anatomic plane is the coronal plane otherwise known as the frontal plane. The coronal

plane is a vertical plane that is parallel to the front or the back of the body and is used to divide the body or a specific component of the anatomy into front and rear parts. The third anatomic plane is the midsagittal plane. The midsagittal plane is a vertical plane like the coronal plane, however it runs down the middle of the body and separates the body into left an right halves.

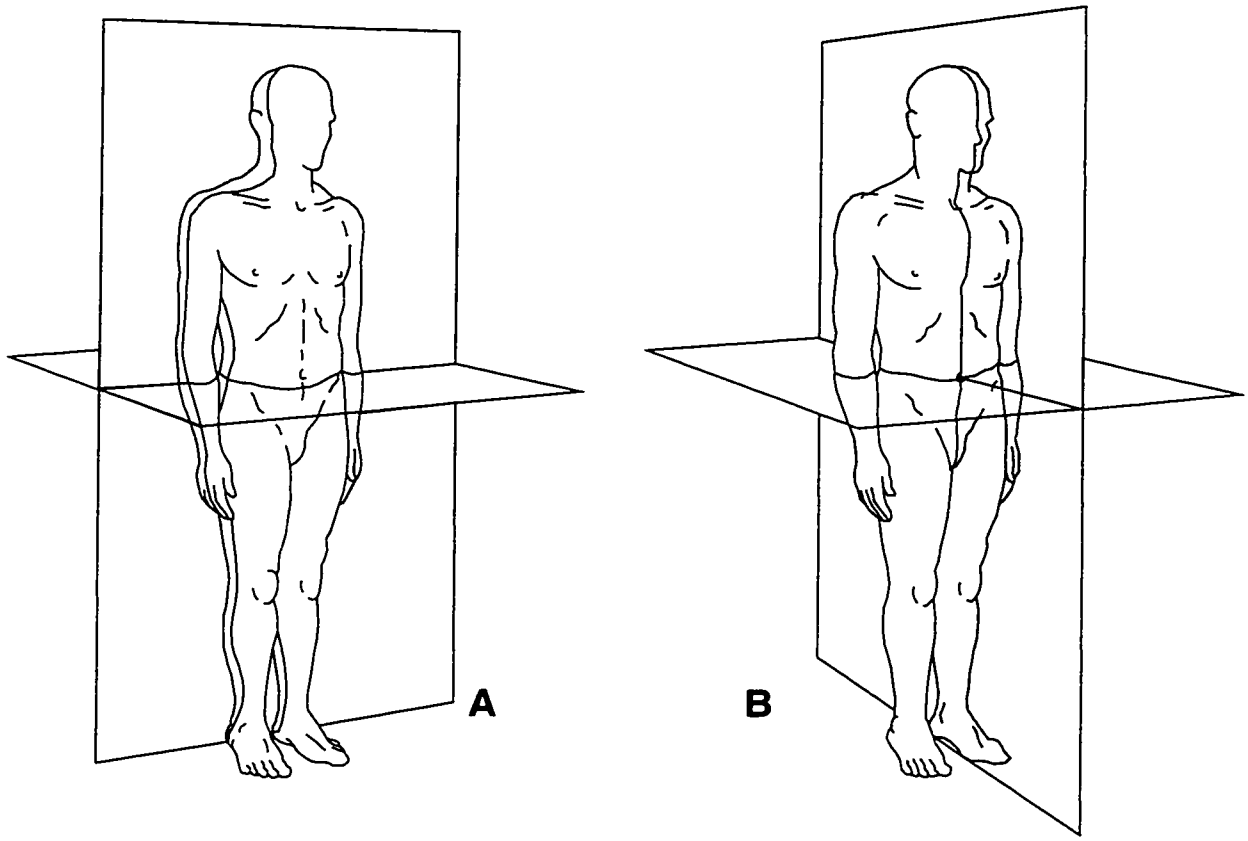

Figure 1: Diagrams demonstrating the anatomic position and the three anatomic planes. The coronal (gray) and transverse planes are shown on the left (A). The midsagittal (gray) and transverse planes are presented on the right (B). Diagrams adapted from Jenkins.[33]

The anatomic directions are used in reference to the anatomic planes. For the transverse plane there are the superior and inferior directions, which simply mean up or down with respect to the location of the transverse plane. Movement with respect to the transverse plane can be described as movement superiorly or inferiorly. With respect to the coronal plane there are the anterior and posterior directions, which refer to ahead of and behind

the coronal plane, respectively. Anteriorly refers to movement forward of the coronal plane, and posteriorly refers to movement behind the coronal plane. Left and right are commonly used for the midsagittal plane. However, the terms medial and lateral are also used. Medial is used to describe some part of a structure that is closer to the midsagittal plane, while lateral is used to describe some part of a structure that is farther away from the midsagittal plane. Additionally, movement with respect to the midsagittal plane can be described as movement medially, or toward the midsagittal plane, and movement laterally, or away from the midsagittal plane. Combinations of these directions can be put together to describe a direction or motion, such as anteromedial, which means forward with respect to the coronal plane and towards the midsagittal plane.

5.1.2 Bony Anatomy

The spinal column can be divided into five distinct regions: cervical, thoracic, lumbar, sacral and coccygeal (Figure 2). The basic unit in each of these regions is the vertebra. In a typical column there are 33 individual vertebrae: seven cervical, twelve thoracic, five lumbar, five fused sacral vertebrae, and three or four fused coccygeal vertebrae. The spinal region of interest in this study is the cervical spine.

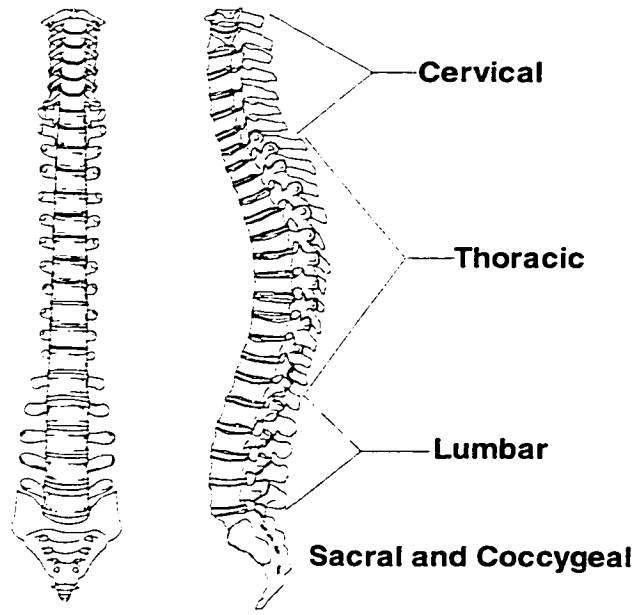

Figure 2: Anatomical sections of the human spinal column.

A typical vertebra is composed of several structures that together form a single bone (Figure 3). The vertebral body is the largest of these structures. It is composed of a core of trabecular (or spongy) bone covered by a thin shell of cortical (or dense/hard) bone. Extending posteriolaterally from the vertebral body are the pedicles. The pedicles together with the laminae form the vertebral arch. The space encompassed by the vertebral arch and the posterior aspect of the vertebral body is known as the vertebral foramen (foramen meaning opening or hole). When all of the vertebrae are correctly aligned their individual vertebral foramen form the bony boundary of the spinal canal, which houses the spinal cord and its associated structures. Extending laterally as well as superiorly and inferiorly from the junction of the pedicles and laminae are the articular pillars. The articular pillars provide the underlying support structure for the superior and inferior articular processes or facets. These facets provide articulation surfaces between a vertebra and those adjacent to it. Extending laterally and anteriorly from the vertebral body and articular pillars are the transverse processes. The spinous process is a bony prominence extending posteriorly from the junction of the laminae.

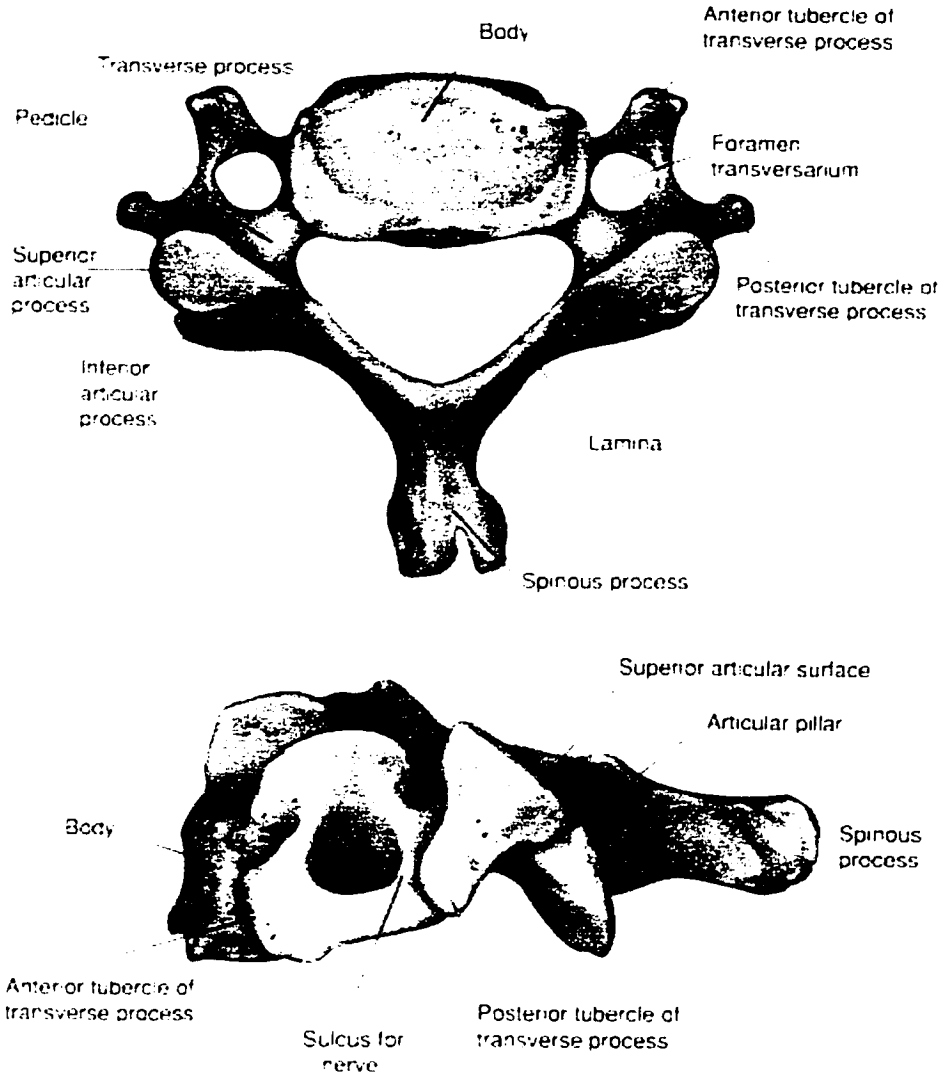

Figure 3: Graphical representation bony components of the typical cervical vertebra (adapted from Heller and Pedlow Jr. [30]).

There are two morphologically distinct vertebrae and five "typical" vertebrae in the cervical spine. The two morphologically distinct vertebrae are C1, the atlas, and C2, the axis. The atlas is the vertebra responsible for joining the cervical spine with the base of the skull (the occiput or C0). The axis and the atlas together form the atlanto-axial joint. The five "typical" vertebrae are C3 through C7. These vertebrae are generally characterized by the fact that their transverse processes have a foramen, the transverse

foramen.[33] However, these vertebrae can also be characterized by the angle of the facets. The superior facets of C3 through C7 are oriented at an angle of approximately 45 degrees relative to the frontal plane, which is different from the orientations of facets in the thoracic and lumbar spines.[90]

Two adjacent vertebrae along with their intervening/interconnecting soft-tissues constitute a functional spinal unit (FSU). The functional spinal unit consists of one motion segment between two vertebrae including the intervertebral disc, facet joints and ligaments connecting these structures. These soft-tissue structures will now be discussed in detail as they pertain to a single FSU.

5.1.3 Soft-Tissue Anatomy

5.1.3.1 Intervertebral Disc

The primary loadbearing connection between two cervical vertebra is the intervertebral disc (Figure 4). Intervertebral discs are composed of three different structures: the cartilaginous *endplates*, the *annulus fibrosis*, and the *nucleus pulposus*. The endplates make up the superior and inferior surfaces of the vertebral body and are composed of hyaline cartilage. The endplates separate the vertebral body from the other components of the disc. The annulus forms the outer wall of the disc and consists of concentric layers of collagen fibers (see Figure 4). The fibers in a given layer are oriented at approximately 30 degrees to the transverse plane. In successive layers the orientation alternates between + and – 30 degrees.[90] The orientation of these fibers allows the disc to resist torsion across a motion segment. The inner layers of the annulus are attached to the endplate while the layers closer to the periphery actually attach to the bony vertebra. The nucleus pulposus is a strongly hydrophilic, incompressible proteoglycan gel intermingled with a random collagen matrix.[80] Under compression the pressure in the nucleus increases. This increased pressure causes endplates to bulge. It also causes the annulus to bulge radially putting the outer fibers of annulus in tension.

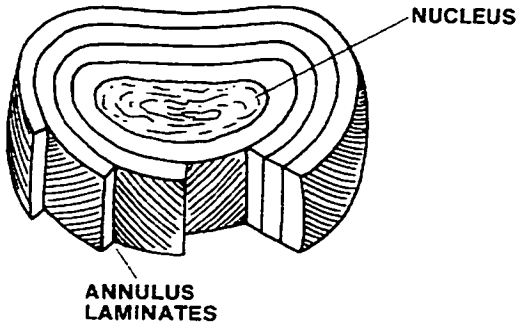

Figure 4: Representation of the cross-section of a typical intervertebral disc showing the annulus fibrosis and the nucleus pulposus (adapted from White and Panjabi [90])

5.1.3.2 Facet Joints

The facet joints are formed by adjacent articular facets. In these joints the superior facet of an inferior vertebra is closely apposed to the inferior articular facet of a superior vertebra. Covering the bone where the surfaces come in contact is a layer of articular cartilage. The joint is enclosed with ligaments and filled with synovial fluid, which lubricates the interface between the layers of articular cartilage. The facet joints of the spine serve two purposes. The facet joints, in concert with the intervertebral disc, are responsible for bearing anterior shear and compressive loads.[90] Further, these joints act to define the functional kinematics of a particular motion segment. The orientation and geometry of facet joints provides the motion segment with a motion guide. Specifically in the cervical spine, the facet joints allow a significant amount of flexion and extension.[90]

5.1.3.3 Ligaments

Ligaments are bundles of parallel collagen fibers that attach between bones or across bones. The nature of their construction limits ligaments to loadbearing in tension. In the cervical spine there are a number of ligaments: the *intertransverse* ligaments, the *anterior longitudinal* ligament (ALL), the *posterior longitudinal* ligament (PLL), the *ligamentum flavum*, the *interspinous ligament*, the *supraspinous ligment* and the *capsular* ligaments

(see Figure 5). These ligaments act to limit excessive joint motion at individual motion segments.

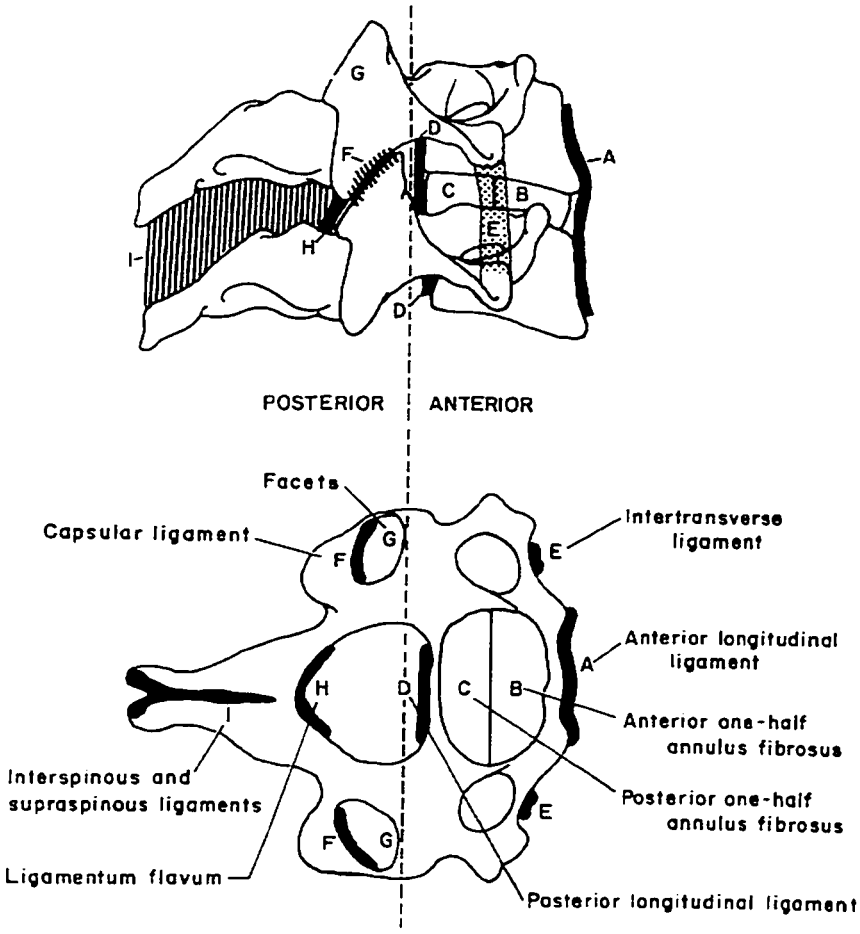

Figure 5: Schematic of the placement of the different ligaments associated with the cervical spine (adapted from White and Panjabi [90]).

5.1.4 Spinal Cord

The spinal cord provides the direct link between the brain and the rest of the body. It starts at the base of the brainstem as an extension of the medulla. Exiting the skull through a large opening in the occipital bone, the foramen magnum, it typically extends to just below the inferior aspect of the first lumbar vertebra. The cross-section of the spinal cord can be grossly divided into two parts: the gray matter and white matter. The gray matter exhibits a very distinct symmetrical H-shape, and is composed primarily of

neuron cell bodies, which gives it the gray appearance. It is these cell bodies that give rise to the spinal nerve roots. The white matter surrounds the gray matter and is composed primarily of axons, which are white in color. The gray and white matter working in conjunction provide the necessary neurological pathways for conducting motor information to the muscles and sensory information to the brain.

5.1.5 Cervical Spine Motion and Loading

There are three primary types of pure midsagittal plane loading that the cervical spine experiences. These primary loading types are axial loading, bending, and shear (Figure 6). All three primary types can be further broken down into subtypes. Axial loading breaks down into tension and compression. Bending breaks down into flexion and extension. And, shear breaks down into anteroposterior (AP) and posteroanterior (PA). The complete midsagittal plane loading environment at any level in the cervical spine can be defined by combining axial loading, bending, and shear components. Often, though, the shear component is left out and the loading environment is described based on the axial loading and bending components present (e.g. compression-flexion, compression, flexion, etc...)

Coincidentally, the midsagittal plane motions of the cervical spine are related to the loads defined above and can be described using the same terminology (Figure 6). For example, the application of flexion bending produces flexion rotation. A complete description of the motion at given location can be produced by combining axial displacement, bending rotation, and shear displacement components.

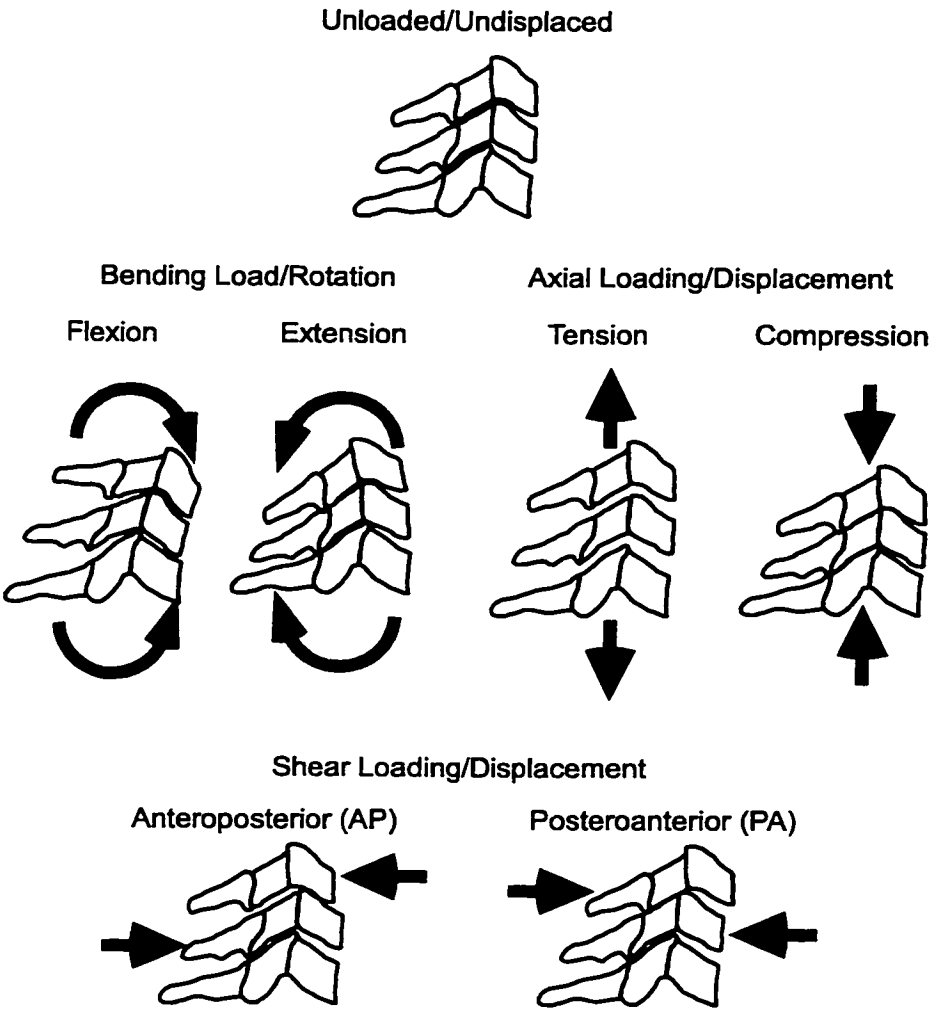

Figure 6: Schematic diagram of the primary midsagittal plane loads and motions of the cervical spine.

5.2 Literature Review

5.2.1 Epidemiology

There are numerous studies that have examined the epidemiology of injury to the cervical spine and the cervical spinal cord. These studies have provided a great deal of information regarding the incidence, costs, and etiologies (causes) of cervical spine/spinal cord injuries.

In general the epidemiological literature indicates that the majority of spinal trauma, as well as the majority of spinal cord injuries, occur in the cervical spine.[11, 26, 75] Estimates indicate that 52 to 65% of all spinal injuries occur in the cervical spine.[11, 26, 75] Considering only cervical cord injuries the National Head and Spinal Cord Injury Severity Survey found that each year there are more than 10,000 new cases of cervical spinal cord injury with quadriplegia.[45] If we assume the current population of the US to be 285,406,533 people (per US Census Bureau October 22, 2001) then we might expect that annually approximately 1 out of every 29,000 people will suffer a cervical spine injury resulting in quadriplegia. At first glance this seems like a small number. However, it does not include other degrees of neurologic injury such as partial paralysis, and it is out of context without consideration for the monetary and psychological costs to individuals and society.

The lifetime medical costs for the partial or complete quadriplegic patient have been estimated to range from $757,000 to $941,000 in 1992 dollars.[48] That equates to between $7.6 billion and $9.4 billion dollars for the lifetimes of the 10,000 new cases every year. Looking at the numbers on an annual basis, it has been estimated that medical costs for *all* individuals with cervical spinal cord injury is approximately $5.3 billion dollars, in 1992 dollars.[48] When costs such as emergency services, lost productivity, legal costs, and the psychosocial effects on an individual and their family and friends are factored in, the annual estimate rises to $12 billion, in 1992 dollars.[48] It cannot be denied that these numbers represent significant costs to the people involved and society as a whole, but how can a price be placed on quality of life? When all is said and done living a full life is priceless, but numbers like these are needed to make society aware of the significance of the problem.

As society has become more aware of the consequences of cervical cord injury, efforts have been made to elucidate its etiologies. In general, there are four primary etiological categories relating to cervical spinal cord injury: transportation, recreation, fall, and

gun/missile related. Figures from the National Spinal Cord Injury Data Research Center show that auto accidents (36.7% of reported cervical spinal cord injuries), falls (15.9%), gunshot wounds (11.7%), shallow water diving (10.6%), and motorcycle accidents (6.2%) represent the top 5 causes of cervical spinal cord injury.[52] These top 5 etiologies account for 81.1% of all cervical cord injuries.

Several authors have examined the mechanisms of cervical spine injury within and across the various etiologies.[5, 10, 84, 96] With the exception of gunshot wounds, the consensus from these various studies is that the most common cervical spine injury mechanism is axial compression. Generally, axial compression results from an incident where the head is suddenly stopped and the still moving torso drives the neck into the base of the skull.

The epidemiological literature gives a clear idea of the devastating scope of the cervical cord injury epidemic. Cervical spine/cord injuries are more common than injuries occurring in other parts of the spine. But, cervical spine/cord injuries occur in a relatively small segment of the population. Yet, the medical costs of these injuries are disproportionately large, not to mention the high psychosocial costs. Fortunately, the predominant etiologies and mechanisms of these terrible injuries have been elucidated. Excluding injuries caused by guns and missiles, the predominant etiologies are associated with transportation (auto and motorcycle accidents) and recreation. With regard to the predominant mechanism of injury the literature suggests that most cervical spine injuries are the result of axial compression.

5.2.2 Classification of Cervical Spine Injury

Classifications of cervical spine injury represent important communication tools within and between the epidemiological, clinical, and biomechanical realms. Classifications seek to define injury characteristics and generate categories with distinct sets of characteristics that also have unique prognoses and requirements for treatment. In the epidemiological realm classifications can provide a way to track the incidence and severity of specific types of injuries. In the clinical realm, where classifications are generally developed, they can be effective tools for enhancing medical treatment and can provide distinct injury categories for clinical outcome studies. In the biomechanical realm classifications can provide direction to research projects aimed at investigating cervical spine injury mechanics and developing injury prevention strategies. Across the three realms, classifications can provide a language that allows results from each community to be shared seamlessly.

At present there are numerous classification schemes described in the literature. However, no single scheme is universally accepted. Lack of universal acceptance inhibits communication.[51] Moreover, the absence of any studies that evaluate the functionality and reliability of the available classification schemes inhibits universal acceptance. It has been suggested that:

> *"Any classification scheme, be it nominal, ordinal, or scalar, should be proved (scientifically) to be a workable tool before it is used in a discriminatory or predictive manner."* [12]

To the author's knowledge there are no studies that evaluate the functionality and reliability of any of the available cervical spine injury classifications.

The available classification schemes can essentially be broken into two groups: those based on gross head and neck motion and those based on the local loading environment (mechanism) at the level of injury. Rogers [78], Holdsworth [32], Whitley and Forsyth [91], Babcock [7], and Kazarian [36, 37] used reviews of case reports, radiographs, postmortem

examinations, and operative information to generate their classifications. They all clearly state, or indicate, that their classifications relate the injury observed in the cervical spine to the gross overall motions of the head and neck. That is to say that the overall motions of the head and neck take the structures of the cervical spine beyond their mechanical limits, resulting in failure.

In 1960 Roaf [76] conducted experimental work demonstrating that classifications based on gross motions of the head and neck are not reliable for defining injury mechanisms. Instead, the injury is more likely to be a function of the loads applied at the injury level. In 1972 he conceived of a classification scheme that related the observed injury to the local loading environment at the injury site.[77] Roaf's findings have been supported by the research of Nightingale et al. who demonstrated that multiple injury mechanisms can be induced without significant head or neck motion.[56] Moreover, they suggested that observed injury patterns were a function of the loading environment at the level of injury. Unfortunately, they were unable to determine the actual loading environments to demonstrate a relationship between mechanism and injury pattern.

White and Panjabi [89] generated their own classification scheme, acknowledging that the inspiration was, in part, drawn form the classification that Roaf [77] described. In their scheme they defined the loading environment responsible for injury by a single loading vector, which they called the Major Injuring Vector (MIV). A limitation, in the author's opinion, of the MIV classification scheme is that it attempts to reduce the loading responsible for injury down to a single vector without consideration for coupled loading conditions. For example, in situations where it is clear that compression and midsagittal plane bending (flexion or extension) are at play, the MIV concept tries to chose the one most responsible. By choosing a single vector valuable information is lost regarding the true mechanism, which is actually a combination of loads.

Allen et al [5] generated a well organized classification of injury to the lower cervical spine based on 165 cases of fractures and dislocations. Their schema, termed "Mechanistic

Classification," is arguably the most commonly used classification today. In their study they segregated injuries into groups based on mechanisms of injury, which were defined using combined loads. The five mechanisms of injury that they defined were compressive-flexion, vertical compression, compressive-extension, distractive-flexion, distractive-extension, and lateral-flexion, and, although it wasn't explicitly stated, these mechanisms appear to be defined *based on the local loading environment (mechanism) at the level of injury.*

Allen et al. [5] took a big step ahead of other classifications in two critical areas: injury descriptions and neurologic injury potential. With regard to injury descriptions, they did not utilize previous naming conventions for injuries (e.g. burst, wedge-compression, hyperflexion, etc...), which reflected old patterns of thought and in some ways confusing jargon. Instead they described the injuries based on the damage observed in specific structures that they felt best described the injury. Thus, *they attempted to link the injury mechanism to the injury pattern.*

Neurologic injury potential was also addressed in the Allen et al. [5] classification. The classification scheme broke each mechanism down into stages, which were ordered from low to high by the severity of structural injury as denoted in the observed injury pattern. Examining their compilation of associated spinal cord injuries, it appears that the structural severity may be directly related to neurologic injury severity. The assertion they made regarding the relationship between structural injury severity and neurologic injury potential is best described in their words.

> *"It is evident that the higher stages of injury within each phylogeny (mechanism) are more likely to show a severe cord injury than are the lower stages. Higher stages are reflective of a more severe injury to the spine and predictably show a more severe cord involvement."*

Furthermore, an examination of the frequency of spinal cord injury within each injury mechanism suggests that *the injury mechanism may be related to neurologic injury potential.* Thus, they attempted to account for the neurologic outcome in their

classification scheme, which is arguably the most important factor in determining patient outcome.

More recently Myers and Winkelstein [52, 92, 93] revisited the concept of cervical spine injury classification. They conducted a thorough review of the clinical literature regarding classification and a thorough review of the biomechanical literature to tease out the best injury classification scheme. They concluded that the mechanistic classification described by Allen et al. [5] represented the best fit with the available biomechanical and clinical literature. Synthesizing the literature they were able to expand on the Allen et al. classification. Ultimately, they suggested a high degree of agreement between injury mechanism and structural injury pattern.

A shortcoming of the Myers and Winkelstein classification [52, 92, 93] was that they did not incorporate neurologic sequelae in their classification. So, their classification scheme is apt for sorting out mechanisms as they relate to structural damage, but it stops there. The reality is that the Myers and Winkelstein mechanistic classification scheme needs clinical field data to help tease out relationships between structural damage and neurologic injury severity in a similar fashion to the classification of Allen et al.[5]

Before concluding this review it is important to point out a hole in the mechanistic classification that is vital to understanding the objective of this dissertation work. The hole in the mechanistic classification is its primary hypothesis that *different injury mechanisms produce distinct injury patterns that can be accurately classified by mechanism alone*. The mechanisms that Allen et al.[5] used in their classification scheme were perceived mechanisms, meaning they assigned an injury pattern to a mechanism based on their perception that it was created by that mechanism. Unfortunately, they did not present any experimental data to verify that their mechanisms were correct.

Myers and Winkelstein[52, 92, 93] used experimental data along with clinical data to develop their mechanistic classification. Nonetheless, as will be demonstrated in the next section,

they still made "educated guesses" as to the mechanism responsible for different injury patterns. Therefore, it is important that some investigation be conducted to investigate the hypothesis that *different injury mechanisms produce distinct injury patterns that can be accurately classified by mechanism alone.*

The review of the literature presented here suggests that the best classification scheme for communicating within and between the epidemiologic, clinical, and biomechanical realms is the mechanistic classification. It can define the characteristics of distinct groups of injuries, which all three groups need for purposes of identifying injuries created naturally and experimentally. If properly developed it can also provide information on neurologic injury potential, which is primarily of benefit to the clinician for treatment decisions. Primarily, though, the mechanistic classification conveys information about the mechanism responsible for creating specific injury characteristics. Clinically, knowledge of the injury mechanism can provide insight into the forces applied during injury and the direction(s) in which post-injury instability may be an issue. Biomechanically, knowledge of the mechanism is beneficial for devising experiments to investigate injuries and schemes to prevent injuries. However, the fundamental hypothesis behind the mechanistic classification, *that different injury mechanisms produce distinct injury patterns that are classifiable by mechanism alone*, remains untested.

5.2.3 Mechanics of Compressive Cervical Spine Injury

Historically, biomechanical investigations of compressive cervical spine trauma have been conducted using whole cadavers, isolated cadaver head and cervical spine

specimens, and isolated cadaver cervical spine specimens. [2, 18, 31, 42, 44, 46, 53-57, 60, 61, 68, 73, 97-101] The methods employed to apply compressive loading include dropping whole cadavers onto their heads,[2, 31, 42, 60, 61, 99, 100] dropping isolated head and cervical spine specimens onto their heads (simulated torso mass used),[53-55, 57] dropping weights onto isolated cervical spines,[18] using loading frames to apply load to the head of an isolated head and cervical spine,[42, 68, 97-99, 101] and using loading frames to apply load to isolated cervical spines.[18, 42, 44, 46, 56, 68, 73, 97-99, 101] These studies have demonstrated that it is possible to generate clinically relevant injuries in the cervical spine under compressive loading.

A byproduct of these previous biomechanical studies is a clear understanding that it is nearly impossible to predict the location of injury or the type (pattern) of injury that will result. Some studies have shown that similar loading protocols applied to different specimens produce injuries that appear to be the result of different injury mechanisms (e.g. compression-flexion, compression, and compression-extension). Others have demonstrated that the same specimen can have multiple injuries, with each injury appearing to be the result of a different injury mechanism. The obvious question is: how can such variability be explained?

The seminal work of Nightingale et al. [53-55, 57] provided a great deal of insight into the variability of injury site, pattern, and mechanism. In their experiments they used isolated head and cervical spine specimens. The specimens were inverted and dropped onto the head with a simulated torso mass attached at the base of the cervical spine. In their results they noted significant variations in the site(s) of injury and the plausible mechanism(s) of injury (they did not compute the loading environment at the injury site). More importantly, though, their results provided the first conclusive evidence that the cervical spine buckles under axial compressive impact loading. They hypothesized that buckling results in loading environment variations along the length of the cervical spine,

and that these loading environment variations are responsible for the variations in injury site, pattern, and mechanism previously observed.

In several well-written review articles Myers and Winkelstein [52, 92, 93] synthesized the available clinical and biomechanical literature regarding injury mechanism, taking into account the findings of Nightingale et al.[53-55, 57] Considering that the cervical spine buckles when loaded under axial compression they suggested that the buckled shape dictates the loading environment at different positions along the cervical spine (Figure 7). For the configuration shown in Figure 7 it becomes clear that the line of action of the axial force F relative to the positions of the intervertebral joints dictates the loading environment. With this type of configuration one section of the cervical spine could be sustaining compression-flexion loading, another section compression-extension loading, and yet another section compression loading. Thus, the injury mechanism, injury type (pattern), and injury site will vary depending on the susceptibility of a given segment to failure by the loading environment and loading magnitudes applied to it.

Another important contribution of Myers and Winkelstein [52, 92, 93] was the introduction of a simple, yet novel, variable for representing injury mechanism. This new variable was called the eccentricity. Eccentricity, can be defined as the moment arm required to resolve the compressive force and midsagittal plane moment produced at the level of injury into a compressive force at a distance from the centroid of the intervertebral disc (Figure 8). Thus, a loading environment consisting of a compressive force and a midsagittal plane moment can be represented by a single variable, eccentricity.

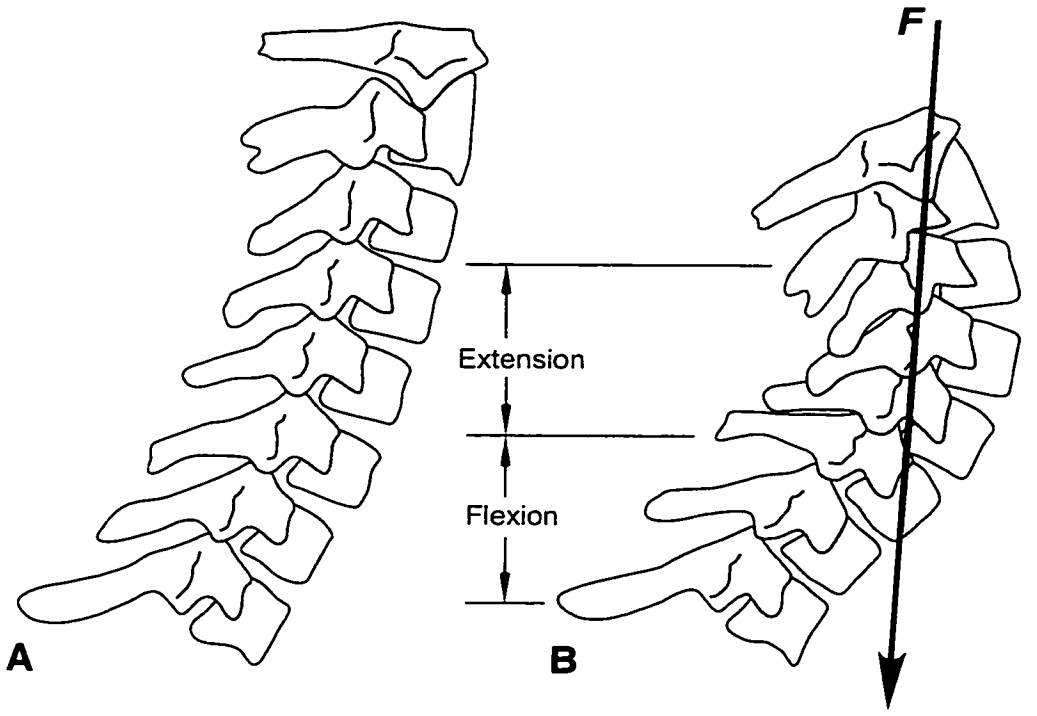

Figure 7: Adaptation of Figure 4 from Winkelstein and Myers [92]. The figure shows the normal spinal alignment (A) and the buckled spinal alignment (B) produced by the axial impact force F.

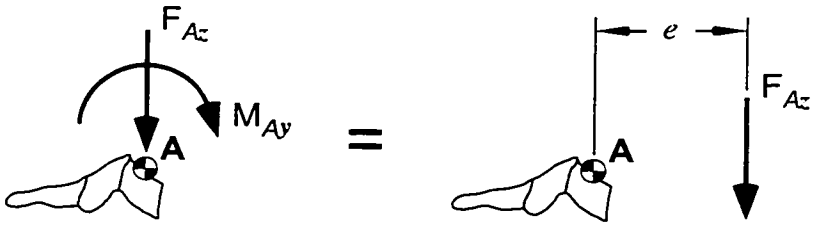

Figure 8: Schematic representation of the resolution of compressive force and midsagittal plane moment into a compressive force at a distance. The distance the compressive force is shifted is known as the eccentricity. The reference point A was established at the centroid of the intervertebral disc superior to the injured level. In this diagram a compression-flexion loading is applied.

Using the concept of eccentricity to define loading environment, Myers and Winkelstein [52, 92, 93] hypothesized that injuries traditionally attributed to compressive mechanisms could be represented by an eccentricity spectrum. In other words, they hypothesized that injury mechanism, as defined by eccentricity, predicts the type (pattern) of injury. The diagram provided in Figure 9 demonstrates their hypothesized relationship between the traditional injury description and injury mechanism as defined by eccentricity.

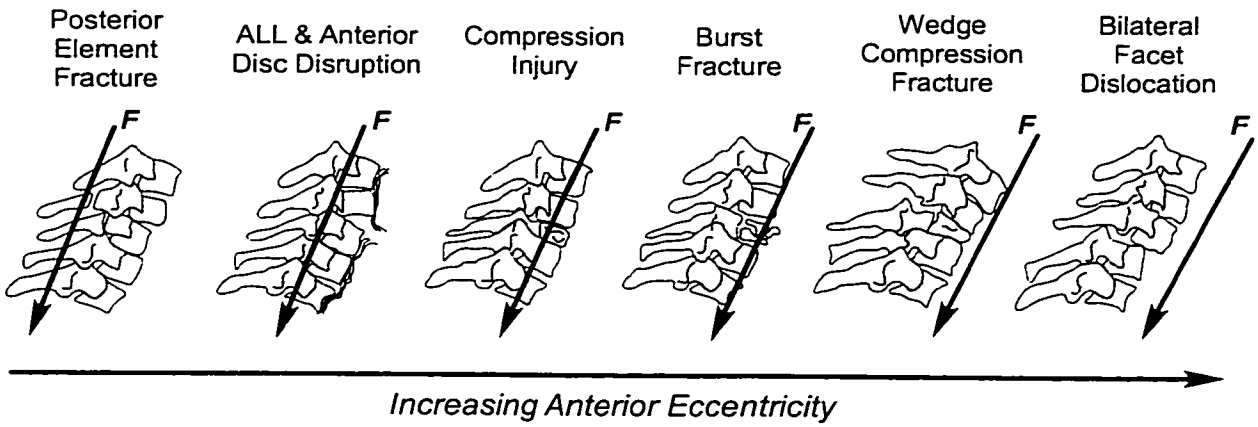

Figure 9: Diagram relating traditional injury descriptions to mechanism of injury as established using eccentricity. As the axial force moves from posterior to anterior the injury mechanism changes from compression-extension to compression and finally to compression-flexion. Figure adapted from Winkelstein and Myers [92]

Myers and Winkelstein's[52, 92, 93] hypothesis that *different injury mechanisms, as defined by eccentricity, produce different types of injury (patterns of injury)*, while logical, has never been experimentally tested. The lack of experimental validation of this hypothesis represents a significant gap in the biomechanical literature regarding the mechanics of compressive trauma. Even Myers and Winkelstein [52] indicated that an experimental study investigating this hypothesis would be a welcome addition to the literature.

There are a two studies that have come close to testing the hypothesis that injury mechanism dictates injury pattern.[22, 83] Both of these studies used 2 FSU segments as their experimental model, which is considered to be the shortest segment of the spine in which injury can be studied.[24] Using the 2 FSU experimental model avoids the issues associated with models that involve the whole cervical spine. Specifically, using the 2 FSU model eliminates buckling and localizes injury to a single vertebra and its adjacent intervertebral joints.

Crowell et al.[22] subjected human 2-FSU cervical spine specimens to quasistatic flexion rotation and flexion rotation with compression translation to generate flexion and flexion-compression loading. After testing, they dissected each specimen and examined the posterior ligaments, facet capsules, intervertebral discs, and vertebral bodies for injury.

They concluded that similar patterns of injury can occur in both flexion and flexion-compression; however, they did not demonstrate their conclusion statistically. Furthermore, while they did specify loads at failure, they did not specify where the loads were measured/computed. Based on a review of their article it appears that the loads were not transformed into the specimen to provide the local loading environment in the specimen at failure. Thus, they did not clearly define the mechanism at the level of injury nor did they statistically test the hypothesis that injury mechanism dictates injury pattern.

Southern et al.[83] tested porcine 2 FSU cervical segments. A dropweight-style protocol was used to deliver high-speed impact loading. The impactor was 14.5 kg and the drop height was 1.1 m, which corresponds to an impact velocity of 4.6 m/s, under frictionless conditions. The specimens were subjected to compression, compression-extension, and compression-flexion injury mechanisms by shifting a roller assembly attached to the top of the specimen. A compression injury mechanism was defined when the roller assembly was aligned such that the initial impact force from the impactor was directed through the centroid of the segments middle vertebral body. Compression-flexion and compression-extension mechanisms were defined when the initial impact force was directed 1 cm anterior to and 1 cm posterior to the centroid of the middle vertebral body, respectively.

In their analysis Southern et al.[83] gave each anatomic structure in the segment an injury score based on an arbitrary injury severity scale. Then they used the nonparametric equivalent of a one-way ANOVA to determine if the injury scores for each individual structure were significantly different across the three injury mechanisms. They determined that some structures sustained more severe injuries depending on the injury mechanism. Compression-extension produced the greatest severity of injury in the discs, anterior longitudinal ligaments, posterior longitudinal ligaments, articular facets, and pedicles. The spinous processes, laminae, ligamentum flavii, and interspinous ligaments, sustained the most severe injuries in compression flexion. The compression mechanism produced the least amount of injury.

Southern et al.[83] came close to statistically testing the hypothesis that different injury mechanisms produce distinct injury patterns. Ultimately, though, their statistical analysis was incapable of specifically testing the hypothesis because it didn't consider the multidimensional nature of the injury patterns. Instead their analysis looked for differences shown by individual structures across each injury mechanism group. Also, they did not demonstrate, via measurement or computation, that their experimental procedure produced loading environments at the time of injury consonant with the three injury mechanisms they were investigating. Furthermore, since their specimens were porcine their results have limited applicability to humans.

Hence, there are no previous studies that have specifically tested the hypothesis: different injury mechanisms, as defined by eccentricity, produce different types of injury (patterns of injury).

This review of the biomechanical literature concerning compressive cervical spine trauma demonstrates that a significant amount of work has been done to understand the mechanics of injury. However, the fundamental link between injury mechanism and injury pattern remains ill defined. Recent reviews by Myers and Winkelstein have hypothesized that injury mechanism can be defined by eccentricity and that different injury mechanisms produced different injury patterns. At present, though, no studies exist which examine the hypothesis that *different injury mechanisms, as defined by eccentricity, produce distinctly different injury patterns.*

5.2.4 Mechanics of Cord Injury

Structural damage alone does not make cervical spine injury dangerous. It is the significant potential that a cervical spine injury may lead to a spinal cord injury resulting

in paralysis or death that makes cervical spine injury dangerous. It is generally accepted that the neurologic component of a cervical spine injury has the greatest effect on the patient's outcome. Physicians can repair structural damage in the cervical spine quite effectively, but there is currently no way of repairing damage to neural tissues.

When the cervical spine sustains a structural injury there is the possibility that displaced structural components, such as bone fragments or ligaments, may impinge upon the spinal cord. Numerous clinical studies have suggested that canal occlusion (reduction in midsagittal diameter) is a mechanism of cord injury, based on post-injury occlusion measurements using radiographs or CT's.[9, 23, 27, 29, 35, 39, 43, 79] However, the data also shows that there are patients who do not exhibit significant post-injury occlusion but present with incomplete or complete neurologic deficit. It has been suggested that this discrepancy occurs because the post-injury measurements of canal geometry from radiographs and CT scans are poor predictors of the occlusion produced during the injury.

It is widely held that the neurologic injury is initiated by the initial mechanical deformation of the cord during spinal trauma.[62, 66, 87] This concept has been echoed since the first spinal cord injury studies conducted by Reginald Allen in the early 1900's.[3, 4] Recently, Anderson [6] and Kearney et al. [38] conducted elegant studies subjecting the spinal cords of ferrets to controlled compressive displacements. The midsagittal diameters (MSDs) of the spinal cords were compressed by various amounts at different velocities, followed by a controlled release. The results of these studies indicated that the amount of cord deformation and the velocity of that deformation was predictive of spinal cord injury severity, in terms of post-insult recovery (Figure 10). If cord injury can be related to the dynamics of cord compression than it would be advantageous to monitor the spinal canal for changes in midsagittal diameter during cervical spine trauma experiments.

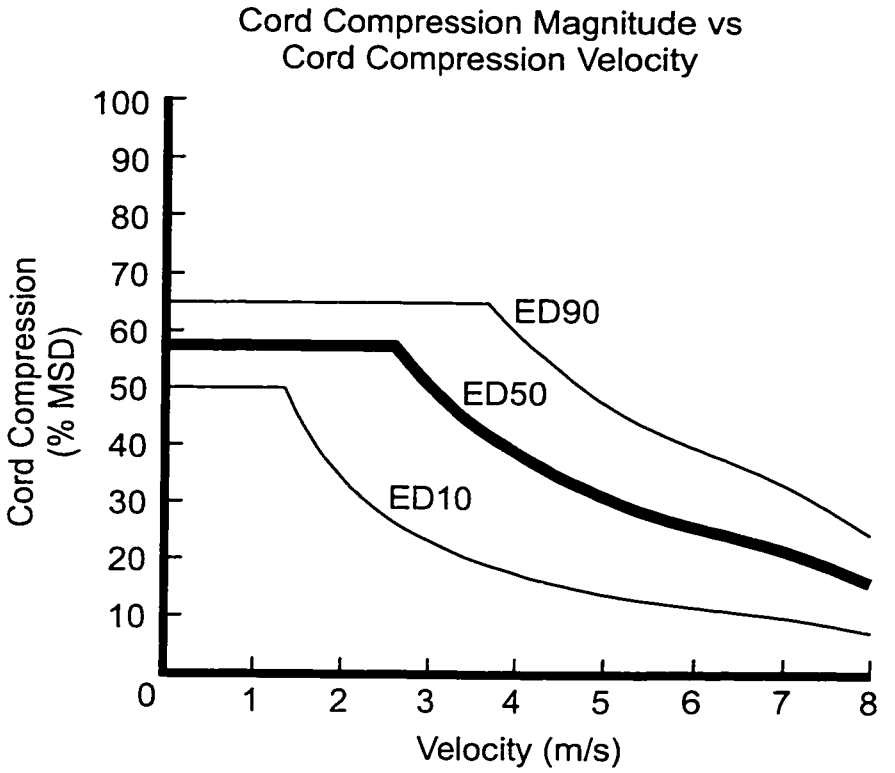

Figure 10: Adaptation of figure 15 from Kearney et al. [38] demonstrating the propesed relationships between spinal cord injury, the amount of cord compression, and the velocity of the compression. The three curves represent the estimated doses necessary for 10% probability of complete neurologic injury (ED10), 50% probability of complete neurologic injury (ED50), and 90% probability of complete neurologic injury (ED90).

Traditionally, biomechanical studies of cervical spine structural injury have paid little attention to the concept of neurologic injury as it relates to the mechanism or type (pattern) of structural injury. Biomechanical studies of cervical spine injury mechanics that also investigate linkages to neurologic injury have only recently begun to appear.[8, 17, 18, 20, 66, 69-71, 85] The common element of these studies has been some method for transducing changes in the spinal canal environment during compressive trauma. The studies conducted by Bates-Carter et al.,[8] Carter et al.,[17, 18] Chang et al.,[20] Panjabi et al.,[66] and Tran et al. [85] used specially designed transducers to monitor changes in the midsagittal diameter (MSD) of the spinal canal. These studies are based on the idea that monitoring the canal during injury can elucidate the linkage between structural trauma and neurologic trauma in cervical spine injuries.

The studies that have monitored the midsagittal diameter have done so in experiments involving compression of isolated ligamentous human cervical spines,[8, 17, 18, 20] isolated ligamentous human thoracolumbar spines,[66] and isolated bovine lumbar spines.[85] These studies have demonstrated that large canal occlusions (reductions in MSD) are generated during injury. Further, they have demonstrated that the large occlusions observed during injury are transient in nature and are not predicted by the occlusions that are observed post injury. Moreover, they have shown that loading rate can have a significant effect on not only the occlusion produced during injury but also on the occlusion observed post-injury. At present, however, no studies exist which examine the relationship between injury mechanism and potential for neurologic injury.

The fact that there aren't any biomechanical studies that investigate the relationship between injury mechanism and injury pattern, begs the question: "Is there evidence that injury mechanism affects neurologic injury potential?" The mechanistic classification created by Allen et al. [5] indicates that injury mechanism may have a significant effect on neurologic injury potential. As can be seen in Figure 11 the frequency of cord injuries increases as the mechanism shifts from compression-extension to compression-flexion. Thus, the injury mechanism may have a profound effect on the neurologic outcome of a cervical spine injured patient. Therefore, research should be performed to investigate the hypothesis that *cervical spine injury mechanism is related to the potential for cervical spinal cord injury.*

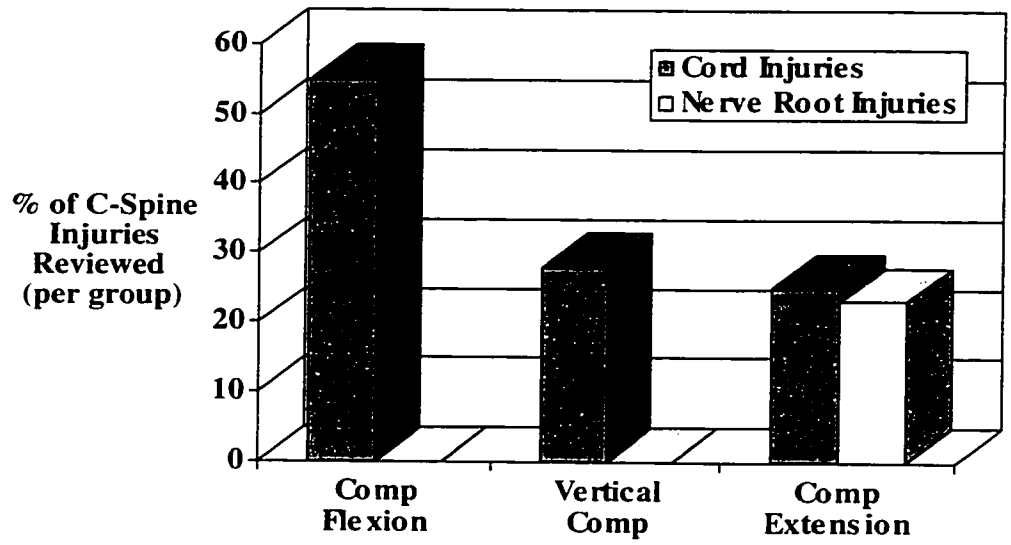

Figure 11: Bar graph representing the percentage of cord and nerve root injuries exhibited for each compression related mechanism in the study of Allen et al. [5]. The numbers are the percentage of injuries per the number of individuals in a mechanism group.

In summary, this literature review concerning the mechanics of spinal cord injury reveals that compression of the spinal cord can lead to neurologic injury. In cervical spine trauma spinal cord compression is generally considered to occur when disrupted structures are displaced into the canal such that they impinge on the spinal cord. When the cord is compressed it has been demonstrated that the magnitude and velocity of the compression dictate the degree of neurologic injury. This understanding has recently been integrated into biomechanical investigations of compressive cervical spine trauma through the use of specially designed transducers capable of monitoring the spinal canal geometry during injury. These studies have demonstrated that cervical spine compression can generate significant canal occlusion

during injury, and that the occlusion observed post-injury fails to predict the occlusions measured during injury. At present no biomechanical studies exist which investigate *the effect of injury mechanism on neurologic injury potential.* However, such research should be conducted, as there is reason to believe that injury mechanism may have a significant effect on neurologic injury potential.

5.2.5 Summary

Injuries to the spine and spinal cord are the most common in the cervical spine. They affect a small segment of the population, but present a significant burden in terms of monetary and psychosocial costs that ripples out into society. The most common etiologies – accounting for 81.1% of all cervical spine injuries – are auto accidents, falls, gunshot wounds, shallow water diving, and motorcycle accidents. Furthermore, the epidemiological data suggests that axial compressive loading is the most common injury mechanism.

Investigation and progress in the arenas of clinical treatment and injury prevention could benefit from the development of a universal tool for communicating information about cervical spine injuries.[52] The mechanistic classifications that have been most recently developed by Allen et al. [5] and Myers and Winkelstein [52, 92, 93] appear to be effective at placing injury patterns into distinct groups and also presenting information regarding the potential for neurologic injury associated with certain patterns. While no classification scheme has been accepted universally or even validated, the mechanistic classification scheme holds the most promise. With further development it can become not only a useful clinical tool to help guide treatment of patients, but also a useful interfacing tool between epidemiologists, clinicians, and biomechanics researchers. Specifically, the hypothesis that *different injury mechanisms produce distinct injury patterns that can be*

accurately classified by mechanism alone needs to be more thoroughly investigated before the mechanistic classification can be considered a reliable tool.

The current understanding with regard to the mechanics of compressive trauma in the cervical spine has been greatly simplified in this review. Prior to the literature reviews conducted by Myers and Winkelstein [52, 92, 93] and the studies of Nightingale et al. [53-57] most of the biomechanics literature involved testing head-neck-torso, head-neck, and isolated neck specimens. These experiments demonstrated inherent variabilities in injury site, pattern, and mechanism. As a result of these variabilities the focus has been shifted toward examining the local loading environment at the site of injury to better understand how compressive injuries are developed. The primary contribution of Myers and Winkelstein [52, 92, 93] was the hypothesis that the *different injury mechanisms, as defined by eccentricity, produce different injury patterns.* While this hypothesis makes good common sense, it has yet to be validated experimentally.

It is disconcerting that consideration for neurologic injury potential receives so little attention in clinical classification and in biomechanical studies of cervical spine trauma. After all when an individual has a neck injury, their most significant concern pertains to their functional outcome, which is dictated by the degree of neurologic injury. As far as classifications are concerned, the mechanistic classification of Allen et al. [5] is the only one that really speaks to neurologic injury potential. Their data suggests that injury mechanism may be related to neurologic injury potential. From a biomechanical standpoint, few studies have examined the link between cervical spine injury and neurologic injury potential. To date no study has investigated the effect of injury mechanism on neurologic injury potential. Therefore, it is important to undertake research examining *the relationship between injury mechanism and neurologic injury potential.*

5.3 Objective

The review of the literature highlights two very important gaps in our current knowledge. Specifically, it is clear that the relationship between mechanism of injury and injury pattern has not been scientifically validated. The mechanistic classification scheme, as well as the current school of thought regarding the mechanics of compressive cervical spine injury, are based on the hypothesis that different injury mechanisms produce distinct injury patterns and that those injury patterns can be accurately classified by mechanism alone. This hypothesis, while tending to make good common sense, relies primarily on perception and some limited experimental data. To date no scientific study has been performed to examine this hypothesis.

Additionally, there is currently no clear understanding of the relationship between mechanism and neurologic injury potential. The data provided by Allen et al. [5] provide reason to believe that there is a significant relationship. However, the fact that their mechanisms were based on the perception of the loading environment responsible for the injury tends to taint the findings. Thus, it would be extremely valuable to examine the relationship between injury mechanism and neurologic injury potential.

It would be wonderful to conduct a study that looked at every possible injury mechanism to examine the interrelationships of injury mechanism, injury pattern, and neurologic injury potential. But, that would be more consistent with the goal of a "life-long" research program, not a dissertation. Instead this work focused on the area where the epidemiological data demonstrate the greatest need, namely compressive cervical spine trauma.[5, 10, 84, 96] Specifically, this study examined the three primary mechanisms of midsagittal plane compressive trauma: compression-flexion, compression, and compression-extension. [5, 52, 92, 93]

Therefore, the objective of this study was to examine the effect of midsagittal plane compressive loading mechanisms on structural injury patterns and neurologic injury

potential, in cervical spine trauma. To achieve this objective an experimental design was conceived to create injuries in 2-FSU cervical spine segments under the three different mechanisms of axial compressive loading selected. During each experiment canal occlusion was monitored continuously using a specially designed spinal canal occlusion transducer (SCOT), which was developed in the author's laboratory.[74] Post-experiment, each specimen was thoroughly inspected both visually and radiographically (plain radiographs and CT scans) to establish the pattern of structural injury produced. A synthesis of these measurements should fill the void in our understanding of cervical spine injuries and enable the development of enhanced injury prevention and clinical management strategies.

5.4 Hypotheses

To meet the objective of this dissertation, a series of hypotheses were rigorously developed.

1.) Significantly different midsagittal plane compressive injury mechanisms, in terms of eccentricity, produce distinctly different injury patterns. (H_o: Significantly different injury mechanisms do not produce significantly different injury patterns)

2.) Structural injury patterns can be accurately classified by injury mechanism between compression, compression-flexion, or compression-extension injuries. (H_o: The accuracy of classifying injury patterns by injury mechanism is no different from assigning injury patterns to an injury mechanism at random)

3.) Canal occlusions measured at the initiation of structural failure (failure), peak during injury, and immediately post-injury (residual occlusion) are related to injury mechanism. (H_o: Mean canal midsagittal-diameter (MSD) occlusions measured at

failure, at peak during the injury, and immediately post-injury do not change significantly due to changes in injury mechanism)

4.) The peak canal occlusion generated during injury is always greater than the occlusion measured both at failure and the residual occlusion measured immediately post-injury. (H_o: Mean peak canal MSD occlusion measured during injury is no different from mean occlusion measured at failure or mean residual occlusion)

5.) There is no correlation between peak canal occlusion measured during injury and the residual occlusion measured immediately post-injury. (H_o: $\beta = 0$, or the slope of a line relating peak canal MSD occlusion to Residual MSD occlusion is not significantly different from zero)

6 MATERIALS AND METHODS

6.1 Experimental Model

Historically, compressive cervical spine trauma studies have been conducted on experimental models that include the entire cervical spine. However, the work of Nightingale et al.,[53-55, 57] the reviews of Myers and Winkelstein,[52, 92, 93] and the author's personal experience lead to the conclusion that it is not possible to control for the location (i.e. spinal level) or number of injury sites in experiments involving whole cervical spines subjected to compressive loading. Furthermore, in whole cervical spine experiments, the site of injury is typically separated from, and moving with respect to, any load sensing instrumentation. Moreover, there are objects of unknown mass with unknown acceleration (e.g. other vertebral bodies and/or the head) interposed between the injury site and any load sensing equipment. Hence, it is nearly impossible to compute the specific loading environment at the level of injury, which makes defining the injury mechanism equally uncertain. Therefore, using whole cervical spines as a model for examining the effects of injury mechanism in cervical spine trauma is difficult at best.

A better experimental model for investigating the effects of injury mechanism is the 2 FSU segment of the human cervical spine. Edwards suggested that the 2 FSU spinal segment represents the smallest unit of the cervical spine that can be used for studying injury.[24] Using a 2 FSU segment, rather than the whole cervical spine, removes the variability of injury site by limiting the possible sites to one vertebra and its adjacent intervertebral joints. A 2 FSU segment provides the ability to accurately define the loading environment at the injury site by placing it closer to load sensing instrumentation and eliminating objects of unknown mass and acceleration between it and the load sensing instrumentation. Additionally, a 2 FSU specimen provides better control over the mechanism of injury through the elimination of buckling. Thus, to meet the objective of this study a 2 FSU experimental model will be used.

6.2 Specimen Preparation

6.2.1 Harvesting/Inspection

A total of 24 human cadaveric cervical spine specimens (Occiput to T6) were acquired for this research. Specimens were obtained through the willed body programs of the University of Washington, University of California at Davis, and International Institute for the Advancement of Medicine. Each specimen was harvested shortly after death, wrapped in moist towels, and frozen at – 20° C. The specimens were not embalmed to prevent undesirable changes in tissue properties.[88]

After arriving at the Applied Biomechanics Laboratory (ABL) each cervical spine specimen was dissected to remove the surrounding soft-tissue. Care was taken to prevent disruption of the osteoligamentous structures that connect the individual vertebrae. At the end of the dissection procedure each specimen was subjected to a thorough visual inspection for obvious pre-existing pathologies, such as osteophytic growth, or fracture.

Manual manipulation was used to determine the degree of mobility across each intervertebral joint. Mobility was assessed as a binary variable. Each individual intervertebral joint could be either mobile or fused.

Concurrent with manual manipulation, an assessment of intervertebral disc integrity was made. This assessment was made by injecting physiologic saline into the nucleus of the disc. Similar to the mobility assessment, disc integrity was assessed as a binary variable where each disc either held pressure or did not.

Following the visual inspection procedure each specimen was radiographed. Both lateral and anterior/posterior views were taken. The radiographs were taken in an HP Faxitron (model 43855A, Hewlett Packard, McMinnville, OR) at 100 kVp for 30 seconds. The radiographs were used to examine the specimens for pre-existing pathology that may have escaped notice during the visual inspection.

The visual inspection, radiographic inspection, mobility assessment, and disc integrity assessment were combined to evaluate the viability of each vertebra and intervertebral joint in an individual cervical spine. Two adjacent FSU's were selected for this study if they lacked significant pre-existing pathology, had two mobile intervertebral joints and at least one intervertebral disc that held pressure. Preference was given to selecting the C5-7 segment if it met the inclusion criteria. However, due to the variability in specimen quality and limited availability it was decided to harvest one viable 2-FSU segment from each specimen. Selected segments ranged from C2-4 to C6-T1.

Once a two FSU segment was selected, that segment was harvested from the whole cervical spine. The harvesting procedure involved transecting the intervertebral joints at either end of the segment using a scalpel. Care was taken not to damage the bony components or the endplate of the vertebra adjacent to the intervertebral joint. During the harvesting of the segment the spinal cord, dura, and nerve roots were carefully removed.

A total of 24 2-FSU specimens were harvested from 24 different cervical spines. Harvested specimens were randomly assigned to one of the three injury mechanism groups (e.g. compression, compression-flexion, or compression-extension) such that each group contained eight specimens.

All specimen preparation work was conducted utilizing the accepted CDC guidelines for handling human cadaver tissues.[19] Each specimen was thawed at room temperature for approximately 2 hours to minimize degradation prior to preparation work and testing.[34] During preparation stages the specimens were kept moist with copious amounts of physiologic (0.9%) saline to prevent tissue degradation.[67] At the completion of preparation work and testing the specimens were wrapped in moist towels, sealed in plastic bags, and refrozen at – 20° C. It has been demonstrated that freezing, even for extended periods of time (up to a year or more), doesn't have a significant overall effect on the behavior fresh frozen cadaveric spinal tissues.[67, 94] Additionally, it has been

suggested that thawing and refreezing, does not produce significant changes in the mechanics, however, this was only examined for trabecular bone specimens.[41]

6.2.2 Potting

One of the most important components of this type of biomechanical testing is ensuring that the specimen can be held rigidly and with geometric consistency during testing. To facilitate solid purchase by test fixtures the inferior and superior vertebrae in each 2 FSU segment were "potted." Potting essentially encases the superior and inferior vertebrae in a material that is much more rigid than the specimen itself, thus allowing the specimen to be rigidly coupled to the available test fixtures. The potting material used in these experiments was Polymethylmethacrylate (Jet Acrylic – Lang Dental, Wheeler, IL).

Prior to beginning the potting procedure each 2-FSU segment was subjected to a lateral radiograph in its normal (post-mortem) lordotic configuration. The lateral radiograph was used to establish the potting geometry and depth of potting. Using the lateral radiograph a tracing was made of the specimen's midsagittal profile (Figure 12A). Subsequently, a line was drawn between the inferior vertebral body's anteroinferior tip and the inferior tip of the inferior vertebra's spinous process (Figure 12B). This line was designated to represent the inferior-most plane of the specimen and was defined as horizontal. A parallel line was drawn through the superior-most point of the superior vertebra (Figure 12C). This line was considered to be the superior-most plane of the specimen. Two more parallel lines were drawn, one below the superior-most line, and one above the inferiormost line (Figure 12D). The perpendicular distance between the pair of lines for the superior vertebra (Ds) was defined as the potting depth necessary to encase it. Similarly, the pair of lines for the inferior vertebra (Di) defined the potting depth necessary to encase it. The potting depths were established to ensure that the potting compound would hold the specimen rigidly without interfering with either of the two intervertebral joints in the segment.

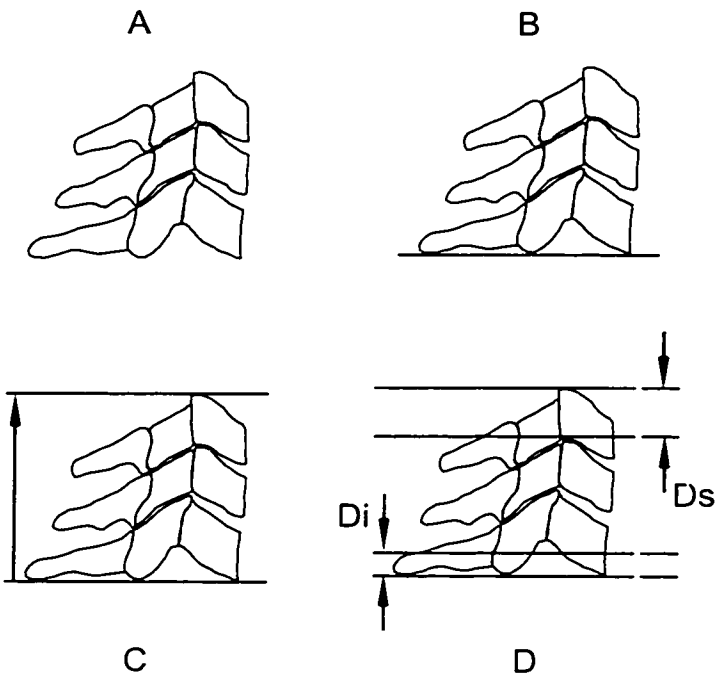

Figure 12:: Schematic representation of the method used to determine the depth of potting needed to encase the superior and inferior vertebra. First a tracing from a lateral radiograph is made (A). Then the horizontal plane was defined (B). Next a line parallel to the horizontal was drawn through the superior most aspect of the superior vertebra (C). Finally, two more lines parallel to the horizontal were generated at levels consistent with the depth of potting required to encase the superior and inferior vertebra without interfering with joint motion (D). The distances Ds and Di represent the potting depths for the superior and inferior vertebrae, respectively.

To help ensure that good purchase would be made between the potting material and the specimen, 0.75 mm diameter 304 stainless steel wires were used. The wires were inserted into the vertebral body, articular pillars, and spinous processes of the superior and inferior vertebra. In addition, a single wire was wrapped around each pedicle of both the superior and inferior vertebrae. Functionally, these wires provided a direct connection between the specimen and the PMMA potting compound, ensuring that loads transferred to the potting molds would be efficiently transferred to the specimen.

Standard potting molds were used for each specimen. These molds were made from 3" ID X 3.5" OD PVC tubing that can be obtained from the plumbing supply section of any hardware store. The tubing was cut into 3/4" (19 mm) long sections.

A custom built potting stand was used to hold the potting cups in place. This potting stand was configured such that the inferior vertebra could be potted first. Once the inferior vertebra was potted, the stand could be reconfigured to invert the specimen and allow for potting of the superior vertebra.

The potting procedure began with placing the mold in the potting mold receptacle on the stand. Then the stand was leveled using a bubble level. Standoff blocks were placed in the bottom of the mold receptacle. These standoff blocks were made to take up the difference between the depth of compound required to encase the vertebra and the overall depth of the potting mold (3/4"). Generally two blocks were used for potting the inferior vertebra. One block went underneath the anteroinferior tip of the vertebral body and the other block went underneath the posteroinferior tip of the spinous process.

Before inserting the inferior vertebra into the potting mold a section of flexible tubing was placed into the spinal canal. The tubing was sized to fill up the total available area of the spinal canal and extend a short distance beyond the superior and inferior ends of the specimen. This tubing was used to prevent the potting material from flowing into and obstructing the spinal canal.

The inferior vertebra was placed into the potting mold with the spinal canal centered over a slightly off-center 3/4" hole (Appendix A drawing 015-A) in the potting mold receptacle. The hole allowed the tubing in the canal to pass through the bottom of the receptacle, which also provided a way to seal off the potting mold to prevent leakage of the potting material. Once the inferior vertebra was resting on the standoff blocks and the potting mold was sealed to prevent leakage. Fourteen small holes were drilled near the top of the potting mold. The ends of the stainless steel wires that had been inserted into the inferior vertebra were threaded through these holes and pulled tight. The wires were configured in this manner to give the potting material better purchase to the specimen.

The potting mold was filled with potting material until the potting material was even with the top of the mold. A cure time of approximately 15 minutes was allowed before proceeding with potting the superior vertebra.

After sufficient time had been allowed for curing of the inferior potting the specimen was removed from the potting stand. The stand was then reconfigured to hold the specimen inverted by the cured inferior potting. A second potting mold was placed into the mold receptacle to pot the inferior vertebra. The same procedure used to pot the inferior vertebra was then repeated for the superior vertebra. Once sufficient time had been allowed for adequate hardening of the potting material, adjacent stainless steel wires were twisted together, trimmed, and crimped. The transition from a freshly harvested 2 FSU segment to a potted and ready for testing 2 FSU segment is shown in Figure 13.

Figure 13: Photograph showing the primary stages of specimens preparation. On the left is a freshly harvested 2 FSU segment. In the middle is a 2 FSU segment with the superior and inferior vertebra wired in preparation for potting. On the right is the end product of the potting procedure.

6.3 Experimental Equipment and Instrumentation

6.3.1 Loading Frame

A custom-manufactured high-rate 15,000 N capacity servohydraulic test frame was used to generate the compressive loading required for this project (Figure 14). The test frame was manufactured by MTS (MTS Systems Corporation, Eden Prairie, MN) and given the

custom model number 318.10S. The frame was based on an MTS 810 single-axis test frame with the hydraulic ram mounted in the crosshead. To achieve high stroke rates the ram was outfitted with a 10 gallon accumulator pack, a high-rate manifold, and a high-rate servo-valve. The unit was digitally controlled using TestStar™ II software and hardware (MTS Systems Corporation, Eden Prairie, MN). In closed-loop operation the frame was capable of achieving stroke rates of approximately 3 m/s. Operating in open-loop mode the frame was capable of achieving stroke rates on the order of 10m/s.

The displacement of the hydraulic ram was monitored using a linear variable differential transformer or LVDT (model 244.11 LVDT, S/N 1028919, MTS, Eden Prairie, MN), which was built into the crosshead of the frame. The LVDT was supplied with the loading frame and came pre-calibrated based on a National Institute for Standards and Technology traceable standard (Part # 115682-01A).

6.3.2 Loading Fixtures

To transmit the loads developed by the test frame to a test specimen custom loading fixtures were designed in house and manufactured by Limited Productions Inc., Bellevue, WA. These fixtures were designed to: hold the specimen rigidly during load application, prevent axial rotation, provide the ability to position the specimen for load application, and allow for application of either compression, compression-flexion, or compression-extension loading. The entire loading fixture assembly, including the loading frame described above, and six-axis load cell described below, is shown in Figure 14. Additionally, the individual design drawings for the fixture components can be found in Appendix A.

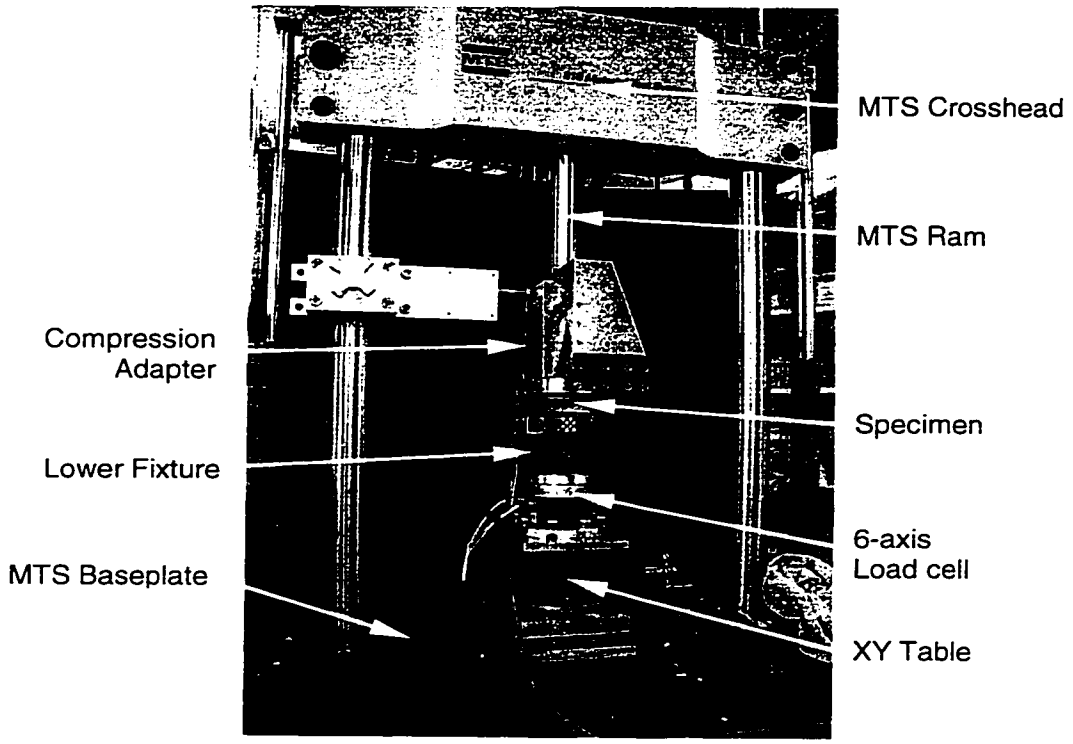

Figure 14: Overall view of loading fixture configuration and componentry. TShis picture shows a representative configuration used to test the specimens assigned to the compression group.

6.3.3 Six-Axis Load Cell

A custom-designed six-axis load cell was used to monitor the loads transmitted through a specimen during testing (Model 4526, Robert A. Denton, Inc., Rochester Hills, MI). The design of this load cell is based on the design of the six axis load cells used to measure neck loads in Hybrid III crash test dummies. The basic design has been proven to have more than adequate dynamic fidelity in years of use in automotive crash testing. Thus, the load cell design was deemed to be more than adequate for the purposes of the testing in this project.

The load cell used here had the following measurement capacities: F_x – ± 4,448 N, F_y – ± 4,448 N, F_z – ± 11,120 N, M_x – ± 338.9 N-m, M_y – ± 338.9 N-m, and M_z – ± 203.4 N-m. Prior to testing, the load cell was calibrated by the manufacturer. The calibration was traceable to the National Institute of Standards and Technology under the Morehouse

Instrument Company Report number F538145KJ2799. According to the calibration the total uncertainty for any channel at maximum capacity was 0.02% (F_x – 0.9 N, F_y – 0.9N, F_z – 2.2 N, M_x – 0.07 N-m, M_y, 0.07 N-m, and M_z – 0.04 N-m).

In designing the loading fixtures described above, the load cell was included as an integral part of the overall structure. The load cell's position in the loading apparatus is shown in Figure 14.

6.3.4 Spinal Canal Occlusion Transducer

In terms of instrumentation the most important component of the experimental setup was the Spinal Canal Occlusion Transducer (SCOT). The primary function of this device, as its name implies, is to measure occlusion or narrowing of the spinal canal. Moreover, it affords the capability of measuring canal occlusion dynamically, making it invaluable for this study. The SCOT was researched, developed, and characterized in house. Its operational characteristics are well understood and have been thoroughly described elsewhere.[74]

Even though the design and operational characteristics of the transducer have been previously described a brief technical introduction is warranted here. In general the transducer operates based on the first principle of electronics...Ohm's Law (V = IR). For this study the transducer was constructed from compliant (durometer 35 +/- 5) 9.5 mm ID × 0.79 mm Wall × 150 mm long natural rubber tubing (Primeline Industries, Akron, OH) and filled with physiologic saline. Six wire electrodes pierce the tubing with regular separations between individual electrodes of 20 mm (Figure 15). This electrode spacing approximates the distance from the centerline of one intervertebral disc to the centerline of an adjacent intervertebral disc in the spinal canal, or roughly one third of a the canal length for a 2 FSU segment, in a normal healthy cervical spine. The electrodes at the far ends of the tube are used as source and sink electrodes. The intervening electrodes are designated to serve as sensing electrodes.

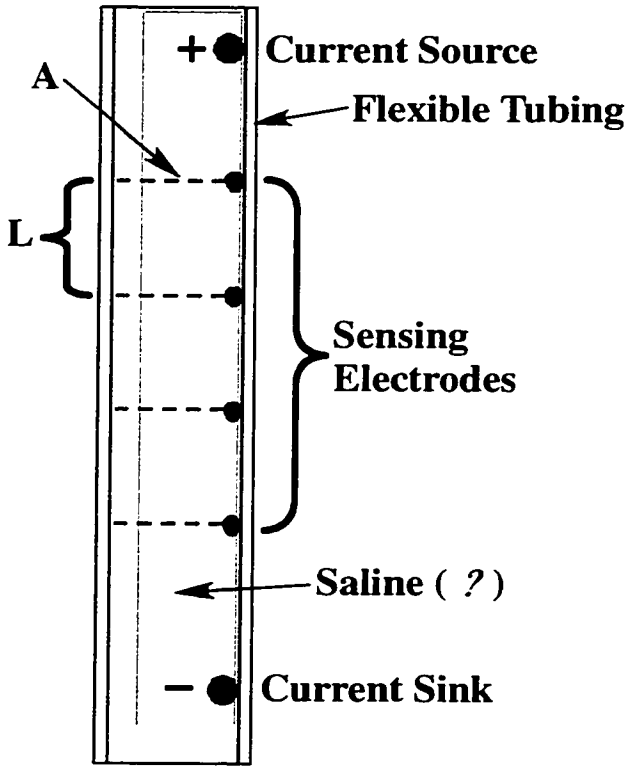

Figure 15: Schematic diagram of spinal canal occlusion transducer.

During operation a 2 kHz constant-amplitude alternating current is input at the source electrode and travels, with constant current density, to the sink electrode. When a section of tubing between two electrodes is occluded (narrowed) the result is a reduced cross-sectional area of the conducting media. According to the fundamental equation for resistance in a continuous conducting media (Equation 1) a reduction in cross-sectional area results in an increase in resistance for a resistor of constant length. Combining this with Ohm's Law demonstrates that a reduction in cross-sectional area leads to an increase in voltage, if the current remains constant. Thus, the output from the SCOT takes on the form of an amplitude modulated 2 kHz alternating voltage.

$$R = \rho \cdot \frac{L}{A} \qquad \text{Equation 1}$$

At present there isn't a way to relate a change in cross-sectional area to neurologic injury potential. Current spinal cord injury mechanics studies use a reduction in MSD as the

correlate to neurologic injury.[6, 38] Thus, the output of the SCOT needs to be converted so that it measures a displacement that can be related to a change in MSD. Realizing that the cross-sectional area of the SCOT is a function of its diameter provides a way to use the SCOT to measure displacement. Equation 1 can be rewritten such that resistance becomes a function of the SCOT's diameter (D). With this new equation a change in diameter effects a change in resistance, thereby resulting in a change in output voltage. In this case a reduction in D, produced by compressing the tube, results in a reduction in cross-sectional area, which leads to an increase in the amplitude of the output signal.

$$R = \rho \cdot \frac{L}{f(D)} \qquad \text{Equation 2}$$

Investigations have been conducted to understand the measurement error experienced during both static and dynamic usage of the SCOT.[59, 74] These studies suggest that under normal operating conditions the maximum measurement error is less than or equal to 5% of Full Scale Output (FSO). That equates to an error in the measured tubing diameter of less than 0.5 mm at maximum tubing occlusion.

Under dynamic operating conditions the SCOT has been found to faithfully follow occlusion inputs with rise times as short as 1 msec.[58, 74] An examination of the biomechanical literature suggests that a rise time of 2 msec is the shortest that might be expected in a study such as this. Thus, the SCOT possesses adequate dynamic range to monitor canal occlusions in this study.

6.3.5 High-Speed Video

For this study high-speed video was used to provide visual feedback on the responses of individual specimens to the loads imposed on them. The high-speed video camera used here was the Kodak Ektapro RO-1000 (Eastman Kodak Company, Motion Analysis Systems Division, San Diego, CA). The camera provided the capability to record an experiment at 1000 frames-per-second in 24-bit color with a resolution of 512 X 384.

Thus, the camera provided more than adequate visual monitoring capabilities for this study.

6.3.6 Data Acquisition

Two personal computers were used to acquire data during testing. These computers were virtually identical in their configurations. Both computers were manufactured by Gateway™ and had the same model number (E-5200, Gateway™, Sioux Falls, ND). One, designated by the name MTS-High, had a 500 MHz Pentium® III processor and 256 MB of RAM, while the other one, designated by the name MTS-Low, had a 600 MHz Pentium® III processor and 256 MB of RAM. Both machines were equipped with high-speed data acquisition boards (PCI-6071E, National Instruments™, Austin, TX). Data acquisition on each machine was controlled by custom designed LabVIEW™ virtual instruments (VIs) (LabVIEW™, National Instruments™, Austin, TX). A schematic diagram of the data acquisition setup is shown in Figure 16.

The MTS-High machine was configured to acquire loads from the six-axis load cell and ram displacement via the crosshead LVDT. This machine was also responsible for communicating software commands to the loading frame's digital controller, and operating the high-speed video camera (Figure 16).

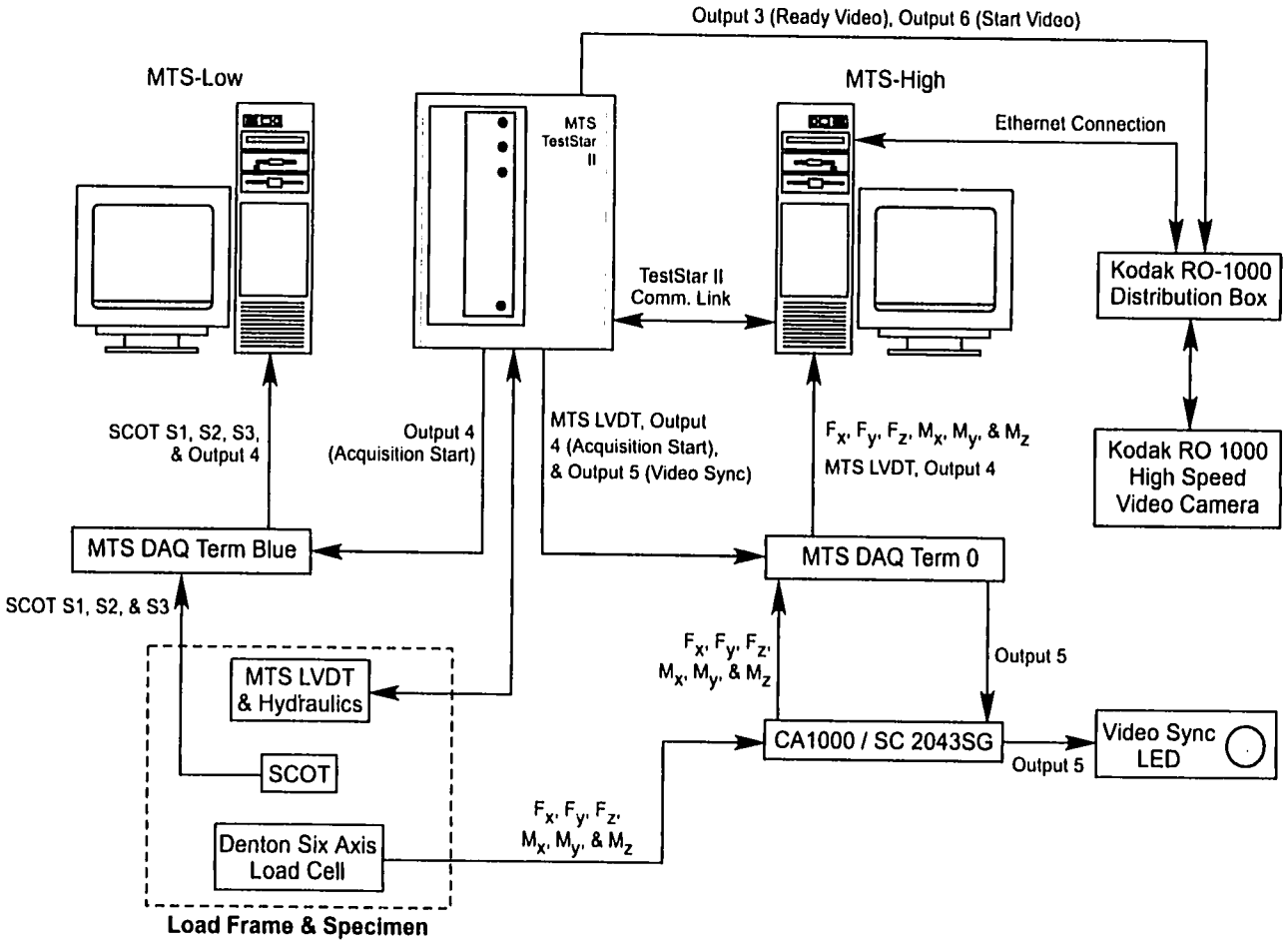

Figure 16: Schematic diagram of the data acquisition and experiment control configuration used for this project.

Prior to being sampled with MTS-High, the six-axis load cell's output was conditioned by an eight-channel strain gauge conditioner (SC-2043-SG, National Instruments™, Austin, TX). This conditioning unit provided sufficient gain to the load cell outputs for acquisition. The conditioner was also equipped with a single-pole low-pass 1.6 kHz buffered RC anti-aliasing filter. This anti-aliasing filter meets the SAE J211-1 recommended practice for a channel frequency class (CFC) 1000 filter.

The MTS-Low machine was dedicated to acquiring only SCOT data. All of the necessary signal conditioning for the SCOT was accomplished by custom-designed dedicated electronics. Therefore, no additional signal conditioning was necessary.

The sampling rate used in this study was 40 kHz for a duration of 1 second. Both data acquisition machines were triggered using a common TTL signal produced by the MTS load frame's digital controller. The individual acquisition processes on both machines were found to initiate within one sample (0.000025 sec) of each other using this method.

6.4 Experimental Protocol

Before testing, each specimen was thawed in room temperature water for approximately 2 hours, consistent with the protocol suggested by Kaigle et al.[34] All experimentation was conducted at a room temperature of about 21 to 24° C (70 to 75° F). Although human tissue normally operates at a temperature of 37° C (98.6° F), it has been demonstrated that *in-vitro* testing of fresh-frozen cervical spine specimens at room temperature is not significantly different from testing at body temperature.[46] Again, all specimens were bathed with physiologic saline on a regular basis to maintain proper hydration. If the specimen had to be out for a prolonged period before the commencement of testing it was bathed in saline and wrapped in damp towels to maintain hydration.

6.4.1 Geometric Measurements

Several measurements were made to provide intact spinal canal MSDs for later use in data reduction. These canal MSD measurements were made at the levels of the superior, central, and inferior vertebrae. Prior to taking these measurements lateral radiographs were produced for each specimen with a stainless-steel hose clamp attached to the inferior potting such that the bottom edge of the clamp was coplanar with the bottom surface of the potting. The hose clamp was used as a scaling phantom for the radiographs, providing a known length at the level of the specimen's midsagittal plane. After completing the radiograph it was scanned for computer analysis.

Using ImageJ (Freeware programmed by Wayne Rasband, Research Services Branch, National Institute of Mental Health, Bethesda, Maryland) three MSD measurements were made at each vertebral level (image resolution on average was 0.05 mm/pixel ± 0.0002 mm/pixel). Each measurement was made between the posterior aspect of the vertebral body and the spinolaminar line along a line parallel to the bottom surface of the inferior potting, which was the assumed horizontal plane for each specimen. The three MSD measurements were then averaged to provide a single value for the MSD of each vertebral level. The average MSDs and standard deviations for each specimen are provided in Table 1.

Table 1: Tabulation of mean midsagittal diameter (MSD) measurements made for each specimen.

		Superior Vertebra		Middle Vertebra		Inferior Vertebra	
Group	Spec #	Mean [mm]	Std Dev [mm]	Mean [mm]	Std Dev [mm]	Mean [mm]	Std Dev [mm]
Compression	2	14.0	0.16	13.8	0.18	13.4	0.39
	10	13.0	0.68	13.9	0.15	14.4	0.43
	12	15.1	0.39	14.7	0.12	14.8	0.13
	23	16.0	0.06	16.2	0.25	15.0	0.39
	28	12.9	0.35	13.0	0.25	12.9	0.12
	40	15.4	0.27	14.9	0.17	15.1	0.31
	44	16.6	0.28	16.2	0.47	16.4	0.04
	46	15.0	0.09	14.9	0.09	13.0	0.08
Comp-Flexion	3	12.9	0.04	12.7	0.24	12.2	0.13
	5	13.7	0.35	12.9	0.07	14.0	0.33
	7	14.8	0.08	13.8	0.16	14.8	0.12
	8	13.3	0.10	13.3	0.16	13.4	0.10
	15	15.6	0.32	15.8	0.52	15.5	0.16
	17	13.5	0.13	13.0	0.19	13.2	0.18
	27	12.6	0.35	12.2	0.04	12.7	0.07
	48	14.2	0.52	13.9	0.00	14.5	0.52
Comp-Extension	14	11.5	0.11	12.2	0.36	12.3	0.08
	29	16.5	0.64	12.8	1.32	11.2	0.15
	39	11.1	0.51	12.6	0.11	11.6	0.05
	41	13.6	0.49	13.8	0.46	15.3	0.39
	43	12.2	0.82	14.6	0.86	16.4	0.35
	45	14.4	0.38	14.3	0.27	15.6	0.14
	47	14.4	0.57	13.4	0.19	15.9	0.36
	49	15.3	0.52	14.7	0.58	14.7	0.58

Utilizing the same lateral radiograph used for measurement of MSD the location of the inferior intervertebral disc's centroid was determined for each specimen. Horizontal and vertical measurements to the disc centroid were made relative to the center of the inferior potting's bottom surface. Again, the inferior potting's bottom surface was treated as the horizontal plane for the specimen.

6.4.2 SCOT Calibration

The SCOT was subjected to a complete calibration immediately before each test. The calibration was carried out in a custom built calibration jig (Figure 17) equipped with a linear variable differential transformer (LVDT) (model 1000-DCD, s/n 5077, Schaevitz Engineering, Pennsauken, NJ). A 10 mm X 10 mm block occluder was attached to the LVDT core and used to displace the transducer tubing during calibration. The backplane

was designed to represent the shape of the posterior portion of a typical cervical spine's canal.

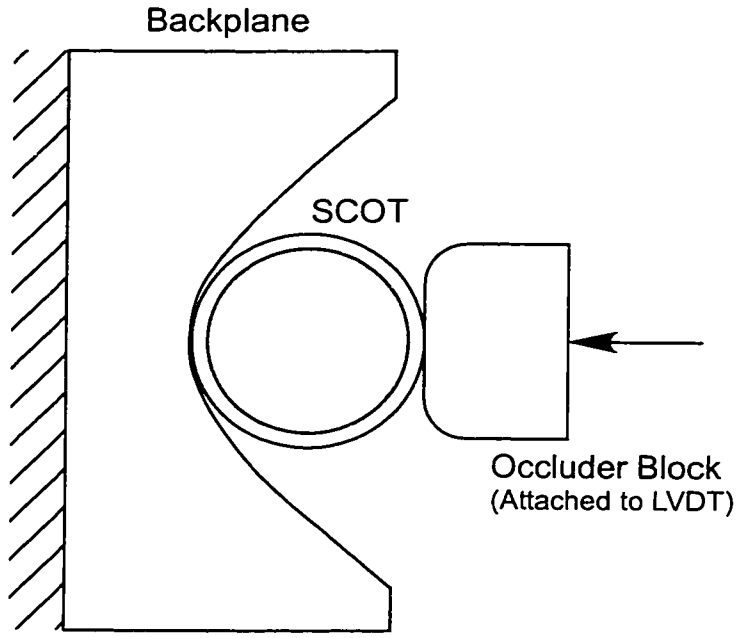

Figure 17: Schematic of custom jig used to calibrate the SCOT.

The transducer was placed up against the backplane and oriented with its longitudinal centerline directly in the "midsagittal" plane of the backplane. Subsequently, the transducer was shifted vertically so that the centerline of the occluder block would split the difference between the sensing electrodes of the desired sensing section. The occluder block was brought into contact with the transducer to establish the calibration zero point. Then the occluder block was slowly driven posteriorly until it came in contact with the backplane. A custom designed LabVIEW™ VI monitored the output of each sensing section and the displacement of the occluder as measured by the LVDT. The resulting curve of transducer output (V) versus displacement (mm) is shown in Figure 18. This calibration curve was used to generate a calibration lookup table for later use during the analysis of the SCOT data.

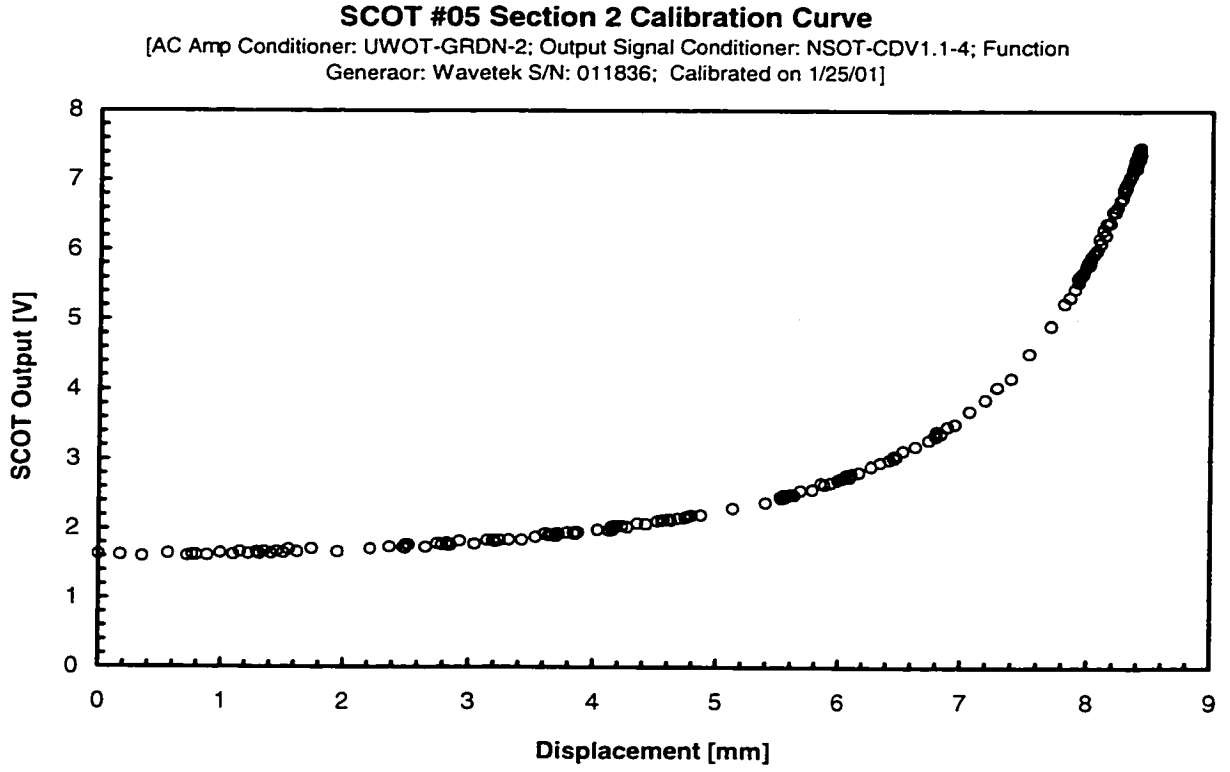

Figure 18: Typical SCOT calibration curve demonstrating the relationship between tubing deformation and transducer output.

6.4.3 Test Configuration

Just prior to a test the thawed specimen received the calibrated SCOT. With the SCOT in place the specimen was rigidly mounted to the loading frame by its inferior potting mold. The interface between the specimen's upper potting mold and the MTS ram was dictated by the desired injury mechanism.

6.4.3.1 Compressive Injury Mechanism Configuration

It is generally accepted that the compression injury mechanism is produced when the eccentricity is smaller than the distance from the centroid of the disc to the anterior and posterior boundaries of the vertebral body. Therefore, the objective of the loading scheme for producing the compressive injury mechanism was to keep the axial force within the boundaries of the vertebral body up to the point of failure. Two previous

studies demonstrated that a loading scheme where the ends of the specimen were fixed to prevent rotation and anterior/posterior translation (fixed-fixed end condition) might provide the kind of control over eccentricity necessary to meet this objective.[56, 72] Thus, a fixed-fixed end condition loading scheme was developed.

Preliminary nondestructive testing using the fixed-fixed scheme demonstrated that the axial load vector tended to remain in the area between the PLL and the centroid of the inferior intervertebral disc. Thus, the fixed-fixed end condition was considered to be the best way to produce the compression injury mechanism.

To produce a fixed end condition at the superior potting mold a custom compression fixture was used. The compression fixture was designed to accept the cylindrical upper potting mold, provide a flat mating surface for applying compression, prevent the specimen from rotating, and prevent the potting mold from shifting in the horizontal plane during compression.

In preparation for testing the custom compression fixture, which was attached directly to the ram of the MTS load frame, was brought into proximity of the upper potting mold (Figure 19A). With the attachment fixture in proximity the XY-table was used to adjust the position of the specimen to properly align the upper potting mold for coupling (Figure 19A). Once the specimen was ready to be coupled the MTS ram was slowly moved downward until the top surface of the upper potting mold was fully engaged with the compression fixture.

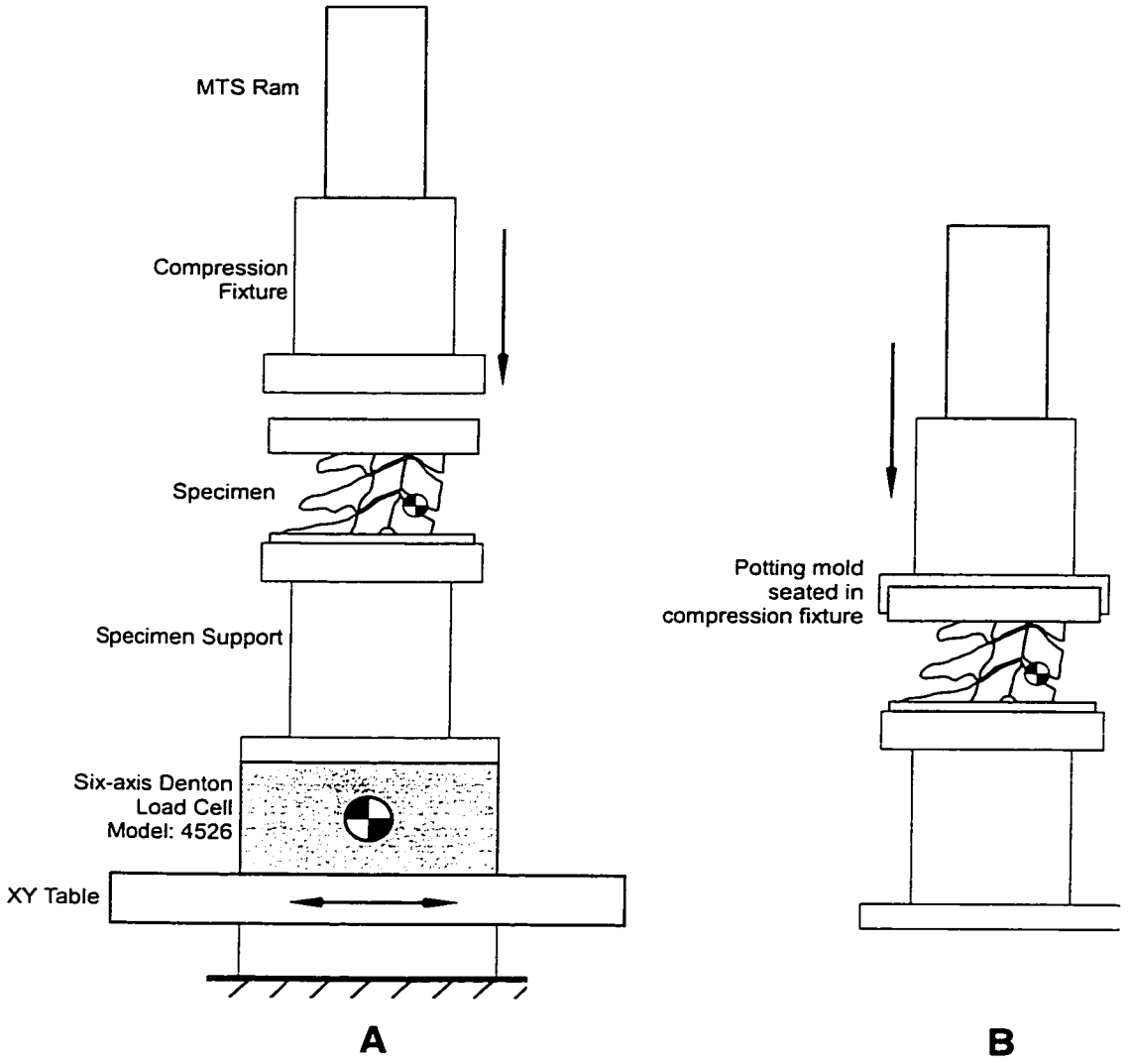

Figure 19: Schematic of the process conducted to prepare a specimen for a compression test. Initially, the compression fixture is brought into proximity with the upper potting mold of the specimen followed by adjustment of the specimens position using the XY-table (A). Once the specimen is ready to be coupled to the compression fixture the compression fixture is moved downward until the specimen's superior potting mold seats into the compression fixture (B).

6.4.3.2 Compression-Flexion and Compression-Extension Configuration

The objective of the configurations for generating the compression-flexion and compression-extension injury mechanisms was to move the axial load vector in the midsagittal plane beyond the boundaries of the vertebral body. The concept of moving

the axial load vector outside the boundaries of the vertebral body to create compression-flexion and compression-extension injury mechanisms is consistent with the current thought regarding these injury mechanisms.[52, 92, 93] For the compression-flexion group the axial load vector was required to be anterior to the anterior aspect of the vertebral body at the point of failure. Similarly, the axial load vector was required to be posterior to the posterior aspect of the vertebral body at the point of failure for the compression-extension group. To accomplish the objective a fixed-free loading scheme was developed. In this scheme the specimen's inferior potting mold was fixed, while the superior potting mold was allowed to translate and rotate in the midsagittal plane.

A custom-built bending fixture was attached to the superior potting mold to produce the free end condition. The bending fixture was equipped with a set of two idler-roller bearings (CAMROL CCF-1-S, McGill MFG CO Inc., Valparaiso, IN), each having a 2,225 lbf dynamic capacity. The design of this bending fixture placed the roller bearings on the left and right sides of the specimen, equidistant from the midsagittal plane, such that their roll axes were approximately at the level of the centroid of the specimen's middle vertebral body and oriented perpendicular to the midsagittal plane. In addition, the bending fixture provided for anterior/posterior adjustment of the bearing centerlines with respect to the centroid of the specimen's inferior intervertebral disc (Figure 20).

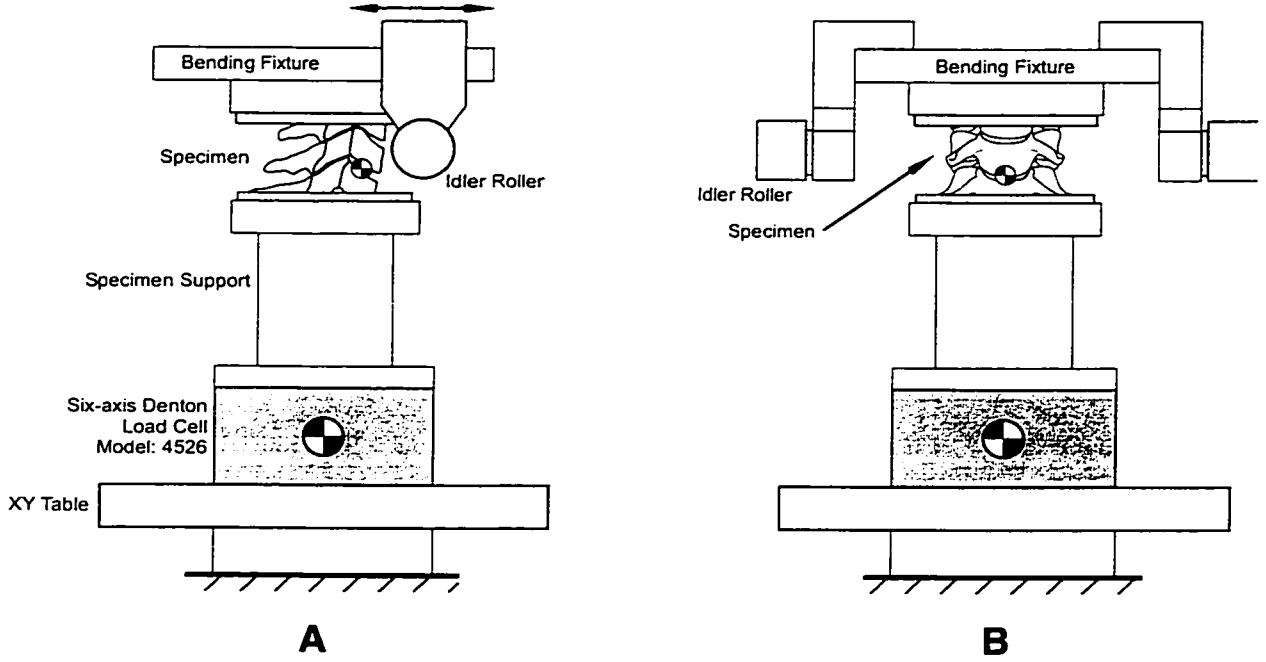

Figure 20: Schematic showing the attachment of the bending fixture to the specimen from a right lateral (A) and an anterior viewpoint (B). This schematic also demonstrates how the bending fixture allows for anterior/posterior adjustment of the idler rollers.

An aluminum yoke with heat treated 440C stainless runners (Appendix A Drawings 019-A & 024-A) was used as the interface between the MTS ram and the bearings attached to the bending fixture. Using this yoke, downward motion of the MTS ram was transferred into the bending fixture through the idler rollers. Shifting the idler-rollers anteriorly or posteriorly with respect to the disc centroid produced an "initial eccentricity" (e_i), which provided a mechanism to convert the downward motion of the ram into compression-flexion or compression-extension loading environments, respectively. The schematic shown in Figure 21 depicts the configuration used to produce compression-flexion. Configuring the system to produce compression-extension is easily accomplished by simply moving the idler rollers posteriorly on the bending fixture such that they are behind the centroid of the inferior disc.

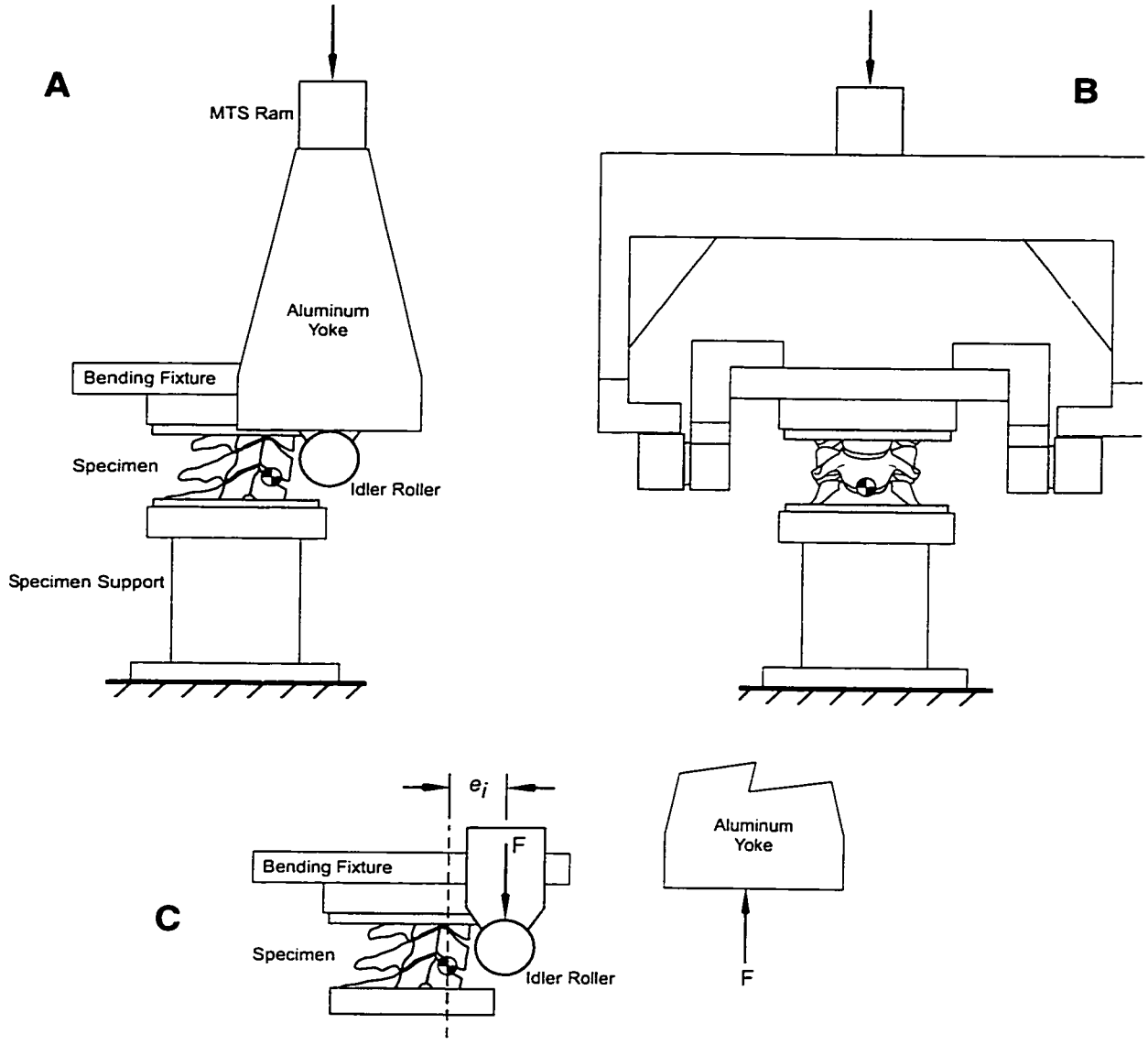

Figure 21: Schematic representation of the interface between the MTS ram and the specimen used to generate compression-flexion loading in a specimen. The schematic shows the configuration from the right lateral perspective (A) and the anterior perspective (B). Additionally, the schematic depicts the initial eccentricity (e_i) between the point of load application and the centroid of the intervertebral disc used to produce compression-flexion (C). The system can easily be reconfigured to produce compression-extension by shifting the idler rollers posteriorly on the bending fixture such that they are a distance e_i behind the centroid

The primary issue in creating the compression-flexion and compression-extension injury mechanisms was defining the initial eccentricity needed to generate them. McElhaney et al. [46] suggested that compression-flexion and compression-extension injury mechanisms

could be produced in whole cervical spines using initial eccentricities of 1 cm forward or rearward, respectively. That places the load vector just beyond the edges of the vertebral body if the vertebral body is assumed to have a MSD of between 16 and 19 mm.[64]

To ensure that compression-flexion and compression-extension were created in this study it was decided to apply axial load beyond the 1 cm suggested by McElhaney et al.[46] For the compression-flexion specimens the idler rollers were placed forward of the inferior disc centroid by an initial eccentricity equivalent to the anterior/posterior depth of the middle vertebral body. Likewise, the bearing centerlines were placed behind the centroid of the inferior intervertebral disc by the same amount for the compression-extension specimens. Using the anterior/posterior depth of the vertebral body normalized the load application point to the size of the specimen, which was intended to eliminate inconsistencies in the results arising from size variations within the specimen pool.

One preliminary experiment was conducted for each mechanism group to confirm that the configurations would work. The preliminary experiments demonstrated that the axial load vector was anterior to the anterior aspect of the vertebral body for compression-flexion and posterior to the posterior aspect of the vertebral body for compression-extension.

6.4.4 Test Execution

With the specimen installed in the loading frame and all of the instrumentation connected, the last step was the application of load using the MTS load frame's hydraulic ram. For this testing it was decided early on to use a displacement control methodology to apply load to the test specimens. This decision was made knowing that the MTS load frame provided excellent closed loop displacement control at velocities up to 3 m/s. The axial displacement profile used was created to produce peak displacements of between 4 and 20 mm, have a velocity profile consistent with a Haversine pulse, and have a 16 msec

pulse-width. The balance of this section will describe how this particular loading profile was derived for use in this study.

In developing the loading profile for this testing the author first turned to previous 2 FSU experiments. There are several experiments that have been conducted on 2 FSU segments of the cervical spine.[22, 63, 65, 72, 82, 83, 95, 102] These studies were either conducted quasistatically in servohydraulic testing frames [22, 72, 82, 95] or dynamically using a dropweight-style methodology.[63, 65, 83, 102] Yingling et al. [95] provided information on displacement at failure, but the test specimens were porcine, which raises questions regarding applicability to human cadaver testing. The dropweight-style studies [63, 65, 83, 102] provided impact velocity data; however, the velocities were well beyond the capability of the MTS frame (> 3 m/s) and they didn't measure displacement. Additionally, these studies were conducted on porcine specimens, again raising questions regarding applicability to human cadaver testing.

Of the eight 2 FSU studies only the studies of Crowell et al.[22] and Shea et al.[82] provided useful data for developing a loading profile for this testing. They used a specially designed servohydraulic planar testing apparatus (PTA) to apply combined axial displacement and flexion rotation to 2 FSU human cervical spines quasistatically. Their PTA results indicate that on average 2 FSU human cervical segments fail at an axial displacement of 4.7 ± 1.6 mm combined with 25.8 ± 3.4 degrees of flexion rotation. Unfortunately, their experiments were conducted quasistatically and didn't provide any information relevant to setting velocities for this research.

There are several studies concerning axial compressive loading of the entire human cervical spine that provide velocity information for developing the loading profile used in this study.[2, 31, 46, 47, 53, 61, 68, 98, 100, 101] All of these studies were conducted dynamically at velocities ranging from 0.45 m/s up to 11 m/s. This range of velocities is far too broad to be useful for the testing being conducted here. Fortunately, McElhaney et al. [47] provided a velocity threshold of 3.1 m/s which is generally accepted as the axial velocity across the

whole cervical spine required to generate a neck injury. This threshold velocity was used as the basis for determining the velocities that were used in the current study.

Three of the studies just mentioned provide information regarding axial displacement at failure for whole cervical spine specimens.[46, 98, 101] From these three studies a failure displacement range of 17 to 42 mm for the whole cervical spine was suggested. This range of displacements was used as a starting point for defining the axial displacements to be used in this study.

While the whole cervical spine data mentioned above was beneficial it still wasn't directly applicable to testing 2 FSU cervical segments. What was needed was a method for converting the velocities and displacements suggested by whole cervical spine experiments into velocities and displacements compatible with 2 FSU testing. In a recent article, W. T. Edwards[24] suggested that when conducting short segment testing the displacements and velocities used should be scaled down from what is expected or observed across the whole cervical spine. His suggested methodology involved treating the whole cervical spine (C1 to T1) as a series of equivalent stiffness springs. Using this first order approximation it was possible to estimate the displacement and velocity across a 2 FSU cervical segment by multiplying the total displacement by 2/7 (# of FSU's in short segment of interest/# of FSU's in total cervical spine). Thus, the threshold velocity suggested by McElhaney et al. [47] is converted to 0.89 m/s. And, the failure displacement range of 17 to 42 mm is reduced to a range of 4.9 to 12 mm. The lower end of this displacement range is consistent with the axial displacements at failure reported by Crowell et al.[22] and Shea et al.[82] for 2 FSU testing.

The establishment of velocities and displacements for 2 FSU testing was very helpful, however, it was still necessary to determine an appropriate displacement profile to use as a control template for the MTS. To define a reasonable profile a previously validated rigid body dynamic model of the human head and cervical spine was examined.[14-16] The model was based on, and validated with, experimental data produced in drop tests where

human cadaver head/neck/torso specimens were dropped on or near the vertex of the head with impact velocities of roughly 3.2 m/s.[53-55, 57] The output files from the model were graciously provided by its developer, Daniel Camacho.

A thorough examination of the axial displacements, velocities, and accelerations from 2 FSU segments of the model revealed that a Haversine velocity pulse was the most appropriate basis for generating a displacement profile for control the MTS ram. The graph shown in Figure 22 demonstrates how close the Haversine velocity pulse comes to approximating the relative velocity across the C57 segment of the model. Comparisons of displacement and accelerations are provided in Figure 23 and Figure 24.

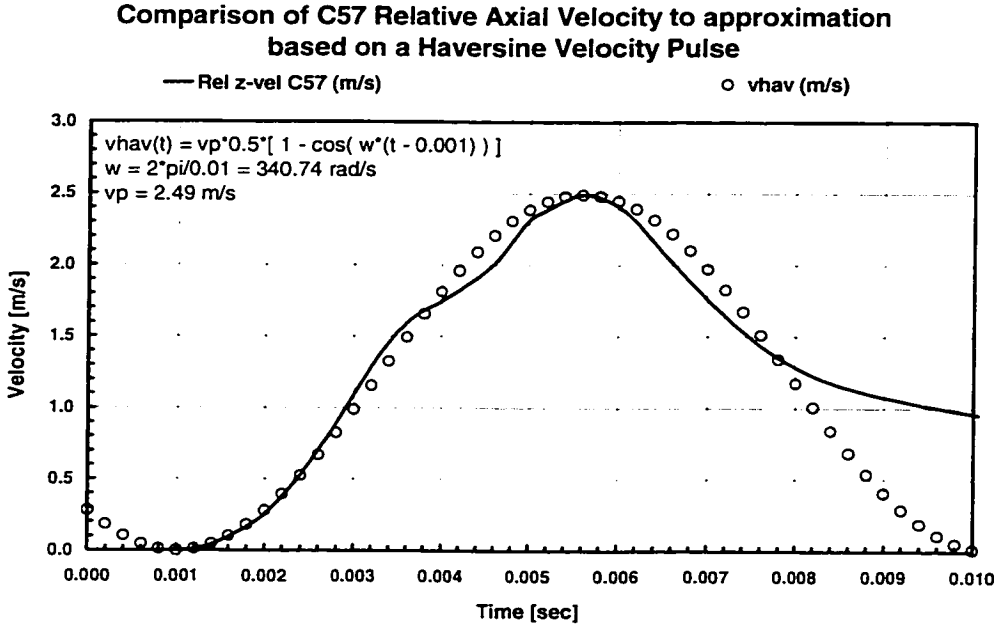

Figure 22: Comparison of the axial velocity across the C57 segment observed in the Camacho et al. model [14-16] with a Haversine velocity pulse. The equation for the Haversine velocity pulse is provided in the upper left hand corner.

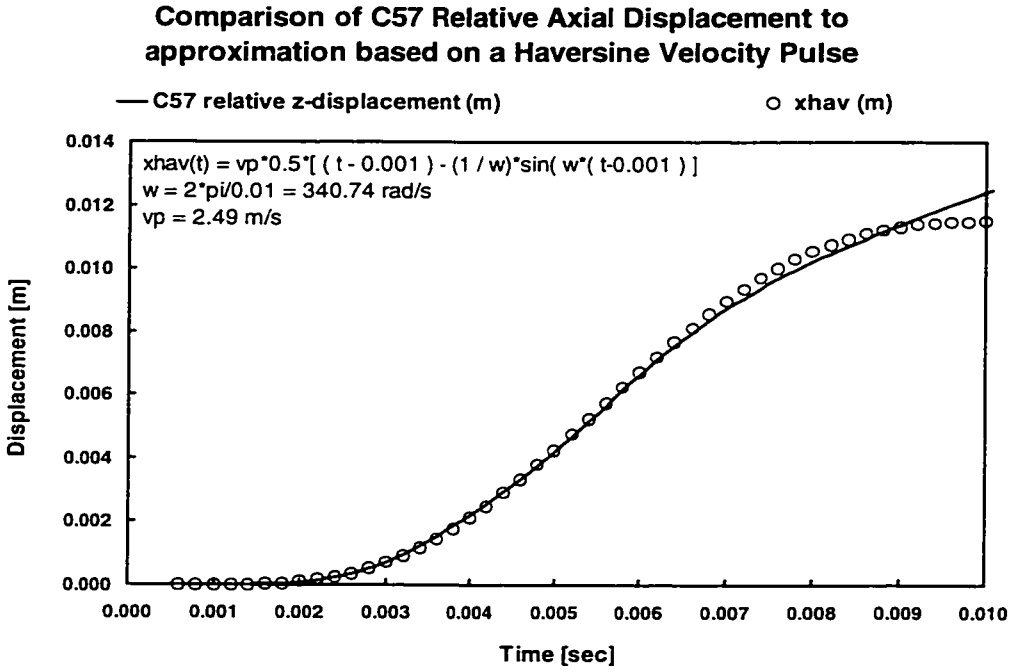

Figure 23: Comparison of the axial displacement across C57 produced by the model of Camacho et al. [14-16] with displacement derived from a Haversine velocity pulse. The displacement equation is provided in the upper left hand corner of the graph.

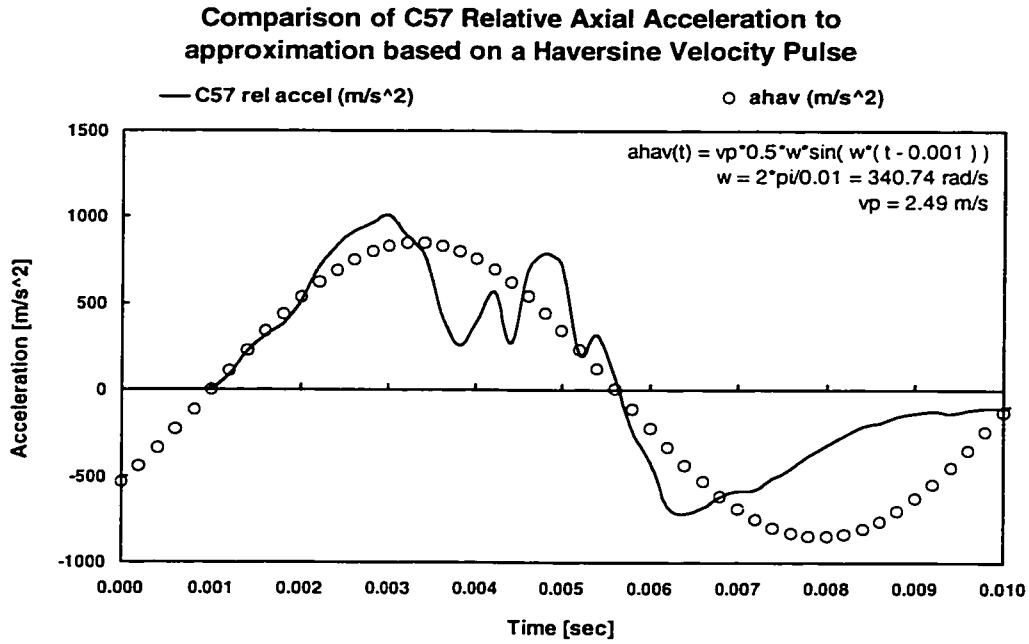

Figure 24: Comparison of axial acceleration across the C57 segment produced by the model of Camacho et al. with acceleration derived from a Haversine velocity pulse. The acceleration equation is provided in the upper right-hand corner of the graph.

Additional examination of the Camacho et al. model revealed that multiplying the overall axial velocities and displacements of the whole cervical spine by 2/7, as suggested by W. T. Edwards, to get the relative velocity across a 2-FSU segment, was not wholly accurate. In fact, the model suggests that the axial velocity across a given 2-FSU segment increases moving from C24 to C57, such that at C24 the relative axial velocity is approximately 2/7 the axial velocity across the whole cervical spine, while the relative axial velocity across C57 is approximately 2/3 the axial velocity across the whole cervical spine. A similar pattern was observed in the relationship between 2 FSU relative axial displacement and overall axial displacement of the whole cervical spine, with the low end being at 1/5 and the high end being approximately 1/2 the total axial displacement of the whole cervical spine. These further findings expanded the range of possible target velocities and displacements. Putting it into numbers the target velocity range became 0.89 to 2.1 m/s and the target displacement range became 3.4 mm to 21 mm.

Having such a broad range of potential velocities and displacements to work with meant that it would be very difficult to know just how much each specimen would require to generate a visible and clinically relevant failure. The general assumption during the development of the testing protocol was that the specimens in the compression-flexion and compression-extension groups would require more displacement to generate failure than those in the compression group. This assumption was based on the work of Nightingale et al. [56] who showed that axial stiffness decreases by a factor of 12 between a fully constrained end condition, which is consistent with the compression group in this study, and an unconstrained end condition, which is consistent with the compression-flexion and compression-extension groups in this study.

So, if the compression-flexion and compression-extension groups require more displacement is it reasonable to use the same input velocity or should the input velocity be allowed to vary based on the amount of displacement input? Nightingale et al. [56] apparently had a similar quandary and solved it using a unique time based loading scheme. Instead of keeping a constant velocity in the face of varying displacements they loaded each specimen over the same time frame. It should be noted that they were not dealing with velocities in the range being considered in this testing. However, the concept of holding the loading time frame constant appeared reasonable. Therefore, it was decided to keep the pulse-width of the input Haversine velocity profile constant, set a desired displacement in the range of 3.4 to 21 mm, and allow the velocity to vary accordingly.

Having decided to run the tests using a constant pulse-width scheme it was necessary to determine an appropriate pulse width. The search for a previous study with such information led to an article by Nightingale et al.[53] The study described in that article was used to validate the model of Camacho et al. described above. In this study time from impact to injury was reported. The time frames reported ranged from 2.2 msec to 30.5 msec with an average of 14.1 msec. Initially, it was decided to maintain a pulse

width of 14 msec. However, due to potential control problems with the MTS, a slightly pulse-width of 16 msec was used.

With all of the above information considered a displacement profile for test execution was finally decided upon. The displacement profile used was derived from a Haversine velocity pulse with a constant pulse-width of 16 msec. The desired peak axial displacement was chosen to lie between 4 and 20 mm. The computed peak velocity achieved during a given test was 2 times the peak displacement multiplied by the pulse-width. The graph provided in Figure 26 is representative of the displacement and velocity profiles used during a given test. The graph shows the loading phase (A) with its Haversine velocity pulse, the holding phase (B), and the unloading phase (C), which is based on a Haversine velocity pulse as well. Additionally, prior to imparting the displacement input a compressive preload of roughly 45 N (headweight) was applied.

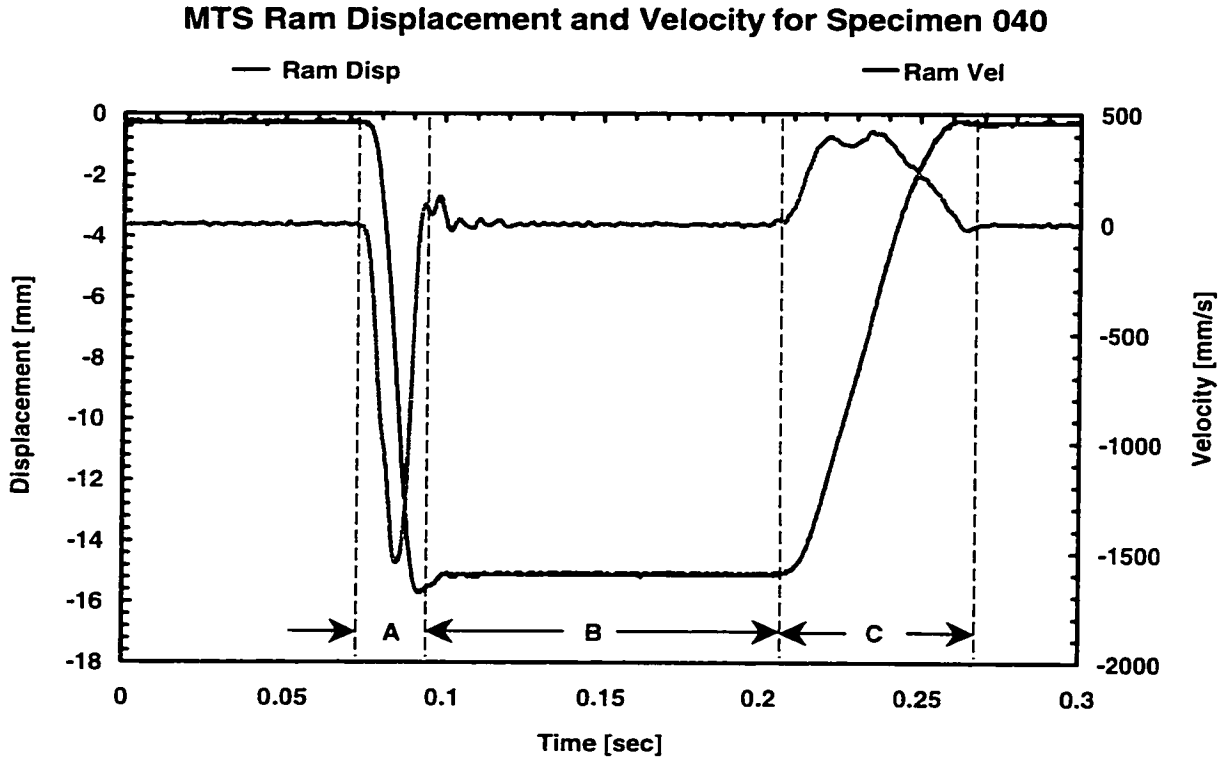

Figure 25: Dual axis plot of axial displacement and axial velocity for specimen 40, which was a member of the compression group. The graph demonstrates the entire test execution sequence, which includes a loading phase (**A**), a holding phase (**B**), and an unloading phase (**C**). Both the loading phase and unloading phases are based on Haversine velocity pulses.

6.5 Post-Experiment Protocol

6.5.1 Post-Test SCOT Readings

Before the specimen was removed from the loading frame a sequence of post-test SCOT readings were generated. First, a measurement was taken without moving or detaching anything from the specimen. This first measurement was used as the immediate post-injury measurement to be compared with the failure and peak occlusions. Second, the specimen was brought to "zero load" by moving the ram away if necessary in the compression group, or by removing the bending fixture attached to the upper potting mold for the compression-flexion and compression-extension group. Once, at "zero load" another reading of the SCOT was taken.

6.5.2 *High-Speed Video Download*

The full 1,000 frames of high-speed video stored on the high-speed video camera were viewed using an external monitor attached to the camera. After viewing the high-speed video, only the frames necessary to sync the video with the force, displacement, and SCOT data and demonstrate the complete motion of the specimen during the test were downloaded to the MTS-High machine's hard drive. The downloaded video was stored as individual frames in Kodak's proprietary Bayer format. Using Kodak's PC Color v 3.0 program the individual Bayer files (BAY) were converted into Tagged Image Format Files (TIFF) for processing into Audio Video Interlaced (AVI) video files. The AVI video files were composed using a VideoMach v 2.4.0 (Gromada.com, Copyright 2001 Zeljko Nikolic and Robert Tibljas), which provided the ability to combine the individual frames downloaded from the camera into a single digital video file.

6.5.3 *Visual Inspection*

A post-test visual inspection of each specimen was performed by the author as the first stage in establishing the injury pattern. During the visual inspections the intact/injured status of all structures that could be readily evaluated visually were noted. Any structure that was determined to be intact was given a score of "0." Injured structures received a score of "1." Care was taken during the visual inspection stage to document without further injury, meaning only blunt instruments were used and limited force was applied to prevent further structural damage.

The results of the visual inspection were entered into a blank "Injury Pattern Scoring Sheet," which can be found in Appendix B. A listing of all of the structures examined in this study is provided in Table 2. The structures that are listed in the scoring sheet are based on the structures that Southern et al.[83] inspected in their study.

Table 2: Listing of all of the anatomic structures that were inspected in this study. The specific structure and its abbreviation are provided in the left-hand column. The locations where that structure was inspected are in the right-hand column. V1 represents the superior vertebra in the 2 FSU segment. V2 represents the middle vertebra. V3 represents the inferior vertebra. V1-2 represents the intervertebral joint between V1 and V2. V2-3 represents the intervertebral joint between V2 and V3.

Anatomic Strucutre	Anatomic Locations
Anterior longitudinal ligament (ALL)	V1, V1-2, V2, V2-3, V3
Anterior body (AVB)	V1, V2, V3
Anterior disc/endplate (AVD)	V1-2, V2-3
Posterior body (PVB)	V1, V2, V3
Posterior disc/endplate (PVD)	V1-2, V2-3
Posterior longitudinal ligament (PLL)	V1, V1-2, V2, V2-3, V3
Pedicle (PED)	V1, V2, V3 (left and right)
Articular pillar (AP)	V1, V2, V3 (left and right)
Anterior facet capsule (AFC)	V1-2, V2-3 (left & right)
Medial facet capsule (MFC)	V1-2, V2-3 (left & right)
Lateral facet capsule (LFC)	V1-2, V2-3 (left & right)
Posterior facet capsule (PFC)	V1-2, V2-3 (left & right)
Ligamentum flavum (LF)	V1-2, V2-3
Spinous process (SP)	V1, V2, V3
Lamina (LAM)	V1, V2, V3 (left & right)
Interspinous ligament (ISL)	V1-2, V2-3
Supraspinous ligament (SSL)	V1-2, V2-3

6.5.4 Computed Tomography Inspection

It was often difficult to determine the intact/injured status of the bony components and intervertebral discs during the visual inspection. To overcome this difficulty each specimen was subjected to an axial CT scan with 1.25 mm slice separation. Each CT scan was carefully reviewed by the author on a slice-by-slice basis looking for evidence of bony disruption and/or disruption of the intervertebral discs. The same binary intact/injured scoring system was used and the results were entered into the specimen's injury pattern scoring sheet (Appendix B).

6.6 Data Reduction

6.6.1 Load Data

The load cell configuration was set to provide the sign convention detailed in Table 3. For all load cells the outputs are considered to be measured at the centroid of the load cell. So, the direct measurements from the load cell describe the applied loading environment at its centroid.

In this study it was desired to measure the loading environment at the centroid of the specimen's inferior intervertebral disc. Transforming the load to this location defines the loads applied to the specimen and allows for the computation of eccentricity, which is integral in defining the injury mechanism.

Table 3: Sign convention used for six-axis load cell output.

	Sign Convention	
Load	**Positive**	**Negative**
Fx	Anterior	Posterior
Fy	Left	Right
Fz	Tension	Compression
Mx	Right lateral bending	Left lateral bending
My	Flexion	Extension
Mz	Counterclockwise	Clockwise

In order to measure the loading environment at the centroid of the inferior disc it was necessary to geometrically transform the loads from the centroid of the load cell using the static equilibrium equations ($\Sigma F = 0$, $\Sigma M_o = 0$). To use the static equilibrium equations for this purpose the following assumptions were made: the centroid of the intervertebral disc is stationary and the linkage between the load cell centroid and the disc centroid is rigid. The free body diagrams shown in Figure 26, Figure 27, and Figure 28 were used to generate the equations necessary to transform the loads to the centroid of the disc.

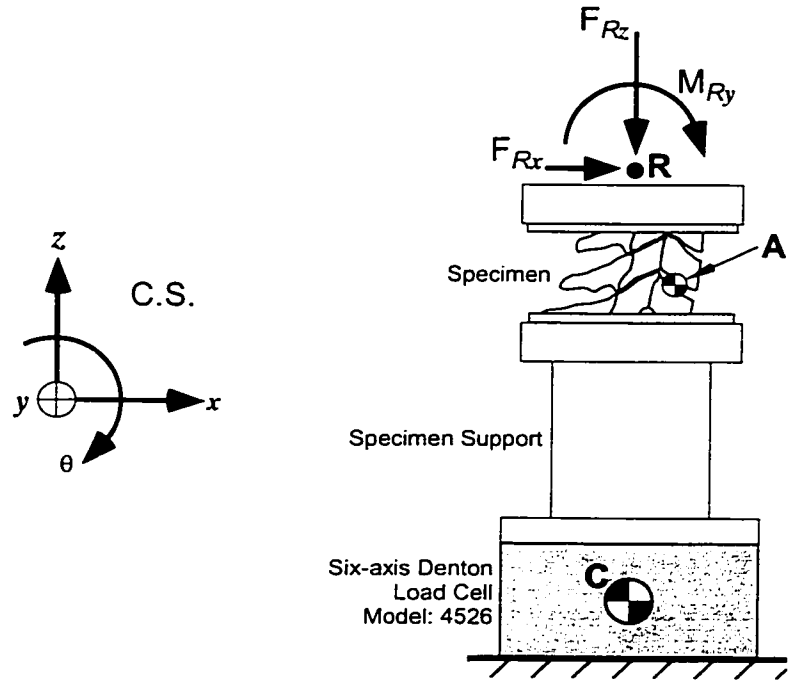

Figure 26: Basic free-body diagram showing the relationship between the position of the specimen and the position of the load cell. The coordinate system for this diagram and the subsequent diagrams is shown in the upper left hand corner. The loading environment at R is intended to generically represent loads applied to the upper potting mold of the specimen by the MTS load frame.

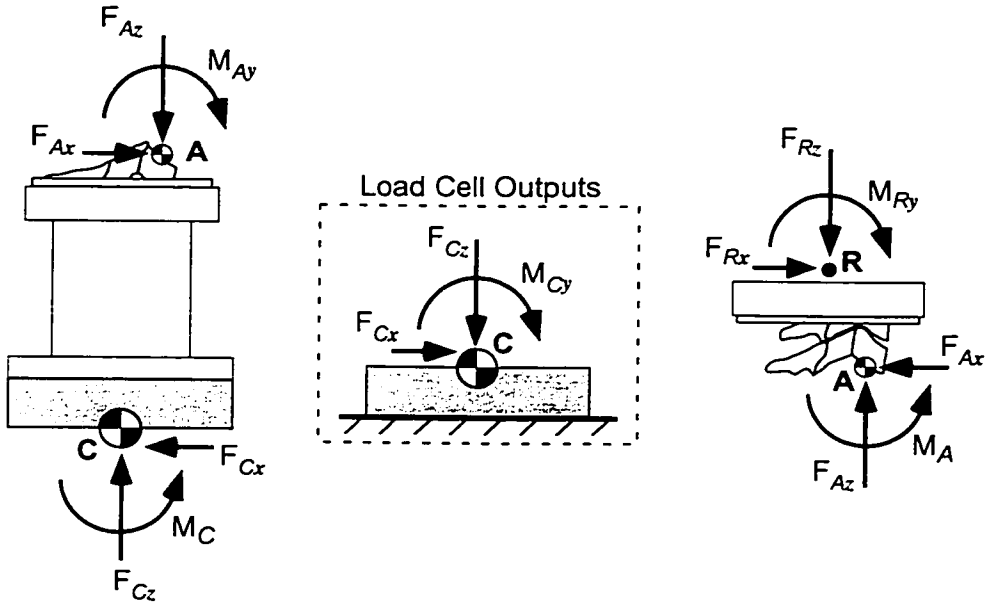

Figure 27: Shows the breakdown of the overall free-body diagram into sub-diagrams. The diagrams of importance are the one on the left and the one in the middle. The diagram on the left provides the basis for developing load transfer equations between the load cell centroid (point C) and the centroid of the specimen's inferior intervertebral disc (point A). The diagram in the middle shows the directionality of the loads that would be measured by the load cell for this scenario given the directionality of the loads shown at point C in the diagram on the left.

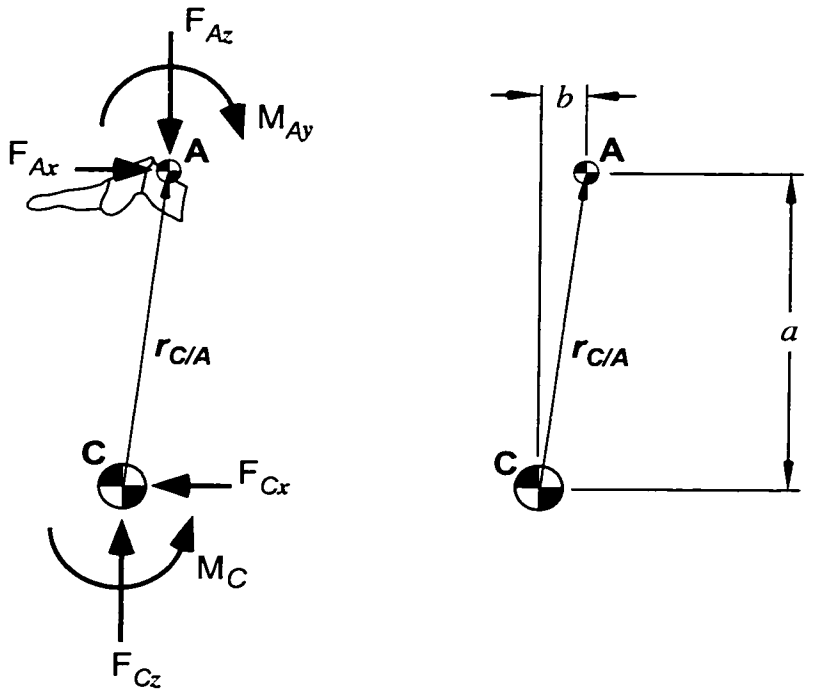

Figure 28: Diagram showing the geometric relationship between the centroid of the load cell (point C) and the centroid of the specimen's inferior intervertebral disc (point A).

To begin the derivation of the transfer equations we start with the static equilibrium equations as they relate to the free-body diagram shown in Figure 28. The forces at the load cell centroid (point C) are related to the forces at the disc centroid (point A) as shown in Eq 5. As can be seen by Eq 5 the relationships between the forces at the two locations are independent of the geometrical relationship between the locations.

$$\sum \bar{F} = 0 \qquad \text{Eq 3}$$

$$\bar{F}_A + \bar{F}_C = 0 \qquad \text{Eq 4}$$

$$F_{Ax} = -F_{Cx} \quad F_{Ay} = -F_{Cy} \quad F_{Az} = -F_{Cz} \qquad \text{Eq 5}$$

The geometry between the two locations does, however, play a role in transferring the moments at the load cell to the disc. The fundamental relationship used to set of the equations for transferring moments is given in Eq 7.

$$\sum \bar{M}_C = 0 \qquad \text{Eq 6}$$

$$\bar{M}_C + \bar{M}_A + (\bar{r}_{A/C} \times \bar{F}_A) = 0 \qquad \text{Eq 7}$$

Taking the determinant in Eq 7 and collecting by direction vectors the following equations are produced.

$$\bar{i} \quad M_{Cx} + M_{Ax} + (r_{A/Cy} \cdot F_{Az} - r_{A/Cz} \cdot F_{Ay}) = 0 \qquad \text{Eq 8}$$

$$\bar{j} \quad M_{Cy} + M_{Ay} + (r_{A/Cz} \cdot F_{Cx} - r_{A/Cx} \cdot F_{Az}) = 0 \qquad \text{Eq 9}$$

$$\bar{k} \quad M_{Cz} + M_{Az} + (r_{A/Cx} \cdot F_{Ay} - r_{A/Cy} \cdot F_{Ax}) = 0 \qquad \text{Eq 10}$$

The values for the components of $r_{A/C}$ are provided below (Eq 11) and are based on the assumption that the disc centroid and the load cell centroid both lie in the midsagittal plane. In practice the offset between the disc centroid was measured to be no more than 4 mm left or right of the load cell centroid with most specimens lying between ± 2 mm. Thus, the assumption that the disc centroid and load cell centroid are both in the midsagittal plane was reasonable.

$$r_{A/Cx} = b \quad r_{A/Cy} = 0 \quad r_{A/Cz} = a \qquad \text{Eq 11}$$

The values a and b represent the vertical and horizontal offsets between the centroid of the load cell and the centroid of the specimen's inferior intervertebral disc. The actual values used in this study can be found in Table 4.

Table 4: Tabulation of the horizontal (b) and vertical (a) offsets between the load cell centroid and the specimen's inferior intervertebral disc centroid. These measurements incorporate the horizontal and vertical offset measurements made in Section 6.4.1.

Group	Spec #	b (mm)	a (mm)
Compression	2	20	140
	10	25	144.5
	12	20	144.5
	23	18	142.5
	28	20	141.5
	40	21.5	144
	44	19.5	140.5
	46	22	142
Comp-Flexion	3	17.5	145
	5	24	140.5
	7	19.5	142.5
	8	25	142.5
	15	20	143.5
	17	21	145
	27	24	144.5
	48	23	141.5
Comp-Extension	14	19.5	142
	29	20	142.5
	39	27	145
	41	23.5	142.5
	43	23.5	143.5
	45	23	142.5
	47	24	143
	49	18.5	145.5

Substituting the components of $r_{A/C}$ into Eq 8, Eq 9, and Eq 10 and solving for the moments about point A (Figure 26) the following equations are obtained.

$$M_{Ax} = -M_{Cx} + a \cdot F_{Ay} \qquad \text{Eq 12}$$

$$M_{Ay} = -M_{Cy} - \left(a \cdot F_{Ax} - b \cdot F_{Az}\right) \qquad \text{Eq 13}$$

$$M_{Az} = -M_{Cz} - b \cdot F_{Ay} \qquad \text{Eq 14}$$

The forces and moments shown in Figure 26 at point C are reactions to the loads actually being applied to and measured by the load cell. Thus they are of the same magnitude as

the measured loads but opposite in direction. The forces at point *A* in Figure 26 (F_{Ax}, F_{Ay}, & F_{Az}) have opposite sign to those at point *C* and therefore have the same sign as the loads measured by the load cell directly (Eq 15). With this in mind Eq 12, Eq 13, and Eq 14 can be further modified to incorporate the loads measured by the load cell (F_x, F_y, F_z, M_x, M_y, & M_z). The results of such modifications are shown in Eq 16, Eq 17, and Eq 18.

$$F_{Ax} = -F_{Cx} = F_x \quad F_{Ay} = -F_{Cy} = F_y \quad F_{Az} = -F_{Cz} = F_z \qquad \text{Eq 15}$$

$$M_{Ax} = M_x + a \cdot F_y \qquad \text{Eq 16}$$

$$M_{Ay} = M_y - (a \cdot F_x - b \cdot F_z) \qquad \text{Eq 17}$$

$$M_{Az} = M_z - b \cdot F_y \qquad \text{Eq 18}$$

So, the forces at point *A* are equivalent in magnitude and direction to the forces measured by the load cell directly, and the magnitudes and directions of the moments at point *A* can be found using Eq 16, Eq 17, and Eq 18. Therefore, the loading environment at point *A* (inferior disc centroid) can be known completely.

This study revolves around the concept of imparting distinctly different loading environments, namely compression, compression-flexion, and compression-extension. Computing the six-axis forces and moments at the inferior disc centroid provides all of the information about the applied loading environment. Nonetheless, no single force or moment value can be used to quantify the loading environment for statistical comparison. The simplest way to quantify the loading environment for statistical comparison is to compute the midsagittal plane moment arm or axial eccentricity (*e*). The axial eccentricity is found when the midsagittal plane moment (M_{Ay}) is resolved into a force at a distance from the centroid (Figure 29). The resolving force of interest is the axial force (F_{Az}). The computation itself is relatively simple and only requires that the measured moment be divided by axial force to obtain the eccentricity and multiplied by – 1 to obtain the proper sign (Equation 19). At the point of structural failure the value of axial

eccentricity provides a single number representative of the loading environment observable at the centroid of the inferior intervertebral disc.

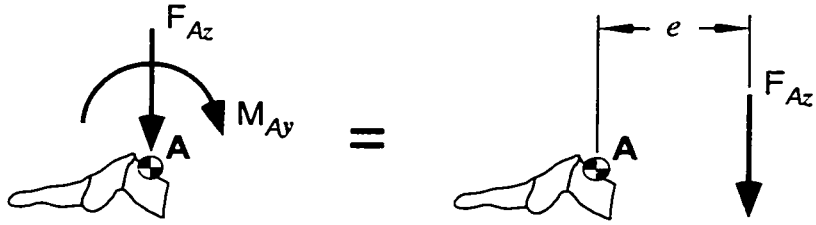

Figure 29: Schematic representation of the computation of eccentricity.

Equation 19: Formula used to compute eccentricity.

$$e = -\left(\frac{M_{Ay}}{F_{Az}}\right)$$

All of the computations defined above were performed post-test using a custom designed LabVIEW VI. Before making any of the computations the VI subjected all of measured load data to a forward-backward 4-pole low-pass Butterworth digital filter with a 3 dB cutoff of 1 kHz (CFC 600 per SAE J211-1). The forward-backward part of the filter description refers to the fact that the selected data array is first passed from front to back (forward in time) and then from back to front (backward in time). This forward/backward method provides for phaseless filtering of the data and is recommended in the SAE J211-1. The SAE J211-1 also recommends the use of a 4-pole Butterworth digital filter, which is supported by the year 2000 NHTSA final rule.[25] With regard to the CFC of 600, the SAE J211-1 recommends a CFC 600 filter for neck moment data and a CFC 1000 for neck force data. However, in the final rule on injury criteria proposed by the NHTSA[25] it was recommended that all neck load data be consistently filtered with a CFC 600 filter. Thus, for this study all load data was consistently filtered using a CFC 600 filter.

The following time histories were output directly from the load data reduction VI:

1.) Load cell outputs F_x, F_y, F_z, M_x, M_y, & M_z

2.) Moments about the inferior disc centroid M_{Ay} and M_{Ax}

3.) Eccentricity (e)

6.6.2 MTS Ram Velocity

As was previously mentioned (see Sections 6.3.1 and 6.3.6) the displacement of the MTS ram was monitored by a built in LVDT. However, the velocity of the ram was not. A custom designed LabVIEW VI was used to compute velocity by differentiating the ram displacement signal. As differentiation tends to accentuate high frequency fluctuations it was necessary to subject the ram velocity output to a forward-backward 4-pole low-pass Butterworth filter. The frequency cutoff used in this case was 1 kHz (CFC 600).

6.6.3 Injury Pattern Data

The visual inspection and computed tomography inspections described above (see Sections 6.5.3 and 6.5.4) put the injury pattern data into a basic format for analysis. However, to simplify the statistical analysis the injury pattern data produced was pared down in the following ways. First, all of the structures were segregated into "hard" and "soft" tissue groups. This segregation was primarily used to help visualize the injury patterns by type of tissue affected. Second, sidedness was removed reducing structures with a left and right parts down to a single representative value. This reduction of sidedness was accomplished by assigning a 0 to a structure with both its left and right parts intact. A 1 was assigned to a structure where one or both of its left and right components were injured. Third, all of the level-by-level data was reduced down to a single representative value for each structure. For the hard tissues a score of 1 was given if a structure was injured in any or all of the three vertebrae in the segment. For the soft tissues a structure received a 0 if it was intact at either joint level or a 1 if it was injured at one or both intervertebral joint levels.

6.6.4 SCOT Data

Data reduction for the SCOT was made complicated because the output was an amplitude modulated 2 kHz alternating voltage. To decouple the actual occlusion signal from the SCOT output it was essential to demodulate the signal. Again, a custom designed LabVIEW VI was employed to process the SCOT output signals.

The first step in the demodulation process was to pass through the test data file and find the peaks and valleys of the alternating voltage signal. The peak/valley detection was facilitated by a peak detection algorithm supplied with LabVIEW. This peak detection algorithm was designed to search a data array and find peaks using a quadratic fit of a specified number of adjacent data points. For the purposes of this study the number of adjacent data points used for the quadratic fit was five. The output of the peak detection algorithm was a set of four arrays containing the locations of the peaks, the peak amplitudes, the locations of the valleys, and the valley amplitudes.

The second step was DC offset compensation. While the SCOT signal conditioning equipment was designed to provide an AC coupled output (no DC offset), some leakage was always present resulting in a signal that was not completely AC coupled. At the beginning of each data acquisition file was a section of baseline data where no occlusions were being imparted to the transducer. This baseline data was used to compute the DC offset.

The average amplitudes of the first 150 peaks and the first 150 valleys from the baseline data were computed. The average peak and valley amplitudes were then averaged to find

the DC offset. The DC offset was then subtracted from all of the peak and valley amplitudes.[1]

After compensating for DC offset the equivalent of a full wave rectification was performed. The first step in the rectification process was to take the absolute values of the valley amplitudes. The peak amplitudes and rectified valley amplitudes were then interleaved into one data array based on the location information generated during the peak detection process. The result was a demodulated voltage signal representing the output of the SCOT.

Once a demodulated voltage output was produced for each sensing section the calibration lookup tables created during the pre-test calibrations were used to convert the voltage signals into displacement signals. Using the average midsagittal diameters measured at each vertebral level (see Section 6.4.1) the displacement signals for each sensing section were then converted into percent midsagittal diameter (*%MSD*) occlusion signals. The equation used to make the conversion is shown below (Equation 20). The variables used in the equation were canal midsagittal diameter (*MSD*), SCOT nominal tubing diameter (*TD*), and displacement as measured by the SCOT (x).

Equation 20: Equation used to compute the percent decrease in midsagittal diameter from the SCOT deformation output.

$$\%MSD = \left(\frac{MSD - TD + x}{MSD} \right) \cdot 100$$

[1] This method of computing DC offset is not the appropriate method. The two common methods for determining DC offset are: compute the average of all of the samples in the baseline signal or pass the entire signal through a low-pass filter with a cutoff frequency that is substantially lower than the signals fundamental frequency (2 kHz in this case). Alternatively, LabVIEW comes with a built in AC/DC estimator virtual instrument that can be easily incorporated to provide DC offset values. All three of these methods were compared with the method of computing DC offset used by the author. The maximum difference observed was 0.025 volts suggesting that the author's method, while inappropriate, had a negligible effect.

6.7 Data Analysis

6.7.1 Load Data

6.7.1.1 Peak and Failure Loads

The first step in analyzing the load data involved establishing the maximum and minimum values for the primary loads of interest measured at the centroid of the inferior intervertebral disc (F_{Ax}, F_{Az}, and M_{Ay}). The max and min values, or peaks, and their occurrence times were found by way of a simple search of the load time histories generated during the experiment.

The second step in the analysis of the load data was the establishment of the loading environment at failure. Before the failure loads could be determined a definition for the occurrence of failure had to be established. In previous axial compression experiments failure, in terms of load and not stress, has been defined as the peak axial load prior to a reversal, with a reversal being defined as a decrease in load in the presence of increasing displacement.

After examining all of the load data produced in this study it was clear that looking for a reversal in the axial load was not the best indicator of failure for all circumstances. In this study the axial load (F_{Az}) and the moment about the y-axis (M_{Ay}) were examined together to determine failure. Examining the load histories for both F_{Az} and M_{Ay} proved to be more sensitive, as there were times when looking at one without the other would have led to the conclusion that a failure did not occur at a specific point. An example of such an occurrence is depicted in Figure 30.

Once a failure was located the axial load (F_{Az}), shear load (F_{Ax}), moment (M_{Ay}), and time of failure were segregated from the data. The time of failure was of particular importance because it was used to search the time histories of other variables, such as canal occlusion, for their values at failure. The failure loads for each specimen were tabulated

and averages, standard deviations, and 95% confidence intervals were computed for the different loading groups.

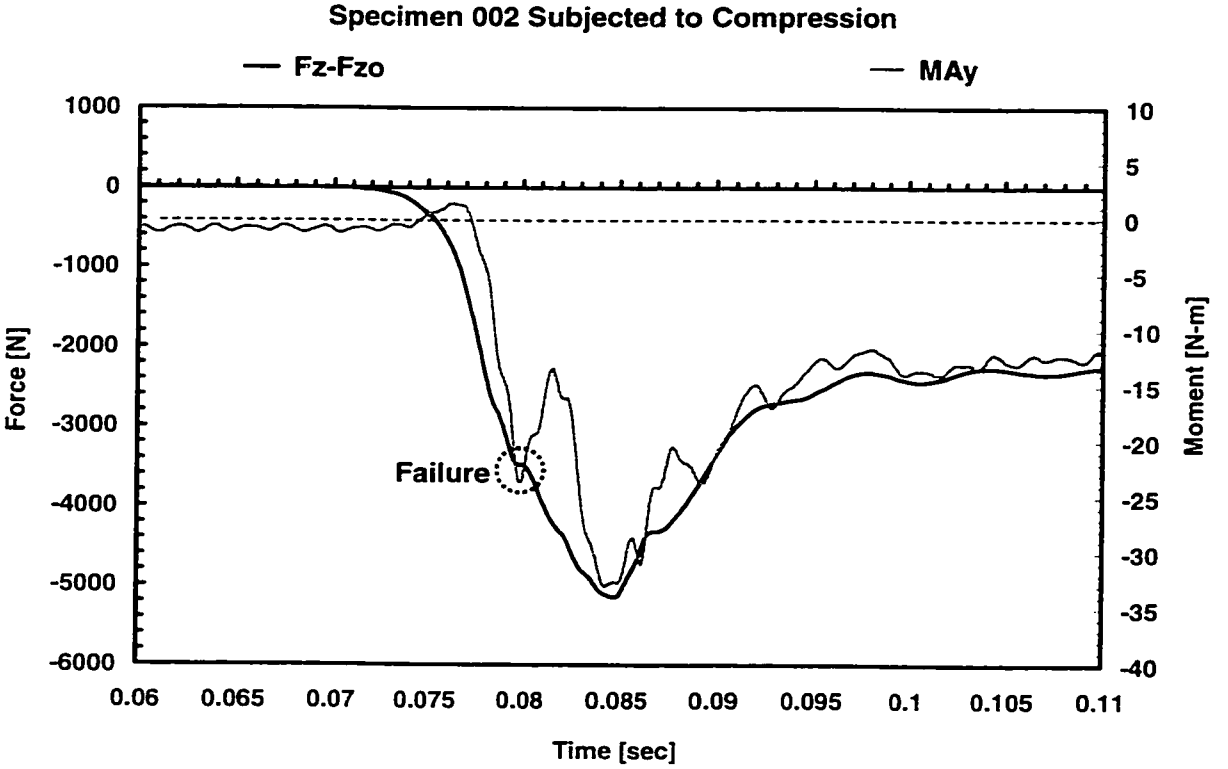

Figure 30: Graph providing an example where examining only the axial force trace (Fz-Fzo) prevented a clear determination of the failure. In this case the moment about the centroid of the inferior intervertebral disc (MAy) provided additional information to help define when failure occurred.

6.7.1.2 Axial Eccentricity at Failure

An important part of this project was ensuring that the three groups were subjected to three different loading environments. To demonstrate that distinct loading environments were applied the axial eccentricity at the point of failure was determined for each specimen. The eccentricities for each test group (compression-flexion, compression, or compression-extension) were tabulated and subjected to a One-Way ANOVA using SPSS statistical software (SPPS v 10.0.5, SPSS Inc., Chicago, IL). The significance level, or alpha level, was set at 0.05. The null hypothesis was: there exists no difference in eccentricity at failure across each of the three test groups.

6.7.2 Displacement and Velocity

Maximum displacement and velocity during the loading phase of the test were acquired by simply searching the time histories for maxima. Displacement and velocity at failure were found using time at failure as a search critieria. These displacement and velocity values were tabulated and their group averages, standard deviations and 95% confidence intervals were computed in Microsoft Excel 2000 (Microsoft Corp., Redmond, WA).

To provide feedback as to how similar the inputs for the three test groups were the maximum displacement and velocity values were subjected to a One-Way ANOVA using SPSS statistical software (SPSS v. 10.0.5, SPSS Inc., Chicago, IL). The objective of the analysis was to test the null hypothesis that there was no difference in the mean peak displacement or mean peak velocity inputs across the three loading groups. Significance was established at an alpha level of 0.05.

Additionally, an ANOVA was performed on displacement at failure data to provide some insight into the relationship between ram displacement at failure an injury mechanism. Should research similar in nature to this research be performed in the future it may be beneficial to have a better idea how the amount of ram displacement required to generate an injury will vary. The type of analysis used was a One-way ANOVA, which was conducted with SPSS statistical software, using a significance level of 0.05.

6.7.3 Injury Pattern Data

In hypothesis number 2 (see Section 5.4) the assertion is made that structural injury patterns can be accurately classified based on injury mechanism. To evaluate this hypothesis a quantitative method for classification is needed. This classification method should preserve the multidimensional information provided by each specimen's injury pattern. Furthermore, it should provide feedback regarding the accuracy with which an injury pattern can be classified by injury mechanism. The author has determined that the best statistical method for establishing a classification relationship between injury

mechanism and injury pattern without disrupting the multidimensional information is known as Discriminant Analysis (DA). The DA for this study was performed using a SPSS v. 10.0.5 (SPSS Inc., Chicago, IL).

Generally, the objective of the DA technique is the development of predictive equations that can be used to classify subjects that are described by a multidimensional vector into distinct groups. These classification equations are then used in the future to predict what group a new subject, which was not subjected to the original analysis, might belong to. A distinct advantage of Discriminant analysis is its capability to determine which components of the multidimensional vector describing a subject are the best *discriminators* for group membership. Thus, it is possible to limit the amount of information required to classify a subject into a specific group.

For example, a health insurance company decides to develop a way to assess the risk of providing a potential policyholder with health insurance. To do this they would take current health insurance policyholders and separate them into risk categories, such as high, medium, and low risk, based on dollar amounts expended per year. Then they could describe the people in those categories based on aspects of their health such as whether or not they smoke, if they have high blood pressure, and so on. For the purposes of this discussion lets say the insurance company comes up with 10 factors (health aspects) to describe each policy holder. With all of the information compiled the DA is conducted. The output is a set of three equations, one for each risk group, which can be used to classify a potential policyholder. These equations will be based on the factors that are the best discriminators for risk group membership, which will hopefully be a subset of the 10 factors originally proposed. Thus, the insurance company could give the potential policyholder a questionnaire that provides the information needed for the classification equations and then immediately classify that person to determine the risk of insuring them.

It may seem as though DA is not immediately applicable for use in evaluating hypothesis 2. However, DA does provide a method for addressing how accurately injury patterns can be classified into injury mechanism groups. The method for addressing classification accuracy is called cross-validation.

Cross-validation is a common method for scrutinizing strength of classification, and to a certain extent group distinctiveness, in DA. In cross-validation one subject is removed from the analysis and the remaining subjects are used to generate classification equations. These new classification equations are then used to reclassify the removed subject. This process is repeated for every subject in the analysis. At the end of the cross-validation process a cross-validation rate is computed, which is the number of subjects properly reclassified divided by the total number of subjects and multiplied by 100 to get a percentage. A high reclassification rate indicates that the groups are very distinct in a similar fashion to the way that R^2 indicates the strength of a linear regression.

After determining the reclassification rate it is necessary to determine its significance. A statistical assessment of cross-validation rate significance was provided by Sharma.[81] The test statistic is given in Equation 21, where o is the number of correctly reclassified subjects, e is the expected number of reclassifications due to chance (Equation 22), and n is the total number of subjects used in the Discriminant Analysis. In Equation 22, which is used to compute the expected number of reclassifications due to chance, n_g represents the number of subjects in a particular group and G represents the total number of groups. The test statistic Z^* is assumed to follow an approximately normal distribution.

Equation 21: Test statistic used to assess the statistical significance of the reclassification rate produced by a Discriminant Analysis.

$$Z^* = \frac{(o-e)\sqrt{n}}{\sqrt{e\,(n-e)}}$$

Equation 22: Equation used to computed the expected number or correct reclassifications due to chance.

$$e = \frac{1}{n} \sum_{g=1}^{G} n_g^2$$

A p-value is obtained by referencing Z^* to normal distribution tables. The resulting p-value is the probability that the number of successful reclassifications in the cross-validation is due solely to random chance. For this study a p-value less than 0.05 was considered to indicate that the number of successful reclassifications is significantly greater than what can be ascribed to random chance.

The first hypothesis of this study (see Section 5.4) concerned the idea that different injury mechanisms produce different injury patterns. Using DA the null hypothesis that different injury mechanisms do not produce different injury patterns can be tested. Afifi and Clark [1] have provided a good explanation of the concepts behind testing this hypothesis in Chapter 11 of their book. Essentially, a matrix is generated that makes pairwise comparisons of the "mean" injury pattern for all three injury mechanism groups. This comparison matrix provides a p-value for each pairwise comparison indicating the probability that the "mean" pattern for one group is the same as another group. In this study the significance of injury pattern comparisons was established based on a p-value of 0.05. It should also be noted that the cross-validation rate provides an indication of group distinctiveness, however, it does not lend itself to testing the null hypothesis for hypothesis 1.

6.7.4 SCOT Data

The SCOT data was examined to determine the following: canal occlusion at the initiation of structural failure (failure), peak canal occlusion, and canal occlusion immediately post-injury (residual occlusion). Canal occlusion at failure was obtained simply by searching the SCOT history using time at failure to find the SCOT output at that time. Peak canal occlusion was found by searching the SCOT time history for a

maximum. The immediate post-injury or residual occlusion was the canal occlusion present at the end of the test, when all load had been removed from the specimen. These three canal occlusion values were established for each specimen and then tabulated for each test group.

To test hypotheses 3 and 4 (see Section 5.4) a Two-Way Repeated Measures ANOVA was employed using SPSS statistical software (SPSS v. 10.0.5, SPSS Inc., Chicago, IL). The between-subjects factor for the analysis was loading environment (compression-flexion, compression, and compression-extension) and the within-subjects, or repeated measures, factor was time of measurement (failure, peak, and residual). A significance level of 0.05 was used to establish a significant difference. To test hypothesis 5 (see Section 5.4) a simple linear regression of peak occlusion versus residual occlusion was performed using Microsoft Excel 2000 (Microsoft Corp., Redmond, WA). In this regression all of the data was pooled to perform the analysis.

7 RESULTS

7.1 Load Data

7.1.1 Peak Loads

Table 5 is a summary table demonstrating the mean peak loads and the 95% confidence interval values for each type of load, grouped by the loading environment. The ±95% confidence interval range is the range between the mean peak load minus the 95% CI value and the mean peak load plus the 95% CI value. A complete listing of the peak loads sustained by each specimen as well as the time to peak load can be found in Appendix C

Table 5: Tabulation of mean peak loads and their 95% confidence interval values at the inferior disc centroid grouped by loading environment. Each loading environment group contains 8 specimens..

		Loading Environment					
		Compression-Flexion		Compression		Compression-Extension	
		Mean	95% CI*	Mean	95% CI*	Mean	95% CI*
Tension	[N]	209.9	36.0	49.4	28.4	27.6	9.6
Compression	[N]	1462.4	229.6	6662.5	1080.4	4002.5	669.6
Anterior Shear	[N]	459.9	110.8	903.9	235.7	1070.7	825.9
Posterior Shear	[N]	503.4	72.7	67.8	69.6	563.9	112.6
Flexion	[N-m]	23.1	5.6	1.7	0.9	5.0	6.4
Extension	[N-m]	5.9	1.8	63.8	18.6	195.9	129.6

** 95% CI represents the value used to create the 95% confidence interval about the mean*

7.1.2 Failure Loads

The mean failure loads for the different loading environments and their 95% confidence interval values are displayed in Table 6. The tabulated data is also presented graphically in Figure 31 and Figure 32. It is apparent from the data that the mean axial force (F_{Az}) at failure for the compression and compression-extension loading environments are nearly equal and better than four times larger than their counterpart in the compression-flexion

group. Additionally, the graphical representations give the impression that there is a trend toward increasing shear force (F_{Ax}) and decreasing midsagittal moment (M_{Ay}) moving from the compression-flexion group to the compression-extension group. A complete listing of the failure loads for each specimen along with time to failure can be found in Appendix C.

Table 6: Tabulation of mean failure loads and their 95% confidence interval values at the inferior disc centroid grouped by loading environment. Each loading environment group contains eight specimens.

		Loading Environment					
		Compression-Flexion		Compression		Compression-Extension	
		Mean	95% CI*	Mean	95% CI*	Mean	95% CI*
Axial Force	[N]	-765.5	240.0	-3260.9	707.7	-3472.0	684.4
Shear Force	[N]	-235.5	142.3	320.7	221.0	524.9	127.3
Midsagittal Moment	[N-m]	21.4	6.9	-15.0	5.7	-47.8	13.6

** 95% CI represents the value used to create the 95% confidence interval about the mean*

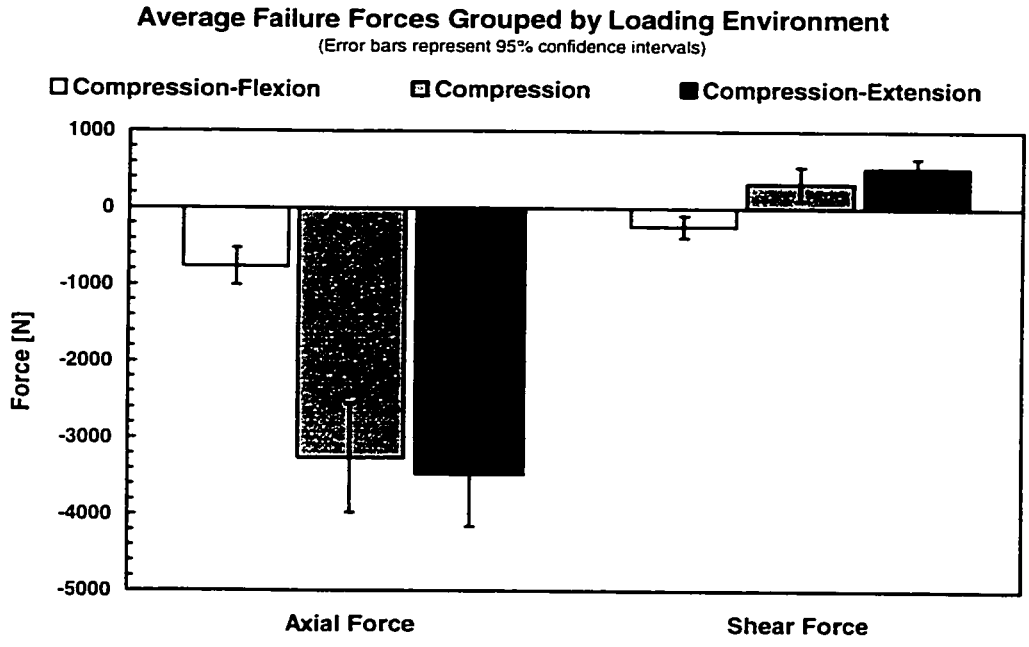

Figure 31: Columnar graph demonstrating the relationships between mean axial force (F_{Az}) at failure across the three loading environments, and mean shear force (F_{Ax}) at failure across the three loading environments.

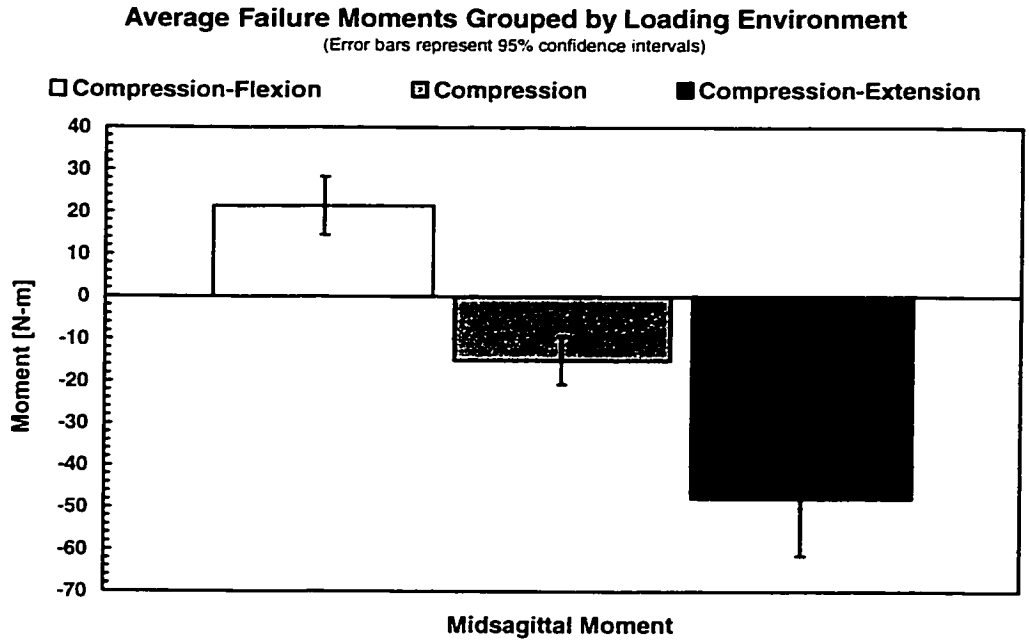

Figure 32: Columnar graph demonstrating the change in midsagittal plane moment (M_{A_y}) at failure as a function of loading environment.

7.1.3 Axial Eccentricity at Failure

Mean axial eccentricity at failure for each of the three loading environment groups is provided in Figure 33. In Figure 34 the individual axial eccentricities computed for each group are plotted in the midsagittal plane. All of the axial eccentricity values plotted in Figure 34 have been normalized to the anterior-posterior width of the vertebral body in the midsagittal plane. This graphical representation shows that the compression-flexion and compression-extension groups exhibited axial eccentricities that tended to extend beyond the anterior and posterior borders of the inferior intervertebral disc/middle vertebral body, respectively. The compression group, on the other hand, exhibited axial eccentricities that tended to lie roughly half way between the disc centroid and the posterior border of the inferior disc/middle vertebral body.

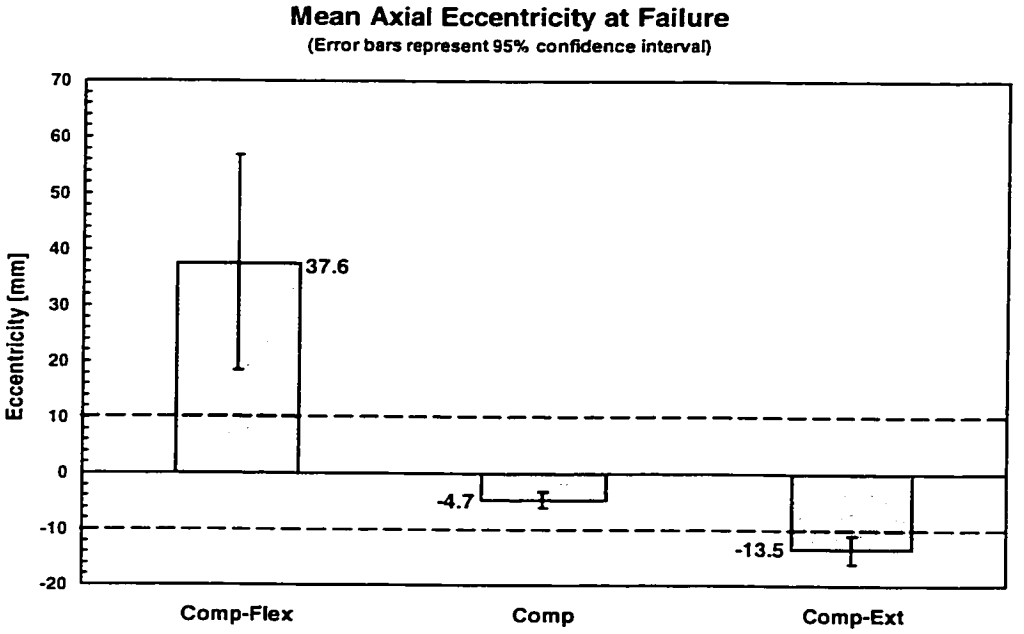

Figure 33: Plot of mean axial eccentricity versus loading environment. The mean values are shown next to each column. Zero on this graph represents the centroid of the inferior intervertebral disc and the dashed lines represent the average locations of the anterior and posterior margins of the vertebral body relative to the inferior disc centroid. The eccentricity values have not been normalized.

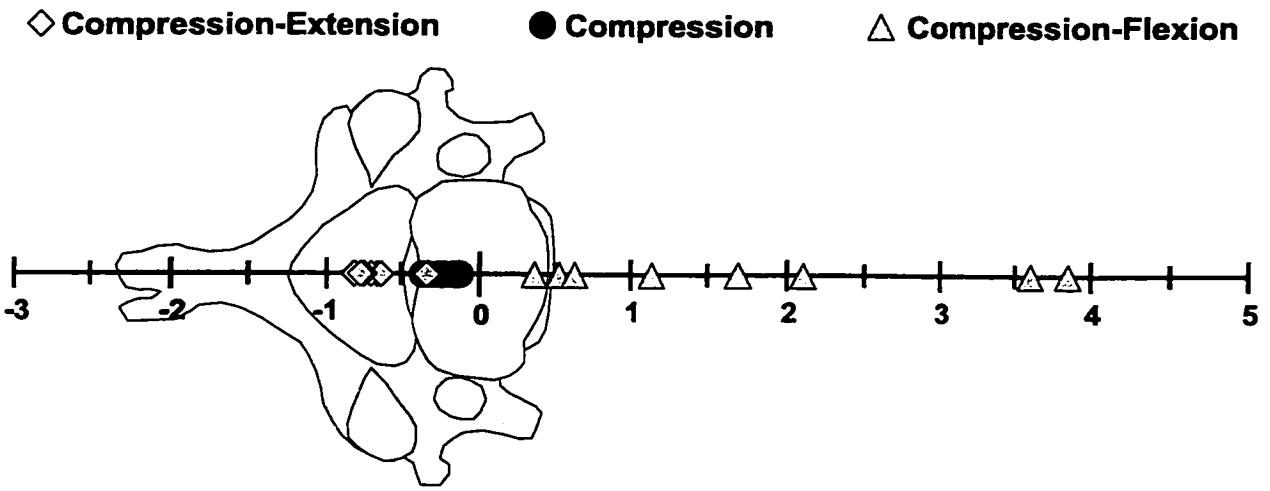

Figure 34: Axial eccentricity values compared to the size of a vertebra. The coordinate system origin is centered on what would be the centroid of the intervertebral disc. The units for the axis are body widths, where one body width represents the distance in the midsagittal plane between the anterior and posterior margins of the vertebral body. The data points are eccentricity values that have been normalized to the anterior-posterior width of their corresponding specimen.

A One-Way ANOVA was conducted to test the null hypothesis that there is no difference in axial eccentricity across the three loading environments applied in this study. The results of the one-way ANOVA and subsequent post-hoc pairwise comparisons demonstrate that the mean eccentricities were significantly different for all three groups ($p < 0.01$). Thus, all three loading groups were distinctly different from one another in terms of the applied loading environment. The complete output for the One-Way ANOVA is provided in Appendix D.

7.2 Displacement and Velocity

The mean failure and peak displacements and peak velocities for each of the three test groups are shown in Table 7. A full tabulation of the peak displacements and velocities for each specimen in each group can be found in Appendix C. The values appear to demonstrate that the peak displacements and velocities are in roughly the same ballpark with the displacements and velocities for the compression group being slightly higher. A One-way ANOVA of the peak displacements and velocities (Appendix E) reveals that there was no significant difference in the mean peak displacement for each of the three test groups ($p > 0.05$). On the other hand, the mean peak velocity analysis was somewhat ambiguous. The ANOVA suggested that there was at least one significant difference between two of the three loading groups ($p = 0.032$). However, when a post-hoc pairwise comparison was performed no significant differences were uncovered ($p > 0.1$). This difference between the inference from the ANOVA and the post-hoc analysis would tend to indicate that the mean peak velocities exhibited by the three groups are right on the edge of being significantly similar/different. Overall, the analysis tends to suggest that the inputs used for the three test groups were similar.

With regard to displacement at failure it appears that there was a significant difference between the three groups; however, this was not specifically tested. Generally, it appears that the compression flexion group required the most displacement of the ram before

failure was observed, the compression group required the least, and the compression-extension group fell in between.

Table 7: Tabulation of mean failure displacements, peak displacements and peak velocities for each of the three test groups. The table also provides ± values for 95% confidence interval determination.

	Loading Environment					
	Compression-Flexion		Compression		Compression-Extension	
	Mean	95% CI*	Mean	95% CI*	Mean	95% CI*
Failure Displacement [mm]	-7.48	1.14	-2.91	0.48	-4.28	0.45
Peak Displacement [mm]	-9.23	1.08	-11.97	2.19	-9.91	1.35
Peak Velocity [m/sec]	-0.85	0.12	-1.14	0.23	-0.86	0.11

** 95% CI represents the value used to create the 95% confidence interval about the mean*

7.3 Injury Pattern

The reduction of injury pattern data described in Section 6.6.3 can be seen in Table 8. As was mentioned in Section 6.7.3 a Discriminant Analysis was performed on the injury pattern data shown in Table 8 using SPSS statistical software (SPSS v. 10.0.5, SPSS Inc., Chicago, IL). The analysis shows that the anterior longitudinal ligament, pedicle, articular pillar, ligamentum flavum, spinous process, and interspinous ligament were the best variables for determining group membership (i.e. they were the best discriminators). The complete results of the DA can be found in Appendix F.

Table 8: Tabulation of structural injury grouped by loading applied loading and by soft and hard tissue structures. The structures listed are as follows: ALL – anterior longitdudinal ligament, AVD – anterior ½ intervertebral disc, PVD – posterior ½ intervertebral disc, PLL – posterior longitudinal ligament, AFC – anterior facet capsule, MFC – medial facet capsule, LFC – lateral facet capsule, PFC – posterior facet capsule, LF – ligamentum flavum, ISL – interspinous ligament, SSL – supraspinous ligament, AVB – anterior ½ vertebral body, PVB – posterior ½ vertebral body, PED – pedicle, AP – articular pillar, LAM – lamina, and SP – spinous process.

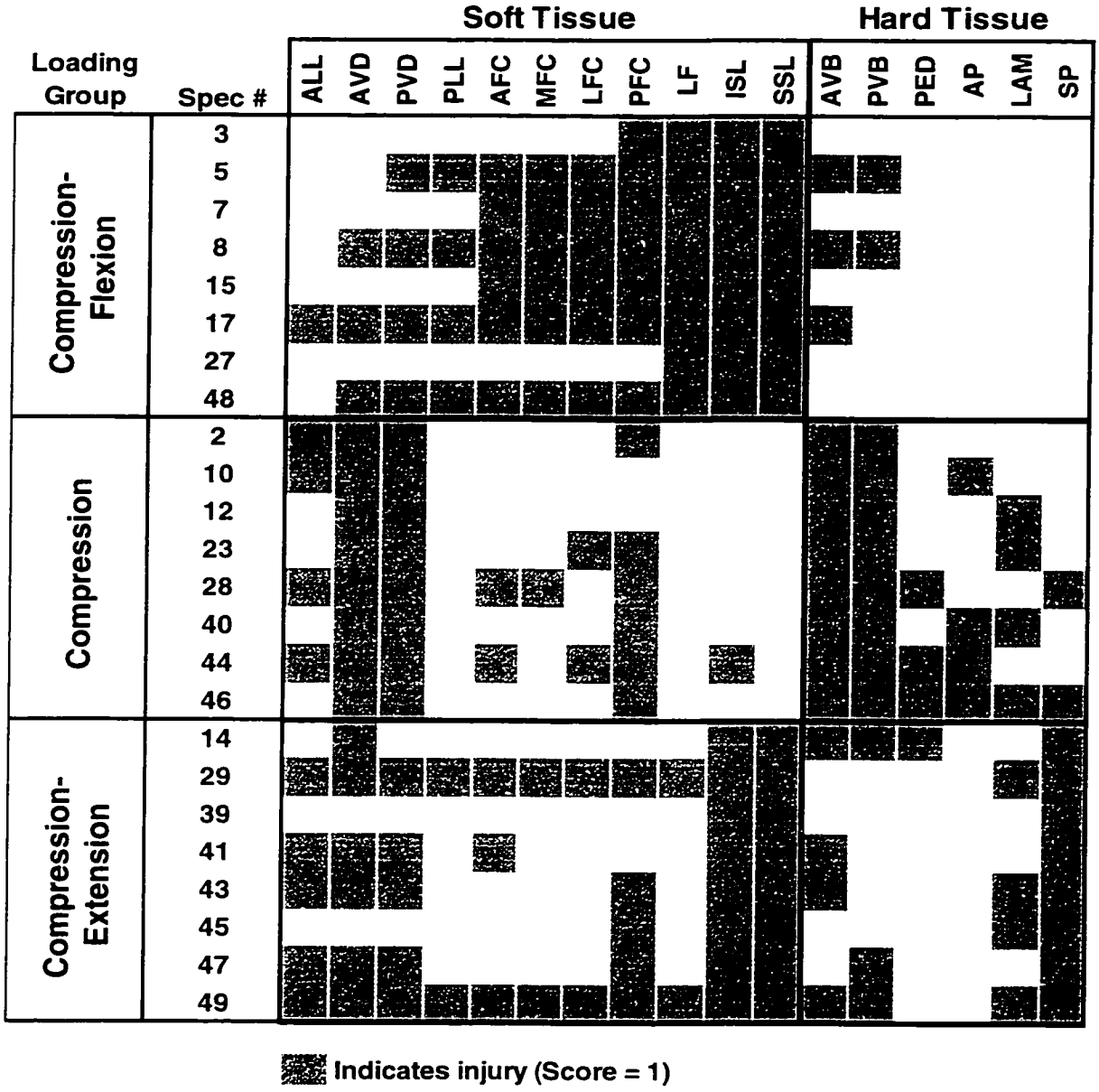

With regard to hypothesis 1 the DA demonstrates that different injury mechanisms produced distinct injury patterns. One part of the DA output was a table of pairwise comparisons that, in effect, compares the mean pattern for each of the three groups to see if significant differences in the patterns exist. In this study all three groups demonstrated significantly different injury patterns on average ($p < 0.001$). The significant difference in injury pattern was also clearly demonstrated in Table 8 and bolstered by the 100% classification accuracy discussed above.

In conjunction with demonstrating that distinct injury patterns are produced by different injury mechanisms, this study sought to determine whether injury patterns can be accurately classified based on injury mechanism alone (Hypothesis 1). The DA demonstrates that the structural injury patterns produced in this study can be accurately classified. In fact the results of the DA indicate a classification accuracy of 100%. In order to demonstrate that this accuracy is significant the test statistic in Equation 21 was calculated as shown below for n = 24, n_g = 8, G = 3, and o = 24. Referencing the Z* value of 6.928 to values for a standard normal distribution demonstrates that there is essentially zero probability of classifying the injury patterns in this study as accurately by random chance. Therefore, the 100% accuracy produced here not only meets the common sense criteria for significance it also meets the statistical criteria for significance.

$$e = \frac{1}{24}(64+64+64) = 8 \quad \Rightarrow \quad Z^* = \frac{(24-8)\sqrt{24}}{\sqrt{8\,(24-8)}} = 6.928$$

7.4 Canal Occlusion

One of the most unfortunate things to occur during this study was the removal of the occlusion data from the compression-flexion series. After a thorough investigation of the data a determination was made that it was unreliable. Close examination of the occlusion

data in conjunction with examination of the high-speed video footage suggested that the SCOT was being pulled and kinked during the compression-flexion tests. As a result the transducer output demonstrated wildly varying oscillations that appeared to travel along the transducer. An example of the typical response is demonstrated in Figure 35. Alternatively, an example of a clean SCOT response is provided in Figure 36.

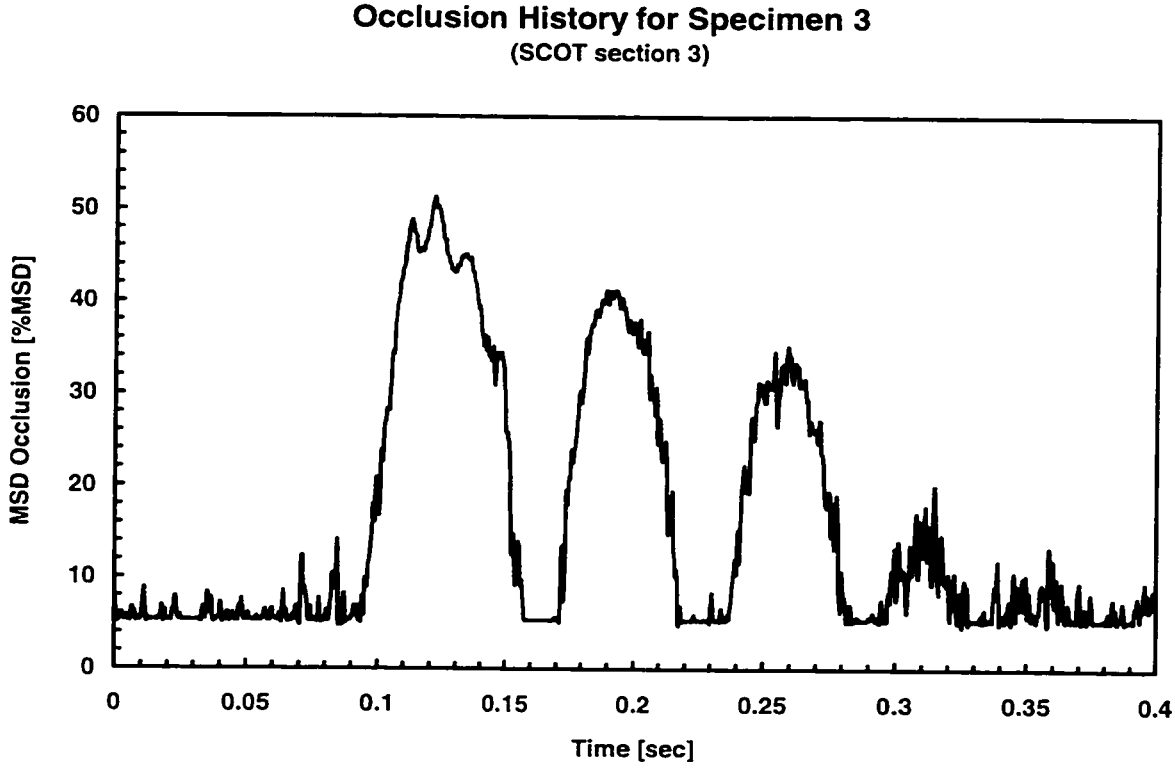

Figure 35: SCOT response from specimen 3, which was subjected to compression-flexion loading. Response demonstrates the typical oscillatory pattern exhibited as a result of the transducer being pulled and kinked during. The ram displacement initiated at 0.078 seconds and failure occurred at 0.090 seconds.

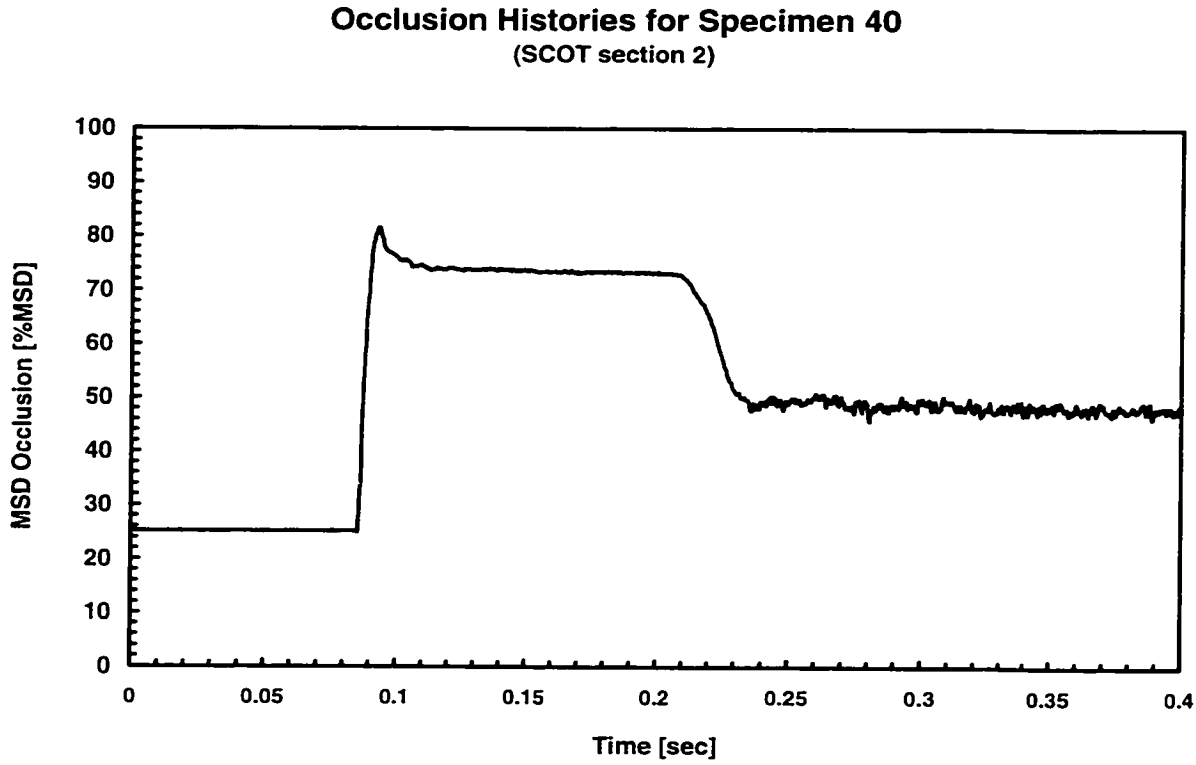

Figure 36: SCOT response from specimen 40, which was subjected to compression loading. Response demonstrates a clean signal from the SCOT during a test. The ram displacement initiated at 0.076 seconds and failure occurred at 0.081 seconds.

Fortunately, the SCOT data from the compression and compression-extension series were unaffected by the problems observed in the compression-flexion series. Therefore, the testing of hypotheses 3, 4, and 5 was conducted using only the compression and compression-extension data sets.

The table (Table 9) and bar graph (Figure 37) provided below contain the mean values for occlusion at the three time points of interest in this study (failure, peak, and residual) in relation to the loading groups compression and compression-extension. The occlusion data gathered during experimentation was lost for one specimen in the compression group and two specimens in the compression-extension group as a result of forgetting to connect the SCOT and improper strain relief of the SCOT sensing electrodes. The complete tabulation of occlusion data can be found in Appendix G. When the mean

values were analyzed in a Two-way Repeated Measures ANOVA (Appendix G) the results clearly confirmed that there was a very significant difference in mean occlusion over time ($p < 0.001$). Post-hoc tests revealed that all three time points were, on average, significantly different from one another ($p < 0.012$). The observed power for the comparisons of occlusions over the three time points was 1.0. Thus, null hypothesis for hypothesis 4 was rejected.

Table 9: Tabulation of mean occlusion values measured at each of the three time points of interest and grouped by applied loading. The table also provides the number of samples in each group, and the computed ± 95% confidence interval values.

	Loading Environment					
	Compression			Compression-Extension		
	Mean	N	95% CI*	Mean	N	95% CI*
Occlusion at Failure [%MSD]	4.28	7	6.66	12.42	6	10.15
Peak Occlusion [%MSD]	58.71	7	7.53	59.96	6	3.56
Residual Occlusion [%MSD]	22.25	7	11.86	32.48	6	10.74

** 95% CI represents the value used to create the 95% confidence interval about the mean*

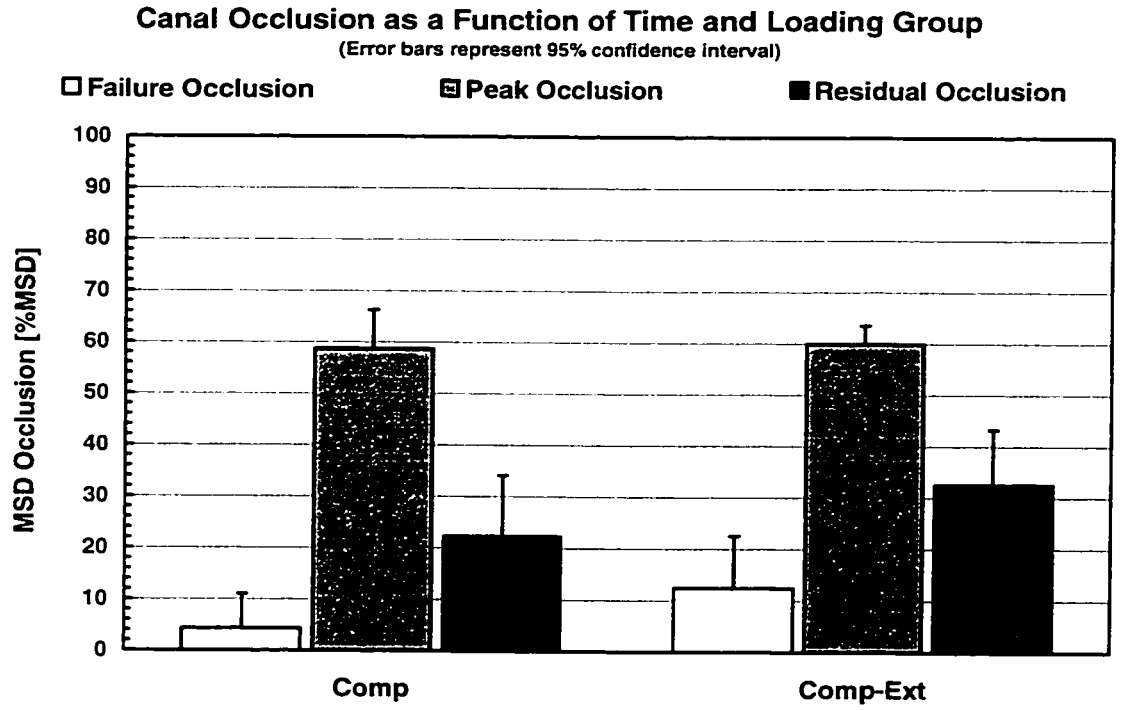

Figure 37: Graphical representation of the average canal occlusion data as a function of time and loading group. Failure occlusion represents the occlusion measured at the point where the loading history demonstrates a failure in the specimen. The peak occlusion is the maximum occlusion measured during the experiment. Post-injury occlusion is the occlusion measured immediately post-injury after the specimen was unloaded.

The repeated measures analysis also provided some insight into the effect of injury mechanism on canal occlusion (Hypothesis 3). As can be seen in the table (Table 9) and graph (Figure 37) above it appears that the peak occlusions, in particular, are nearly equal for both loading groups. The mean occlusion at failure and the mean residual occlusion for the compression-extension group appear similar to, but slightly larger than, their counterparts in the compression group. In the repeated measures analysis the main effect of loading group was found to be insignificant ($p = 0.187$). Thus, the null hypothesis for hypothesis 3 was accepted. However, the observed power for the test was a very low 0.251, indicating that there existed an almost 75% chance that the null hypothesis would be accepted when it should be rejected (Type II error). To increase the power would require the addition of more specimens to both groups. Therefore, it is indicated that

injury mechanism does not have an effect on canal occlusion, however, this result lacks the statistical power to make it truly definitive.

A simple linear regression was performed to elucidate the relationship, if any, between peak occlusion and residual occlusion. A plot of peak occlusion versus residual occlusion is provided in Figure 38. The plot also shows the output from the linear regression. The linear regression output reveals that the strength of the relationship is very weak ($R^2 = 0.207$) and that the slope is not significantly different from zero (Slope Sig. = 0.118). Based on this analysis the null hypothesis for hypothesis 5 was accepted. Therefore, there does not appear to be a direct relationship between peak occlusion and residual occlusion for the data generated in this study.

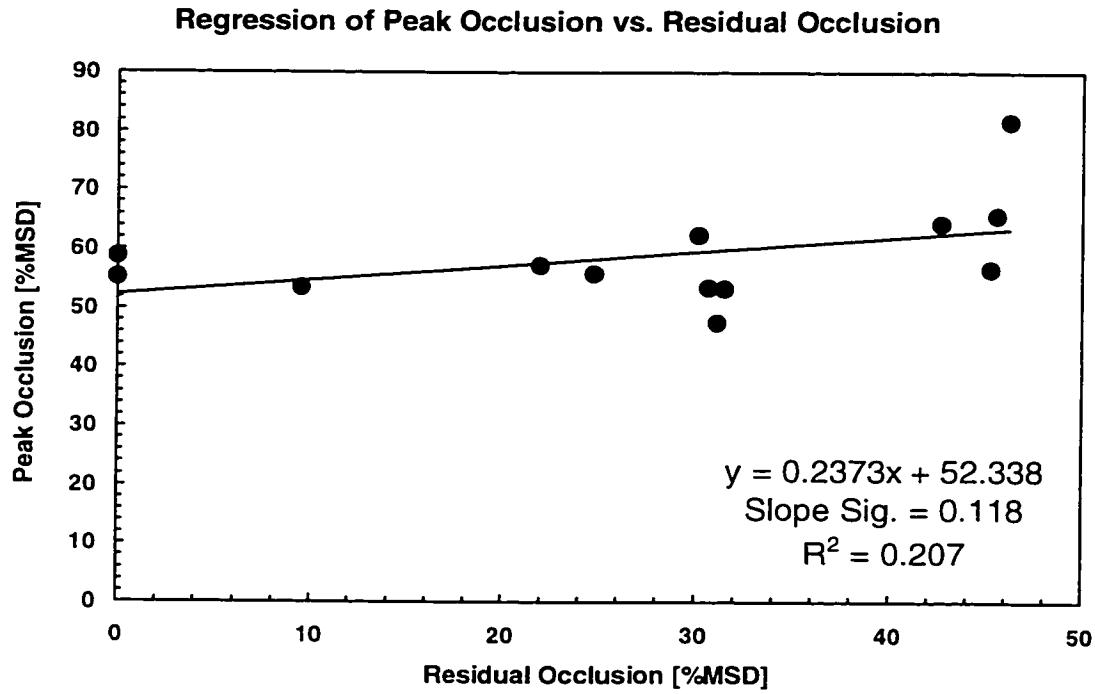

Figure 38: Plot of peak occlusion versus residual occlusion. Line represents linear regression through data. The equation for the line as well as statistics with regard to the significance and strength of the linear relationship between peak occlusion and residual occlusion are provided in the lower right hand corner of the graph.

8 DISCUSSION

The objective of this study was to examine the effect of midsagittal plane compressive loading mechanisms on structural injury patterns and neurologic injury potential, in cervical spine trauma. This objective was broken down into five hypotheses, which were evaluated by an experimental approach. The first null hypothesis was rejected indicating that different injury mechanisms produce distinct injury patterns. The second null hypothesis was also rejected indicating that structural injury patterns can be accurately classified by their injury mechanism (compression, compression-flexion, or compression-extension). The methods used to test these first two hypotheses provide a statistical basis for classification of compressive-type injury mechanisms by their injury pattern that is both discriminatory and accurate. The third null hypothesis was accepted suggesting that there is not a relationship between canal occlusion and injury mechanism, regardless of when the occlusion was measured (i.e. at structural failure, at peak occlusion, or immediately post-injury). Null hypothesis four was rejected indicating that the peak canal occlusion (during injury) was greater than that observed at structural failure and immediately post-injury. Finally, null hypothesis five was accepted demonstrating that there is no correlation between the peak occlusion measured during injury and the occlusion measured immediately post-injury. Therefore, with regard to spinal canal occlusion, a statistical difference was established between canal measurements made during failure, at peak, and post-injury; however, these differences did not elucidate a pattern to suggest a relationship with a particular injury mechanism nor did they provide predictive measures of peak occlusion given a post-injury (clinical) measurement. The implications of these findings will be discussed in the paragraphs to follow.

In recent years there has been some debate in the clinical community about classification schemes in general. Much of this debate has focused on the publication of classification schemes that lack scientific validation. In a 1993 Editorial in the Journal of Bone and Joint Surgery Albert Burstein stated that classification schemes are in essence part of a surgeons toolkit.[12] He later suggested that, before a classification scheme can be used as

a tool it should be examined in an appropriately structured experiment that shows that the tool is valid.[13]

In this study the concept of the mechanistic classification originally proposed by Roaf [77] and later refined and popularized by White and Panjabi [90], Allen et al. [5], and Myers and Winkelstein [52] was used as the basis for investigation. Three distinct injury mechanisms were applied to 2-FSU segments of the cervical spine. The resulting injury patterns were defined by examining all of the anatomical structures for the presence/absence of injury. Statistical analysis of the injury pattern data revealed that the three different injury mechanisms produced three distinct injury patterns. Additionally, three equations were developed providing the ability to classify an injury pattern by the injury mechanism that created it. These equations are efficient, in that they require knowledge of the status (intact/injured) of only a small subset of the available anatomical structures. Thus, these equation represent the basis for a Quantitative Mechanistic Classification scheme.

The most startling outcome of this study was the accuracy of the Quantitative Mechanistic Classification equations. The analysis shown in Appendix F provides the classification equation coefficients developed in this study (Table 10). These equations use the anterior longitudinal ligament (ALL), pedicle (PED), articular pillar (AP), ligamentum flavum (LF), spinous process (SP), and interspinous ligament (ISL) to assign an injury pattern to an injury mechanism. And, while, it remains to be seen how intra- and inter-observer effects will influence the accuracy of the classification equations, the analysis demonstrates that they were 100% accurate.

As can be seen in Table 10 the DA produced three sets of classification function coefficients, one set for each injury mechanism. Using these coefficients three separate equations can be produced to represent each injury mechanism. The equations are linear combinations of the coefficients multiplied by the binary injury status variable (i.e. intact and injured) for each structure considered (ALL, PED, AP, LF, SP, or ISL) plus the constant. To use these equations the binary injury status for each of the structures must

be known. The individual injury status values are then input into each of the three equations. The result of each equation is a scalar value. Group membership, for the pattern in question, is dictated by the equation that produces the largest scalar value. Thus, the evaluation of group membership is quantitative and simple.

Table 10: Tabulation of the function coefficients for each injury mechanism. These coefficients were produced by the Discriminant Analysis procedure. The anatomic structures selected by the Discriminant analysis were the anterior longitudinal ligament (ALL), pedicle (PED), articular pillar (AP), ligamentum flavum (LF), spinous process (SP), and interspinous ligament (ISL).

Classification Function Coefficients

	Injury Group		
	Comp	Comp-Flex	Comp-Ext
ALL	2.710	-4.742	2.710
PED	3.316	-11.053	-24.316
AP	6.079	-13.263	-27.079
LF	-.802	14.529	-1.907
SP	-1.961	19.182	67.671
ISL	-4.671	44.924	64.961
(Constant)	-3.503	-30.528	-66.503

Fisher's linear discriminant functions

The results of this study reveal a method with the potential to provide a simple and reliable quantitative mechanistic classification scheme. Furthermore, this quantitative mechanistic classification is "scaleable." As future experimental studies investigate the relationship between injury mechanism and injury pattern the results can be combined with previous results and upgraded classification equations developed. In this way continuous improvement of the classification will be possible, which is a characteristic that previous classification schemes do not possess.

A potential roadblock to the quantitative mechanistic classification scheme is usability. It is not difficult to deduce that clinicians will shy away from a classification if it is cumbersome. Harris suggested that a classification scheme should be simple, pragmatic, and understandable with equal application to the clinician and theorist (biomechanician).[28] The quantitative mechanistic classification is simple because it only

asks the clinician to examine a few structures for injury. It is pragmatic if and only if imaging studies (CT and MRI) are generated to observe the few structures required. It is understandable because it reduces previously complex and misleading descriptions down to simple "on" or "off" binary examinations with a clear quantitative output. Thus, the quantitative mechanistic classification has the potential to be highly usable, especially when compared to previous classification schemes.

Although, the different injury mechanisms in this study produced distinctly different injury patterns, the affect was not carried over to neurologic injury potential. Unfortunately, this comparison could only be made for the compression and compression-extension mechanisms because the data for the compression-flexion series was found to be unreliable. Nonetheless, the results demonstrate that injury mechanism did not have a significant affect on magnitude of canal occlusion at any point before, during, or after the injury. Thus, for the conditions of these tests there was no significant difference in neurologic injury potential when injury mechanism was considered.

Previous studies have suggested a significant affect of loading rate on peak canal occlusion for the same injury mechanism. [18, 85] Coupling the results of those studies with the results of this study, where similar displacements and loading rates were used with different injury mechanisms, leads to the conclusion that loading rate may have a greater effect on neurologic injury potential than mechanism. Further investigation will be required to truly elucidate the relationships between mechanism, loading rate, and neurologic injury potential.

A previous study by the author demonstrated that the peak canal occlusion measured during injury was always larger than occlusion measured post-injury.[18] The results of this study provide further support for that finding. In addition, the results of the present study demonstrated that the peak occlusion was always larger than occlusion measured at structural failure, and that the occlusion measured immediately post-injury was, on average, significantly larger than occlusion measured at the point of structural failure.

Putting the occlusion results in context, it appears that little or no occlusion is created prior to structural failure, then once failure occurs the occlusion begins to rapidly increase until the peak displacement is reached. As the load is released and the specimens "decompress" the occlusion falls off, and, generally, a significant residual occlusion remains. The obvious implication would be that preventing structural failure (injury) prevents neurologic injury. The results also support the idea that the peak occlusion measured during injury is the primary variable responsible for initiating neurologic injury, especially when its magnitude is compared to the occlusions measured at failure and immediately post-injury.

What a clinician sees, in terms of occlusion, is comparable to the results for occlusion measured immediately post-injury. An obvious question is, if the peak occlusion is the primary variable responsible for neurologic injury potential can it be predicted based on the occlusion measured immediately post-injury? The answer to this question is, in all likelihood, no. The regression of peak occlusion versus occlusion measured immediately post-injury (Figure 38) demonstrated that there wasn't a significant relationship. This finding supports the idea that the occlusion measured immediately post-injury is merely a snapshot of a moving target. [18, 21] As a patient is treated the damaged elements in his/her cervical spine are likely to shift, thereby resulting in a time-varying post-injury occlusion.[5]

Measurements of the reduction in canal space available to the spinal cord are ultimately meaningless unless they can be related in some way to neurologic injury. There are two studies which can provide some meaningful insight. In 1982 Anderson [6] used a plunger type device to apply well-controlled high-velocity insults (2 m/s) to ferret spinal cords. They were able to quantify the degree of damage and relate it back to the amount of cord deformation. They found that a 10-30% spinal cord occlusion (by midsagittal diameter) did not produce significant neurologic impairment. Between 40 and 60% cord occlusion they observed impaired neuronal conduction, which they felt could be partially, but not

completely, recovered from. Above 75% cord occlusion their was no functional recovery.

In 1988 Kearney et al. expanded on the work of Anderson and performed a comprehensive set of experiments to relate the amount of spinal cord occlusion and the velocity of occlusion to neurologic deficit.[38] They found that as occlusion velocity increased up to ~ 3 m/s complete neurologic impairment was highly likely for cord occlusions above 50%, which was consistent with the results of Anderson's study.[6] For occlusion velocities beyond ~ 3 m/s the amount of occlusion required to create complete neurologic impairment decreased monotonically relative to the 50% required for occlusion velocities below 3 m/s (Figure 10). Generally, they noted that, regardless of rate, a cord occlusion of 50% or more was indicative of complete neurologic injury.

In the present study the maximum canal occlusion measured was 81.6% in specimen 40. A calculation based on the size of the canal and the time to reach peak occlusion suggests that the occlusion velocity was ~ 1 m/sec. The occlusion velocity for specimen 40 represents the highest occlusion velocity observed in this study and falls into the 0 to 3 m/s occlusion velocity range where the studies of Anderson [6] and Kearney et al. [38] provide data useful for examining neurologic injury potential. Thus, the neurologic injury potentials for the tests conducted in this study were assessed based on the work of Anderson [6] and Kearney et al.[38]

To assess the neurologic injury potential for this study the cord MSD occlusion was estimated from the canal MSD occlusion so that comparisons could be made with the studies by Anderson [6] and Kearney et al.[38] This estimation was performed using Equation 23 where $\%MSD_{CANAL}$ is the measured canal occlusion, MSD_{CANAL} is the intact MSD of the canal at the level of the middle vertebra, and MSD_{CORD} is average MSD of the human cervical spinal cord. The variables $\%MSD_{CANAL}$ and MSD_{CANAL} are known results of this study. The variable MSD_{CORD} was obtained from Lang [40] whose cord MSD

measurements indicate that the average human cervical spinal cord is ~ 8.3 mm in diameter.

Equation 23: Equation used to estimate cord MSD occlusion ($\%MSD_{CORD}$) from canal MSD occlusion ($\%MSD_{CANAL}$). This equation uses the intact canal MSD at the level of the middle vertebra (MSD_{CANAL}) and the average cord MSD derived from the measurements of Lang [40] (MSD_{CORD}) to compute the cord occlusion estimate.

$$\%\ MSD_{CORD} = \left(\frac{\left(\frac{\%\ MSD_{CANAL}}{100} \right) \cdot MSD_{CANAL} - (MSD_{CANAL} - MSD_{CORD})}{MSD_{CORD}} \right) \cdot 100$$

The results of estimating the cord occlusion using Equation 23 can be found in Table 11. Using the threshold levels provided by Anderson [6] and Kearney et al. [38] it would appear that the cord occlusion produced in the test of specimen 40 is consistent with a non-recoverable neurologic injury. Specimens 28, 14, 39, 43, 45, and 47 sustained cord occlusions that would be consistent with a partially recoverable neurologic injury. And, specimens 10, 12, 23, 44, 46, and 41 sustained non-injurious cord occlusions. Thus, this study produced a broad range of neurologic injury potentials.

Table 11: Results of converting the canal MSD occlusions measured in this study into cord MSD occlusions using Equation 23.

Mechanism	Specimen	Canal MSD Occ (% MSD)	Canal MSD - Middle Vertebra (mm)	Cord MSD Occ (% MSD)
Compression	10	56	13.9	26
	12	55	14.7	20
	23	53	16.2	8
	28	59	13	36
	40	82	14.9	68
	44	48	16.2	0
	46	54	14.9	17
Compression-Extension	14	53	12.2	31
	39	57	12.8	34
	41	57	13.8	29
	43	66	14.6	40
	45	64	14.3	38
	47	62	13.4	39

A closer review of the data contained in Table 11 reveals a link between canal occlusion and neurologic injury potential, namely the initial diameter of the spinal canal. The results of estimating the cord occlusion from the canal occlusion suggest that larger spinal canals offer more protection to the spinal cord. Thus, any study evaluating neurologic injury potential should pay close attention to the initial diameter of the spinal canal as it relates to the size of the spinal cord.

9 LIMITATIONS

The following is a discussion of some areas where the results of this research are limited. Additionally, the following discussion will provide insight regarding the overall effects of these limitations and/or describe areas where further research is needed to overcome a given limitation.

The average age of the specimens used in this study was approximately 70 years (range 30 to 94 years). Since axial compressive injuries are most common for individuals in the second and third decades of life, are the results of this study useful for application to the segment of the population most at risk? With respect to injury pattern there may be some effect of age, however, it appears to be small in comparison to the effect of injury mechanism. Specifically, the different injury mechanisms applied in this study produced distinctly different injury patterns, even though a broad range of ages were present in each group (compression – 34 to 84 years, compression-flexion – 34 to 90 years, and compression-extension – 55 to 94 years). With respect to canal occlusion, age also appears to play a limited role, as there were instances where younger specimens, with approximately equivalent canal sizes, exhibited larger canal occlusions for similar inputs. Nevertheless, age does play some role and its effects on injury pattern and canal occlusion should be studied more closely in future studies.

Originally, this study was designed test 24 C5-7 2-FSU specimens. However, the limited availability and quality of cervical spine tissues made it difficult to collect the required number of C5-7 specimens. So, the decision was made to harvest C5-7 if it met the inclusion criteria, however, if it did not then the nearest 2-FSU specimen to C5-7, which met the inclusion criteria, was harvested for testing. As a result the harvested levels varied from C2-4 to C6-T1.

The analyses performed in this study did not take into account differences in harvest location. In part, some of the variability associated with harvest location was eliminated

by randomly assigning specimens, regardless of harvest location, to each of the three injury mechanism groups. Regardless, there may still be an effect of harvest location. Unfortunately, there are not enough specimens in this data set to examine it. Further study where different mechanisms are applied to groups segregated based on harvest location is required to adequately tease out a relationship between harvest location and injury pattern or canal occlusion.

All of the specimens in this study were osteoligamentous, meaning that all of the musculature was removed. Generally it is assumed that lack of musculature is of little significance to studies where axial compressive loading is applied to the cervical spine, because the musculature cannot bear compressive loads. In this study the compression and compression-extension mechanisms did not exhibit motions during injury that would tend to suggest an increased contribution of the musculature. In contrast, the compression-flexion series demonstrated that musculature may play a significant role in the injury event. Specifically, it was noted that the compression-flexion specimens exhibited primarily soft-tissue failures that progressed from the rear of the specimen (i.e. supraspinous ligament) forward. The progression of soft-tissue failure from posterior to anterior was primarily due to splaying of the posterior elements by the applied flexion moment. In this context musculature may have played a role in defining the injury, because the tendency of the posterior elements to splay under the application of flexion moment would result in the production of tension in the posterior spinal musculature, which could affect the load required to produce failure and potentially the appearance of the injury. Further study is suggested to investigate the effect of spinal musculature on compression-flexion injuries.

Two different types of boundary condition were applied to the test specimens in this research: fixed-fixed (compression) and fixed-free (compression-flexion and compression-extension). For the compression series the fixed-fixed boundary condition was effective in keeping the compressive load focused over the vertebral body. For the

compression-flexion and compression-extension series the fixed-free boundary condition allowed the compressive load to migrate beyond the vertebral body in the anterior and posterior directions, respectively. Thus, it was possible to effectively apply the three different injury mechanisms examined in this study. However, within the cervical spine the boundary conditions for a given 2-FSU segment will be neither fixed-fixed or fixed-free. Instead, it is more likely that the boundary conditions at either end of a segment will be variable, and lie somewhere between fixed and free. Therefore, the boundary conditions used in this study, while being reasonable first order approximations, do not represent the actual boundary conditions for a 2-FSU segment under axial compressive loading. Further research is needed to investigate methods for applying more realistic boundary conditions when conducting 2-FSU testing.

A significant limitation of this study is related to the fact that the author was solely responsible for inspecting the tested specimens and defining injury patterns. Although the author has more than 8 years of experience investigating cervical spine trauma, there is still a need to address inter- and intra-observer reliability to fully assess the results of the injury pattern analysis and the efficacy of the Quantitative Mechanistic Classification. Nonetheless, it is reasonable that a high degree of inter- and intra-observer reliability will be found when examining the injury patterns produced in this study, because each individual structure is evaluated in a simple binary manner – injured or uninjured – making it much more likely that independent observations will agree.[49, 50]

In this study hard-tissue injuries were primarily assessed by CT, a standard clinical tool, while soft-tissue injuries were primarily assessed by dissection. Even though dissection represents the "gold standard" for assessing musculoskeletal injury, it cannot be applied clinically. This begs the question, how can the proposed Quantitative Mechanistic Classification be useful if three of the six structures it relies on require dissection to determine their injury status? In a recent study, Vaccaro et al. demonstrated that injuries to the soft-tissues of the cervical spine can be accurately assessed using Magnetic

Resonance Imaging (MRI).[86] Thus, the Quantitative Mechanistic Classification may indeed be useful if MRI is used to define soft-tissue injuries.

The Quantitative Mechanistic Classification scheme described in this dissertation provides a method for defining how an injury was produced. In the clinical realm, though, a classification scheme should also provide information regarding relevant clinical factors, such as instability, recommended treatment/management, and prognosis. Thus, the Quantitative Mechanistic Classification is, at present, limited in its applicability to patient care. It is hoped that the results of this study will encourage future investigations to incorporate clinical factors and make the Quantitative Mechanistic Classification a useful tool.

A significant component of this research revolved around investigating the effect of injury mechanism on neurologic injury potential through the measurement of canal occlusion. Unfortunately, the effect of injury mechanism on canal occlusion could only be investigated for the compression and compression-extension injury mechanisms. The data from compression-flexion series was not included in the analysis because it was found to be unreliable.

Examination of the canal occlusion data from the compression-flexion series revealed that the SCOT was being placed in tension and kinked during the tests, which revealed itself as large oscillations in the SCOT output in each sensing section. These large oscillations considered alone would suggest that the tube was being occluded and released several times during the test. Review of the high speed film, however, did not suggest such an occurrence. It appears that the SCOT may be ill suited for measuring canal occlusion in an environment where it is placed under tension. Further investigation should be conducted to examine the behavior of the SCOT under tensile loading and develop, if possible, a means for overcoming this apparent limitation of the SCOT.

The fundamental relationship between canal occlusions measured in this study and actual human neurologic injury is unknown and represents a limitation when interpreting the canal occlusion data. In order to get an idea of the degree of neurologic injury produced by a certain magnitude of canal occlusion, a given canal occlusion can be compared to animal studies relating occlusion to spinal cord injury severity. Needless to say, an animal study may not be directly applicable to the human condition. However, since comparable human data can never be generated, the use of animal data provides the best tool for assessing neurologic injury potential from canal occlusion measurements.

10 CONCLUSIONS

The objective of this study was to examine the effect of midsagittal plane compressive loading mechanisms on structural injury patterns and neurologic injury potential, in cervical spine trauma. The results of this study clearly indicate that injury mechanism does have a significant effect on injury pattern. Not only did the analysis show that compression-flexion, compression, and compression-extension result in distinct injury patterns, it was determined that the injury patterns could be classified by injury mechanism with 100% accuracy. Although the effects of inter- and intra-observer variability remain to be investigated, there may be significant potential for the use of injury pattern analysis, like that conducted in this study, to develop a clinically reliable classification tool.

With respect to the affect of injury mechanism on neurologic injury potential, this study did not show a significant effect. However, in examining the compression and compression-extension data, there did appear to be a slight trend toward larger occlusions at failure and post-injury for the compression-extension group. Also, the peak occlusions during injury represent a significant potential for neurologic injury as on average ~ 60% of the available midsagittal diameter was pinched off during injury in both the compression and compression-extension groups. Unfortunately, this finding only applies to the compression-extension and compression injury mechanism groups, as the occlusion data for the compression-flexion series was not reliable.

Analysis of the time histories of occlusion demonstrated that there is a significant overall effect of the time at which occlusion is measured. The peak occlusion produced during an experiment was always larger than occlusion measured at the point of structural failure or immediately post-injury. And, there was no relationship between the peak occlusion and the residual occlusion. Also, there was a significant difference between occlusion measured at failure, which generally tended toward a value of zero, and occlusion measured immediately post injury. These results reinforce the findings of the author's

earlier work concerning the time history of occlusion in compressive cervical spine trauma. [18]

11 POTENTIAL FOR FUTURE RESEARCH

Further development of the Quantitative Mechanistic Classification for cervical spine trauma has the potential to stimulate a significant amount of future research. Part of this future research may result from the fact that the Quantitative Mechanistic Classification is upgradeable, which is a feature not inherent to previous classification schemes. It can be upgraded by the addition of injury pattern data for specific injury mechanisms. With the additional injury pattern data the equations, which form the foundation of the classification, can be refined and redefined, as necessary. Considering the number of potential injury mechanisms associated with cervical spine trauma there is a significant amount of clinical and biomechanical research that can be conducted to unearth more injury pattern data for upgrading the classification. Furthermore, research to uncover the effects of injury mechanism on neurologic injury potential and instability coupled with clinical research regarding treatment, management, and prognosis will provide valuable data for improving the Quantitative Mechanistic Classification. Thus, there are a vast number of opportunities for future research associated with the investigation of the Quantitative Mechanistic Classification.

12 LIST OF REFERENCES

1. Afifi, A.A. and V. Clark, *Computer Aided Multivariate Analysis*. 3rd ed. 1996, New York, NY: Chapman and Hall.

2. Alem, N.M., G.S. Nusholtz, and J.W. Melvin. *Head and Neck Response to Axial Impacts*. in *Proceedings of the 28th Stapp Car Crash Conference*. 1984.

3. Allen, A.R., *Surgery of Experimental Lesion of Spinal Cord Equivalent to Crush Injury of Fracture Dislocation of Spinal Column.* JAMA, 1911. **57**(11): p. 878-80.

4. Allen, A.R., *Remarks on the Histopathological Changes in the Spinal Cord Due to Impact: An Experimental Study.* J Nerv Ment Dis, 1914. **41**: p. 141-7.

5. Allen, B.L., et al., *A Mechanistic Classification of Closed, Indirect Fractures and Dislocation of the Lower Cervical Spine.* Spine, 1982. **7**(1): p. 1-27.

6. Anderson, T.E., *A Controlled Pneumatic Technique for Experimental Spinal Cord Contusion.* J Neurosci Methods, 1982. **6**: p. 327-33.

7. Babcock, J.L., *Cervical Spine Injuries: Diagnosis and Classification.* Archives of Surgery, 1976. **111**: p. 646-651.

8. Bates-Carter, J.W., R.P. Ching, and A.F. Tencer. *Transient Changes in Canal Geometry During Axial Burst Fracture of the Cervical Spine*. in *Proceedings of the 5th Annual Symposium on Injury Prevention through Biomechanics*. 1995. Detroit: Centers for Disease Control.

9. Braakman, R. and L. Penning, *Mechanisms of Injury to the Cervical Cord.* Paraplegia, 1973. **10**(4): p. 314-20.

10. Burke, D.C., H.T. Burley, and G.H. Ungar, *Data on Spinal Injuries-Part I. Collection and Analysis of 352 Consecutive Admissions.* Austr N.Z. J Surg, 1985. **55**: p. 3-12.

11. Burney, R.E., et al., *Incidence, Characteristics, and Outcome of Spinal Cord Injury at Trauma Centers in North America.* Arch Surg, 1993. **128**(5): p. 596-9.

12. Burstein, A.H., *Fracture Classification Systems: Do They Work and Are They Useful? [Editorial] [See Comments].* J Bone Joint Surg Am, 1993. **75**(12): p. 1743-4.

13. Burstein, A.H., *Fracture Classification Systems: Do They Work and Are They Useful? Replies to Letters [Letter; Comment].* J Bone Joint Surg Am, 1993. **75**(12): p. 789-793.

14. Camacho, D.L., et al. *Experimental Flexibility Measurements for the Development of a Computational Head-Neck Model Validated for near-Vertex Head Impact.* in *Proceedings of the 41st Stapp Car Crash Conference.* 1997: SAE.

15. Camacho, D.L.A., *Dynamic Response of the Head and Cervical Spine to near-Vertex Head Impact: An Experimental and Computational Study*, in *Biomedical Engineering.* 1998, Duke University: Durham, NC. p. 193.

16. Camacho, D.L.A., R.W. Nightingale, and B.S. Myers, *Surface Friction in near-Vertex Head and Neck Impact Increases Risk of Injury.* Journal of Biomechanics, 1999. **32**: p. 293-301.

17. Carter, J.W., et al. *Transient Changes in Cervical Spinal Canal Geometry During Wedge Compression Fracture.* in *6th Injury Prevention through Biomechanics Symposiumq.* 1996. Detroit: CDC.

18. Carter, J.W., et al., *Canal Geometry Changes Associated with Axial Compressive Cervical Spine Fracture.* Spine, 2000. **25**(1): p. 46-54.

19. Cavanaugh, J.M. and A.I. King, *Control of Transmission of Hiv and Other Bloodborne Pathogens in Biomechanical Cadaveric Testing.* J Orthop Res, 1990. **8**: p. 159-166.

20. Chang, D.G., et al., *Geometric Changes in the Cervical Spinal Canal During Impact.* Spine, 1994. **19**(8): p. 973-80.

21. Ching, R.P., *Residual Stability in Thoracolumbar Spine Fractures: A Biomechanical Study*, in *Mechanical Engineering.* 1992, University of Washington: Seattle, Washington. p. 172.

22. Crowell, R.R., et al., *Cervical Injuries under Flexion and Compression Loading.* J Spinal Disord, 1993. **6**(2): p. 175-81.

23. Denis, F., *The Three Column Spine and Its Significance in the Classification of Acute Thoracolumbar Spinal Injuries.* Spine, 1983. **8**: p. 817-831.

24. Edwards, W.T., *Principles of Cervical Spine Biomechanical Testing*, in *Frontiers in Head and Neck Trauma*, N. Yoganandan, et al., Editors. 1998, IOS Press: Washington, D.C. p. 217-231.

25. Eppinger, R., et al., *Supplement: Development of Improved Injury Criteria for the Assessment of Advanced Automotive Restraint Systems - Ii.* 2000, National Highway Transportation Safety Administration. p. 40.

26. Fife, D. and J. Kraus, *Anatomic Location of Spinal Cord Injury: Relationship to the Cause of Injury.* Spine, 1986. **11**(1): p. 2-5.

27. Fontijne, W.P., et al., *Ct Scan Prediction of Neurological Deficit in Thoracolumbar Burst Fractures [Published Erratum Appears in J Bone Joint Surg Br 1993 Jan;75(1):169].* J Bone Joint Surg, 1992. **74B**(5): p. 683-5.

28. Harris, J.H., B. Edeiken-Monroe, and D.R. Kopaniky, *A Practical Classification of Acute Cervical Spine Injuries.* Orthop Clin North Am, 1986. **17**(1): p. 15-30.

29. Hashimoto, T., K. Kaneda, and K. Abumi, *Relationship between Traumatic Spinal Canal Stenosis and Neurologic Deficits in Thoracolumbar Burst Fractures.* Spine, 1988. **13**(11): p. 1268-72.

30. Heller, J.G. and F.X. Pedlow, Jr., *Anatomy of the Cervical Spine*, in *The Cervical Spine*, C.R. Clark, Editor. 1998, Lippincott-Raven: Philadelphia, PA. p. 3-36.

31. Hodgson, V.R. and L.M. Thomas. *Mechanisms of Cervical Spine Injury During Impact to the Protected Head.* in *Proceedings of the 24th Stapp Car Crash Conference.* 1980.

32. Holdsworth, F., *Fractures, Dislocations, and Fracture-Dislocations of the Spine.* J Bone Joint Surg Am, 1970. **52**(8): p. 1534-51.

33. Jenkins, D.B., *Hollinshead's Functional Anatomy of the Limbs and Back.* 6th ed. Functional Anatomy of the Limbs and Back, ed. M.M. Biblis. 1991, Philadelphia, PA: W.B. Saunders Company.

34. Kaigle, A., et al. *Minimum Thawing Time of Frozen Spinal Specimens Used for in-Vitro Biomechanical Testing.* in *XVIIth ISB Congress.* 1999. Calgary, Alberta, Canada: ISB.

35. Kang, J.D., M.P. Figgie, and H.H. Bohlman, *Sagittal Measurements of the Cervical Spine in Subaxial Fractures and Dislocations.* J. Bone Joint Surg., 1994. **76A**(11): p. 1617-28.

36. Kazarian, L., *Injuries to the Human Spinal Column: Biomechanics and Injury Classification.* Exercise and Sports Sciences Reviews, 1981. **9**: p. 297-352.

37. Kazarian, L., *Classification of Simple Spinal Injuries*, in *Impact Injury of the Head and Spine*, C.L. Ewing, et al., Editors. 1983, Charles C. Thomas: Springfield, Illinois. p. 72-93.

38. Kearney, P.A., et al., *Interaction of Contact Velocity and Cord Compression in Determining Severity of Spinal Cord Injury.* J Neurotrauma, 1988. **5**(3): p. 187-207.

39. Kiwerski, J., *The Influence of the Mechanism of Cervical Spine Injury on the Degree of the Spinal Cord Lesion.* Paraplegia, 1991. **29**(8): p. 531-6.

40. Lang, J., *Clinical Anatomy of the Cervical Spine*. 1993, New York, NY: Thieme Medical Publishers, Inc.

41. Linde, F. and H.C. Sorensen, *The Effect of Different Storage Methods on the Mechanical Properties of Trabecular Bone.* J Biomech, 1993. **26**(10): p. 1249-52.

42. Maiman, D.J., et al., *Compression Injuries of the Cervical Spine: A Biomechanical Analysis.* Neurosurgery, 1983. **13**(3): p. 254-60.

43. McAfee, P.C., et al., *The Value of Computed Tomography in Thoracolumbar Fractures: An Analysis of One Hundred Consecutive Cases and a New Classification.* J Bone Joint Surg, 1983. **65A**: p. 461-473.

44. McElhaney, J.H., et al., *Combined Bending and Axial Loading Responses of the Human Cervical Spine.* Transactions of the SAE, 1988. **SAE Paper #881709**: p. 1090-97.

45. McElhaney, J.H. and B.S. Myers, *Biomechanical Aspects of Cervical Trauma*, in *Accidental Injury: Biomechanics and Prevention*, A.M. Nahum and J.W. Melvin, Editors. 1993, Springer-Verlag: New York. p. 311-361.

46. McElhaney, J.H., et al., *Cervical Spine Compression Responses.* Proceedings of the 27th Stapp Car Crash Conference, 1983: p. 163-177.

47. McElhaney, J.H., et al., *Biomechanical Analysis of Swimming Pool Neck Injuries.* Transactions of the SAE, 1979. **88**: p. 494-500.

48. Miller, T.R., et al., *Costs of Head an Neck Injury and a Benefit-Cost Analysis of Bicycle Helmets*, in *Head and Neck Injury*, R.S. Levine, Editor. 1994, Society of Automotive Engineering: New York. p. 211-40.

49. Mirza, S., *Personal Communication*. Personal Communication. 1996

50. Mirza, S.K. *Assessment of Instability in the Lower Cervical Spine: Application of the White and Panjabi Criteria and Anatomic Scoring to Cervical Spine Injuries.* in *Cervical Spine Res Soc.* 1996.

51. Myers, B.S., J.H. McElhaney, and R. Nightingale, *Cervical Spine Injury Mechanisms*, in *Head and Neck Injury*, R.S. Levine, Editor. 1994, Society of Automotive Engineers, Inc.: Warrendale, PA. p. 107-155.

52. Myers, B.S. and B.A. Winkelstein, *Epidemiology, Classification, Mechanism, and Tolerance of Human Cervical Spine Injuries.* Crit Rev Biomed Eng, 1995. **23**(5-6): p. 307-409.

53. Nightingale, R.W., et al. *The Dynamic Responses of the Cervical Spine: Buckling, End Conditions, and Tolerance in Compressive Impacts.* in *Proc. 41st Stapp Car Crash Conference.* 1997. Orlando, FL: SAE.

54. Nightingale, R.W., et al., *Experimental Impact Injury to the Cervical Spine: Relating Motion of the Head and the Mechanism of Injury.* J Bone Joint Surg, 1996. **78A**(3): p. 412-21.

55. Nightingale, R.W., et al., *Dynamic Responses of the Head and Cervical Spine to Axial Impact Loading.* J Biomechanics, 1996. **29**(3): p. 307-18.

56. Nightingale, R.W., et al. *The Influence of End Condition on Human Cervical Spine Injury Mechanisms.* in *Proc. 35th Stapp Car Crash Conference.* 1991.

57. Nightingale, R.W., W.J. Richardson, and B.S. Myers, *The Effects of Padded Surfaces on the Risk for Cervical Spine Injury.* Spine, 1997. **22**(20): p. 2380-7.

58. Nuckley, D.J., *Dynamic Response of Scot.* Personal Communication. 2001

59. Nuckley, D.J., *Neural Space Occlusion Transducer Error Analysis.* Personal Communication. 2001

60. Nushlotz, G.S., et al. *Response of the Cervical Spine to Superior-Inferior Head Impact.* in *Proceedings of the 25th Stapp Car Crash Conference.* 1981.

61. Nusholtz, G.S., et al. *Cervical Spine Injury Mechanisms.* in *Proceedings of the 27th Stapp Car Crash Conference.* 1983.

62. Ogata, T., et al., *Role of Aspartate in Ischemic Spinal Cord Damage.* J Orth Res, 1996. **14**: p. 504-10.

63. Oxland, T.R., et al., *An Anatomic Basis for Spinal Instability: A Porcine Trauma Model.* J Orthop Res, 1991. **9**(3): p. 452-62.

64. Panjabi, M.M., et al., *Cervical Human Vertebrae. Quantitative Three-Dimensional Anatomy of the Middle and Lower Regions.* Spine, 1991. **16**(8): p. 861-9.

65. Panjabi, M.M., et al., *Multidirectional Instabilities of Traumatic Cervical Spine Injuries in a Porcine Model.* Spine, 1989. **14**(10): p. 1111-1115.

66. Panjabi, M.M., et al., *Dynamic Canal Encroachment During Thoracolumbar Burst Fractures.* J Spinal Disord, 1995. **8**(1): p. 39-48.

67. Panjabi, M.M., et al., *Biomechanical Time-Tolerance of Fresh Cadaveric Human Spine Specimens.* J Orthop Res, 1985. **3**(3): p. 292-300.

68. Pintar, F., et al. *Biodynamics of the Total Human Cervical Spine.* in *32nd Stapp Car Crash Conference.* 1990.

69. Pintar, F.A. *Spinal Cord Injury Potential Using an Experimental Biomechanical Model.* in *Proc American Assoc Neurol Surgeons Ann Mtg.* 1995. Orlando, FL.

70. Pintar, F.A., et al., *Instrumented Artificial Spinal Cord for Human Cervical Pressure Measurement.* Biomed Matrls Engr, 1996. **6**(3): p. 219-229.

71. Pintar, F.A., et al., *Measurement of Dynamic Spinal Cord Pressure*, in *Crashworthiness and Occupant Protection in Transportation Systems.* 1993, Am Soc Mech Engr.

72. Pintar, F.A., et al., *Cervical Vertebral Strain Measurements under Axial and Eccentric Loading.* J Biomech Eng, 1995. **117**(4): p. 474-8.

73. Pintar, F.A., et al. *Kinematic and Anatomical Analysis of the Human Cervical Spinal Column under Axial Loading.* in *Proc. 33rd Stapp Car Crash Conf.* 1989.

74. Raynak, G.C., et al., *Transducers for Dynamic Measurment of Spine Neural-Space Occlusions.* Journal of Biomechanical Engineering, 1998. **120**: p. 787 - 791.

75. Riggins, R.S. and J.F. Kraus, *The Risk of Neurologic Damage with Fractures to the Vertebrae.* The Journal of Trauma, 1977. **17**(2): p. 126-133.

76. Roaf, R., *A Study of the Mechanics of Spinal Injuries.* The Journal of Bone and Joint Surgery, 1960. **42 B**(4): p. 810-23.

77. Roaf, R., *International Classification of Spinal Injuries.* Paraplegia, 1972. **10**(1): p. 78-84.

78. Rogers, W.A., *Fractures and Dislocations of the Cervical Spine.* J Bone Joint Surg, 1957. **39A**(2): p. 341-76.

79. Schneider, R.C., G. Cherry, and H. Pantek, *The Syndrome of Acute Central Cervical Spinal Cord Injury: With Special Reference to the Mechanisms Involved in Hyperextension Injuries of the Cervical Spine.* J Neurosurg, 1954. **11**: p. 546-577.

80. Schultz, A.B. and J.A. Ashton-Miller, *Biomechanics of the Human Spine*, in *Basic Orthopaedic Biomechanics*, V.C. Mow and W.C. Hayes, Editors. 1991, Raven Press: New York, NY. p. 337-376.

81. Sharma, S., *Applied Multivariate Techniques.* 1996, New York, NY: John Wiley & Sons Inc.

82. Shea, M., et al., *Variations of Stiffness and Strength Along the Human Cervical Spine.* J Biomech, 1991. **24**(2): p. 95-107.

83. Southern, E.P., et al., *Cervical Spine Injury Patterns in Three Modes of High-Speed Trauma: A Biomechanical Porcine Model.* J-Spinal-Disord, 1990. **3**(4): p. 316-28.

84. Torg, J.S., et al., *National Football Head and Neck Injury Registry: Report on Cervical Quadriplegia.* Am J Sports Med, 1979. **7**(2): p. 127-32.

85. Tran, N., et al., *Mechanism of the Burst Fracture in the Thoracolumbar Spine: The Effect of Loading Rate.* Spine, 1995. **20**: p. 1984-88.

86. Vaccaro, A.R., et al., *Magnetic Resonance Imaging Analysis of Soft Tissue Disruption after Flexion-Distraction Injuries of the Subaxial Cervical Spine.* Spine, 2001. **26**(17): p. 1866-72.

87. Viano, D.C., et al., *Injury Biomechanics Research: An Essential Element in the Prevention of Trauma.* J Biomechanics, 1989. **22**(5): p. 403-17.

88. Viidik, A. and T. Lewis, *Changes in Tensile Strength Characteristics and Histology of Rabbit Ligaments Induced by Different Modes of Post-Mortal Storage.* Acta Orthop Scand, 1966. **37**: p. 141.

89. White, A.A., III and M.M. Panjabi, *Clinical Biomechanics of the Spine.* 1978, Philadelphia: JB Lippincott Company.

90. White, A.A., III and M.M. Panjabi, *Clinical Biomechanics of the Spine*. 2nd Edition ed. 1990, Philadelphia: JB Lippincott Company.

91. Whitley, J.E. and H.F. Forsyth, *The Classification of Cervical Spine Injuries.* Archives of Surgery, 1976. **83**(4): p. 633-644.

92. Winkelstein, B.A. and B.S. Myers, *The Biomechanics of Cervical Spine Injury and Implications for Injury Prevention.* Med Sci Sports Exerc, 1997. **29**(7): p. S246-S255.

93. Winkelstein, B.A. and B.S. Myers, *Determinants of Catastrophic Neck Injury*, in *Frontiers in Head and Neck Trauma*, N. Yoganandan, et al., Editors. 1998, IOS Press: Washington, D. C. p. 266-295.

94. Woo, S.L., et al., *Effects of Postmortem Storage by Freezing on Ligament Tensile Behavior.* J Biomech, 1986. **19**(5): p. 399-404.

95. Yingling, V.R., J.P. Callaghan, and S.M. McGill, *Dynamic Loading Affects the Mechanical Properties and Failure Site of Porcine Spines.* Clinical Biomechanics, 1997. **12**(5): p. 301-5.

96. Yoganandan, N., et al. *Epidemiology and Injury Biomechanics of Motor Vehicle Related Trauma to the Human Spine.* in *Proc. 33rd Stapp Car Crash Conf.* 1989.

97. Yoganandan, N., et al., *Strength and Motion Analysis of the Human Head-Neck Complex.* J Spinal Disorders, 1991. **4**(1): p. 73-85.

98. Yoganandan, N., et al., *Strength and Kinematic Response of Dynamic Cervical Spine Injuries.* Spine, 1991. **16**(10 Suppl): p. S511-7.

99. Yoganandan, N., A. Sance, Jr., and F. Pintar, *Biomechanical Evaluation of the Axial Compressive Responses of the Human Cadaveric and Manikin Necks.* J Biomech Engr, 1989. **111**: p. 250-255.

100. Yoganandan, N., et al., *Experimental Spinal Injuries with Vertical Impact.* Spine, 1986. **11**(9): p. 855-60.

101. Yoganandan, N., et al., *Injury Biomechanics of the Human Cervical Column.* Spine, 1990. **15**(10): p. 1031-9.

102. Zhu, Q., et al., *Traumatic Instabilities of the Cervical Spine Caused by High-Speed Axial Compression in a Human Model.* Spine, 1999. **24**(5): p. 440-44.

103. Zolman, J.F., *Popular Post Hoc Multiple Comparison Tests*, in *Biostatistics: Experimental Design and Statistical Inference*. 1993, Oxford University Press: New York. p. 147-152.

13 APPENDICES

Appendix A Fixture Drawings

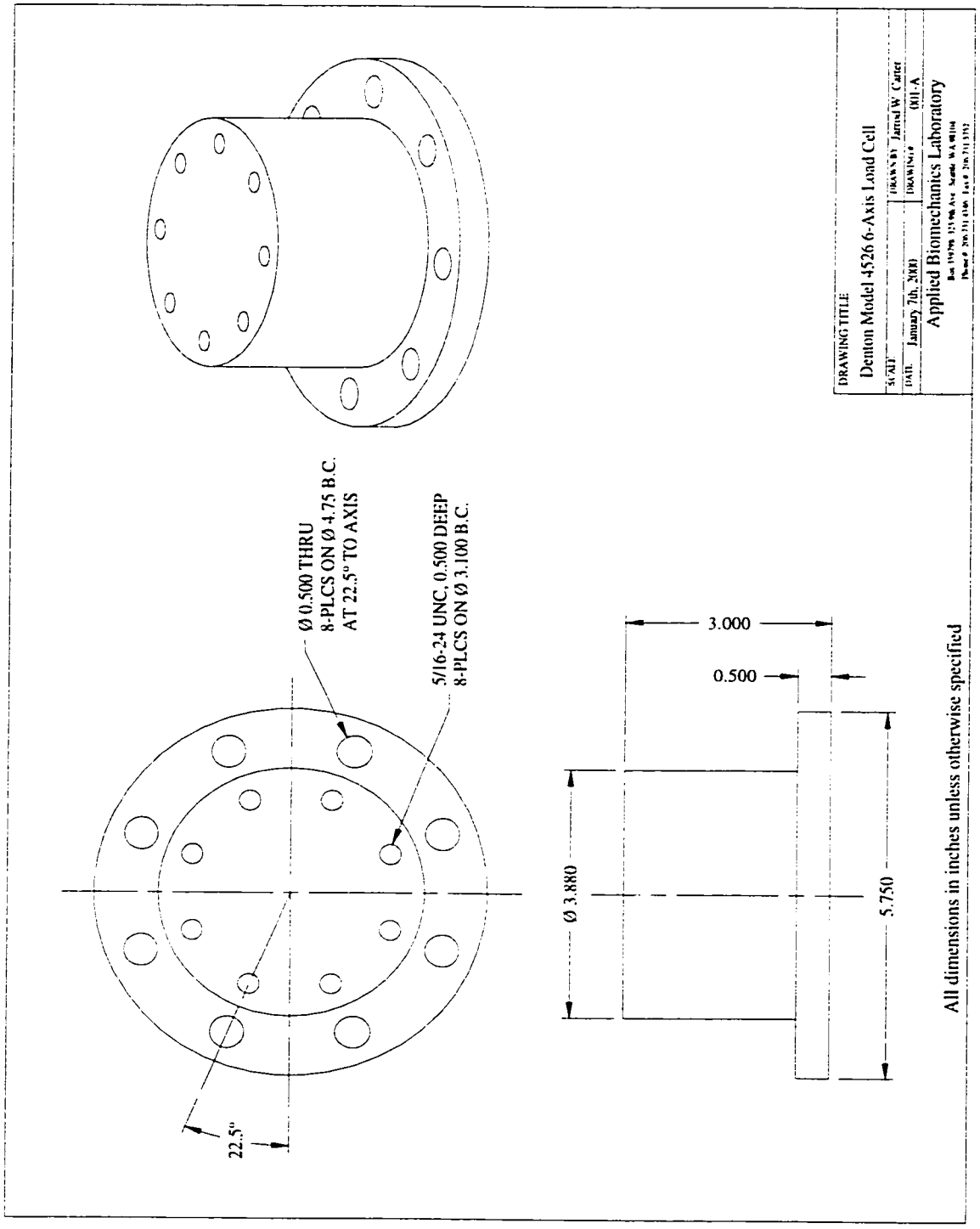

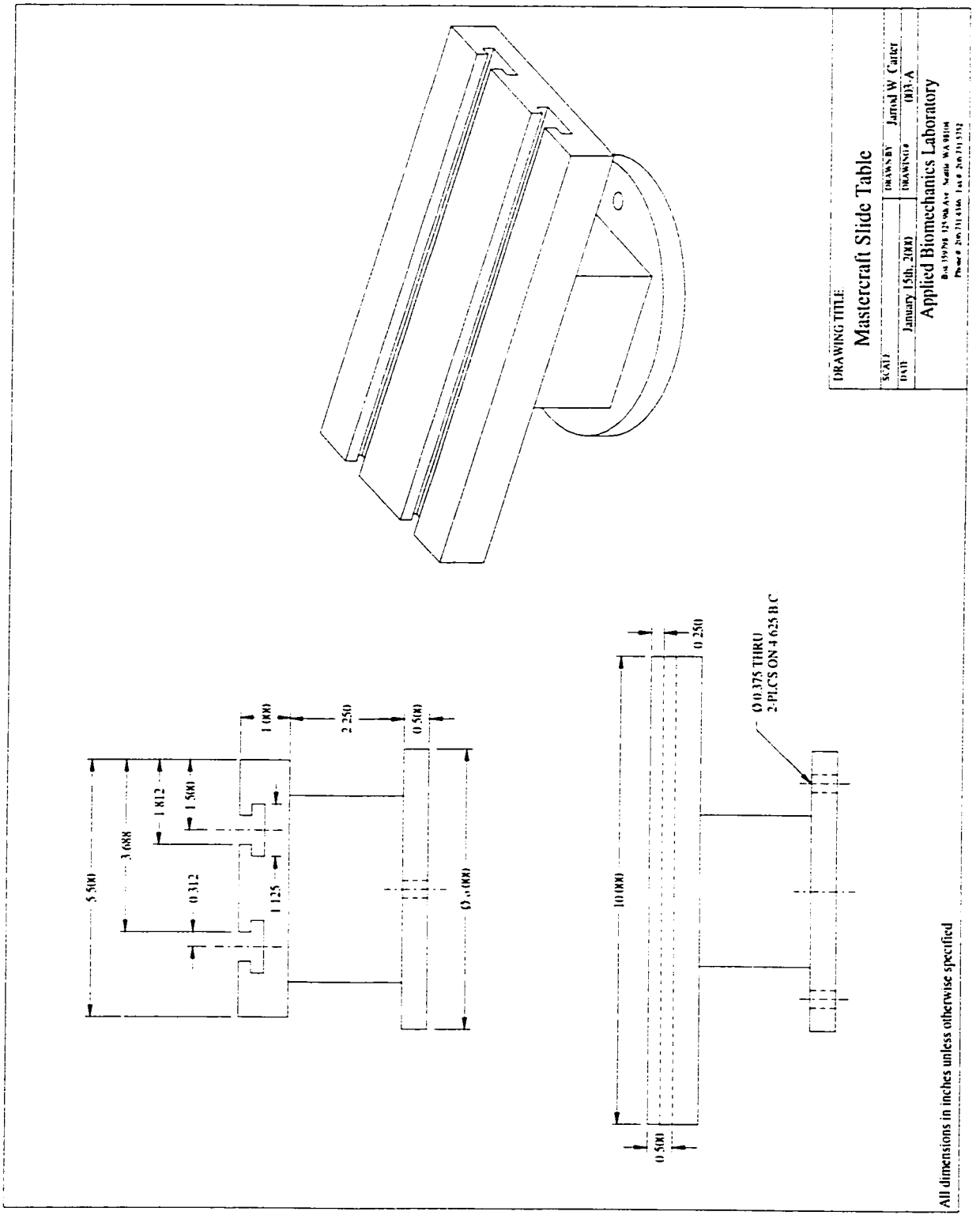
DRAWING TITLE
Mastercraft Slide Table
SCALE
DATE
January 15th, 2000
DRAWN BY
Jarrad W Carter
DRAWING #
003-A
Applied Biomechanics Laboratory
All dimensions in inches unless otherwise specified
5.500
3.688
1.812
1.500
0.312
1.125
1.000
2.250
0.500
10.000
0.500
0.250
Ø 0.375 THRU
2 PLCS ON 4.625 B.C.

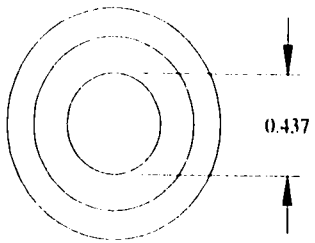

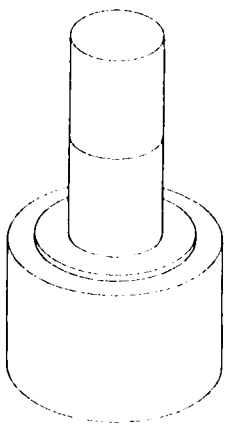

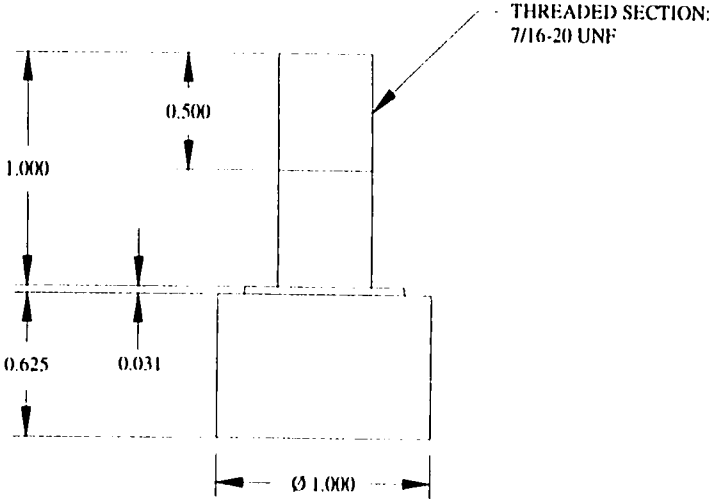

All dimensions in inches unless otherwise specified

DRAWING TITLE
McGill CAMROL CF-1-S Bearing

SCALE 15" = 12" (1.25X)	DRAWN BY Jarrod W. Carter
DATE January 14th, 2000	DRAWING # 004-A

Applied Biomechanics Laboratory

Box 359768 325 9th Ave Seattle WA 98104
Phone # 206.731.4366 Fax # 206.731.3192

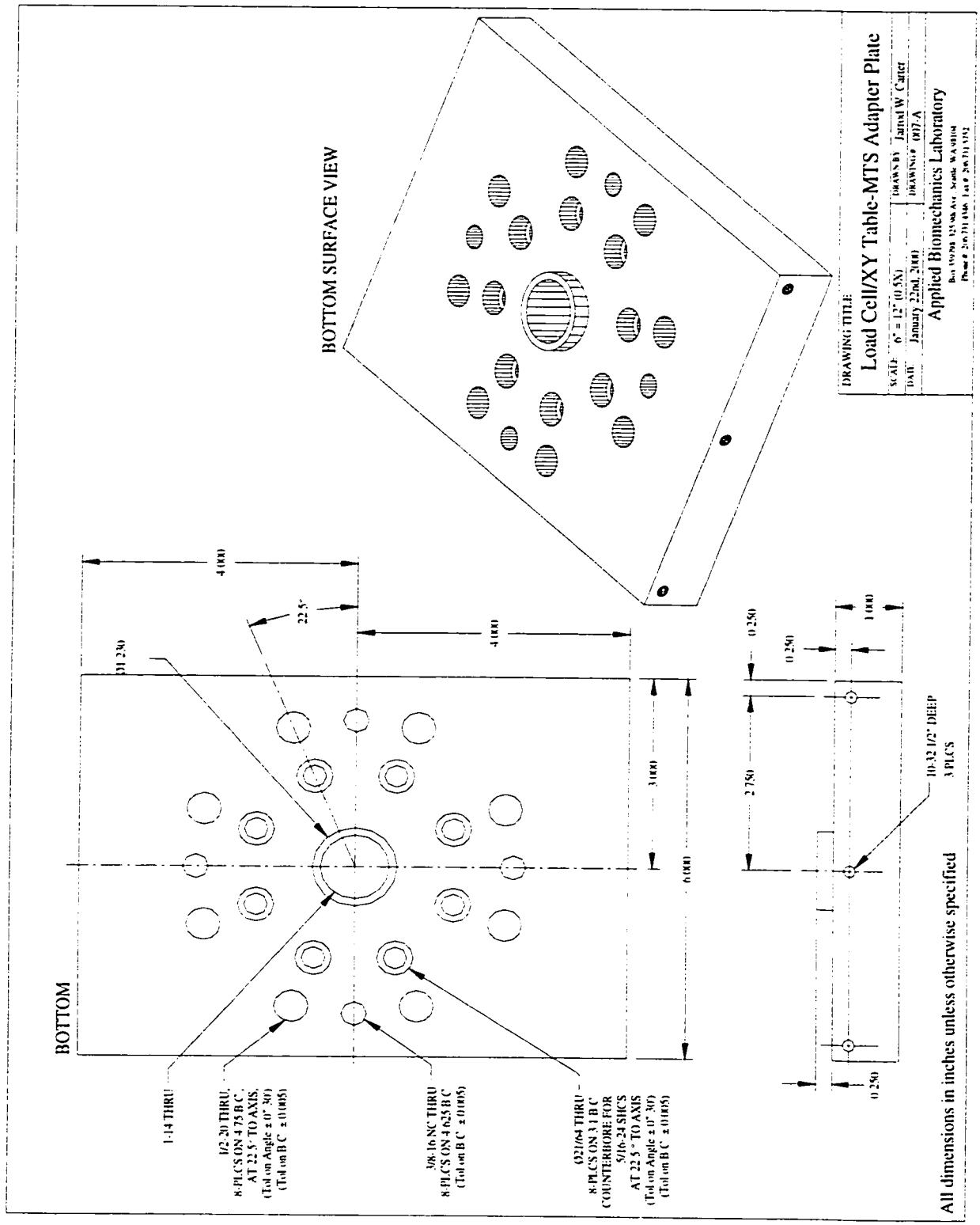
BOTTOM SURFACE VIEW
BOTTOM
DRAWING TITLE:
Load Cell/XY Table-MTS Adapter Plate
Applied Biomechanics Laboratory
All dimensions in inches unless otherwise specified
1-14 THRU
1/2-20 THRU, 8 PLCS ON 4.75 B.C. AT 22.5° TO AXIS, (Tol on Angle ± 0° 30') (Tol on B.C. ± 0.005)
3/8-16 NC THRU 8 PLCS ON 4.625 B.C. (Tol on B.C. ± 0.005)
0.21/64 THRU - 8 PLCS ON 3.1 B.C. COUNTERBORE FOR 5/16-24 SHCS AT 22.5° TO AXIS (Tol on Angle ± 0° 30') (Tol on B.C. ± 0.005)
10-32 1/2" DEEP 3 PLCS
4.000
3.000
2.750
0.250
1.000
22.5°

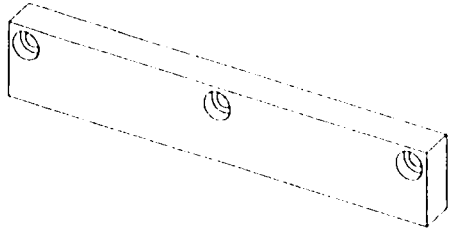

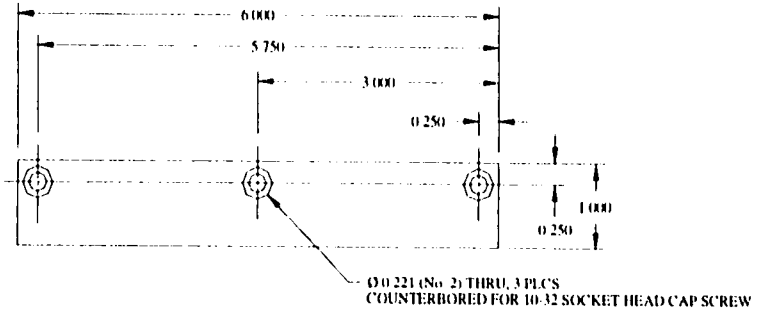

All dimensions in inches unless otherwise specified

DRAWING TITLE

LC/XY-MTS Adapter Retaining Plate

SCALE	6" = 12" (0.5X)	DRAWN BY	Jarrod W. Carter
DATE	January 24th, 2000	DRAWING #	008-A

Applied Biomechanics Laboratory

Box 359798 125 9th Ave Seattle WA 98104

Phone # 206.731.4166 Fax # 206.731.3252

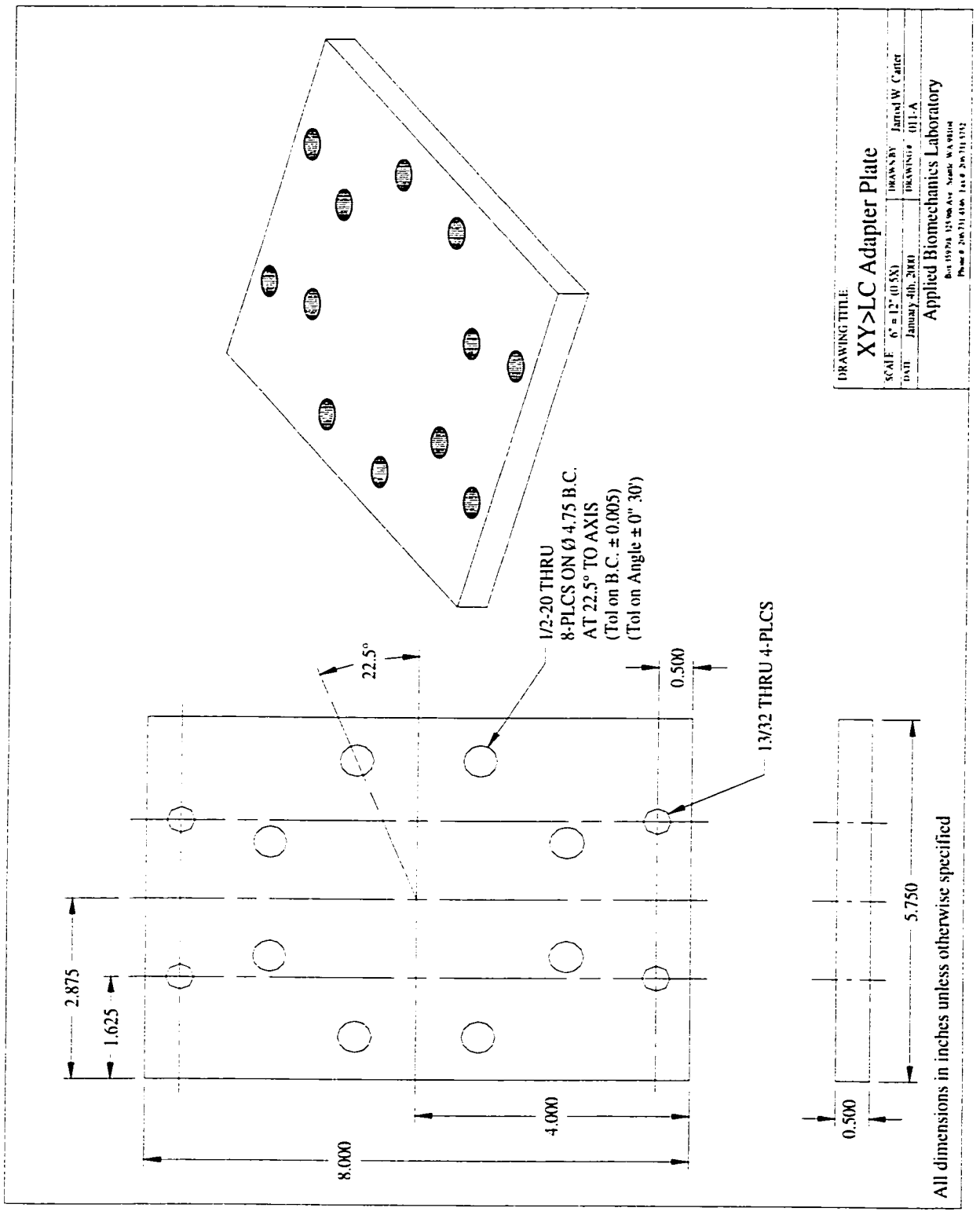
DRAWING TITLE
XY>LC Adapter Plate
SCALE 6" = 12" (0.5X)
DRAWN BY James W Carter
DATE January 4th, 2001
DRAWING # 011-A
Applied Biomechanics Laboratory
1/2-20 THRU
8-PLCS ON Ø 4.75 B.C.
AT 22.5° TO AXIS
(Tol on B.C. ± 0.005)
(Tol on Angle ± 0° 30')
13/32 THRU 4-PLCS
22.5°
0.500
2.875
1.625
4.000
8.000
0.500
5.750
All dimensions in inches unless otherwise specified

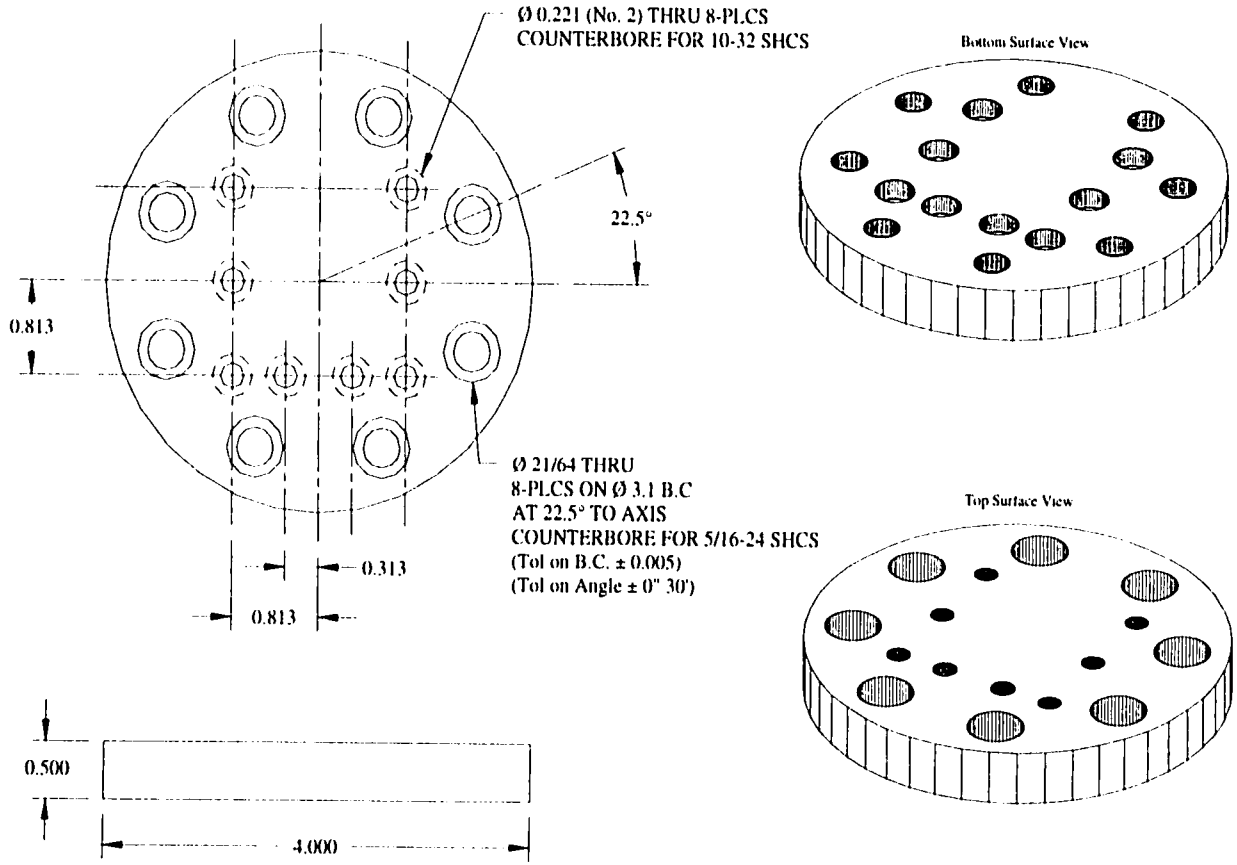

All dimensions in inches unless otherwise specified

DRAWING TITLE

LC>Specimen Mount Adapter Plate

SCALE	8" = 12" (0.67X)	DRAWN BY	Jarrod W. Carter
DATE	March 27th, 2000	DRAWING #	012-B

Applied Biomechanics Laboratory

Box 354700, 325 9th Ave. Seattle, WA 98104
Phone # 206.731.4346 Fax # 206.731.3252

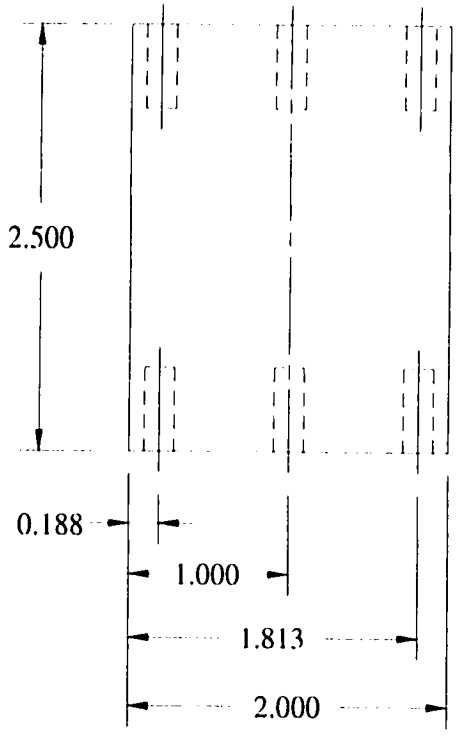

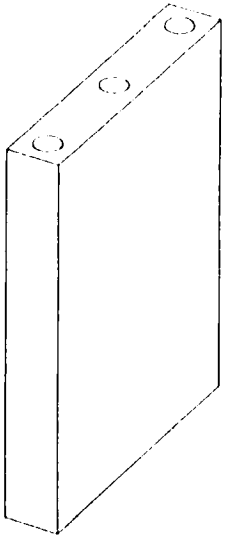

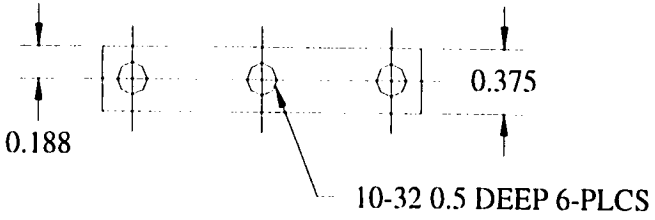

All dimension in inches unless otherwise specified

DRAWING TITLE
LC>Specimen Mount Strut

SCALE	1" = 1" (1X)	DRAWN BY	Jarrod W. Carter
DATE	February 7th, 2000	DRAWING #	013-A

Applied Biomechanics Laboratory

Box 354765 · 325 9th Ave · Seattle WA 98104
Phone # 206.731.4846 · Fax # 206.731.3752

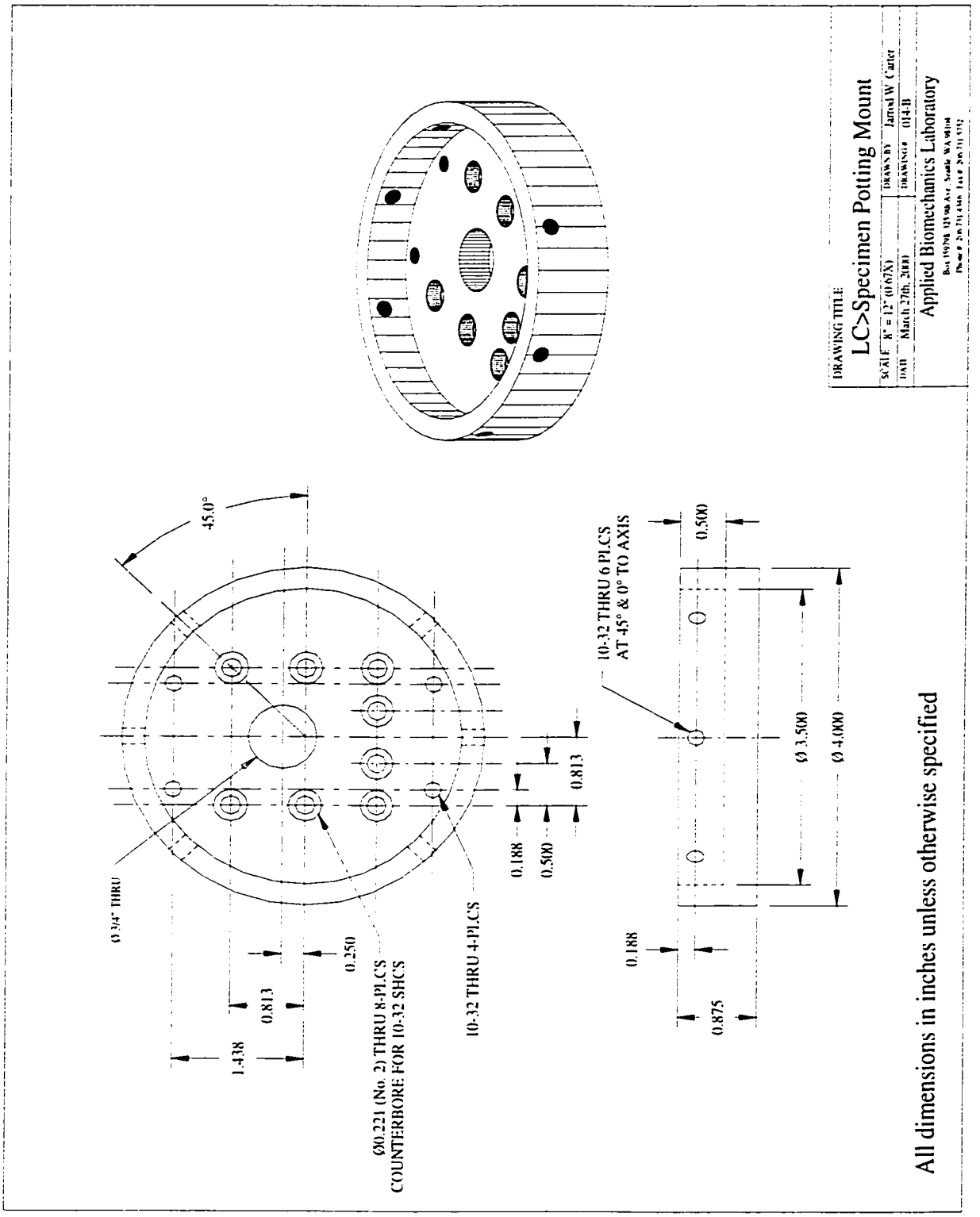
DRAWING TITLE
LC>Specimen Potting Mount
Applied Biomechanics Laboratory
45.0°
Ø.221 (No. 2) THRU 8-PLCS
COUNTERBORE FOR 10-32 SHCS
10-32 THRU 4-PLCS
10-32 THRU 6 PLCS
AT 45° & 0° TO AXIS
0.188
0.500
0.813
1.438
0.250
0.875
Ø 3.500
Ø 4.000
All dimensions in inches unless otherwise specified

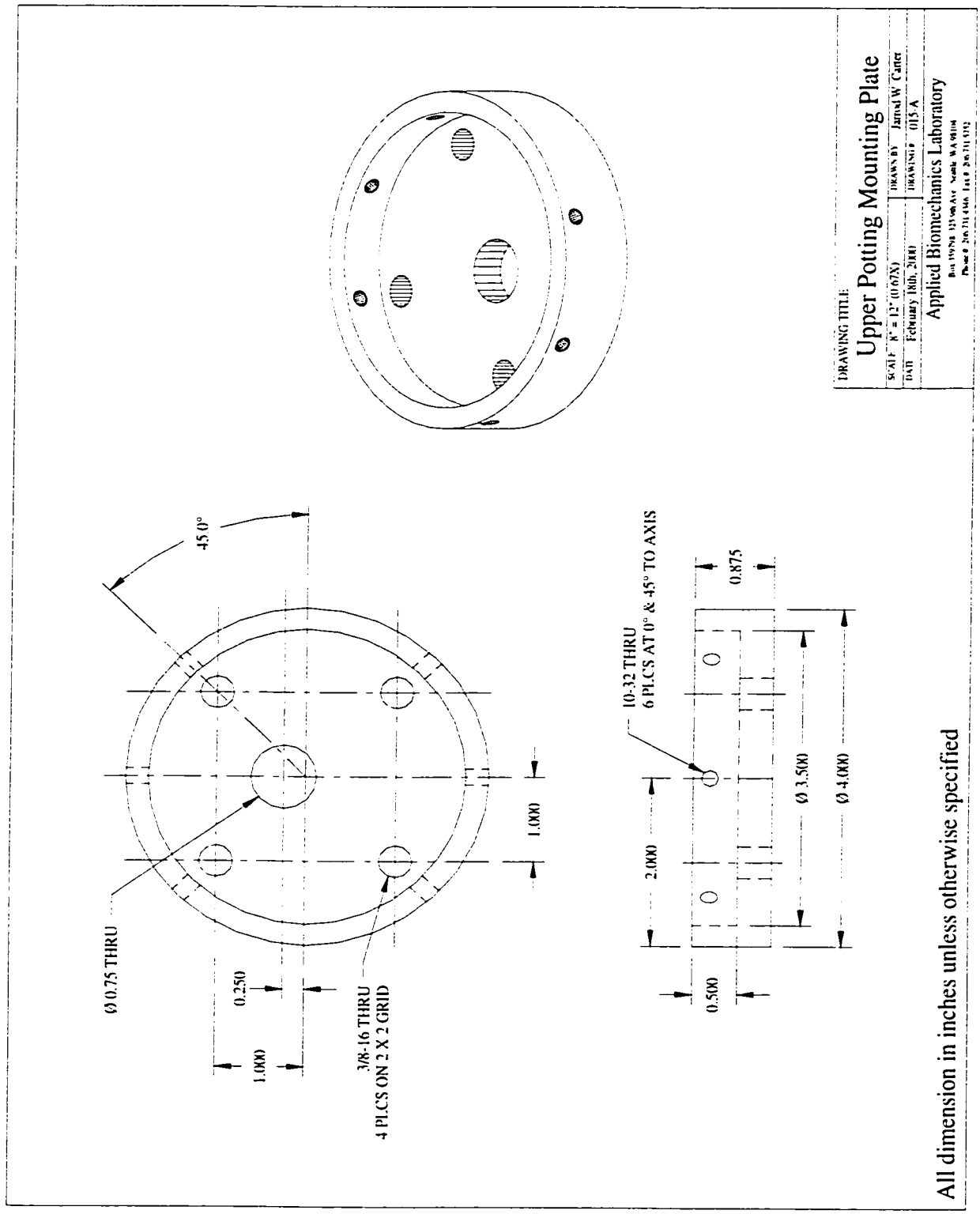
DRAWING TITLE:
Upper Potting Mounting Plate
SCALE: N = 12" (0.67X)
DRAWN BY: Jamal W. Carter
DATE: February 18th, 2000
DRAWING #: 0115 A
Applied Biomechanics Laboratory
45.0°
Ø 0.75 THRU
0.250
1.000
3/8-16 THRU
4 PLCS ON 2 X 2 GRID
1.000
10-32 THRU
6 PLCS AT 0° & 45° TO AXIS
0.875
2.000
Ø 3.500
Ø 4.000
0.500
All dimension in inches unless otherwise specified

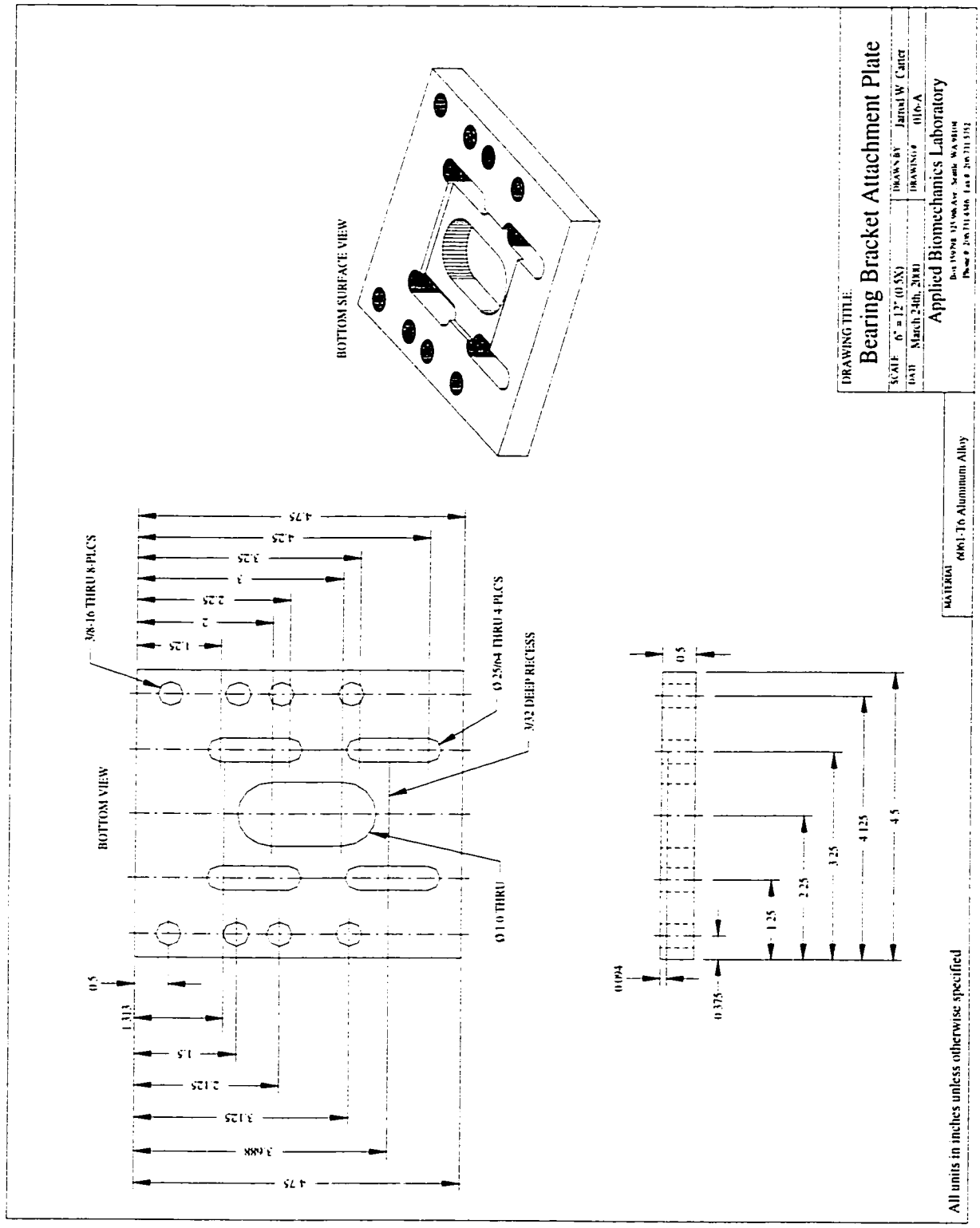
BOTTOM SURFACE VIEW
BOTTOM VIEW
3/8-16 THRU 8 PLCS
Ø 25/64 THRU 4 PLCS
3/32 DEEP RECESS
Ø 1.0 THRU
DRAWING TITLE
Bearing Bracket Attachment Plate
SCALE 6" = 1.2" (0.5X)
DATE March 24th, 2000
DRAWN BY Jamal W Carter
DRAWING # 016-A
Applied Biomechanics Laboratory
MATERIAL 6061-T6 Aluminum Alloy
All units in inches unless otherwise specified

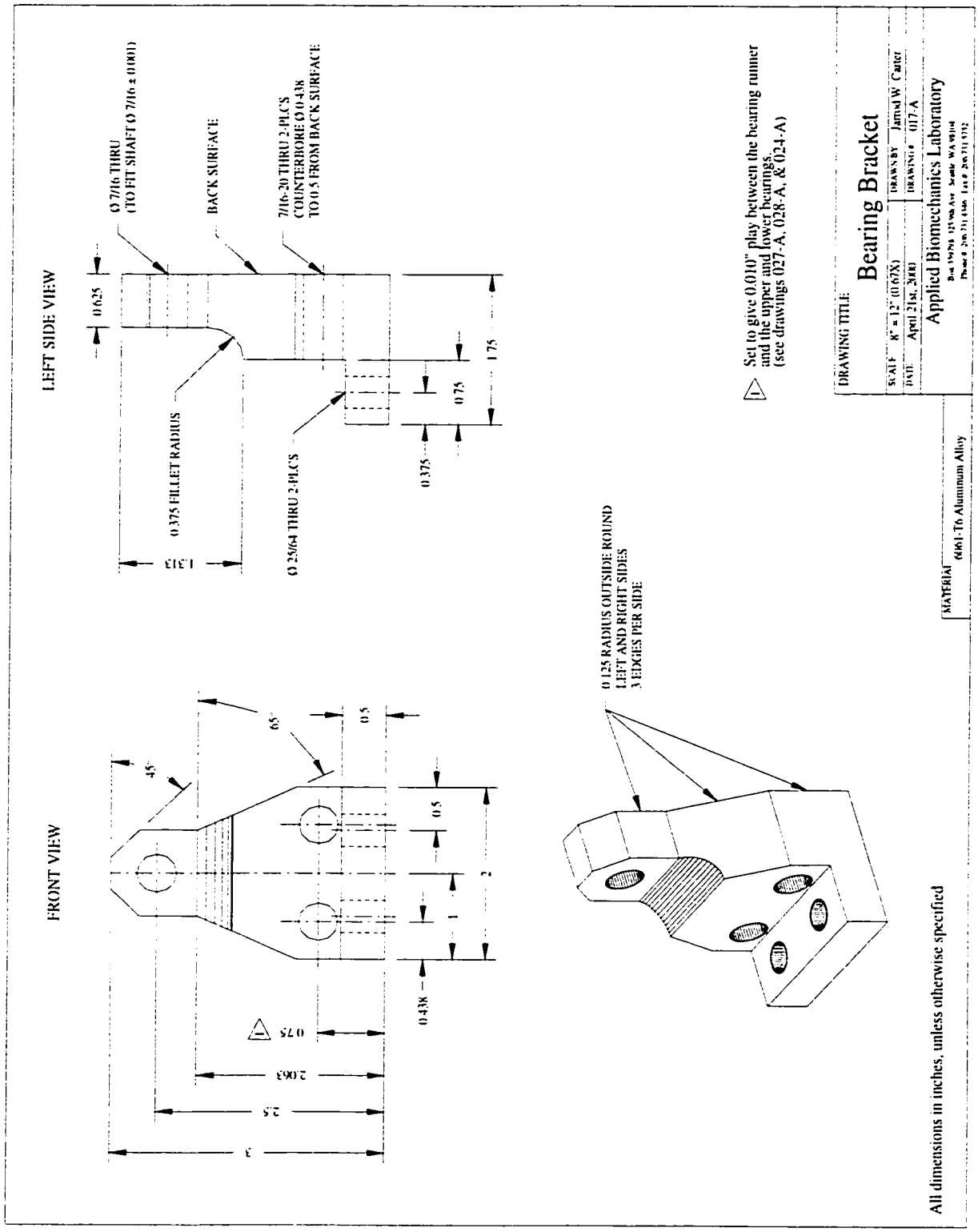
LEFT SIDE VIEW
FRONT VIEW
Ø 7/16 THRU
(TO FIT SHAFT Ø 7/16 ± 0.001)
BACK SURFACE
7/16-20 THRU 2-PLCS
COUNTERBORE Ø 0.438
TO 0.5 FROM BACK SURFACE
0.625
0.375 FILLET RADIUS
1.313
Ø 25/64 THRU 2-PLCS
0.375
0.75
1.75
0.5
65°
45°
0.5
0.5
2
1
0.438
0.75
2.063
2.5
3
0.125 RADIUS OUTSIDE ROUND
LEFT AND RIGHT SIDES
3 EDGES PER SIDE
Set to give 0.010" play between the bearing runner
and the upper and lower bearings.
(see drawings 027-A, 028-A, & 024-A)
All dimensions in inches, unless otherwise specified
MATERIAL
6061-T6 Aluminum Alloy
DRAWING TITLE
Bearing Bracket
SCALE
1" = 1" (0.667X)
DRAWN BY
James W Carter
DATE
April 21st, 2000
DRAWING #
017-A
Applied Biomechanics Laboratory

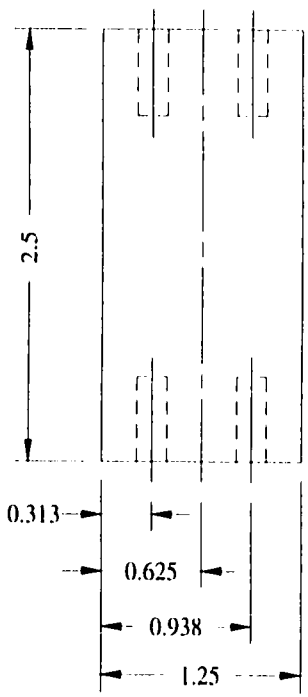

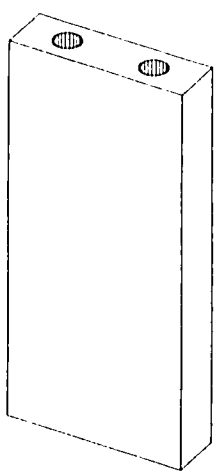

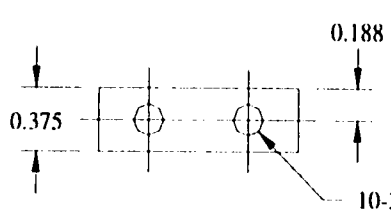

All dimensions in inches unless otherwise specified

MATERIAL
6061-T6 Aluminum Alloy

DRAWING TITLE
LC>Specimen Aux. Strut

SCALE	DRAWN BY Jarrod W. Carter
DATE March 28th, 2000	DRAWING # 018-A

Applied Biomechanics Laboratory

Box 354798, 325 9th Ave., Seattle, WA 98104
Phone # 206.731.4386, Fax # 206.731.5712

FRONT SURFACE VIEW

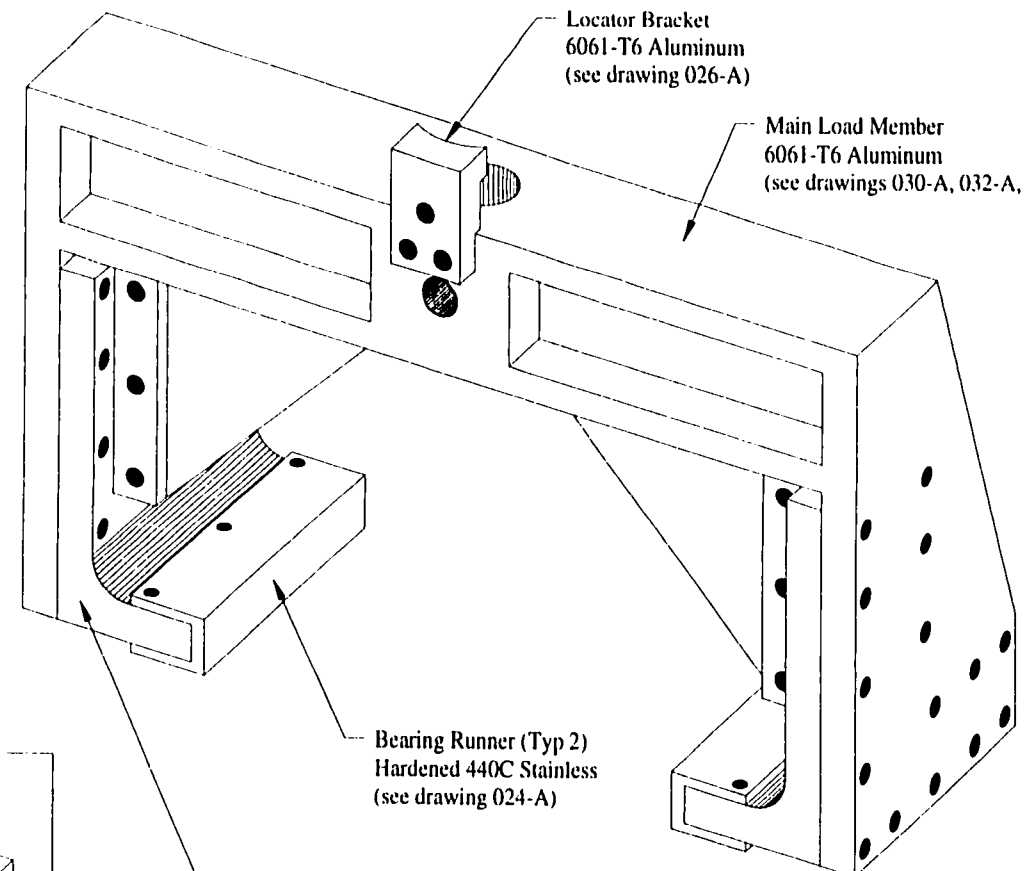

BACK SURFACE VIEW

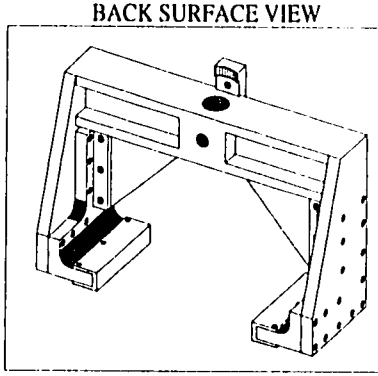

DRAWING TITLE

Yoke Assembly

SCALE	6" = 12" (0.5X)	DRAWN BY	Jarrod W. Carter
DATE	March 5th, 2000	DRAWING #	019-A

Applied Biomechanics Laboratory

Box 355061 325 9th Ave., Seattle WA 98104
Phone # 206.731.4540 Fax # 206.731.5752

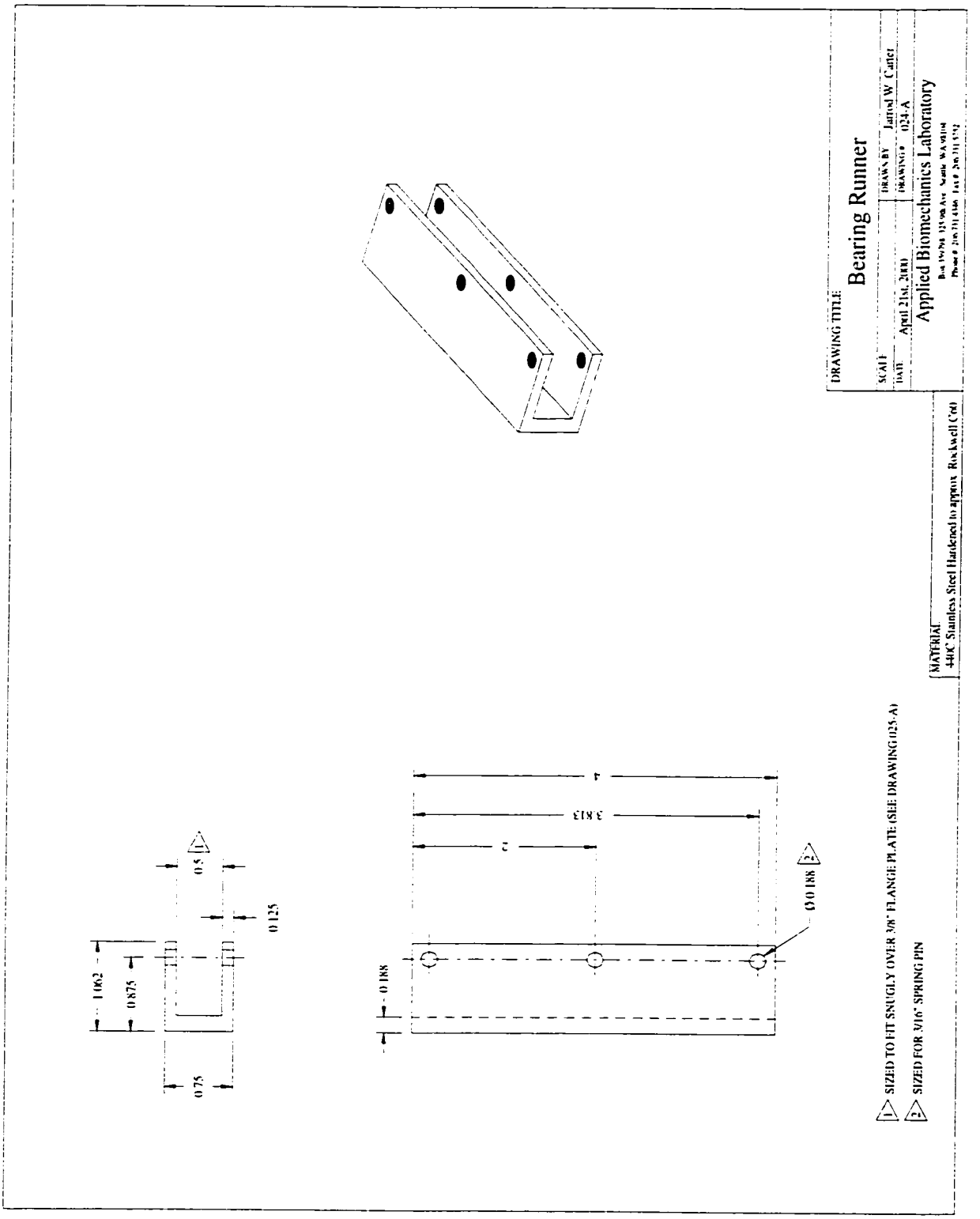
DRAWING TITLE
Bearing Runner
SCALE
DATE
April 21st, 2008
DRAWN BY
Jarred W Carter
DRAWING #
024-A
Applied Biomechanics Laboratory
MATERIAL
440C Stainless Steel Hardened to approx Rockwell C60
1 SIZED TO FIT SNUGLY OVER 3/8" FLANGE PLATE (SEE DRAWING 025-A)
2 SIZED FOR 3/16" SPRING PIN
0.5
0.125
1.062
0.875
0.75
0.188
3.813
3
2
0.188

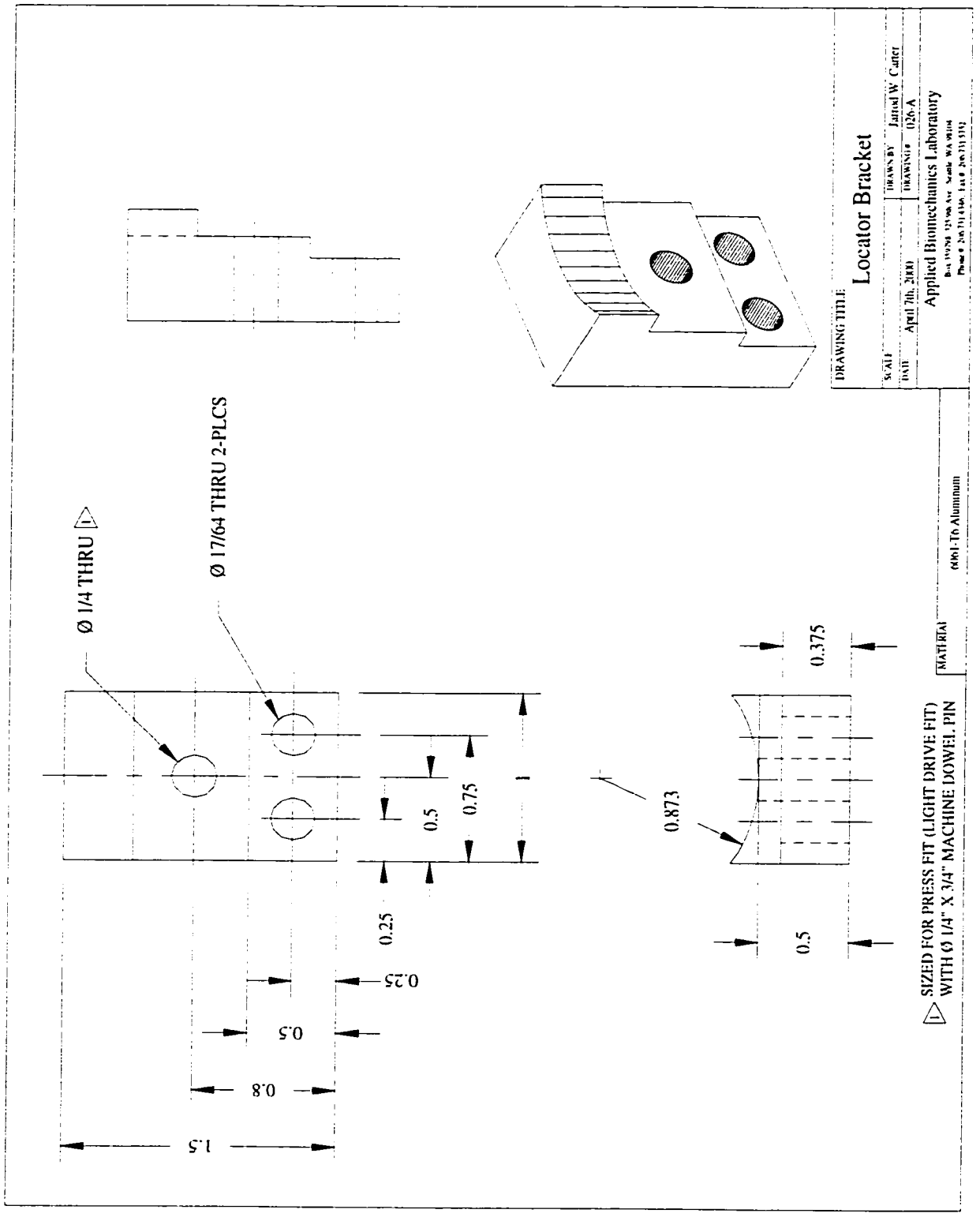
Ø 1/4 THRU 1
Ø 17/64 THRU 2-PLCS
0.25
0.5
0.75
1
0.873
0.375
0.5
0.25
0.5
0.8
1.5
1 SIZED FOR PRESS FIT (LIGHT DRIVE FIT) WITH Ø 1/4" X 3/4" MACHINE DOWEL PIN
MATERIAL
6061-T6 Aluminum
DRAWING TITLE
Locator Bracket
SCALE
DATE
April 7th, 2000
DRAWN BY
Jarad W. Cutter
DRAWING #
026-A
Applied Biomechanics Laboratory

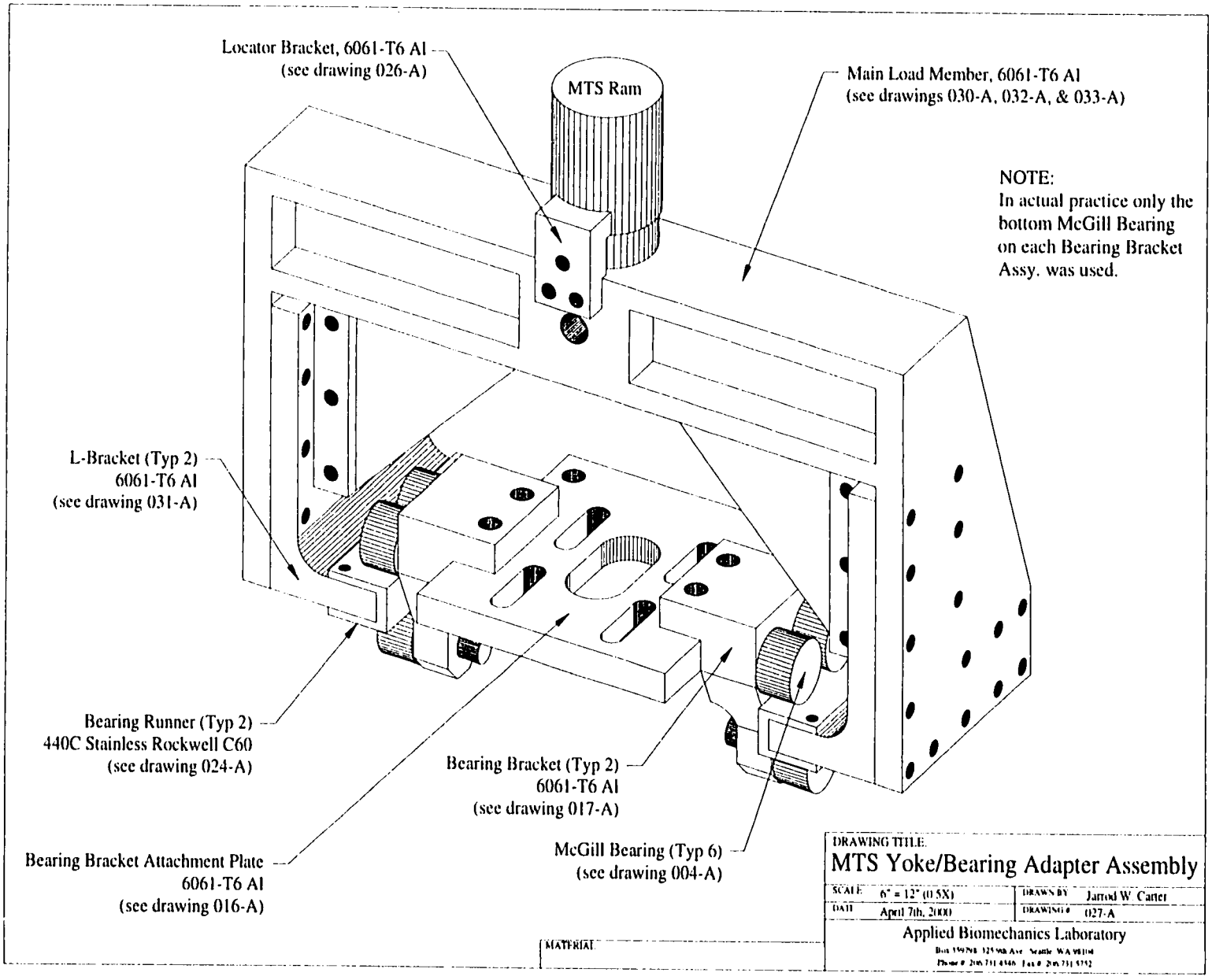
Locator Bracket, 6061-T6 Al
(see drawing 026-A)
MTS Ram
Main Load Member, 6061-T6 Al
(see drawings 030-A, 032-A, & 033-A)
NOTE:
In actual practice only the bottom McGill Bearing on each Bearing Bracket Assy. was used.
L-Bracket (Typ 2)
6061-T6 Al
(see drawing 031-A)
Bearing Runner (Typ 2)
440C Stainless Rockwell C60
(see drawing 024-A)
Bearing Bracket (Typ 2)
6061-T6 Al
(see drawing 017-A)
Bearing Bracket Attachment Plate
6061-T6 Al
(see drawing 016-A)
McGill Bearing (Typ 6)
(see drawing 004-A)
DRAWING TITLE:
MTS Yoke/Bearing Adapter Assembly
SCALE: 6" = 12" (0.5X)
DRAWN BY: Jarrod W. Carter
DATE: April 7th, 2000
DRAWING #: 027-A
Applied Biomechanics Laboratory
MATERIAL:

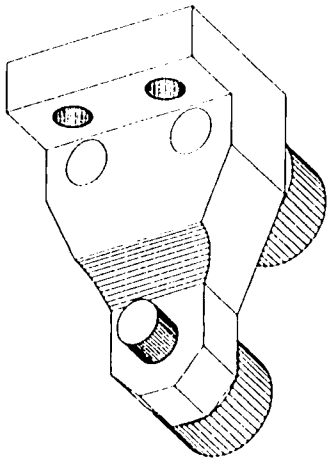

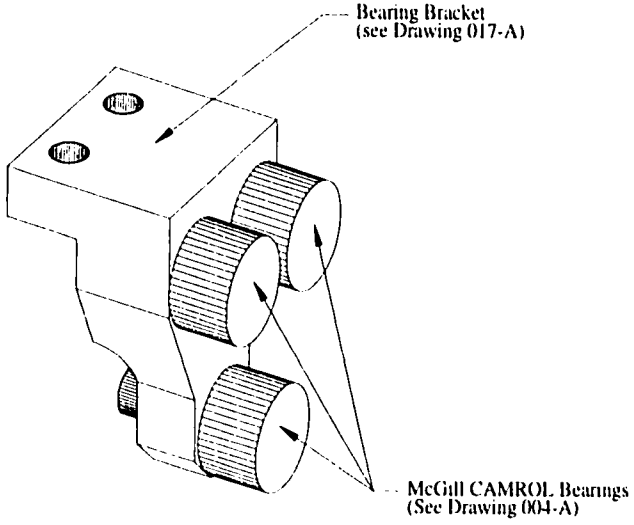

NOTE:
In practice only the bottom McGill Bearing was used.

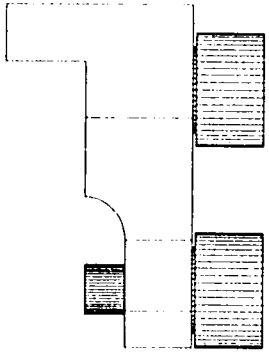

MATERIAL

DRAWING TITLE
Bearing Bracket Assembly

SCALE	8" = 12" (0.67X)	DRAWN BY	Jarrod W. Carter
DATE	April 7th, 2000	DRAWING #	028-A

Applied Biomechanics Laboratory

Box 357420 325 9th Ave Seattle, WA 98104
Phone # 206.731.4360 Fax # 206.731.3752

RIGHT SIDE VIEW (SECTION A-A)

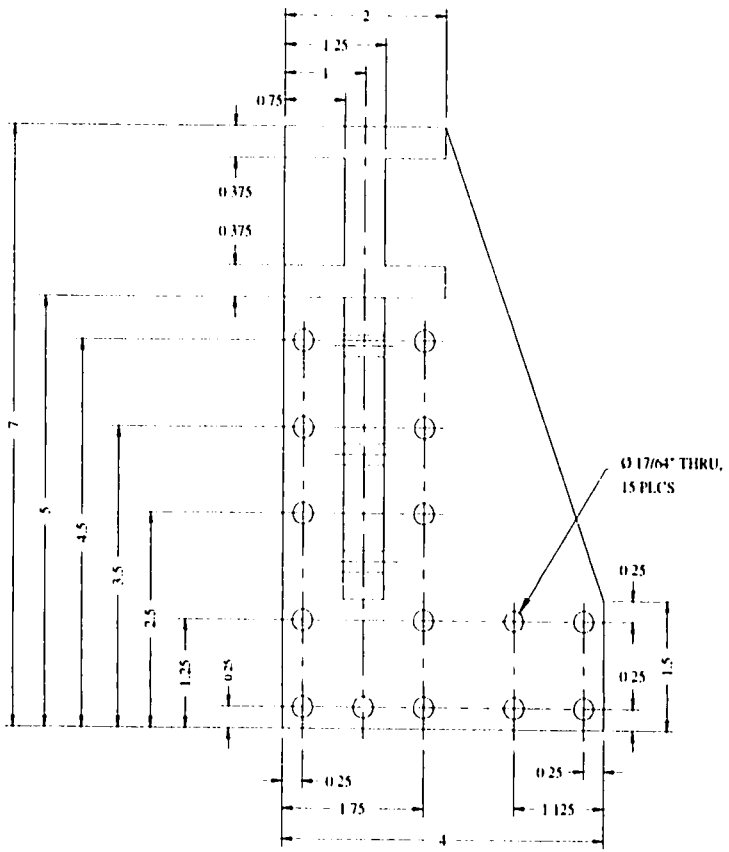

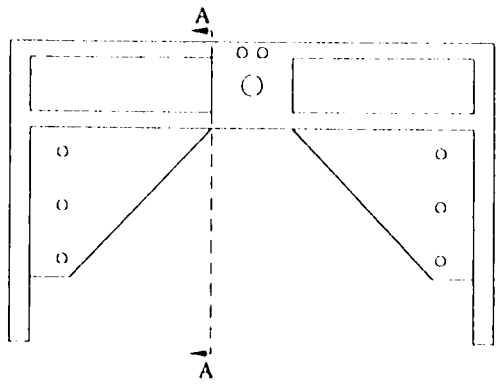

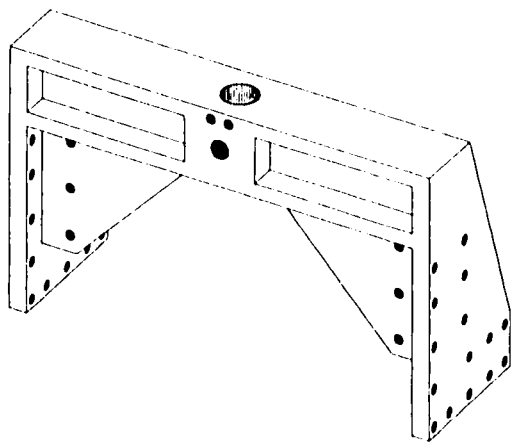

All dimensions in inches, unless otherwise specified

MATERIAL 6061-T6 Aluminum Alloy

DRAWING TITLE
Main Load Member (Side On View)

SCALE		DRAWN BY	Jarrod W. Carter
DATE	April 21st, 2003	DRAWING #	030-A

Applied Biomechanics Laboratory

Box 354768 325 9th Ave Seattle WA 98104
Phone # 206.731.4346 Fax # 206.731.4352

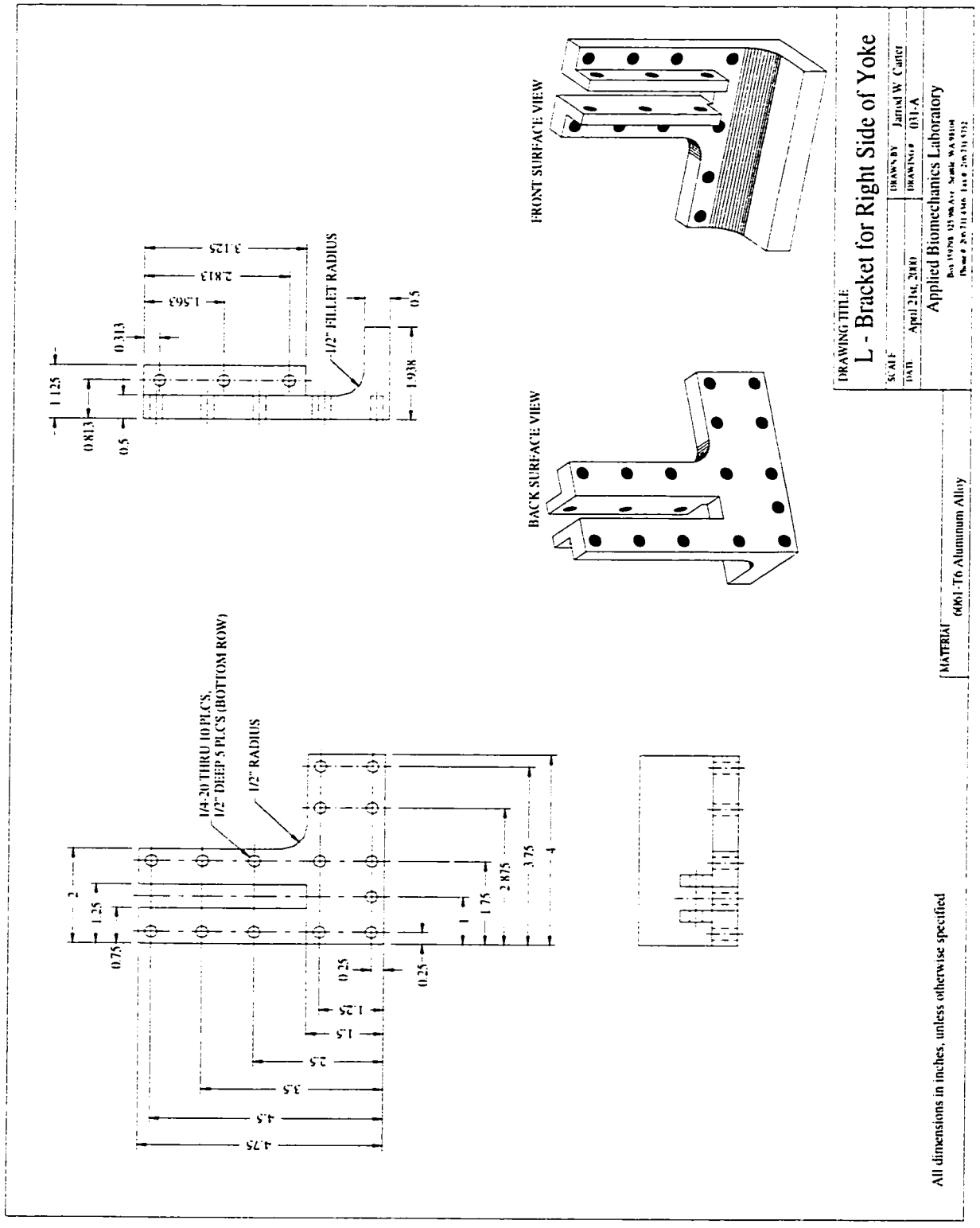
FRONT SURFACE VIEW
BACK SURFACE VIEW
1/2" FILLET RADIUS
1/4-20 THRU 10 PLCS.
1/2" DEEP 5 PLCS (BOTTOM ROW)
1/2" RADIUS
DRAWING TITLE
L - Bracket for Right Side of Yoke
SCALE
DATE
April 21st, 2000
DRAWN BY
Jamal W. Carter
DRAWING #
031-A
Applied Biomechanics Laboratory
MATERIAL
6061-T6 Aluminum Alloy
All dimensions in inches, unless otherwise specified

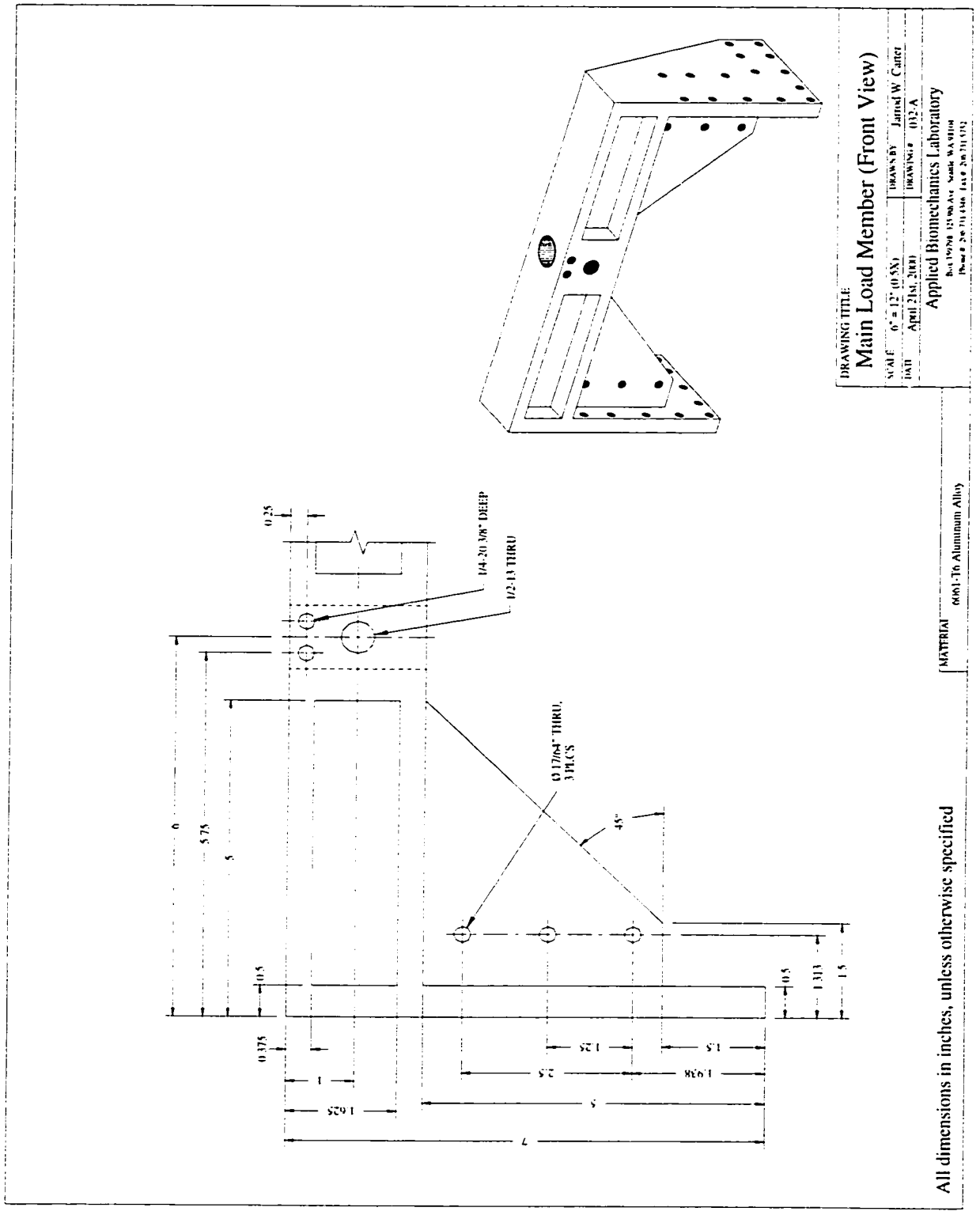
DRAWING TITLE
Main Load Member (Front View)
SCALE 6" = 12" (0.5X)
DATE April 21st, 2000
DRAWN BY Jarrod W. Carter
DRAWING # 012-A
Applied Biomechanics Laboratory
All dimensions in inches, unless otherwise specified
MATERIAL 6061-T6 Aluminum Alloy
1/4-20 3/8" DEEP
1/2-13 THRU
Ø 17/64" THRU, 3 PLCS
45°
0.25
0.5
5.75
5
0.375
1
1.625
1.25
2.5
1.938
5
7
1.5
1.313

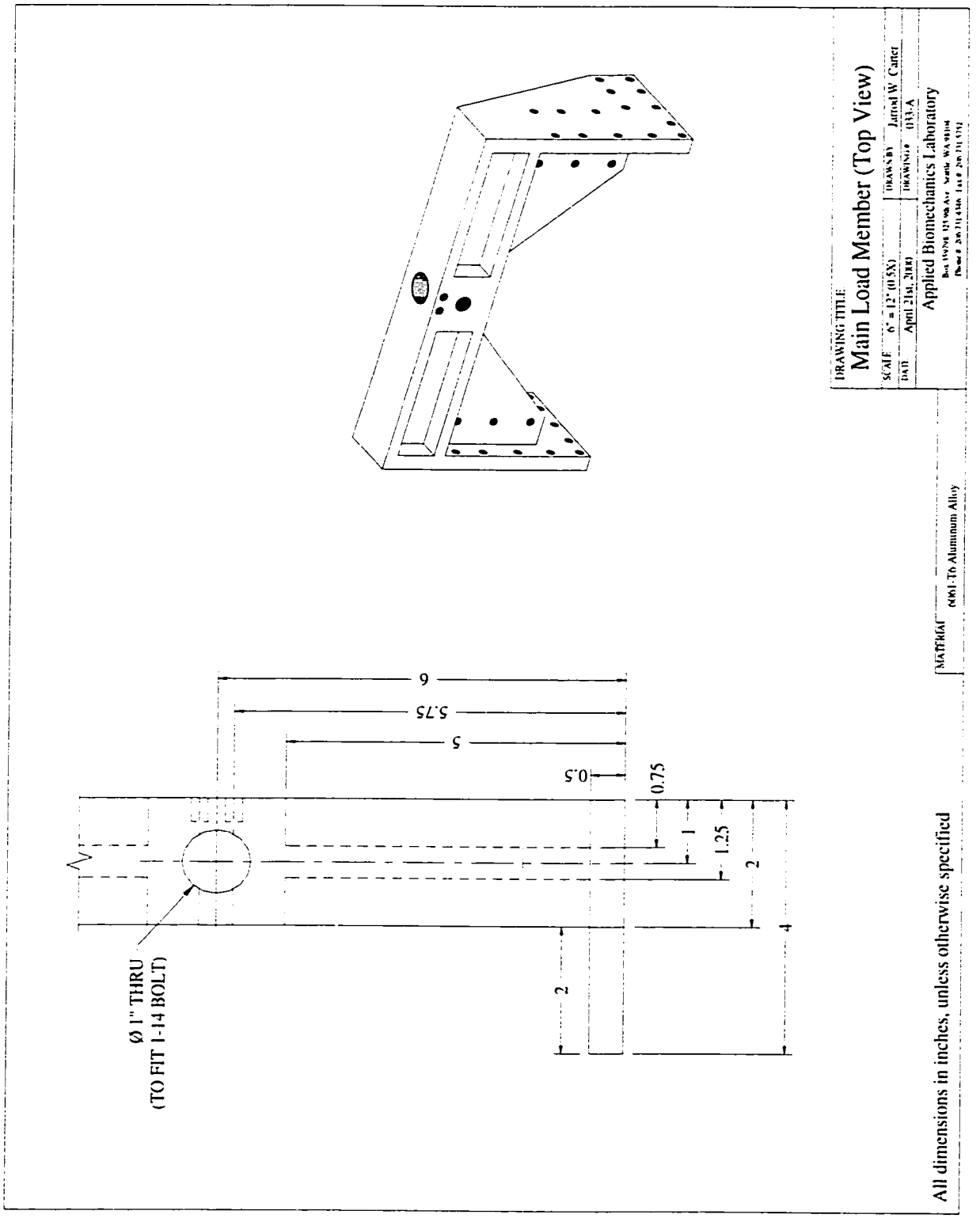
DRAWING TITLE
Main Load Member (Top View)
SCALE 6" = 12" (0.5X)
DATE April 21st, 2000
DRAWN BY Jarrod W Carter
DRAWING # 033-A
Applied Biomechanics Laboratory
MATERIAL
6061-T6 Aluminum Alloy
All dimensions in inches, unless otherwise specified
Ø 1" THRU
(TO FIT 1-14 BOLT)
6
5.75
5
0.5
0.75
1
1.25
2
4
2

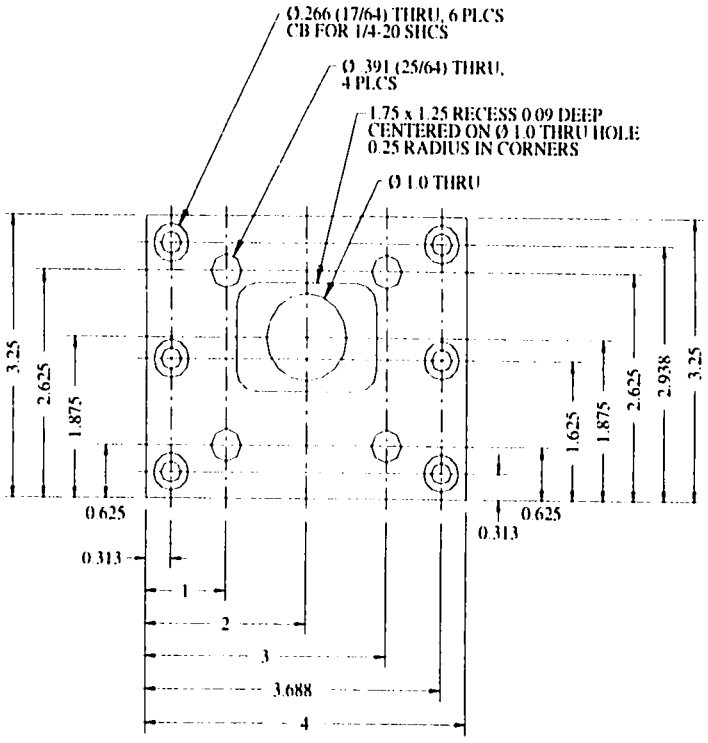

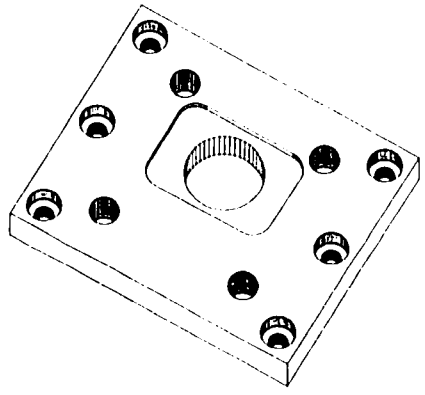

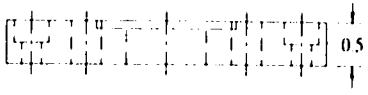

DRAWING TITLE:
Direct Compression Adapter Plate

SCALE:	DRAWN BY: J. W. Carter
DATE: April 27th, 2000	DRAWING #: 034-A

MATERIAL:
6061-T6 Aluminum

All dimensions in inches, unless otherwise specified

Applied Biomechanics Laboratory
Box 359798, 325 9th Ave., Seattle, WA 98104
Phone #: 206.731.4346; Fax #: 206.731.5752

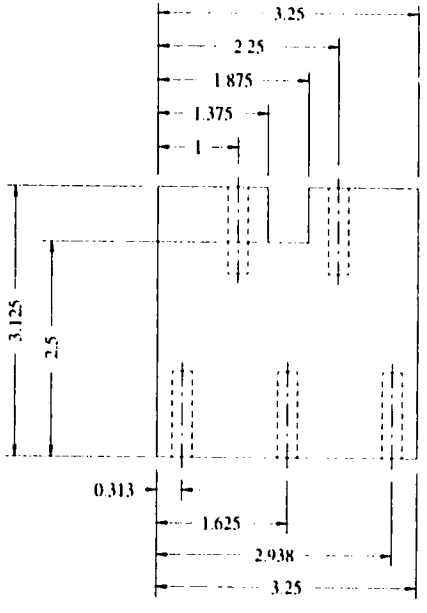

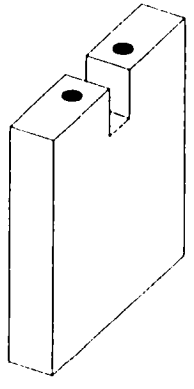

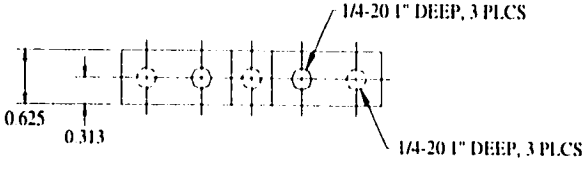

DRAWING TITLE:
Direct Compression Adapter Strut

SCALE: 6" = 12" (0.5 X)	DRAWN BY: J. W. Carter
DATE: April 27th, 2000	DRAWING #: 035-A

MATERIAL:
6061-T6 Aluminum

Applied Biomechanics Laboratory
Box 359798, 325 9th Ave , Seattle, WA 98104
Phone #: 206.731.4346; Fax #: 206.731.5752

All dimensions in inches, unless otherwise specified

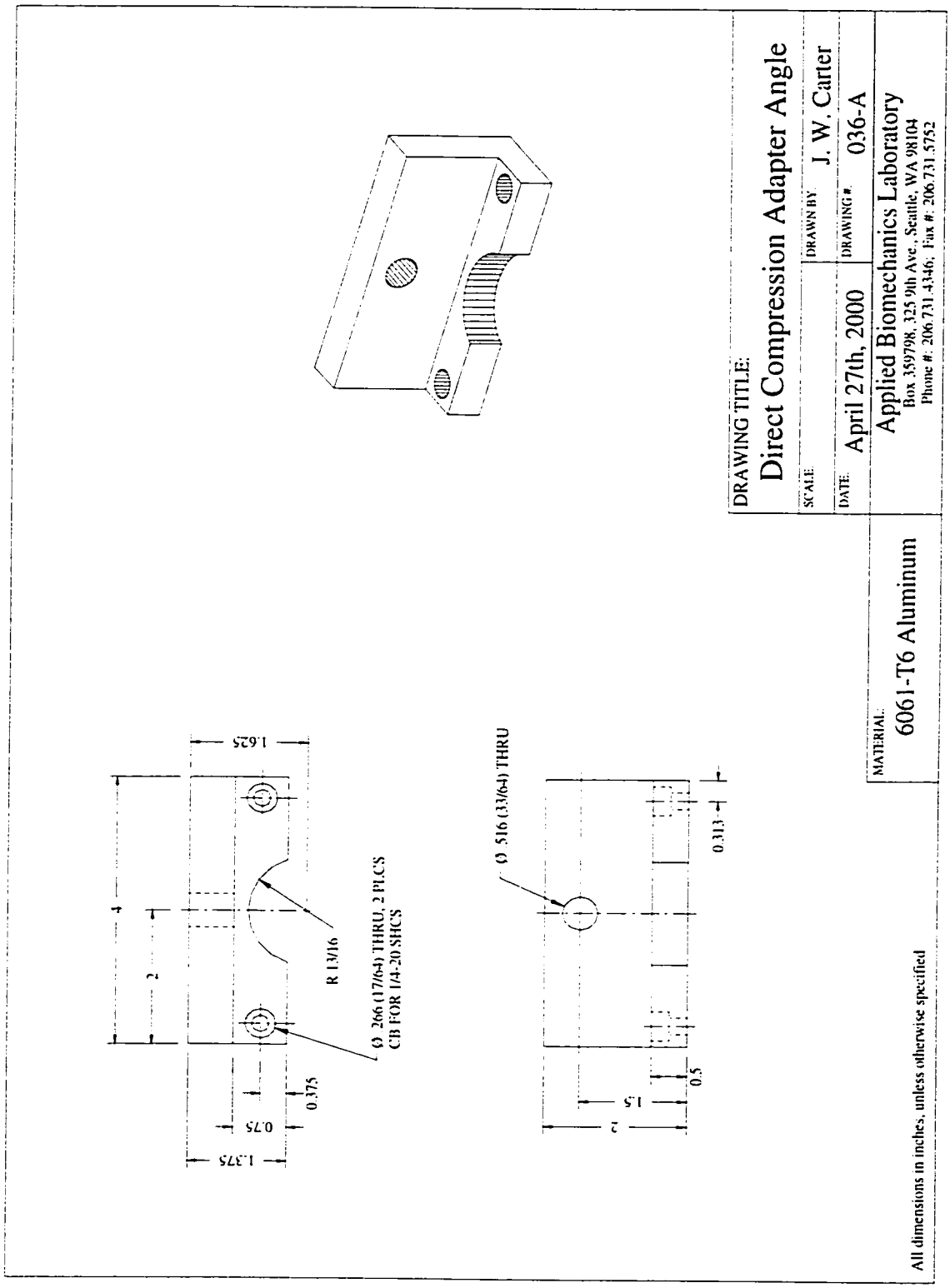
DRAWING TITLE:
Direct Compression Adapter Angle
SCALE
DRAWN BY J. W. Carter
DATE April 27th, 2000
DRAWING # 036-A
MATERIAL:
6061-T6 Aluminum
Applied Biomechanics Laboratory
Box 359798, 325 9th Ave., Seattle, WA 98104
Phone #: 206.731.4346; Fax #: 206.731.5752
All dimensions in inches, unless otherwise specified
1.625
4
2
R 13/16
Ø .266 (17/64) THRU, 2 PLCS
CB FOR 1/4-20 SHCS
0.375
0.75
1.375
Ø .516 (33/64) THRU
0.313
0.5
1.5
2

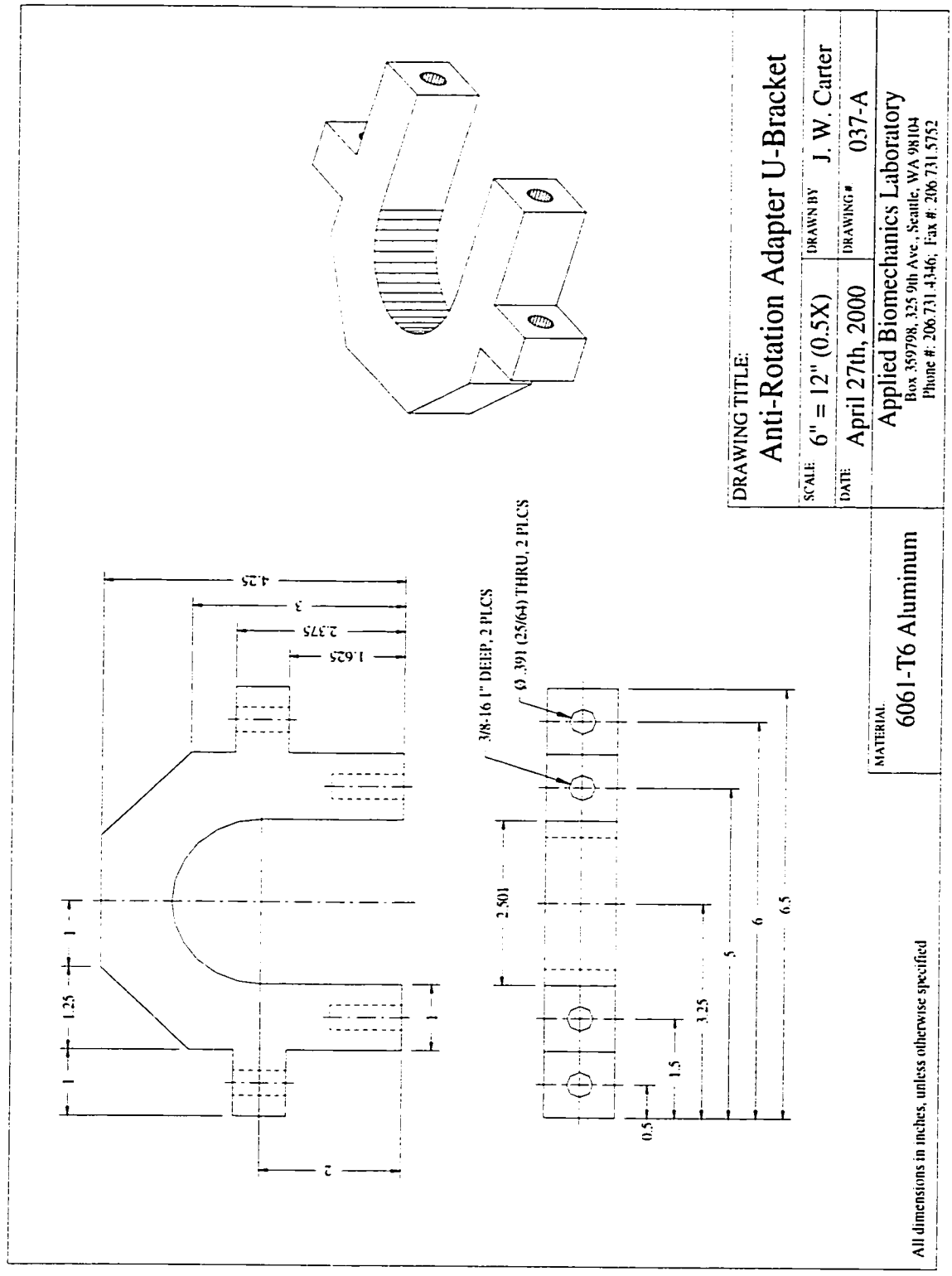
DRAWING TITLE:
Anti-Rotation Adapter U-Bracket
SCALE: 6" = 12" (0.5X)
DRAWN BY: J. W. Carter
DATE: April 27th, 2000
DRAWING #: 037-A
MATERIAL:
6061-T6 Aluminum
Applied Biomechanics Laboratory
Box 359798, 325 9th Ave., Seattle, WA 98104
Phone #: 206.731.4346; Fax #: 206.731.5752
All dimensions in inches, unless otherwise specified
3/8-16 1" DEEP, 2 PLCS
Ø .391 (25/64) THRU, 2 PLCS
4.25
3
2.375
1.625
2.501
1.25
1
2
3.25
1.5
0.5
5
6
6.5

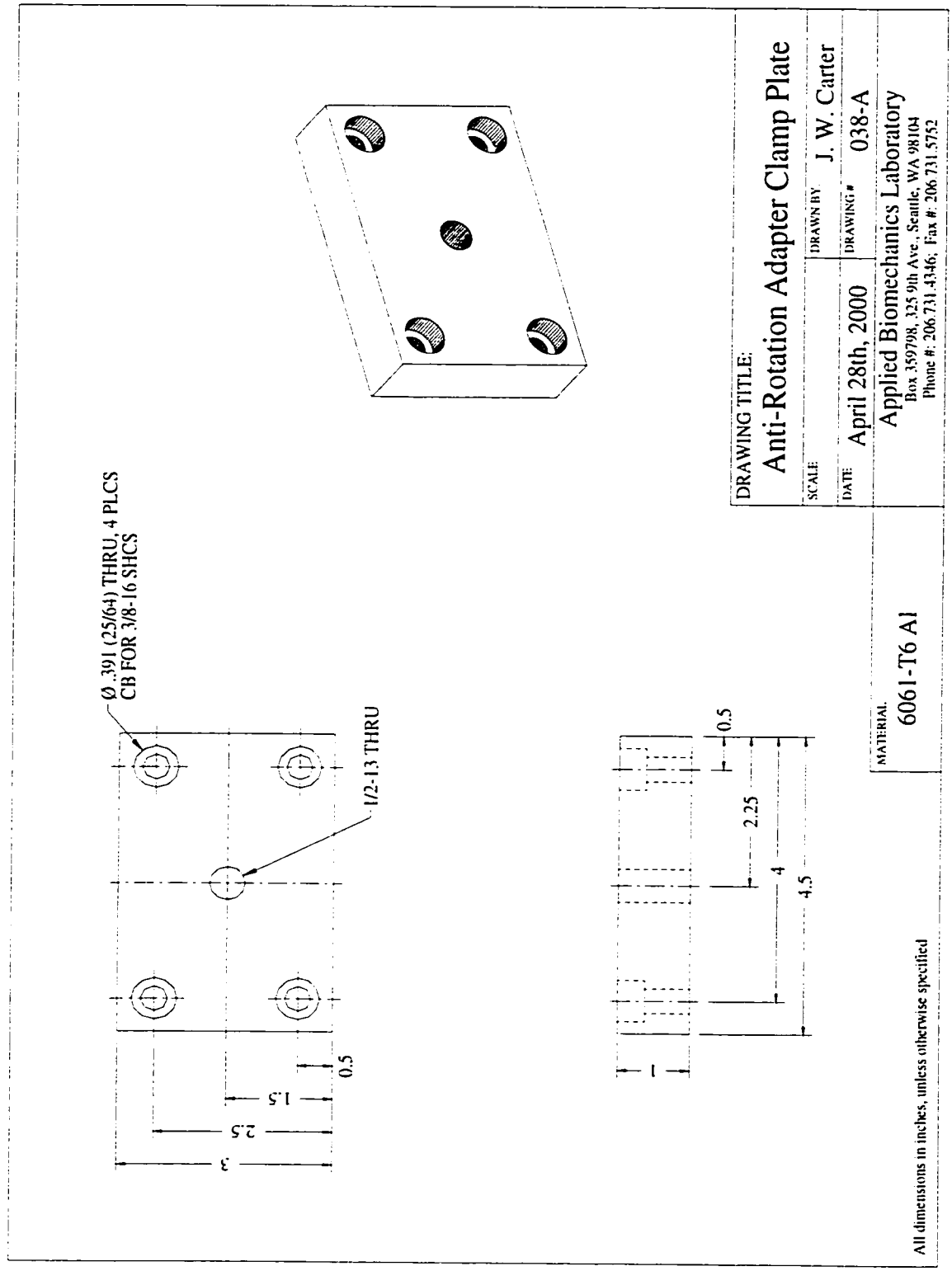
Ø .391 (25/64) THRU, 4 PLCS
CB FOR 3/8-16 SHCS
1/2-13 THRU
3
2.5
1.5
0.5
1
4.5
4
2.25
0.5
All dimensions in inches, unless otherwise specified
MATERIAL
6061-T6 Al
DRAWING TITLE:
Anti-Rotation Adapter Clamp Plate
SCALE
DRAWN BY
J. W. Carter
DATE
April 28th, 2000
DRAWING #
038-A
Applied Biomechanics Laboratory
Box 359798, 325 9th Ave., Seattle, WA 98104
Phone #: 206.731.4346; Fax #: 206.731.5752

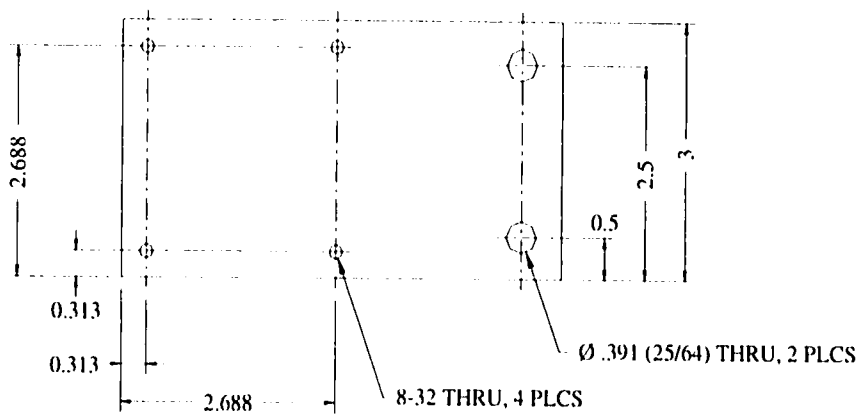

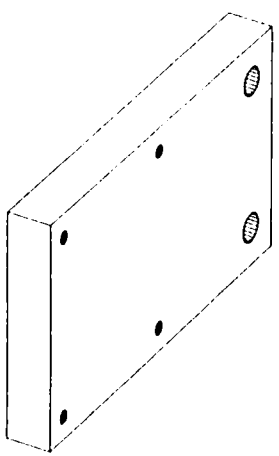

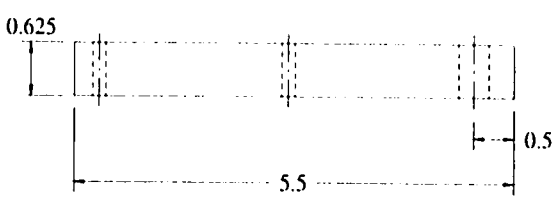

DRAWING TITLE:
Anti-Rotation Adapter Guide Plate

SCALE: 6" = 12" (0.5X)	DRAWN BY: J. W. Carter
DATE: April 28th, 2000	DRAWING #: 039-A

MATERIAL:
6061-T6 Al

All dimensions in inches, unless otherwise specified

Applied Biomechanics Laboratory
Box 359798, 325 9th Ave , Seattle, WA 98104
Phone #: 206.731.4346; Fax #: 206.731.5752

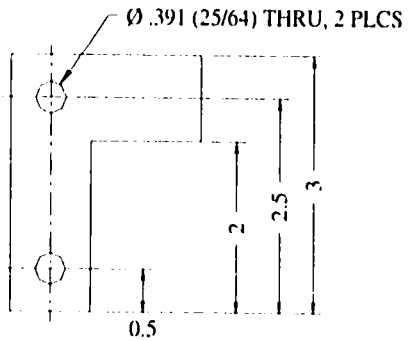

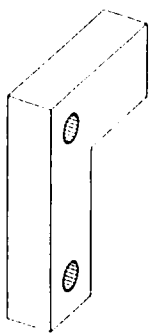

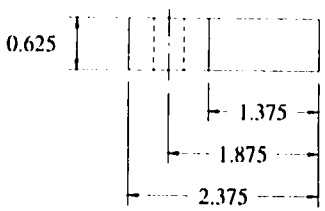

DRAWING TITLE:
Anti-Rotation Adapter L-Plate

SCALE:	DRAWN BY: J. W. Carter
DATE: April 28th, 2000	DRAWING #: 040-A

MATERIAL: 6061-T6 Al

All dimensions in inches, unless otherwise specified

Applied Biomechanics Laboratory
Box 359798, 325 9th Ave., Seattle, WA 98104
Phone #: 206.731.4346; Fax #: 206.731.5752

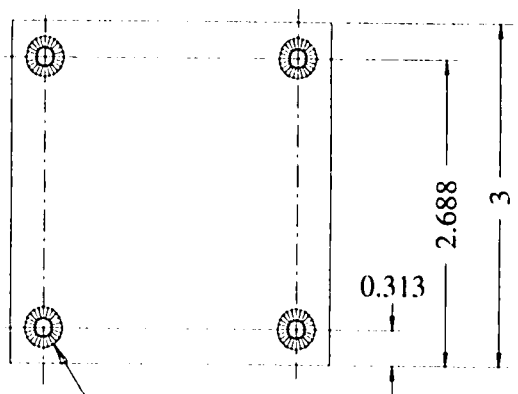

Ø .164 (#8), 4 PLCS
CS FOR 8-32 82¡ SOCKET FLAT
COUNTERSUNK HEAD CAP SCREW

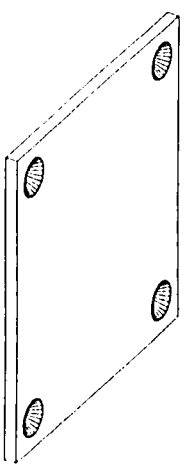

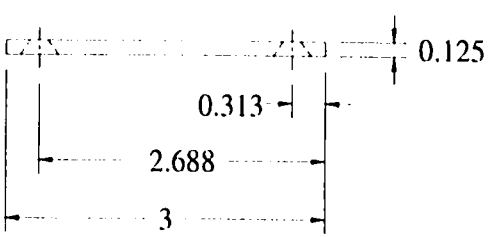

DRAWING TITLE:
Anti-Rotation Adapter Teflon Interface Plate

SCALE:	DRAWN BY: J. W. Carter
DATE: May 1st, 2000	DRAWING #: 041-A

MATERIAL:
Mechanical Grade Teflon Sheet

Applied Biomechanics Laboratory
Box 359798, 325 9th Ave., Seattle, WA 98104
Phone #: 206 731 4346; Fax #: 206 731 5752

All dimensions in inches, unless otherwise specified

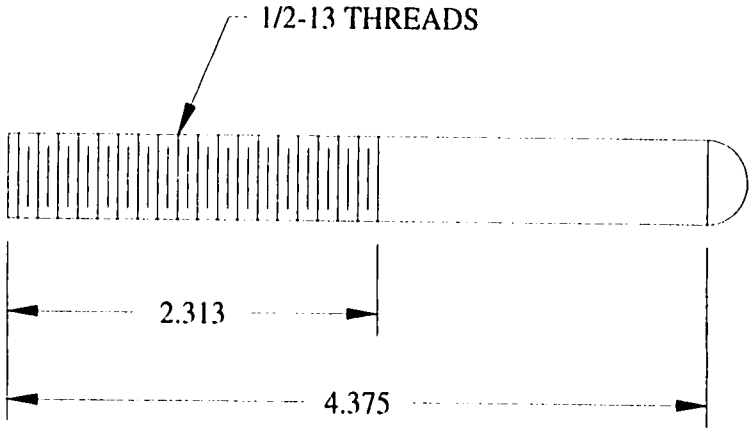

Ø .490 FROM END OF THREADS TO TIP

DRAWING TITLE: Anti-Rotation Adapter Guide Rod		
SCALE: 12" = 12" (1.0X)	DRAWN BY: J. W. Carter	
DATE: May 1st, 2000	DRAWING #: 042-A	
MATERIAL: 6061-T6 Al	Applied Biomechanics Laboratory Box 359798, 325 9th Ave., Seattle, WA 98104 Phone #: 206.731.4346; Fax #: 206.731.5752	

All dimensions in inches, unless otherwise specified

FRONT SURFACE VIEW

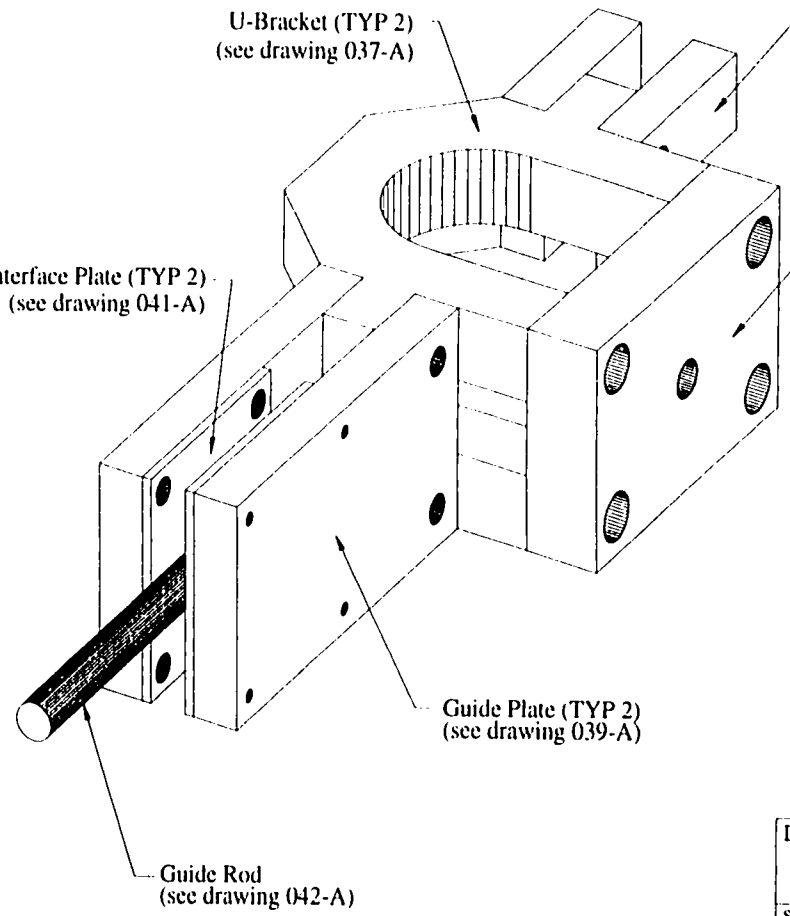

BACK SURFACE VIEW

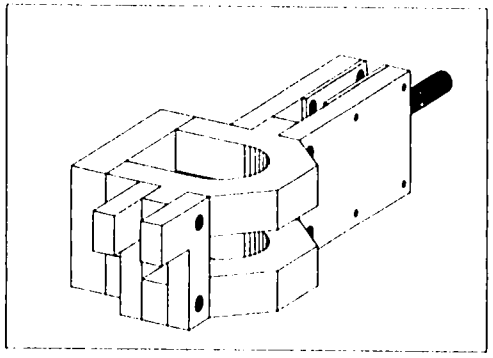

DRAWING TITLE:

Anti-Rotation Adapter Assembly

SCALE:	DRAWN BY: J. W. Carter
DATE: May 1st, 2000	DRAWING #: 043-A
MATERIAL:	

Applied Biomechanics Laboratory
Box 359798, 325 9th Ave., Seattle, WA 98104
Phone #: 206.731.4346; Fax #: 206.731.5752

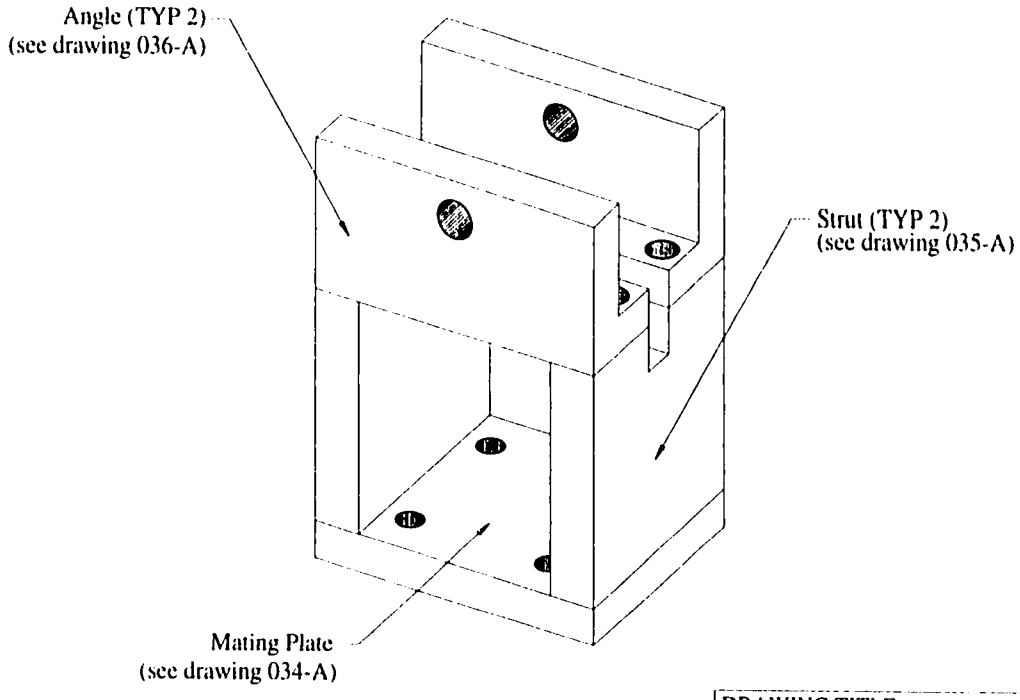

DRAWING TITLE:
Direct Compression Adapter Assembly

SCALE	DRAWN BY: J. W. Carter
DATE: May 1st, 2000	DRAWING #: 044-A
MATERIAL	

Applied Biomechanics Laboratory
Box 359798, 325 9th Ave., Seattle, WA 98104
Phone #: 206.731.4346; Fax #: 206.731.5752

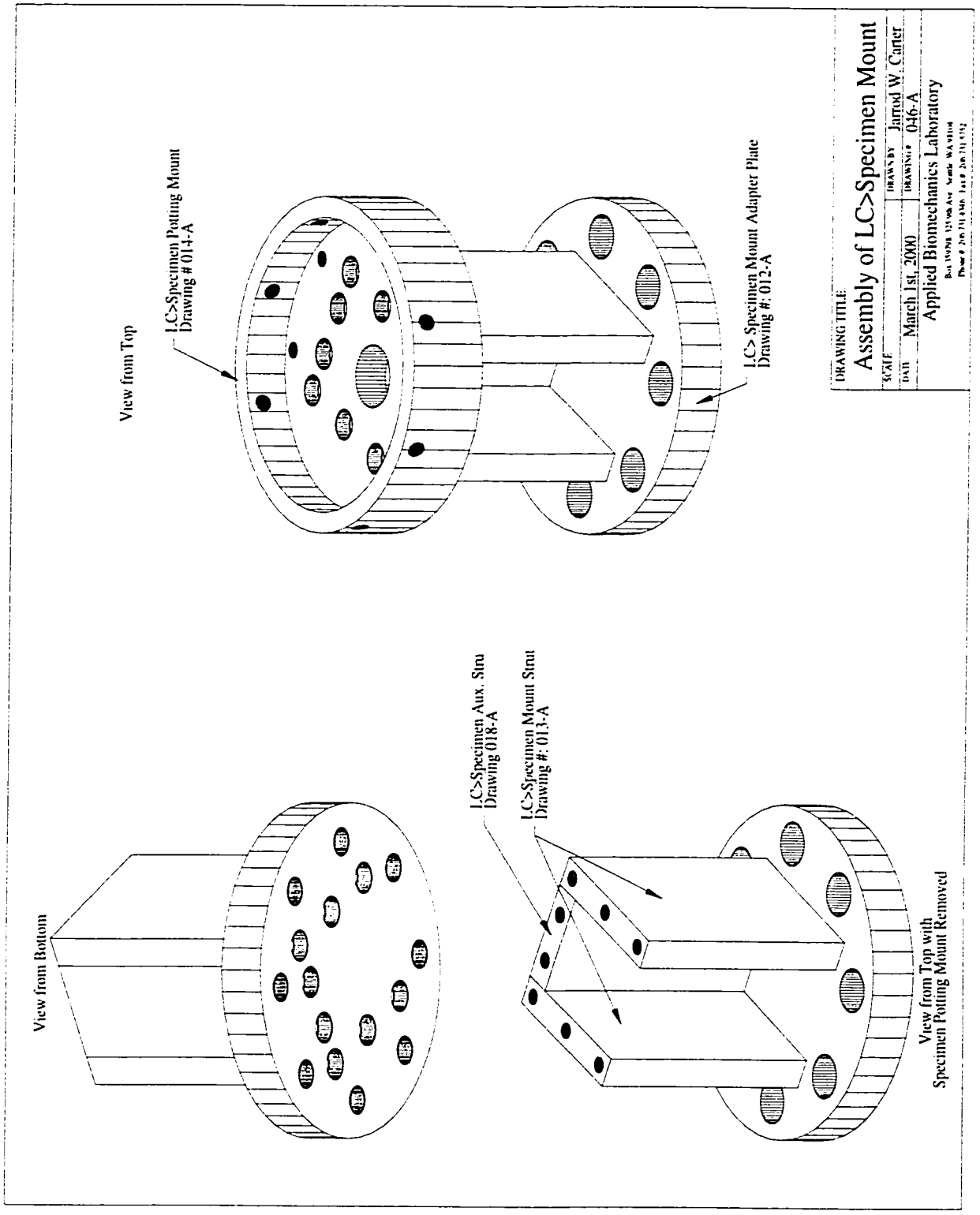
View from Top
LC>Specimen Potting Mount
Drawing # 014-A
LC> Specimen Mount Adapter Plate
Drawing #: 012-A
View from Bottom
LC>Specimen Aux. Stru
Drawing 018-A
LC>Specimen Mount Strut
Drawing #: 013-A
View from Top with
Specimen Potting Mount Removed
DRAWING TITLE
Assembly of LC>Specimen Mount
SCALE
DRAWN BY
Jarrod W. Carter
DATE
March 1st, 2000
DRAWING #
046-A
Applied Biomechanics Laboratory

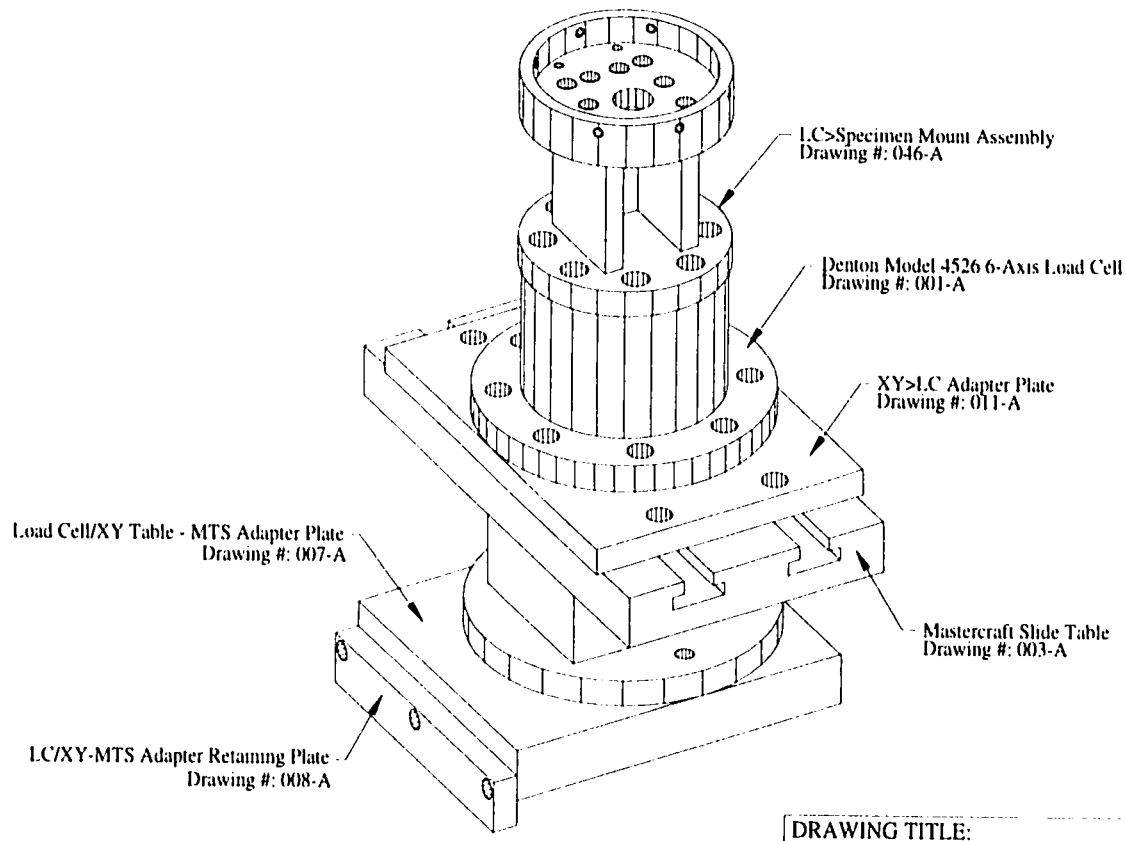

DRAWING TITLE:

MTS>Load Cell>Specimen Assembly

SCALE:	DRAWN BY: J. W. Carter
DATE: 9/5/01	DRAWING #: 047-A

MATERIAL:

All dimensions in inches, unless otherwise specified

Applied Biomechanics Laboratory
Box 359798, 325 9th Ave., Seattle, WA 98104
Phone #: 206.731.4346; Fax #: 206.731.5752

Appendix B Injury Pattern Scoring Sheet

Injury Pattern Scoring Sheet

Specimen #:
Date:
Inspector:

Strucutre	V1	V1-2	V2	V2-3	V3
ALL					
Anterior ½ Disc					
Anterior ½ Body					
Posterior ½ Disc					
Posterior ½ Body					
PLL					
Right Pedicle					
Left Pedicle					
Right Anterior FC					
Right Medial FC					
Right Lateral FC					
Right Posterior FC					
Left Anterior FC					
Left Medial FC					
Left Lateral FC					
Left Posterior FC					
Right Articular Pillar					
Left Articular Pillar					
LF					
Right Lamina					
Left Lamina					
Spinous Process					
ISL					
SSL					

Each structure should be scored with a 0 if uninjured and with a 1 for injured. Any comments with regard to the injury should be noted on the reverse side of this sheet. If you make notes put an N in the corner of the scoring box for that structure.

Structure Abbreviations:
ALL – *Anterior Longitudinal Ligament*
PLL – *Posterior Longitudinal Ligament*
FC – *Facet Capsule*
LF – *Ligamentum Flavum*
ISL – *Interspinous Ligament*
SSL – *Supraspinous Ligament*

Appendix C Load and Displacement Data Tabulation

Compression-Flexion Load Displacement Data

Specimen #		3	5	7	8	15	17	27	48
Sex	[M/F]	F	F	F	F	M	M	F	F
Age	[yrs]	70	90	53	34	50	61	77	72
Levels		C5-7	C5-7	C5-7	C5-7	C5-7	C5-7	C5-7	C5-7
RAM DISPLACEMENT									
Peak Displacement	[mm]	-8.7	-8.6	-8.6	-13.1	-8.7	-8.6	-8.7	-8.8
Time at peak displacement	[sec]	0.092	0.087	0.090	0.086	0.127	0.090	0.099	0.100
Time to peak displacement	[sec]	0.014	0.016	0.016	0.016	0.016	0.016	0.016	0.015
Displacement at Failure	[mm]	-7.8	-5.1	-7.8	-10.3	-8.4	-8.1	-5.7	-6.6
Time at initial displacement	[sec]	0.078	0.072	0.074	0.071	0.110	0.075	0.083	0.084
Peak Velocity	[mm/sec]	-828	-820	-783	-1260	-752	-783	-789	-815
Time at Peak Velocity	[sec]	0.086	0.080	0.081	0.080	0.119	0.083	0.093	0.092
Time to Peak Velocity	[sec]	0.008	0.008	0.007	0.009	0.008	0.009	0.009	0.008
NECK INJURY CRITERIA - Nij									
50th Male Peak Nij	[nondim]	0.43	0.27	0.56	0.40	0.59	0.57	0.41	0.50
5th Female Peak Nij	[nondim]	0.79	0.47	1.00	0.74	1.06	1.03	0.73	0.91
Time at peak	[sec]	0.086	0.079	0.084	0	0.120	0.083	0.091	0.094
Time to peak	[sec]	0.008	0.008	0.010	0.009	0.010	0.008	0.008	0.009
50th Male Nij at Failure	[nondim]	0.06	0.26	0.22	0.13	0.24	0.26	0.32	0.37
5th Female Nij at Failure	[nondim]	0.11	0.47	0.37	0.23	0.44	0.49	0.57	0.67
FAILURE LOAD DATA									
Axial Load	[N]	-330	-930	-1073	-542	-459	-486	-1214	-1091
A/P Shear	[N]	-140	-318	-350	-304	59	58	-415	-473
Midsagittal Moment	[N-m]	18.1	7.0	22.6	23.9	32.2	37.4	13.8	15.9
Time at failure	[sec]	0.090	0.080	0.087	0.082	0.125	0.088	0.093	0.095
Time to failure	[sec]	0.012	0.008	0.013	0.011	0.015	0.013	0.010	0.011
Eccentricity @ Failure	[mm]	54.7	7.6	21.1	44.0	70.3	77.1	11.3	14.6
Lateral Ecc @ Failure	[mm]	-9.7	-2.6	-7.5	-8.4	7.7	2.2	-7.2	-4.3
PEAK LOAD DATA									
Peak Compression	[N]	-1150	-1003	-1709	-1241	-2015	-1631	-1563	-1387
Time at peak	[sec]	0.085	0.079	0.083	0.076	0.119	0.082	0.091	0.093
Peak Tension	[N]	176	139	232	150	292	229	211	250
Time at peak	[sec]	0.093	0.088	0.094	0.102	0.129	0.092	0.101	0.102
Peak Anterior Shear	[N]	396	257	540	341	567	728	541	309
Time at peak	[sec]	0.096	0.090	0.093	0.087	0.129	0.093	0.101	0.101
Peak Posterior Shear	[N]	-420	-318	-574	-456	-613	-604	-467	-574
Time at peak	[sec]	0.087	0.080	0.085	0.079	0.120	0.084	0.091	0.094
Peak Flexion	[N-m]	18.4	13.8	22.6	23.9	32.2	37.4	20.7	16.0
Time at peak	[sec]	0.090	0.100	0.087	0.082	0.125	0.088	0.097	0.095
Peak Extension	[N-m]	-4.6	-3.5	-5.7	-9.0	-4.0	-10.4	-4.0	-5.6
Time at peak	[sec]	0.083	0.104	0.081	0.088	0.116	0.107	0.137	0.090

Compression Load Displacement Data

Specimen #		2	10	12	23	28	40	44	46
Sex	[M/F]	F	M	M	F	F	M	F	M
Age	[yrs]	78	30	80	69	84	41	67	61
Levels		C5-7	C5-7	C5-7	C4-6	C3-5	C5-7	C3-5	C6-T1
RAM DISPLACEMENT									
Peak Displacement	[mm]	-8.3	-15.2	-8.3	-10.0	-10.2	-15.7	-12.6	-15.4
Time at peak displacement	[sec]	0.088	0.093	0.086	0.119	0.092	0.092	0.091	0.087
Time to peak displacement	[sec]	0.016	0.016	0.015	0.049	0.015	0.016	0.015	0.016
Displacement at Failure	[mm]	-4.2	-2.9	-2.9	-3.2	-2.7	-3.2	-1.9	-2.2
Time at initial displacement	[sec]	0.072	0.077	0.070	0.071	0.077	0.076	0.075	0.071
Peak Velocity	[mm/sec]	-774	-1441	-800	-837	-969	-1545	-1286	-1494
Time at Peak Velocity	[sec]	0.078	0.086	0.080	0.079	0.085	0.085	0.084	0.080
Time to Peak Velocity	[sec]	0.007	0.009	0.009	0.008	0.009	0.009	0.009	0.009
NECK INJURY CRITERIA - Nij									
50th Male Peak Nij	[nondim]	1.15	2.12	1.28	1.93	1.68	2.32	1.21	1.51
5th Female Peak Nij	[nondim]	1.96	3.69	2.24	3.36	2.95	4.02	2.04	2.64
Time at peak	[sec]	0.085	0.087	0.084	0.084	0.089	0.090	0.090	0.081
Time to peak	[sec]	0.013	0.010	0.014	0.014	0.012	0.014	0.014	0.010
50th Male Nij at Failure	[nondim]	0.91	0.87	0.74	1.22	0.80	1.21	0.47	0.54
5th Female Nij at Failure	[nondim]	1.59	1.47	1.30	2.17	1.43	2.11	0.80	0.94
FAILURE LOAD DATA									
Axial Load	[N]	-3477	-4110	-2768	-4180	-2656	-4755	-1988	-2153
A/P Shear	[N]	444	-206	307	876	526	338	96	187
Midsagittal Moment	[N-m]	-23.5	-9.7	-8.2	-31.1	-12.7	-13.7	-7.2	-14.0
Time at failure	[sec]	0.080	0.081	0.077	0.076	0.081	0.081	0.079	0.075
Time to failure	[sec]	0.008	0.004	0.006	0.005	0.005	0.005	0.004	0.004
Eccentricity @ Failure	[mm]	-6.8	-2.4	-3.0	-7.4	-4.8	-2.9	-3.6	-6.5
Lateral Ecc @ Failure	[mm]	3.9	0.8	1.1	0.4	2.5	0.5	1.7	4.7
PEAK LOAD DATA									
Peak Compression	[N]	-5154	-8337	-4754	-7477	-6177	-9211	-5742	-6449
Time at peak	[sec]	0.085	0.089	0.084	0.084	0.090	0.090	0.089	0.086
Peak Tension	[N]	47	29	114	110	47	20	13	15
Time at peak	[sec]	0.253	0.227	0.251	0.262	0.255	0.238	0.235	0.225
Peak Anterior Shear	[N]	445	624	735	1282	1313	1281	715	835
Time at peak	[sec]	0.080	0.087	0.092	0.090	0.100	0.101	0.083	0.081
Peak Posterior Shear	[N]	-17	-266	-16	17	-12	4	-82	-170
Time at peak	[sec]	0.096	0.083	0.747	0.436	0.439	-0.028	0.087	0.085
Peak Flexion	[N-m]	1.4	0.6	0.8	3.1	2.5	3.6	0.5	0.8
Time at peak	[sec]	0.076	0.515	0.747	0.436	0.439	0.082	0.442	0.457
Peak Extension	[N-m]	-33.0	-70.2	-28.4	-72.7	-54.8	-105.1	-54.1	-92.4
Time at peak	[sec]	0.084	0.092	0.084	0.086	0.091	0.091	0.089	0.082

Compression-Extension Load Displacement Data

Specimen #		14	29	39	41	43	45	47	49
Sex	[M/F]	F	M	F	M	F	F	M	F
Age	[yrs]	55	88	76	91	87	88	94	86
Levels		C6-T1	C2-4	C6-T1	C3-5	C5-7	C5-7	C5-7	C4-6
RAM DISPLACEMENT									
Peak Displacement	[mm]	-9.8	-14.1	-8.3	-10.6	-8.5	-8.5	-8.8	-10.7
Time at peak displacement	[sec]	0.088	0.088	0.092	0.092	0.089	0.091	0.088	0.109
Time to peak displacement	[sec]	0.016	0.017	0.017	0.016	0.017	0.015	0.015	0.018
Displacement at Failure	[mm]	-4.6	-4.8	-4.2	-4.3	-4.6	-3.4	-3.2	-5.0
Time at initial displacement	[sec]	0.072	0.071	0.075	0.076	0.072	0.075	0.072	0.091
Peak Velocity	[mm/sec]	-891	-891	-698	-927	-704	-799	-753	-1189
Time at Peak Velocity	[sec]	0.081	0.085	0.084	0.086	0.079	0.085	0.082	0.100
Time to Peak Velocity	[sec]	0.009	0.014	0.008	0.010	0.007	0.009	0.009	0.009
NECK INJURY CRITERIA - Nij									
50th Male Peak Nij	[nondim]	1.0	1.4	0.9	2.2	0.7	1.1	1.6	1.1
5th Female Peak Nij	[nondim]	1.9	2.4	1.7	4.0	1.3	2.1	2.9	2.1
Time at peak	[sec]	0.088	0.078	0.093	0.094	0.080	0.092	0.089	0.108
Time to peak	[sec]	0.015	0.007	0.017	0.018	0.008	0.017	0.016	0.017
50th Male Nij at Failure	[nondim]	0.8	1.4	0.8	1.0	0.7	0.7	0.8	1.0
5th Female Nij at Failure	[nondim]	1.4	2.4	1.4	1.8	1.3	1.2	1.4	1.7
FAILURE LOAD DATA									
Axial Load	[N]	-2632	-5676	-3094	-3432	-3036	-2566	-3540	-3800
A/P Shear	[N]	557	830	422	700	335	442	301	613
Midsagittal Moment	[N-m]	-13.7	-80.9	-51.6	-45.6	-40.8	-34.3	-58.8	-56.9
Time at failure	[sec]	0.080	0.078	0.083	0.083	0.080	0.082	0.079	0.099
Time to failure	[sec]	0.007	0.007	0.007	0.007	0.008	0.007	0.006	0.008
Eccentricity @ Failure	[mm]	-5.2	-14.8	-16.7	-13.3	-13.4	-13.4	-16.6	-14.4
Lateral Ecc @ Failure	[mm]	1.1	0.8	-1.1	-4.5	-1.3	-2.1	-0.1	0.7
PEAK LOAD DATA									
Peak Compression	[N]	-3727	-5676	-3725	-5110	-3054	-2814	-4101	-3813
Time at peak	[sec]	0.083	0.078	0.086	0.094	0.080	0.092	0.082	0.099
Peak Tension	[N]	43	23	14	22	22	33	11	51
Time at peak	[sec]	0.224	0.225	0.286	0.232	0.264	0.263	0.230	0.235
Peak Anterior Shear	[N]	765	849	439	983	432	480	639	3978
Time at peak	[sec]	0.081	0.079	0.084	0.094	0.083	0.084	0.081	0.197
Peak Posterior Shear	[N]	-512	-502	-436	-791	-345	-613	-803	-508
Time at peak	[sec]	0.087	0.083	0.093	0.094	0.096	0.095	0.091	0.109
Peak Flexion	[N-m]	2.4	2.1	0.6	1.3	5.3	0.5	0.5	27.7
Time at peak	[sec]	0.451	0.466	0.262	0.476	0.263	0.442	0.456	0.424
Peak Extension	[N-m]	-68.9	-108.1	-81.3	-399.2	-57.3	-123.1	-158.3	-571.0
Time at peak	[sec]	0.088	0.087	0.089	0.094	0.093	0.092	0.088	0.114

Appendix D Axial Eccentricity Anova

The following analysis of variance tests the null hypothesis that there is no difference in axial eccentricity across the three loading environments applied in this study (compression-flexion, compression, and compression-extension.

Notes

Output Created		15-OCT-2001 17:08:21
Comments		
Input	Data	I:\Ecc Reduced Data\Ecc Compare.sav
	Filter	<none>
	Weight	<none>
	Split File	<none>
	N of Rows in Working Data File	24
Missing Value Handling	Definition of Missing	User-defined missing values are treated as missing.
	Cases Used	Statistics for each analysis are based on cases with no missing data for any variable in the analysis.
Syntax		ONEWAY ecc BY test /STATISTICS DESCRIPTIVES HOMOGENEITY /MISSING ANALYSIS /POSTHOC = GH ALPHA(.05).
Resources	Elapsed Time	0:00:00.46

Descriptives

ECC

	N	Mean	Std Dev	Std Error	95% Confidence Interval for Mean		Min	Max
					Lower Bound	Upper Bound		
Comp-Flex	8	37.59	27.66	9.78	14.46	60.71	7.60	77.10
Comp	8	-4.67	1.98	.70	-6.33	-3.02	-7.40	-2.40
Comp-Ext	8	-13.48	3.61	1.28	-16.49	-10.46	-16.70	-5.20
Total	24	6.48	27.50	5.61	-5.13	18.09	-16.70	77.10

ANOVA

ECC

	Sum of Squares	df	Mean Square	F	Sig.
Between Groups	11922.501	2	5961.250	22.866	.000
Within Groups	5474.719	21	260.701		
Total	17397.220	23			

The result of the ANOVA indicates that there exists at least two of the three loading environment groups exhibit significantly different axial eccentricities at failure (Sig = 0.000).

Post-Hoc Tests

Prior to conducting post-hoc pairwise comparisons to determine which groups are significantly different it is necessary to test for homogeneity of variances among the groups. If the null hypothesis that the variances group variances are equal is rejected then an appropriate post-hoc test method should be employed, which accounts for different variances across groups.

Test of Homogeneity of Variances

ECC

Levene Statistic	df1	df2	Sig.
32.680	2	21	.000

The test of homogeneity of variances indicates that the null hypothesis should be rejected (Sig = 0.000). Thus the variances are significantly different across the three groups being examined. Therefore, the Games-Howell post-hoc methodology is employed to compensate for unequal group variances. Zolman [103] recommends the Games-Howell post-hoc methodology for instances where unequal group variances are at issue.

Multiple Comparisons

Dependent Variable: ECC

Games-Howell

(I) TEST	(J) TEST	Mean Difference (I-J)	Std. Error	Sig.	95% Confidence Interval	
					Lower Bound	Upper Bound
Comp-Flex	Comp	42.2625*	8.0731	.008	13.4584	71.0666
	Comp-Ext	51.0625*	8.0731	.003	22.2482	79.8768
Comp	Comp-Flex	-42.2625*	8.0731	.008	-71.0666	-13.4584
	Comp-Ext	8.8000*	8.0731	.000	4.8583	12.7417
Comp-Ext	Comp-Flex	-51.0625*	8.0731	.003	-79.8768	-22.2482
	Comp	-8.8000*	8.0731	.000	-12.7417	-4.8583

*. The mean difference is significant at the .05 level.

The above post-hoc tests demonstrate that the mean axial eccentricities for each of the three test groups are significantly different from one another (Sig < 0.01). Thus, the loading environments applied were significantly different from one another.

Appendix E Displacement and Velocity ANOVA's

One-way ANOVA for Peak Displacements

The following are the most important outputs from the One-way ANOVA of the peak displacement data produced during this study.

Notes

Output Created		10-OCT-2001 16:22:50
Comments		
Input	Data	I:\Ecc Reduced Data\Disp-Vel Data.sav
	Filter	<none>
	Weight	<none>
	Split File	<none>
	N of Rows in Working Data File	24
Missing Value Handling	Definition of Missing	User-defined missing values are treated as missing.
	Cases Used	Statistics for each analysis are based on cases with no missing data for any variable in the analysis.
Syntax		ONEWAY pdisp BY test /STATISTICS DESCRIPTIVES HOMOGENEITY /MISSING ANALYSIS /POSTHOC = TUKEY BONFERRONI SIDAK GH ALPHA(.05).
Resources	Elapsed Time	0:00:00.97

Descriptives

PDISP

	N	Mean	Std. Deviation	Std. Error	95% Confidence Interval for Mean		Min	Max
					Lower Bound	Upper Bound		
Comp-Flex	8	-9.23	1.57	.55	-10.54	-7.92	-13.10	-8.56
Comp	8	-11.96	3.17	1.12	-14.61	-9.31	-15.70	-8.30
Comp-Ext	8	-9.91	1.94	.69	-11.54	-8.29	-14.10	-8.30
Total	24	-10.37	2.52	.52	-11.43	-9.30	-15.70	-8.30

ANOVA

PDISP

	Sum of Squares	df	Mean Square	F	Sig.
Between Groups	32.4	2	16.19	2.98	.073
Within Groups	114.1	21	5.43		
Total	146.5	23			

The ANOVA table indicates that the null hypothesis should be accepted (Sig = 0.073) thus indicating that the average peak displacement applied was no different across the three test groups.

One-way ANOVA for peak velocities

The following are the most important outputs from the One-way ANOVA of the peak velocity data produced during this study.

Notes

Output Created		20-OCT-2001 12:17:55
Comments		
Input	Data	I:\Ecc Reduced Data\Disp-Vel Data.sav
	Filter	<none>
	Weight	<none>
	Split File	<none>
	N of Rows in Working Data File	24
Missing Value Handling	Definition of Missing	User-defined missing values are treated as missing.
	Cases Used	Statistics for each analysis are based on cases with no missing data for any variable in the analysis.
Syntax		ONEWAY pvel BY test /STATISTICS DESCRIPTIVES HOMOGENEITY /MISSING ANALYSIS /POSTHOC = GH ALPHA(.05).
Resources	Elapsed Time	0:00:00.78

Descriptives

PVEL

	N	Mean	Std. Deviation	Std. Error	95% Confidence Interval for Mean		Minimum	Maximum
					Lower Bound	Upper Bound		
Comp-Flex	8	-853.7500	166.0032	58.6910	-992.5322	-714.9678	-1260.00	-752.00
Comp	8	-1143.25	332.0455	117.3958	-1420.8470	-865.6530	-1545.00	-774.00
Comp-Ext	8	-856.5000	160.4921	56.7425	-990.6748	-722.3252	-1189.00	-698.00
Total	24	-951.1667	262.7418	53.6320	-1062.1128	-840.2205	-1545.00	-698.00

Test of Homogeneity of Variances

PVEL

Levene Statistic	df1	df2	Sig.
8.355	2	21	.002

The test for homogeneity of variances suggests that there are in fact significant differences in group variance among the three loading groups. Therefore, if the ANOVA shows a significant difference then any post-hoc testing should be done with a methodology that compensates for unequal variances, such as the Games-Howell method [103].

ANOVA

PVEL

	Sum of Squares	df	Mean Square	F	Sig.
Between Groups	442782.3	2	221391.167	4.061	.032
Within Groups	1144983	21	54523.000		
Total	1587765	23			

The ANOVA table indicates that the null hypothesis should be rejected (Sig = 0.032) thus indicating that at least one pairwise comparison showed a significant difference in mean peak velocity.

Post-Hoc Tests for Peak Velocity Comparison

Multiple Comparisons

Dependent Variable: PVEL
Games-Howell

(I) TEST	(J) TEST	Mean Difference (I-J)	Std. Error	Sig.	95% Confidence Interval	
					Lower Bound	Upper Bound
Comp-Flex	Comp	289.5000	116.7508	.117	-68.6177	647.6177
	Comp-Ext	2.7500	116.7508	.999	-210.9418	216.4418
Comp	Comp-Flex	-289.5000	116.7508	.117	-647.6177	68.6177
	Comp-Ext	-286.7500	116.7508	.119	-643.6002	70.1002
Comp-Ext	Comp-Flex	-2.7500	116.7508	.999	-216.4418	210.9418
	Comp	286.7500	116.7508	.119	-70.1002	643.6002

Normally the post-hoc tests should follow suit with the ANOVA. However, in this case it would appear that the ANOVA is right on the edge showing a significant difference, because the results of the post-hoc tests indicate that there are no significant differences in the mean peak velocities for the three loading groups. The conclusion that one would draw is that the mean peak velocities observed for each group might not be statistically the same, but they are very similar.

One-way ANOVA for Failure Displacements

The following are the most important outputs from the One-way ANOVA of the failure displacement data produced during this study.

Descriptives

Displacement at Failure

	N	Mean	Std. Deviation	Std. Error	95% Confidence Interval for Mean		Min	Max
					Lower Bound	Upper Bound		
Comp-Flex	8	-7.48	1.64	.58	-8.85	-6.10	-10.27	-5.06
Comp	8	-2.91	.70	.25	-3.49	-2.33	-4.24	-1.93
Comp-Ext	8	-4.28	.65	.23	-4.82	-3.74	-4.99	-3.20
Total	24	-4.89	2.22	.45	-5.83	-3.95	-10.27	-1.93

Test of Homogeneity of Variances

Displacement at Failure

Levene Statistic	df1	df2	Sig.
3.749	2	21	.041

The test for homogeneity of variances suggests that there are in fact significant differences in group variance among the three loading groups. Therefore, if the ANOVA shows a significant difference then any post-hoc testing should be done with a methodology that compensates for unequal variances, such as the Games-Howell method [103].

ANOVA

Displacement at Failure

	Sum of Squares	df	Mean Square	F	Sig.
Between Groups	87.914	2	43.957	36.551	.000
Within Groups	25.255	21	1.203		
Total	113.169	23			

The ANOVA table indicates that the null hypothesis should be rejected (Sig = 0.000) thus indicating that at least one pairwise comparison showed a significant difference in mean peak velocity.

Post Hoc Tests for Failure Displacement Comparison

Multiple Comparisons

Dependent Variable: Displacement at Failure

Games-Howell

(I) Test Type	(J) Test Type	Mean Difference (I-J)	Std. Error	Sig.	95% Confidence Interval	
					Lower Bound	Upper Bound
Comp-Flex	Comp	-4.5672*	.5483	.000	-6.3148	-2.8196
	Comp-Ext	-3.1998*	.5483	.002	-4.9396	-1.4601
Comp	Comp-Flex	4.5672*	.5483	.000	2.8196	6.3148
	Comp-Ext	1.3674*	.5483	.003	.4862	2.2485
Comp-Ext	Comp-Flex	3.1998*	.5483	.002	1.4601	4.9396
	Comp	-1.3674*	.5483	.003	-2.2485	-.4862

*. The mean difference is significant at the .05 level.

The post-hoc tests clearly indicate that all pariwise comparisons of mean displacement at failure for the three loading groups show significant differences ($p < 0.003$).

Appendix F injury Pattern Discriminant Anlysis

The following is the output from SPSS generated as part of the Discriminant Analysis of the injury pattern data in this study. The three loading environments in this study (compression-flexion, compression, and compression-extension) were the groups for which classification equations were developed in the analysis. Some sections of the output are not shown here due to their size and the fact that they add little additional information to what is provided.

Notes

Output Created		17-OCT-2001 09:16:06
Comments		
Input	Data	I:\Ecc Injury Pattern\InjPattern-no lateral info.sav
	Filter	<none>
	Weight	<none>
	Split File	<none>
	N of Rows in Working Data File	24
Missing Value Handling	Definition of Missing	User-defined missing values are treated as missing in the analysis phase.
	Cases Used	In the analysis phase, cases with no user- or system-missing values for any predictor variable are used. Cases with user-, system-missing, or out-of-range values for the grouping variable are always excluded.
Syntax		DISCRIMINANT /GROUPS=injgrp(0 2) /VARIABLES=antll avd avb pvd pvb pll ped afc mfc lfc pfc ap lf lam sp isl ssl /ANALYSIS ALL /METHOD=MAHAL /PIN= .05 /POUT= .10 /PRIORS EQUAL /HISTORY /STATISTICS=MEAN STDDEV UNIV COEFF CORR FPAIR TABLE CROSSVALID /PLOT=MAP /CLASSIFY=NONMISSING POOLED .
Resources	Elapsed Time	0:00:00.16

Analysis Case Processing Summary

Unweighted Cases		N	Percent
Valid		24	100.0
Excluded	Missing or out-of-range group codes	0	.0
	At least one missing discriminating variable	0	.0
	Both missing or out-of-range group codes and at least one missing discriminating variable	0	.0
	Total	0	.0
Total		24	100.0

Tests of Equality of Group Means

	Wilks' Lambda	F	df1	df2	Sig.
ALL	.814	2.395	2	21	.116
AVD	.563	8.167	2	21	.002
AVB	.703	4.433	2	21	.025
PVD	.782	2.935	2	21	.075
PVB	.566	8.037	2	21	.003
PLL	.853	1.815	2	21	.187
PED	.825	2.227	2	21	.133
AFC	.818	2.333	2	21	.122
MFC	.689	4.742	2	21	.020
LFC	.771	3.111	2	21	.066
PFC	.944	.618	2	21	.549
AP	.600	7.000	2	21	.005
LF	.257	30.333	2	21	.000
LAM	.566	8.037	2	21	.003
SP	.156	57.000	2	21	.000
ISL	.176	49.000	2	21	.000
SSL	.[a]				

a. Cannot be computed because this variable is constant in each group.

Stepwise Analysis

A stepwise procedure was used to find the best set of discriminating variables from which to build the classification equations. The stepwise process is used when the researcher does not know a priori what the best discriminating variables will be [81]. The stepwise procedure goes through a complicated process to select only those variables which provide the best ability to distinctly separate and classify the subjects into groups. For this project the stepwise procedure used the Mahalanobis distance as the selection criteria for picking the best discriminating variables. The Mahalanobis distances is best used in situations where there are three or more groups of equal size [81].

Variables Entered/Removed[a,b,c,d]

		Min. D Squared					
				Exact F			
Step	Entered	Statistic	Between Groups	Statistic	df1	df2	Sig.
1	LF	.875	Comp and Comp-Ext	3.500	1	21	.075
2	SP	14.375	Comp and Comp-Flex	27.381	2	20	.000
3	ISL	32.375	Comp-Flex and Comp-Ext	39.056	3	19	.000
4	ALL	42.621	Comp-Flex and Comp-Ext	36.532	4	18	.000
5	PED	51.371	Comp-Flex and Comp-Ext	33.269	5	17	.000
6	AP	62.884	Comp-Flex and Comp-Ext	31.941	6	16	.000

At each step, the variable that maximizes the Mahalanobis distance between the two closest groups is entered.

a. Maximum number of steps is 34.

b. Maximum significance of F to enter is .05.

c. Minimum significance of F to remove is .10.

d. F level, tolerance, or VIN insufficient for further computation.

The table titled Variables Entered/Removed shown above provides information on the number of steps used to generate the classification functions and which variables were entered into the classification equations at a given step.

Wilks' Lambda

Step	Number of Variables	Lambda	df1	df2	df3	Exact F			
						Statistic	df1	df2	Sig.
1	1	.257	1	2	21	30.333	2	21	6.410E-07
2	2	.044	2	2	21	37.610	4	40	4.413E-13
3	3	.017	3	2	21	42.785	6	38	2.011E-15
4	4	.012	4	2	21	36.850	8	36	4.395E-15
5	5	.007	5	2	21	37.505	10	34	1.861E-15
6	6	.004	6	2	21	40.406	12	32	7.023E-16

Pairwise Group Comparisons[a,b,c,d,e,f]

Step	Injury Group		Comp	Comp-Flex	Comp-Ext
1	Comp	F		56.000	3.500
		Sig.		.000	.075
	Comp-Flex	F	56.000		31.500
		Sig.	.000		.000
	Comp-Ext	F	3.500	31.500	
		Sig.	.075	.000	
2	Comp	F		27.381	36.667
		Sig.		.000	.000
	Comp-Flex	F	27.381		60.714
		Sig.	.000		.000
	Comp-Ext	F	36.667	60.714	
		Sig.	.000	.000	
3	Comp	F		39.056	52.778
		Sig.		.000	.000
	Comp-Flex	F	39.056		39.056
		Sig.	.000		.000
	Comp-Ext	F	52.778	39.056	
		Sig.	.000	.000	
4	Comp	F		36.532	37.500
		Sig.		.000	.000
	Comp-Flex	F	36.532		36.532
		Sig.	.000		.000
	Comp-Ext	F	37.500	36.532	
		Sig.	.000	.000	
5	Comp	F		33.269	51.000
		Sig.		.000	.000
	Comp-Flex	F	33.269		33.269
		Sig.	.000		.000
	Comp-Ext	F	51.000	33.269	
		Sig.	.000	.000	
6	Comp	F		37.555	73.684
		Sig.		.000	.000
	Comp-Flex	F	37.555		31.941
		Sig.	.000		.000
	Comp-Ext	F	73.684	31.941	
		Sig.	.000	.000	

a. 1, 21 degrees of freedom for step 1.
b. 2, 20 degrees of freedom for step 2.
c. 3, 19 degrees of freedom for step 3.
d. 4, 18 degrees of freedom for step 4.
e. 5, 17 degrees of freedom for step 5.
f. 6, 16 degrees of freedom for step 6.

The most important part of the above table for Pairwise Group Comparisons is the subsection for step 6. This section in effect demonstrates that the mean injury patterns for the three groups are significantly different from one another (Sig = 0.000). Thus, the injury patterns for each group can be considered to be distinctly different from one

another. It should be noted that these comparisons are made based on the six best discriminating variables and not the entire set of 17 variables that the analysis began with.

Summary of Canonical Discriminant Functions

Eigenvalues

Function	Eigenvalue	% of Variance	Cumulative %	Canonical Correlation
1	27.707[a]	77.4	77.4	.982
2	8.088[a]	22.6	100.0	.943

a. First 2 canonical discriminant functions were used in the analysis.

Wilks' Lambda

Test of Function(s)	Wilks' Lambda	Chi-square	df	Sig.
1 through 2	.004	102.936	12	.000
2	.110	40.829	5	.000

Standardized Canonical Discriminant Function Coefficients

	Function	
	1	2
ALL	-.021	.627
PED	-.829	-.060
AP	-.852	.053
LF	.001	-.754
SP	1.160	.629
ISL	1.194	-.398

Structure Matrix

	Function	
	1	2
ISL	.367*	-.338
LAM[a]	.309*	-.240
PFC[a]	.270*	-.057
PVB[a]	-.169*	-.116
PVD[a]	.147*	.124
AP	-.139*	.128
AVB[a]	-.104*	-.023
LF	.097	-.570*
LFC[a]	.301	-.529*
SP	.338	.528*
PLL[a]	.061	-.282*
MFC[a]	-.109	-.282*
AFC[a]	.085	-.274*
ALL	.016	.165*
AVD[a]	-.083	.149*
PED	-.061	.116*

Pooled within-groups correlations between discriminating variables and standardized canonical discriminant functions
Variables ordered by absolute size of correlation within function.

*. Largest absolute correlation between each variable and any discriminant function

a. This variable not used in the analysis.

Functions at Group Centroids

	Function	
Injury Group	1	2
Comp	-6.235	1.675
Comp-Flex	.432	-3.755
Comp-Ext	5.803	2.080

Unstandardized canonical discriminant functions evaluated at group means

Classification Statistics

Classification Processing Summary

Processed		24
Excluded	Missing or out-of-range group codes	0
	At least one missing discriminating variable	0
Used in Output		24

Prior Probabilities for Groups

Injury Group	Prior	Cases Used in Analysis	
		Unweighted	Weighted
Comp	.333	8	8.000
Comp-Flex	.333	8	8.000
Comp-Ext	.333	8	8.000
Total	1.000	24	24.000

Classification Function Coefficients

	Injury Group		
	Comp	Comp-Flex	Comp-Ext
ALL	2.710	-4.742	2.710
PED	3.316	-11.053	-24.316
AP	6.079	-13.263	-27.079
LF	-.802	14.529	-1.907
SP	-1.961	19.182	67.671
ISL	-4.671	44.924	64.961
(Constant)	-3.503	-30.528	-66.503

Fisher's linear discriminant functions

The Classification Function Coefficients table provides the Fisher's standardized linear disciminant function coefficients for the three classifications functions produced in this analysis. To use the functions the values of the six variables listed are taken from a subject injury pattern and multiplied by their corresponding coefficients for each of the three classifications equations. The value of each equation is then determined by

summing terms. The equation with the largest resulting value represents the group that the pattern of interest would be classified into.

Classification Results[b,c]

			Predicted Group Membership			
		Injury Group	Comp	Comp-Flex	Comp-Ext	Total
Original	Count	Comp	8	0	0	8
		Comp-Flex	0	8	0	8
		Comp-Ext	0	0	8	8
	%	Comp	100.0	.0	.0	100.0
		Comp-Flex	.0	100.0	.0	100.0
		Comp-Ext	.0	.0	100.0	100.0
Cross-validated[a]	Count	Comp	8	0	0	8
		Comp-Flex	0	8	0	8
		Comp-Ext	0	0	8	8
	%	Comp	100.0	.0	.0	100.0
		Comp-Flex	.0	100.0	.0	100.0
		Comp-Ext	.0	.0	100.0	100.0

a. Cross validation is done only for those cases in the analysis. In cross validation, each case is classified by the functions derived from all cases other than that case.

b. 100.0% of original grouped cases correctly classified.

c. 100.0% of cross-validated grouped cases correctly classified.

The Classification Results table is important for determining the accuracy of the classification equations that have been developed. The most important section is labeled "Cross-validated." This section provides the best representation of the accuracy of the classification equations. As can be seen here the classification equations that have been developed in this study are 100% accurate. That is to say that if you take a single subject out of the analysis and redevelop the classification equations using the remaining subjects, the left out subject would be properly reclassified (cross-validated) 100% of the time.

The results of this cross-validation also support the results of the Pairwise Group Comparison in that they demonstrate a high level of group/pattern distinctiveness.

Appendix G Canal Occlusion Data

Compression Occlusion Data

Specimen #		10	12	23	28	40	44	46
Sex	[M/F]	M	M	F	F	M	F	M
Age	[yrs]	30	80	69	84	41	67	61
Levels		C5-7	C5-7	C4-6	C3-5	C5-7	C3-5	C6-T1
Failure Occlusion	[%MSD]	0	0	0	26	0	0	0
Peak Occlusion	[%MSD]	56	55	53	59	82	48	54
Time at peak	[sec]	0.093	0.086	0.087	0.093	0.093	0.089	0.088
Time to peak	[sec]	0.016	0.016	0.017	0.016	0.017	0.014	0.017
Residual Occlusion	[%MSD]	25	0	31	0	46	31	31

Compression-Extension Occlusion Data

Specimen #		14	39	41	43	45	47
Sex	[M/F]	F	F	M	F	F	M
Age	[yrs]	55	76	91	87	88	94
Levels		C6-T1	C6-T1	C3-5	C5-7	C5-7	C5-7
Failure Occlusion	[%MSD]	0	0	23	30	0	22
Peak Occlusion	[%MSD]	53	57	57	66	64	62
Time at peak	[sec]	0.129	0.135	0.108	0.098	0.122	0.101
Time to peak	[sec]	0.057	0.060	0.032	0.025	0.046	0.028
Residual Occlusion	[%MSD]	10	22	45	46	43	30

Appendix H Canal Occlusion ANOVA

Two-Way Repeated Measures Analysis of Canal Occlusion Data

Notes

Output Created		15-OCT-2001 15:27:28
Comments		
Input	Data	I:\Ecc Reduced Data\SCOTDataCompare.sav
	Filter	<none>
	Weight	<none>
	Split File	<none>
	N of Rows in Working Data File	13
Missing Value Handling	Definition of Missing	User-defined missing values are treated as missing.
	Cases Used	Statistics are based on all cases with valid data for all variables in the model.
Syntax		GLM hsfail hspeak hsresid BY ecc /WSFACTOR = time 3 Polynomial /METHOD = SSTYPE(3) /PLOT = PROFILE(time*ecc ecc*time) /EMMEANS = TABLES(time) COMPARE ADJ(BONFERRONI) /PRINT = DESCRIPTIVE OPOWER HOMOGENEITY /CRITERIA = ALPHA(.05) /WSDESIGN = time /DESIGN = ecc .
Resources	Elapsed Time	0:00:00.37

Within-Subjects Factors

Measure: MEASURE_1

TIME	Dependent Variable
1	HSFAIL
2	HSPEAK
3	HSRESID

Between-Subjects Factors

		Value Label	N
Eccentricity Group	C	Compression	7
	CE	Compression-Extension	6

Note that this statistical analysis was only performed for the Compression and Compression-Extension series. The Compression-Flexion series occlusion data was determined to be unreliable and was therefore removed from consideration.

Descriptive Statistics

	Eccentricity Group	Mean	Std. Deviation	N
High Section Occ at Failure	Compression	3.67	9.71	7
	Compression-Extension	12.42	13.90	6
	Total	7.71	12.18	13
High Section Peak Occ	Compression	57.99	10.95	7
	Compression-Extension	59.97	4.88	6
	Total	58.90	8.42	13
High Section Residual Occ	Compression	23.44	17.28	7
	Compression-Extension	32.48	14.68	6
	Total	27.62	16.16	13

Mauchly's Test of Sphericity[b]

Measure: MEASURE_1

Within Subjects Effect	Mauchly's W	Approx. Chi-Square	df	Sig.	Epsilon[a] Greenhous e-Geisser	Huynh-Feldt	Lower-bound
TIME	.750	2.878	2	.237	.800	1.000	.500

Tests the null hypothesis that the error covariance matrix of the orthonormalized transformed dependent variables is proportional to an identity matrix.

a. May be used to adjust the degrees of freedom for the averaged tests of significance. Corrected tests are displayed in the Tests of Within-Subjects Effects table.

b.
Design: Intercept+ECC
Within Subjects Design: TIME

Because Mauchly's Test of Sphericity accepts the null hypothesis (Sig = 0.237) then Sphericity is assumed. Therefore, in the Tests of Within-Subjects Effects table below the Sphericity Assumed rows are the ones to look at.

Tests of Within-Subjects Effects

Measure: MEASURE_1

Source		Type III Sum of Squares	df	Mean Square	F	Sig.	Noncent. Parameter	Observed Power[a]
TIME	Sphericity Assumed	17026.9	2.0	8513.4	64.49	.000	128.985	1.000
	Greenhouse-Geisser	17026.9	1.6	10642.5	64.49	.000	103.182	1.000
	Huynh-Feldt	17026.9	2.0	8514.1	64.49	.000	128.975	1.000
	Lower-bound	17026.9	1.0	17026.9	64.49	.000	64.493	1.000
TIME * ECC	Sphericity Assumed	103.0	2.0	51.5	.39	.681	.781	.105
	Greenhouse-Geisser	103.0	1.6	64.4	.39	.637	.624	.099
	Huynh-Feldt	103.0	2.0	51.5	.39	.681	.781	.105
	Lower-bound	103.0	1.0	103.0	.39	.545	.390	.088
Error(TIME)	Sphericity Assumed	2904.1	22.0	132.0				
	Greenhouse-Geisser	2904.1	17.6	165.0				
	Huynh-Feldt	2904.1	22.0	132.0				
	Lower-bound	2904.1	11.0	264.0				

a. Computed using alpha = .05

The tests of Within-Subjects Effects table provides information on the main effect of occlusion measurement period (failure, peak, residual) and the interaction of measurement period and test type (compression or compression-extension). The values given for Sphericity Assumed demonstrate that their exists a significant main effect of measurement period with an observed power of 1.0. Additionally, it is suggested that the there is no interaction effect, however, the observed power is extremely low indicating a high probability of Type II error, which would lead to accepting the null hypothesis that there is no interaction even though it should be rejected. This indicates that the number of specimens is too low to generate the needed power for determining if an interaction effect exists.

Tests of Between-Subjects Effects

Measure: MEASURE_1

Transformed Variable: Average

Source	Type III Sum of Squares	df	Mean Square	F	Sig.	Noncent. Parameter	Observed Power[a]
Intercept	38863.3	1	38863.3	183.0	.000	183.0	1.000
ECC	420.8	1	420.8	1.982	.187	1.982	.251
Error	2335.8	11	212.3				

a. Computed using alpha = .05

The tests of Between-Subjects effects provides information on the main effect of test type (compression vs. compression-extension). The results indicate that there is no effect of test type and that the null hypothesis should be accepted ($p = 0.187$). However, the observed power is very low (0.251) indicating that there is a high probability (~ 75%) of accepting the null hypothesis even though it should be rejected. This suggests that more specimens are needed to more clearly define the individual means and increase the power.

Estimated Marginal Means

Post-Hoc Pairwise Comparisons of Time of Occlusion Measurement

Estimates

Measure: MEASURE_1

TIME	Mean	Std. Error	95% Confidence Interval	
			Lower Bound	Upper Bound
1	8.04	3.28	.818	15.270
2	59.0	2.43	53.6	64.3
3	28.0	4.49	18.1	37.9

Pairwise Comparisons

Measure: MEASURE_1

(I) TIME	(J) TIME	Mean Difference (I-J)	Std. Error	Sig.[a]	95% Confidence Interval for Difference[a]	
					Lower Bound	Upper Bound
1	2	-50.9*	3.781	.000	-61.6	-40.3
	3	-19.9*	5.529	.012	-35.5	-4.3
2	1	50.9*	3.781	.000	40.3	61.6
	3	31.0*	4.052	.000	19.6	42.4
3	1	19.9*	5.529	.012	4.3	35.5
	2	-31.0*	4.052	.000	-42.4	-19.6

Based on estimated marginal means

*. The mean difference is significant at the .05 level.

a. Adjustment for multiple comparisons: Bonferroni.

The pairwise comparisons table provides information on the pairwise comparisons of the individual time periods to one another. What it shows is that all of the measurement periods exhibit significantly different occlusion magnitudes on average. The post-hoc alpha adjustment techniques used was the Bonferroni, which is adequate for multiple comparisons [103]. The Sidak multiple comparisons adjustment was also used. The Sidak pairwise procedure is supposed to be tighter than Bonferroni and limit the increase in Type II error that can be associated with Bonferroni [103]. As can be seen the results were nearly identical.

VITA

Jarrod W. Carter Ph.D.

EDUCATION:

(1988 - Present)

Doctor of Philosophy in Bioengineering
University of Washington, Seattle, Washington
Specialization: Biomechanics
Degree conferred: February 28th, 2002
Dissertation title: Compressive Cervical Spine Injury: The Effect of Injury Mechanism on Structural Injury Pattern and Neurologic Injury Potential.
Research conducted at the Applied Biomechanics Laboratory at Harborview Hospital, Seattle, Washington.

Bachelor of Sciences in Mechanical Engineering
Washington State University, Pullman, Washington
Graduated: May 8th, 1993
Cumulative G.P.A.: 3.77 (on 4.00 scale)
Graduation Honors: Cum Laude
Class Standing: 4th out of 120

EXPERIENCE:

(1988 - Present)

I am an Associate Engineer with the firm of Origin Engineering 12314 East Broadway Avenue, Spokane, Washington. Origin Engineering is a consulting firm specializing in accident reconstruction.

(Up to 1988)

Extensive hands on experience as a commercial fisherman (Kenai, Alaska), truss plant worker (Deer Park, Washington), and farm hand (family farm in Elk, Washington).

ACTIVITIES:

American Society of Mechanical Engineers
- Washington State University Student Section Chair (1992 thru 1993)
Society of Automotive Engineers
- Helped restart society at Washington State University (1992 thru 1993)

AWARDS:

Member of Tau Beta Pi (ΤΒΠ), Phi Kappa Phi (ΦΚΦ) and Golden Key Honor Societies. Presidents Honor Roll Washington State University for 5 semesters.

TEACHING EXPERIENCE:

Washington State Physical Therapists Association, Spring Conference 1996. Taught session on cervical spine injuries in automotive accidents.

University of Washington Rehabilitation Medicine anatomy class entitled "Function of the Locomotor System" (Rehab 445) winter quarters 1996 – 2000. Taught session reviewing cervical spine trauma.

University of Washington Bioengineering class entitled "Orthopaedic Biomechanics" (BIOEN 520) winter quarter 2000. Team taught with four others.

INVITED LECTURES

Compressive Cervical Spine Injury: The Effect of Loading Environment on Structural Injury Pattern and Neurologic Injury Potential. Presentation to Design/Analysis Group at Ford Motor Company, May 15th 2001.

PUBLICATIONS:

Carter JW, Ching RP, Tencer AF: Transient changes in canal geometry during axial burst fracture of the cervical spine. *Fifth Annual Symposium on Injury Prevention Through Biomechanics*, 1995

Carter JW, Ching RP, Tencer AF, Mirza S: Transient changes in cervical spinal canal geometry during wedge compression fracture. *Sixth Annual Symposium on Injury Prevention Through Biomechanics*, 1996

Watson NA, Ching RP, Carter JW, Tencer AF: The effect of post-injury position on canal occlusion in a cervical spine burst fracture model Spine: vol 22, no. 15, pp. 1710-1715, 1997

Ching RP, Carter JW, Raynak GC, Nuckley DJ, Mirza SK, Chapman JR, Tencer AF: Transient and post-traumatic measurement of cervical spinal canal and neuroforaminal deformation: Potential mechanisms for neurologic injury. In: *Frontiers in Head and Neck Trauma: Clinical and Biomechanical*, Eds. Yoganandan, N, Pintar, FA, Larson, SJ, Sances, A Jr., IOS Press, Washington D.C., 1998

Carter JW, Ching RP, Mirza, S, Tencer AF: Canal geometry changes associated with axial-compressive cervical spine fracture. Spine vol. 25, no. 1, pp 46 – 54, 2000

Nuckley DJ, Carter JW, Eck MP, Mirza SK, Ching RP: Compressive Mechanics of the Developing Spine. *Proceedings of the 46th Annual Orthopaedic Research Society Meeting*, 2000

Nuckley DJ, Carter JW, Eck MP, Mirza SK, Ching RP: Compressive Mechanics of the Developing Spine. *Injury Biomechanics Research - Proceedings of the 27th International Workshop,* pp 101 – 104, 1999

David Nuckley, Suzanne Hertsted, Jarrod Carter, Sohail Mirza, and Randal Ching: Compressive Biomechanics of Developing Spinal Tissues. *Proceedings of the 25th Annual Meeting of the American Society of Biomechanics,* pp 55-56, 2001